Final Report

CONTINUATION OF SUPERPAVE PROJECTS MONITORING

UF Project No.: 00073127

Contract No.: BDK-75-977-06

Submitted to:

Florida Department of Transportation
605 Suwannee Street
Tallahassee, FL, 32399

Dr. Reynaldo Roque, P.E.
Sanghyun Chun
Dr. Jian Zou
George Lopp
Dr. Claude Villiers

Department of Civil and Coastal Engineering
College of Engineering
365 Weil Hall, P.O. Box 116580
Gainesville, FL, 32611-6580
Tel: (352) 392-9537 extension 1458
Fax: (352) 392-3394

July 2011

DISCLAIMER

The opinions, findings and conclusions expressed in this publication are those of the authors and not necessarily those of the Florida Department of Transportation.

Prepared in cooperation with the State of Florida Department of Transportation.

SI* (MODERN METRIC) CONVERSION FACTORS

APPROXIMATE CONVERSIONS TO SI UNITS

Symbol	When You Know	Multiply By	To Find	Symbol
	LENGTH			
in	inches	25.4	millimeters	mm
ft	feet	0.305	meters	m
yd	yards	0.914	meters	m
mi	miles	1.61	kilometers	km
	AREA			
in^2	square inches	645.2	square millimeters	mm^2
ft^2	square feet	0.093	square meters	m^2
yd^2	square yards	0.836	square meters	m^2
ac	acres	0.405	hectares	ha
mi^2	square miles	2.59	square kilometers	km^2
	VOLUME			
fl oz	fluid ounces	29.57	milliliters	ml
gal	gallons	3.785	liters	l
ft^3	cubic feet	0.028	cubic meters	m^3
yd^3	cubic yards	0.765	cubic meters	m^3
NOTE: Volumes greater than 1000 l shall be shown in m^3.				
	MASS			
oz	ounces	28.35	grams	g
lb	pounds	0.454	kilograms	kg
T	short tons (2000 lb)	0.907	megagrams	Mg
	TEMPERATURE (exact)			
°F	Fahrenheit temperature	5(F-32)/9 or (F-32)/1.8	Celcius temperature	°C
	ILLUMINATION			
fc	foot-candles	10.76	lux	l
fl	foot-Lamberts	3.426	candela/m^2	cd/m^2
	FORCE and PRESSURE or STRESS			
lbf	poundforce	4.45	newtons	N
psi	poundforce per square inch	6.89	kilopascals	kPa

APPROXIMATE CONVERSIONS FROM SI UNITS

Symbol	When You Know	Multiply By	To Find	Symbol
	LENGTH			
mm	millimeters	0.039	inches	in
m	meters	3.28	feet	ft
m	meters	1.09	yards	yd
km	kilometers	0.621	miles	mi
	AREA			
mm^2	square millimeters	0.0016	square inches	in^2
m^2	square meters	10.764	square feet	ft^2
m^2	square meters	1.195	square yards	yd^2
ha	hectares	2.47	acres	ac
km^2	square kilometers	0.386	square miles	mi^2
	VOLUME			
ml	milliliters	0.034	fluid ounces	fl oz
l	liters	0.264	gallons	gal
m^3	cubic meters	35.71	cubic feet	ft^3
m^3	cubic meters	1.307	cubic yards	yd^3
	MASS			
g	grams	0.035	ounces	oz
kg	kilograms	2.202	pounds	lb
Mg	megagrams	1.103	short tons (2000 lb)	T
	TEMPERATURE (exact)			
°C	Celcius temperature	1.8C + 32	Fahrenheit temperature	°F
	ILLUMINATION			
lx	lux	0.0929	foot-candles	fc
cd/m^2	candela/m^2	0.2919	foot-Lamberts	fl
	FORCE and PRESSURE or STRESS			
N	newtons	0.225	poundforce	lbf
kPa	kilopascals	0.145	poundforce per square inch	psi

* SI is the symbol for the International System of Units. Appropriate rounding should be made to comply with Section 4 of ASTM E380.

(Revised August 1992)

Technical Report Documentation Page

1. Report No.	2. Government Accession No.	3. Recipient's Catalog No.

4. Title and Subtitle	5. Report Date
Continuation of Superpave Projects Monitoring	July 2011
	6. Performing Organization Code 0054539

7. Author(s)	8. Performing Organization Report No.
Reynaldo Roque, Sanghyun Chun, Jian Zou, George Lopp, and Claude Villiers	

9. Performing Organization Name and Address	10. Work Unit No. (TRAIS)
University of Florida Department of Civil and Coastal Engineering 365 Weil Hall P.O. Box 116580 Gainesville, FL 32611-6580	11. Contract or Grant No. BDK-75-977-06

12. Sponsoring Agency Name and Address	13. Type of Report and Period Covered
Florida Department of Transportation Research Management Center 605 Suwannee Street, MS 30 Tallahassee, FL 32399	Final 5/01/08-7/31/11
	14. Sponsoring Agency Code

15. Supplementary Notes

16. Abstract

This study involved the continuous monitoring of material properties and field performance of twelve Superpave project sections in Florida for the establishment of reasonable and effective mixture design guidelines and criteria, the identification and development of material property relations, and the evaluation of ongoing national and Florida design model development efforts. Field performance evaluation was conducted to identify performance-related criteria using the Dominant Aggregate Size Range-Interstitial Component (DASR-IC) parameters, which characterize the mixture gradation. Results indicated that the introduction of DASR-IC criteria into current mix design guidelines and specifications will assure good and consistent performance of Superpave mixtures. Identification of mixture parameters that control cracking performance led to the development of relationships to predict fundamental mixture properties (e.g., fracture energy and creep rate) based on DASR-IC parameters within the acceptable range. Based on the evaluation of existing pavement performance prediction models, the Enhanced Hot-Mix Asphalt Fracture Mechanics based Model (HMA-FM-E) was clearly determined to be the best choice for further top-down cracking prediction model development for use in the design of flexible pavements. It was found that the fracture resistance of asphalt mixtures was significantly reduced in sections subjected to moisture damage, which obviously affected mixture performance in the field. Development of a comprehensive and user-friendly database was continued in this phase. This has resulted in one of the most extensive datasets of research quality Superpave data on real-world projects. Recommendations were made for further investigations on the continuation of Superpave projects monitoring in Florida.

17. Key Word	18. Distribution Statement
Superpave Mix Design, Mixture Characteristics, Component Properties, Material Property Relations, and Performance Prediction Model	No restrictions. This document is available to the public through the National Technical Information Service, Springfield, VA, 22161.

19. Security Classif. (of this report)	20. Security Classif. (of this page)	21. No. of Pages	22. Price
Unclassified	Unclassified	261	

Form DOT F 1700.7 (8-72) Reproduction of completed page authorized

ACKNOWLEDGMENTS

The authors would like to acknowledge and thank the Florida Department of Transportation (FDOT) for providing technical and financial support and materials for this project. Special thanks go to project manager Bruce Dietrich, and engineers and technicians of the Bituminous Section of the State Materials Office for their contributions in terms of their expert knowledge, experience, and constructive advice throughout the course of this work.

Research team would like to especially express our gratitude to Aaron Turner, Mabel Stickles, and Jimmie Self for their invaluable efforts and contributions on binder extraction, testing, and carefully compiling and organizing all the test results. Their efforts are sincerely appreciated and clearly made a positive impact on the quality of the research.

EXECUTIVE SUMMARY

This study involved the continuous monitoring of material properties and field performance of twelve Superpave project sections in Florida for the establishment of reasonable and effective mixture design guidelines and criteria, the identification and development of material property relations, and the evaluation of ongoing national and Florida design model development efforts. The work was a follow-up to an earlier monitoring project conducted on the same pavements from 1999 to 2005.

It was determined that existing mix design criteria, including VMA, gradation control points, and effective asphalt content, do not capture the critical aspects of gradation and mixture volumetric properties found to be the most strongly related to rutting and cracking performance. Superpave mixture performance varied significantly among mixtures that met all existing criteria. Therefore, there was a need to identify and verify additional criteria that can assure better and more consistent Superpave mixture performance.

Field performance evaluation for both rutting and cracking was conducted to identify performance-related criteria using parameters from Dominant Aggregate Size Range – Interstitial Component (DASR-IC) mixture gradation model. Four parameters that characterize mixture gradation were determined to relate well to field performance of Superpave mixtures: DASR porosity, disruption factor (DF), effective film thickness (EFT), and ratio between coarse portion of fine aggregate and fine portion of fine aggregate (CFA/FFA). Results indicated that DASR porosity, which reflects the characteristics of coarse aggregate structure, is the most dominant parameter to control rutting performance. IC characteristics including DF, EFT and CFA/FFA could not overcome the problems associated with a mixture with DASR porosity outside the acceptable range. However, if DASR porosity is within the acceptable range, then DF, EFT and

CFA/FFA may influence rutting performance. For cracking performance, both DASR porosity and IC characteristics are important. The DASR porosity alone appears unable to clearly differentiate field cracking performance. The existence of an acceptable range of DF was identified to achieve good cracking performance. The DASR porosity criterion combined with the DF criterion appear to effectively distinguish the relative cracking performance in the field. Therefore, the introduction of DASR-IC criteria into current mix design guidelines and specifications will help to assure good field rutting and cracking performance of Superpave mixtures. The challenge is to make the system more practical for implementation.

Identification of mixture parameters that control cracking performance also led to the development of preliminary relationships to predict fundamental mixture properties based upon properties and characteristics of mixture components. Relations were developed to predict fracture energy and creep rate, which are the properties known to control cracking performance and are also required for performance model predictions. Basic forms were identified to predict changes in these properties over time (aging). This can serve as the foundation for further development of relationships based on additional field data and laboratory data using more advanced laboratory conditioning procedures currently being developed in other ongoing FDOT research efforts. It is also anticipated that relations will be significantly enhanced to consider binder effect using the newly developed binder fracture energy test.

Evaluation of existing pavement performance prediction models indicated that the Mechanistic-Empirical Pavement Design Guide (MEPDG) bottom-up cracking model appeared to adequately predict observed performance. No bottom-up cracking (BUC) was observed and no BUC was predicted by MEPDG. The PerRoad program appeared to be not as accurate as MEPDG in that it predicted BUC in two sections where none was observed.

For top-down cracking (TDC), the Enhanced Hot-Mix Asphalt Fracture Mechanics based Model (HMA-FM-E) appeared to accurately predict observed time to crack initiation of TDC and resulted in predictions of crack growth that were reasonable and consistent with field observations. The existing TDC model in MEPDG was found to be inadequate in terms of predicting initiation or propagation of TDC. The Energy Ratio (ER) model predicts neither crack initiation time nor crack amount. However, it was found to be suitable for relative evaluation of TDC performance. So, the HMA-FM-E was clearly determined to be the best choice for further TDC performance model development for use in mix and pavement design in Florida. As mentioned earlier, the key is to continue to improve the material property models by taking into account the effects of load-induced damage, moisture-related damage, and aging and healing on mixture properties. This effort was initiated as part of this study.

Moisture damage was visually observed in the form of stripping for Projects 9, 10, 11, and 12 within the first six to seven years after construction. Stripping was particularly prominent at the interface between top and bottom Superpave layers. The use of granite aggregates was common to all moisture-damaged projects. No moisture damage was observed for project sections produced with limestone aggregate. For three of the moisture-damaged projects (Projects 9, 10, and 12), rubber modified binder (ARB-5) was used along with a fine graded mixture. It was identified that the trend of change in mixture properties with aging in the field appears to be strongly affected by the occurrence of moisture damage. In some cases, the air voids increased over time, which appeared to be related to the displacement of material caused by moisture damage. Also, the effect of moisture damage accelerated the rate of reduction in normalized fracture energy and energy ratio with aging. This reflects that the fracture resistance of asphalt mixtures was significantly influenced by moisture damage, which obviously affected

mixture performance in the field. Further investigations of moisture damaged projects are needed to identify various factors that may have contributed to moisture damage and to fully understand and verify mechanism and effect of moisture damage.

Development of a comprehensive and user-friendly database was continued in this phase to include results of comprehensive material testing, performance data collected and interpretation performed on the data into the existing database. This has resulted in the development of one of the most comprehensive datasets of research quality Superpave data on real-world projects, which will be available for further interpretation or validation of findings obtained in this study.

Recommendations were made for further monitoring efforts on existing Superpave project sections to refine and to enhance the Superpave mix design guidelines and specifications to help assure consistently good long-term performance of Superpave mixtures. The need to further develop healing and aging models to complete material property model and to improve existing pavement performance prediction models was also emphasized.

TABLE OF CONTENTS

page

DISCLAIMER i

SI (MODERN METRIC) CONVERSION FACTORS ii

TECHNICAL REPORT DOCUMENTATION PAGE iii

ACKNOWLEDGMENTS iv

EXECUTIVE SUMMARY v

LIST OF TABLES xiii

LIST OF FIGURES xv

CHAPTERS

1 INTRODUCTION 1

1.1 Background 1
1.2 Objectives 2
1.3 Scope 3
1.4 Research Approach 5

2 EVALUATION OF EXISTING PAVEMENT CONDITION AND FIELD DATA COLLECTION 8

2.1 Review of Existing Database 8
2.2 Evaluation of Pavement Condition Survey (PCS) Data 9
2.2.1 Introduction 9
2.2.2 Rut Depth 10
2.2.3 Crack Rating 15
2.2.4 Roughness Data 17
2.2.5 Closure 20
2.3 Field Investigations 21
2.3.1 Introduction 21
2.3.2 Summary of Field Investigation 23
2.3.3 Closure 28
2.4 Field Data Collection and Evaluation 29
2.4.1 Introduction 29
2.4.2 Sampling (Coring) 29
2.4.3 Transverse Profilograph Measurements (TP) 31
2.4.4 Falling Weight Deflectometer Test (FWD) 34
2.4.5 Crack Evaluation on Field Cores 39
2.4.6 Closure 42

3 BINDER RECOVERY AND BINDER TESTS 43

3.1 Introduction 43
3.2 Binder Recovery 44
3.3 Penetration Test 45
3.4 Viscosity Test 46
3.5 Dynamic Shear Rheometer Test (DSR) 48
3.6 Bending Beam Rheometer Test (BBR) 50
3.7 Multiple Stress Creep Recovery Test (MSCR) 52
3.8 Closure 55

4 IMPLEMENTATION OF MIXTURE TESTS ON FIELD CORES FOR SUPERPAVE MIXTURES IN FLORIDA 56

4.1 Introduction 56
4.2 Test Specimen Preparation 57
4.2.1 Measuring, Cataloguing, and Inspecting 57
4.2.2 Cutting 59
4.2.3 Gage Points Attachment 60
4.3 Test Procedure 61
4.3.1 Resilient Modulus Test 61
4.3.2 Creep Test 62
4.3.3 Tensile Strength Test 64
4.4 Superpave IDT Test Results 66
4.5 Moisture-Damaged Projects 76
4.6 Closure 82

5 EVALUATION OF FIELD MIXTURE PERFORMANCE USING DASR-IC (DOMINANT AGGREGATE SIZE RANGE-INTERSTITIAL COMPONENT) MODEL 83

5.1 Introduction 83
5.2 Characterization of Mixture Gradation (DASR-IC Model) 84
5.2.1 Dominant Aggregate Size Range (DASR) 85
5.2.2 DASR Porosity 86
5.2.3 Interstitial Component (IC) of Mixture Gradation 88
5.2.4 Disruption Factor (DF) 89
5.2.5 Effective Film Thickness (EFT) 91
5.2.5.1 Film Thickness Effect 92
5.2.6 CFA/FFA 93
5.3 Gradation Analysis Results for Superpave Projects 94
5.4 Effect of Gradation Characteristics on Mixture Performance 99
5.4.1 Field Performance: Rutting 99
5.4.2 Field Performance: Cracking 103
5.5 Closure 107

6 IDENTIFICATION OF MATERIAL PROPERTY RELATIONS AND MODEL DEVELOPMENT 108

6.1 Introduction 108
6.2 Material Property Models in the HMA-FM-E Model: A Revisit 109
6.2.1 AC Stiffness Aging Sub-Model 109
6.2.2 Fracture Energy Limit Aging Sub-Model 111
6.3 Identification of Material Property Relations 113
6.4 Development of Material Property Prediction Model 115
6.4.1 Models for Initial Material Properties 117
6.4.1.1 Initial Fracture Energy Relation 117
6.4.1.2 Initial Creep Rate Relation 121
6.4.2 Models for Changes in Material Properties 130
6.4.2.1 AC Stiffness Model 131
6.4.2.2 Fracture Energy Limit Model 132
6.5 Closure 135

7 PERFORMANCE MODEL PREDICTIONS AND EVALUATION FOR SUPERPAVE MIXTURES IN FLORIDA 137

7.1 Introduction 137
7.2 Enhanced HMA Fracture Mechanics Based Model (HMA-FM-E) 138
7.2.1 Introduction 138
7.2.2 Input Module 140
7.2.3 Model Prediction Results 141
7.3 Mechanistic-Empirical Pavement Design Guide (MEPDG) Program 144
7.3.1 Introduction 144
7.3.2 Input Module 146
7.3.3 Model Prediction Results 147
7.3.3.1 Prediction Using the BUC Model 147
7.3.3.2 Prediction Using the TDC Model 150
7.4 Perpetual Pavement Design (PerRoad) Program 153
7.4.1 Introduction 153
7.4.2 Input Module 155
7.4.3 Model Prediction Results 156
7.5 Energy Ratio Based Model (ER Model) 157
7.5.1 Introduction 157
7.5.2 Input Module 159
7.5.3 Model Prediction Results 160
7.6 Performance Model Evaluation 161
7.6.1 Introduction 161
7.6.2 Comparison of Model Features 163
7.6.3 Comparison of Prediction Results 166
7.6.3.1 Comparison of BUC Predictions 166
7.6.3.2 Comparison of TDC Predictions 168
7.7 Closure 177
7.7.1 Bottom-Up Cracking Models 177

7.7.2 Top-Down Cracking Models 178

8 DEVELOPMENT OF DATABASE FOR SUPERPAVE MIXTURES IN FLORIDA180

8.1 Introduction 180
8.2 Database Management and Quality Assurance of Data in Database 180
8.2.1 Upgrade Database 180
8.2.2 Enhance Overall Structure of the Database 181
8.2.2.1 Grouping 184
8.2.2.2 Coring Scenario 187
8.2.3 Design New Forms 189
8.2.4 Facilitating Ease of Use 190
8.2.5 Modify Existing Forms 191
8.2.6 Data Entry 192
8.3 Closure 193

9 CLOSURE 194

9.1 Summary and Findings 194
9.2 Conclusions 199
9.3 Recommendations and Future Works 201

LIST OF REFERENCES 203

APPENDICES

A ANALYSIS PROCEDURE TO DETERMINE THE SOURCE OF RUTTING USING TRANSVERSE PROFILOGRAPH MEASUREMENT 208

A.1 Introduction 208
A.2 Digitalization of Graphs 210
A.3 Verification of Layers Moduli and Prediction of Strain Profile 211
A.3.1 Determination of Layers Moduli 211
A.3.2 BISAR Analysis 215
A.4 Interpretation of Transverse Profile 218
A.5 Closure 227

B SOFTWARE DEVELOPMENT 228

B.1 Program Description 228
B.2 Inputs 228
B.3 Outputs 228
B.4 Detailed Functionality 230
B.4.1 GUI: Data Input 231
B.4.2 GUI: Plot Area 234
B.4.3 GUI: Detailed Profile Information 236
B.4.4 GUI: Project Summary 238
B.5 Data Evaluation with Program 239

LIST OF TABLES

Table page

Table 2-1 Rut depth measurement from the transverse profilograph (TP) 10

Table 2-2 Rut depth measurement from the road surface profilograph (RSP) 11

Table 2-3 Rutting performance for Superpave projects 13

Table 2-4 Crack rating data 15

Table 2-5 Crack initiation time and cracking status for Superpave projects 16

Table 2-6 Cracking performance for Superpave projects 16

Table 2-7 IRI rating scale used by FDOT 18

Table 2-8 RN rating scale used by FDOT 18

Table 2-9 IRI and RN for Superpave projects 19

Table 2-10 Finalized coring plan 22

Table 2-11 Initial mixture testing plan and number of cores per coring location 30

Table 2-12 Layer moduli calculated using BISDEF computer program 38

Table 2-13 Crack evaluation results on the field cores 41

Table 3-1 Asphalt binder used on projects 44

Table 4-1 Mixture testing plan 57

Table 4-2 Mixture information for 11 Superpave projects 67

Table 4-3 Project information for moisture-damaged projects 77

Table 5-1 Average void size based on Bailey method 90

Table 5-2 Mixture information of Superpave projects 94

Table 5-3 Gradation parameters calculated for Superpave projects – Layer A 95

Table 5-4 Gradation parameters calculated for Superpave projects – Layer B 96

Table 7-1 Summary of input data characteristics for the HMA-FM-E model 141

Table 7-2 Predicted top-down cracking performance using HMA-FM-E model 142

Table 7-3 Summary of input data characteristics for the MEPDG 147

Table 7-4 Predicted bottom-up cracking using the MEPDG 148

Table 7-5 Predicted top-down cracking using the MEPDG 151

Table 7-6 New coefficients for the BUC model in the PerRoad program 154

Table 7-7 Summary of input data characteristics for PerRoad 156

Table 7-8 Predicted bottom-up cracking using PerRoad 157

Table 7-9 Summary of input data characteristics for ER model 159

Table 7-10 Predicted top-down cracking using the ER model 161

Table 7-11 Observation-based cracking performance 162

Table 7-12 Qualitative comparison of BUC models 164

Table 7-13 Qualitative comparison of TDC models 165

Table 7-14 Comparison of predicted TDC crack status with observation-based performance 176

Table A-1 Summary of available graphs for digitalization 210

Table A-2 Results of comparison of two approaches for 1st and 2nd round of analysis for Project 1 213

Table A-3 Comparison of BISDEF and Backfaa analysis of Project 2 214

Table A-4 Major source of rutting determined for Superpave projects 225

Table B-1 Comparisons of slope difference determined by excel sheet and new program for Location 6 of Project 1 240

LIST OF FIGURES

Figure page

Figure 1-1 Location map of twelve initial Superpave monitoring projects 4

Figure 1-2 Research approach 7

Figure 2-1 Change in RD/ESALs over time 12

Figure 2-2 Rut depth as a function of ESALs 12

Figure 2-3 Rut depth measurement from TP and RSP for Project 1 and 2 14

Figure 2-4. Determination of observed crack initiation time for Project 1 and 2 17

Figure 2-5 IRI for Superpave projects 19

Figure 2-6 RN for Superpave projects 20

Figure 2-7 Field investigation for Project 2 (I-75 SB, Hamilton County) 23

Figure 2-8 Field investigation for Project 4 (I-10 EB, Duval County 24

Figure 2-9 Field investigation for Project 6 (US-301 SB, Marion County) 25

Figure 2-10 Field investigation for Project 8 (I-10 WB, Leon County) 25

Figure 2-11 Field investigation for Project 9 (SR-121 SB, Alachua County) 26

Figure 2-12 Field investigation for Project 10 (SR-16 EB, Bradford County) 27

Figure 2-13 Field investigation for Project 11 (I-295 SB, Duval County) 27

Figure 2-14 Field investigation for Project 12 (SR-73 SB, Calhoun County) 28

Figure 2-15 Schematic of coring operation for each location 30

Figure 2-16 Coring work for Project 8 (I-10 WB, Leon County) 31

Figure 2-17 Transverse profilograph test for Project 9 (SR-121 SB, Alachua County) ... 32

Figure 2-18 Variation of average rut depth over time for Project 1 and 2 33

Figure 2-19 FWD test for Project 9 (SR-121 SB, Alachua County) 34

Figure 2-20 Schematic of loading configuration, deflection basin, and typical pavement structure 35

Figure 2-21 Analysis procedure of FWD test data 36
Figure 2-22 Change of calculated layer moduli over time for Project 1 39
Figure 2-23 Crack evaluation procedure on field cores..... 40
Figure 2-24 Visual inspection for cores obtained from the moisture-damaged projects.. 42
Figure 3-1 Penetration test results for Superpave projects 45
Figure 3-2 Viscosity test results for Superpave projects 47
Figure 3-3 Change in viscosity with aging for Superpave projects..... 48
Figure 3-4 $G^{*}\cdot\sin\delta$, 10 rad/sec at 25 °C (77 °F) for Superpave projects..... 49
Figure 3-5 S(t), 60 seconds loading time at -12 °C (10.4 °F) for Superpave projects..... 51
Figure 3-6 m-value, 60 seconds loading time at -12 °C (10.4 °F) for Superpave projects51
Figure 3-7 MSCR average recovery at 64 °C (147.2 °F) for Superpave projects 53
Figure 3-8 MSCR nonrecoverable compliance at 64 °C (147.2 °F) for Superpave projects54
Figure 4-1 Cross-section layout of typical core..... 58
Figure 4-2 Measuring, cataloguing, and inspecting work for Project 9 (SR-121 SB, Alachua County)..... 58
Figure 4-3 Cutting machine used in this research..... 59
Figure 4-4 Cut specimens for Superpave IDT test..... 60
Figure 4-5 Gage points attachment..... 60
Figure 4-6 Superpave IDT tests..... 61
Figure 4-7 Power model of creep compliance..... 63
Figure 4-8 Determination of fracture energy and dissipated creep strain energy to failure65
Figure 4-9 Change in resilient modulus over time..... 68
Figure 4-10 Change in creep compliance over time..... 69
Figure 4-11 Change in creep rate over time..... 71
Figure 4-12 Change in tensile strength over time..... 72
Figure 4-13 Change in failure strain over time..... 74

Figure 4-14 Change in fracture energy over time 75
Figure 4-15 Change in air voids over time 78
Figure 4-16 Initial rate of reduction in normalized fracture energy over time 80
Figure 4-17 Initial rate of reduction in normalized energy ratio over time 81
Figure 5-1 DASR and IC for three different types of mixture 86
Figure 5-2 Mixture components for calculation of DASR porosity 87
Figure 5-3 Configurations of different DF values 90
Figure 5-4 Conceptual drawing of film thickness effect 93
Figure 5-5 Determination of CFA/FFA 94
Figure 5-6 Rut Depth/ESALs for Superpave projects 100
Figure 5-7 Rut Depth/ESALs for different groups of DASR porosity 101
Figure 5-8 Rut Depth/ESALs for different groups of disruption factor 102
Figure 5-9 Crack initiation time for Superpave projects 104
Figure 5-10 Crack initiation time for different groups of DASR porosity 105
Figure 5-11 Crack initiation time for different groups of disruption factor 106
Figure 6-1 Schematic plot for AC stiffness at surface vs. age 110
Figure 6-2 Schematic plot for creep rate vs. age 111
Figure 6-3 Schematic plot for normalized change in AC stiffness vs. age 112
Figure 6-4 Schematic plot for FE limit vs. age 113
Figure 6-5 Two types of material property relations 115
Figure 6-6 Flowchart for development of material property models 116
Figure 6-7 Relation between initial fracture energy and DASR porosity 118
Figure 6-8 Relation between initial fracture energy and disruption factor 118
Figure 6-9 Relation between initial fracture energy and effective film thickness 119
Figure 6-10 Predicted vs. measured initial fracture energy 121

Figure 6-11 Relation between initial creep rate and DASR porosity 122

Figure 6-12 Relation between initial creep rate and DF 123

Figure 6-13 Relation between initial creep rate and EFT 123

Figure 6-14 Relation between initial creep rate and CFA/FFA 125

Figure 6-15 Effect of polymer modification on initial creep rate relation 126

Figure 6-16 Relation between initial creep rate and viscosity 127

Figure 6-17 Relation between initial creep rate and effective asphalt content 128

Figure 6-18 Relation between initial creep rate and $G^{*}\cdot\sin\delta$ 128

Figure 6-19 Relation between initial creep rate and MSCR average recovery (0.1 kPa) 129

Figure 6-20 Relation between initial creep rate and MSCR nonrecoverable compliance (0.1 kPa) 129

Figure 6-21 Proposed AC stiffness model 132

Figure 6-22 Proposed FE limit model 135

Figure 7-1 General framework of the HMA-FM-E model 139

Figure 7-2 Predicted crack amount increase over time using HMA-FM-E model 144

Figure 7-3 General flowchart for the cracking models in MEPDG program 145

Figure 7-4 Predicted increase of bottom-up crack amount over time using the MEPDG 150

Figure 7-5 Predicted crack amount increase over time using the MEPDG (TDC model) 153

Figure 7-6 Flowchart of the bottom-up cracking model in PerRoad 155

Figure 7-7 General flowchart of ER model 158

Figure 7-8 Comparison of predicted t_i for BUC using MEPDG and PerRoad 167

Figure 7-9 Comparison of predicted t_i for TDC using MEPDG and HMA-FM-E model 170

Figure 7-10 Comparison of predicted crack amount increase over time using different models 175

Figure 8-1 Example of possible error messages upon opening the database 181

Figure 8-2 Layout of the main interface of the database before the CSPM was awarded 182

Figure 8-3 Layout of the main interface of the database after the CSPM was awarded. 183

Figure 8-4 Layout of the general information module..... 183

Figure 8-5 Flow chart of the Superpave monitoring project database..... 185

Figure 8-6 Example of how information in the database is grouped..... 187

Figure 8-7 Options that isolated data for Round-II (Example of core data for Round II – only the appropriate projects are shown) 188

Figure 8-8 Options that isolated data produced during Continuation of Superpave Projects Monitoring (CSPM) phase only (Example of core data extension: Project 1 – only locations 5 and 15 are shown)..... 189

Figure 8-9 Layout of testing protocol for all the different times of coring..... 190

Figure 8-10 Example of modification that made the database more user-friendly..... 191

Figure 8-11 Completed core data CSPM phase entry form..... 192

Figure 8-12 Summary of field investigation form 193

Figure A-1 Schematic approach of elimination process to determine the source of rutting209

Figure A-2 Graphical representation of comparison of two approaches of first round analysis in determining layer moduli for Project 1 212

Figure A-3 Vertical strain distribution at the surface of the subgrade for Location 6.... 215

Figure A-4 Vertical strain distribution at the surface of the subgrade for Location 12.. 216

Figure A-5 Vertical strain distribution at the surface of the subgrade for Location 18.. 216

Figure A-6 Vertical strain distribution at the surface of the subgrade for Location 24.. 217

Figure A-7 Vertical strain distribution at the surface of the subgrade for Location 30.. 217

Figure A-8 Schematic representation of projecting the distribution of the subgrade strain into the rut..... 218

Figure A-9 Overall difference in slope for Project 1 219

Figure A-10 Overall difference in slope for Project 2 219

Figure A-11 Overall difference in slope for Project 3 220

Figure A-12 Overall difference in slope for Project 4 220

Figure A-13 Overall difference in slope for Project 6 221
Figure A-14 Overall difference in slope for Project 7 221
Figure A-15 Overall difference in slope for Project 9 222
Figure A-16 Overall difference in slope for Project 10 222
Figure A-17 Overall difference in slope for Project 11 223
Figure A-18 Overall difference in slope for Project 12 223
Figure A-19 Average slope difference in Projects 1 to 12 (Except Project 5 and 8)..... 224
Figure B-1 GUI display of computer program 231
Figure B-2 The GUI data input field in the program 233
Figure B-3 GUI plot area 235
Figure B-4 Precision pointer example 235
Figure B-5 Hand tool example..... 236
Figure B-6 Detailed profile information 238
Figure B-7 Project summary 239

CHAPTER 1
INTRODUCTION

1.1 Background

The Superpave mix design system was devised in 1993 under the Strategic Highway Research Program (SHRP). This new system represented a major change regarding how asphalt mixtures are designed and constructed. Current pavement design procedures and models were formed based on the performance of older mixtures designed with the Marshall system. Therefore, it is extremely important to monitor the performance and material characteristics of Superpave project sections as well as to establish a database so that the design procedures and models can be updated. This is also especially important with AASHTO's recent interim adoption of the Mechanistic-Empirical Pavement Design Guide (MEPDG) and several ongoing research projects to refine the models in the interim MEPDG.

The Florida Department of Transportation (FDOT) along with other state agencies has implemented the Superpave system in the years since its debut. Superpave mixtures can be significantly different than mixtures produced in the past under the Marshall system. A lack of basic data and limited information with Florida material in terms of the performance as affected by mixture characteristics, performance-related properties, traffic, and Florida environments has been the main obstacle to assess and improve the Superpave system in Florida. Therefore, the idea of monitoring Superpave projects was conceived and introduced to evaluate construction and performance data to establish appropriate and realistic performance based specifications for this new generation of asphalt mixtures.

The first phase (Phase I) of Superpave monitoring project was conducted from 1999 to 2005. The current research, which is the second phase (Phase II) of Superpave monitoring project conducted from 2008 to 2011, was entitled as "Continuation of Superpave Projects Monitoring." In the first phase of Superpave monitoring projects, an extensive database was developed with regard to design, construction, and field performance for twelve Superpave project sections in Florida. This database is composed of comprehensive material testing and performance data for 30 test locations along five-mile stretches of each project. The database represents one of the most extensive collections of research quality Superpave data on real world projects.

It is important that performance data and changes in material properties on these projects are collected continuously from construction throughout their service life, updated into the existing database, analyzed and provided for use in ongoing national and Florida design model development efforts. This information is also very useful in the establishment of reasonable and effective mixture design guidelines and criteria, performance-related laboratory properties and parameters, identification and evaluation of material property models, and calibration and validation of pavement performance prediction models.

1.2 Objectives

Based on the discussion presented above, the primary objectives of this research are as follows:

- Continue to obtain material properties, structural characteristics, and performance data for twelve Superpave project sections.

- Continue to populate the comprehensive database so that it can support the evaluation of the long-term performance of Superpave mixtures in Florida.
- Evaluate the effects of different factors on observed field performance including the effects of mixture properties and characteristics, pavement structure, traffic, aging, and healing.
- Evaluate the performance of different Superpave mixtures on the basis of gradation characteristics.
- Identify changes in material properties in the field as well as develop material property prediction models.
- Evaluate pavement performance prediction models in terms of their ability to predict observed performance of Superpave mixtures in Florida.
- Provide recommendations for improved pavement performance prediction models, Superpave mixture design guidelines and specifications, and future monitoring efforts for these twelve existing project sections or other sections.

1.3 Scope

The scope of this project was mainly focused on the continuation of study and evaluation of twelve projects designed and placed using Superpave mix design technology in different parts of Florida. These twelve projects, composed of interstate highway and state roads, were selected to cover a broad range of materials, mixture types, contractors, traffic levels and environments. Approximately five-mile sections of travel lane were monitored for each project and coring locations were selected to exclude culverts, bridges, overpasses, and entrance and exit ramps. Figure 1-1 shows the location of the twelve projects. Project 5, which is located on northbound I-

95 in Brevard County (District 5), was excluded from the Phase II study since it had been completely resurfaced before the field data collection were conducted for this research.

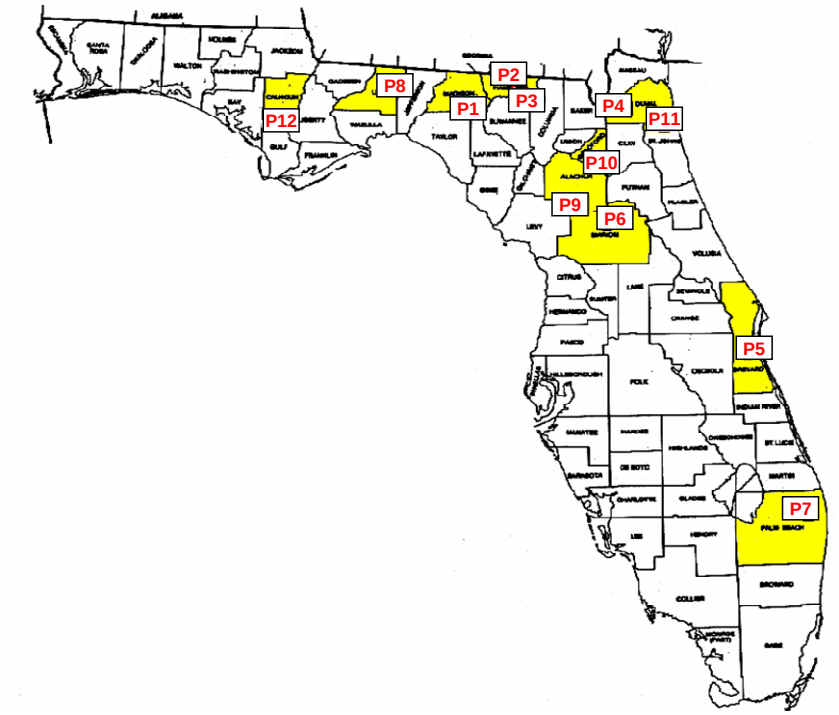

Figure 1-1 Location map of twelve initial Superpave monitoring projects

Asphalt mixture and performance data needed to meet the objectives of this study was obtained from the following sources:

- Data developed during the course of this project: Continuation of Superpave Monitoring Project – Phase II (2008 – 2011)
  - Mixture properties from field cores
  - Binder properties from extracted binders
  - Moduli of unbound materials from back-analysis of falling weight deflectometer (FWD) tests

  - Rut depth measured with transverse profilograph (TP)
- Data available in the existing database, which was developed as a part of the results of Phase I Superpave Monitoring Project (1999 – 2005), including:
  - Design, construction and placement data (e.g., in-place gradations) from the Contractor, the District Construction Office, and the State Materials Office
  - Mixture properties from field cores
  - Binder properties from extracted binders
  - Moduli of unbound materials from back-analysis of falling weight deflectometer (FWD) tests
  - Rut depth measured with transverse profilograph (TP)
- Data available in the pavement condition survey (PCS) database maintained by Florida Department of Transportation
  - Crack rating data
  - Rutting and roughness data obtained from road surface profilograph (RSP)

1.4 Research Approach

This study primarily focused on the continuous monitoring of material properties, structural characteristics, and field performance data for twelve Superpave projects for the establishment of reasonable and effective mixture design guidelines and criteria, performance-related laboratory properties and parameters, identification of material property relation and prediction model evaluation, and for calibration and validation of pavement performance prediction models. The overall approach used to meet all the objectives of this project are stipulated as follows:

- Review the existing database, conduct field data collection and evaluate field data collected over time including rut depth, crack rating, roughness data, and falling weight deflectometer test results.
- Conduct binder recovery and tests to characterize key asphalt binder properties and to identify how these properties change in the field throughout the pavement life.
- Perform mixture tests using Superpave IDT to identify the changes in important mixture properties as a function of age and environment for Superpave project sections.
- Perform gradation analyses to identify performance related gradation parameters and to provide parameters needed for material property relationships.
- Identify material property relationships and develop material property prediction models for initial material properties and for changes in material properties with time.
- Conduct performance model prediction and evaluation using four different existing models, including HMA-FM-E Model, MEPDG, PerRoad, and ER Model.
- Enhance and continue to populate the comprehensive database for use in evaluating the long-term performance of Superpave mixtures in Florida.

The overall framework of the research is represented in Figure 1-2. The main parts of the research are composed of six sub-tasks, including field data collection, laboratory tests, gradation analysis, performance model prediction, material property models and database development.

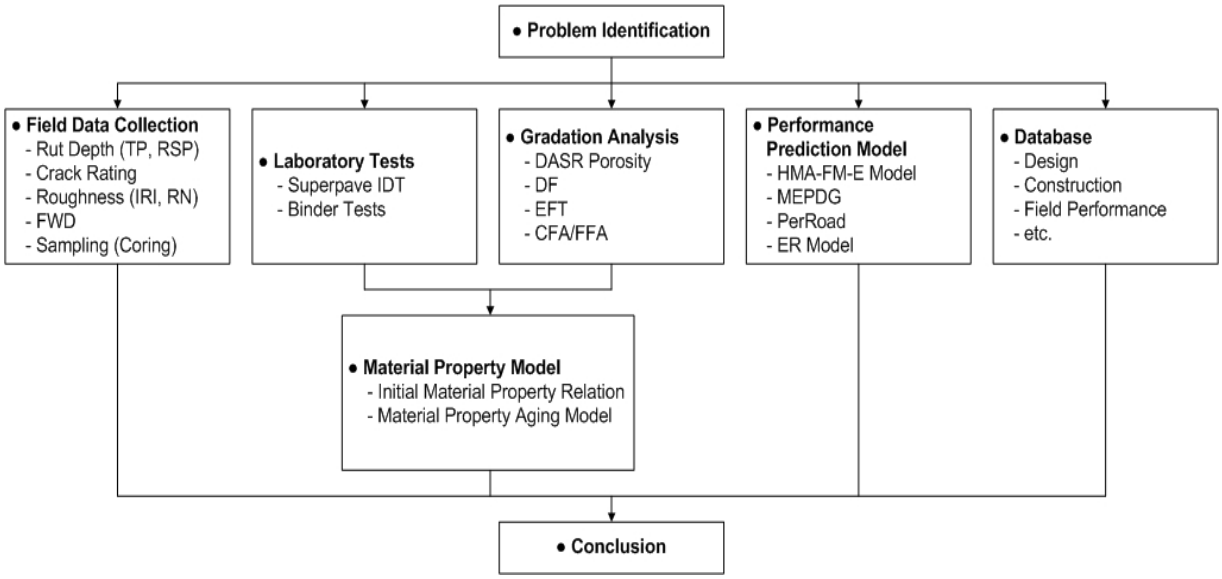

Figure 1-2 Research approach

CHAPTER 2
EVALUATION OF EXISTING PAVEMENT CONDITION AND FIELD DATA COLLECTION

2.1 Review of Existing Database

In Phase I of the Superpave monitoring project, a comprehensive database was developed for FDOT at the University of Florida with regard to design, construction, and field performance of Superpave mixtures. This database contains all data generated and reduced including mixture, construction, core, and field data of twelve Superpave project sections. In addition, all publications including journal papers, progress reports, and final reports were included in the database as well as an inclusive user manual for users to access and modify the database.

Phase II of the project, the results of which are presented in this report, began with a thorough review of the existing database to determine the most appropriate locations for further detailed study and to establish a suitable plan for coring. The database was evaluated and updated to determine the locations associated with the changes in mixture design or other anomalies including construction variability, structural or subgrade differences that were likely to result in performance differences within particular sections.

The most recent pavement condition survey (PCS) information and traffic data provided by FDOT were obtained and included in the database. The coring plan was finalized based on findings from the review of the information summarized, on independent field investigations conducted by the UF research team.

2.2 Evaluation of Pavement Condition Survey (PCS) Data

2.2.1 Introduction

According to the State Highway System Mileage Report introduced by Florida Department of Transportation (FDOT), the Florida State Highway Lane Miles, which is the product of centerline miles and the number of lanes on the road including interstates, turnpikes, and all other roads under the jurisdiction of the state of Florida was approximately 42,432 miles in the 2008 record. To manage this pavement system effectively, FDOT conducts an annual pavement condition survey (PCS). Visual inspections of the pavement surface are performed and ride quality and rut depth measurements are obtained by road surface profiler (RSP). The PCS data provide a detailed summary of pavement condition to identify distressed pavement which requires major maintenance or rehabilitation work. Measured ride quality and structural deficiency are used to make appropriate pavement management decisions.

In this study, three different categories of PCS data, including rut depth, crack rating, and roughness data, were evaluated to identify the pavement condition history of the eleven Superpave project sections. The most recent PCS data for each project were provided by FDOT, and the data obtained were updated into database for evaluation. In addition, a comprehensive review was conducted to identify project sections that had exhibited unique or unusual trends. The most recent rut depth data measured using both transverse profilograph (TP) and road surface profilograph (RSP) were added to the database to assess pavement performance. Similarly the most recent crack rating data, which was considered and used as one of the indicators of cracking performance, was obtained to update the database. In addition, international roughness index (IRI) and ride number (RN) through 2010 were obtained and included in the database. All data were evaluated to conduct a comprehensive evaluation of

performance that would help to guide the selection of section for continued monitoring during Phase II.

2.2.2 Rut Depth

Rut depth is an indicator of the structural and/or mixture performance in asphalt pavement. Most state agencies, including the Florida Department of Transportation (FDOT), use the road surface profilograph (RSP) to measure rut depth. In this study, rut depths were obtained for eleven Superpave project sections from RSP measurements obtained by FDOT as a part of their annual pavement condition survey. In addition, rut depth using transverse profilograph (TP) measurements were obtained by the University of Florida research team during coring operations. Rut depth measurements were obtained on the traffic lane of each project section and Tables 2-1 and 2-2 summarize the rut depth for the eleven Superpave project sections using TP and RSP, respectively.

Table 2-1 Rut depth measurement from the transverse profilograph (TP)

Project (UF) ID	US Route	County	Date Measured	Rut Depth, in		
				RWP	LWP	Average
1	I-10 WB	Madison	Aug, 2009	0.32	0.27	0.30
2	I-75 SB	Hamilton	Sep, 2009	0.69	0.39	0.54
3	I-75 SB	Hamilton	Sep, 2009	0.32	0.22	0.27
4	I-10 EB	Duval	Jul, 2009	0.28	0.28	0.28
6	US-301 SB	Marion	Aug, 2010	0.33	0.27	0.27
7	Turnpike NB	Palm Beach	Aug, 2010	0.18	0.23	0.21
8	I-10 WB	Leon	Dec, 2009	0.18	0.20	0.19
9	SR-121 SB	Alachua	Jun, 2009	0.23	0.18	0.21
10	SR-16 EB	Bradford	Jun, 2009	0.18	0.11	0.14
11	I-295 SB	Duval	Jul, 2009	0.31	0.24	0.28
12	SR-73 SB	Calhoun	Dec, 2009	0.21	0.22	0.21

Note: 1. RWP denotes “Right Wheel Path” and LWP denotes “Left Wheel Path”
2. Average indicates the average value of RWP and LWP

Table 2-2 Rut depth measurement from the road surface profilograph (RSP)

Project (UF) ID	US Route	County	Date Measured	Rut Depth, in
				Average
1	I-10 WB	Madison	Jan, 2010	0.16
2	I-75 SB	Hamilton	Jan, 2010	0.28
3	I-75 SB	Hamilton	Jan, 2010	0.16
4	I-10 EB	Duval	Mar, 2010	0.21
6	US-301 SB	Marion	Aug, 2009	0.18
7	Turnpike NB	Palm Beach	Jan, 2010	0.11
8	I-10 WB	Leon	Jan, 2010	0.09
9	SR-121 SB	Alachua	Apr, 2010	0.20
10	SR-16 EB	Bradford	May, 2009	0.05
11	I-295 SB	Duval	Mar, 2010	0.23
12	SR-73 SB	Calhoun	Mar, 2010	0.02

In general, rut depth measured from the right wheel path is higher than for the left wheel path. Project 2 exhibited the highest average rut depth as measured by the RSP and TP. The high rut depth for Project 2 was verified visually during field investigations. However, for the purpose of data analysis, rut depth per ESALs (RD/ESALs) was used to normalize the effect of differences in traffic volume between different Project sections. Figure 2-1 presents RD/ESALs for different rounds (time periods) of measurements. Rounds I, II, III, and IV correspond to approximately one year after construction, two years after construction, four years after construction, and the measurements obtained in this phase of the project. Hence, the time interval for measurement between Rounds III and IV varies depending on the project sections. Figure 2-2 shows rut depth as a function of ESALs for all Superpave projects. The average rut depth measured by the TP was used.

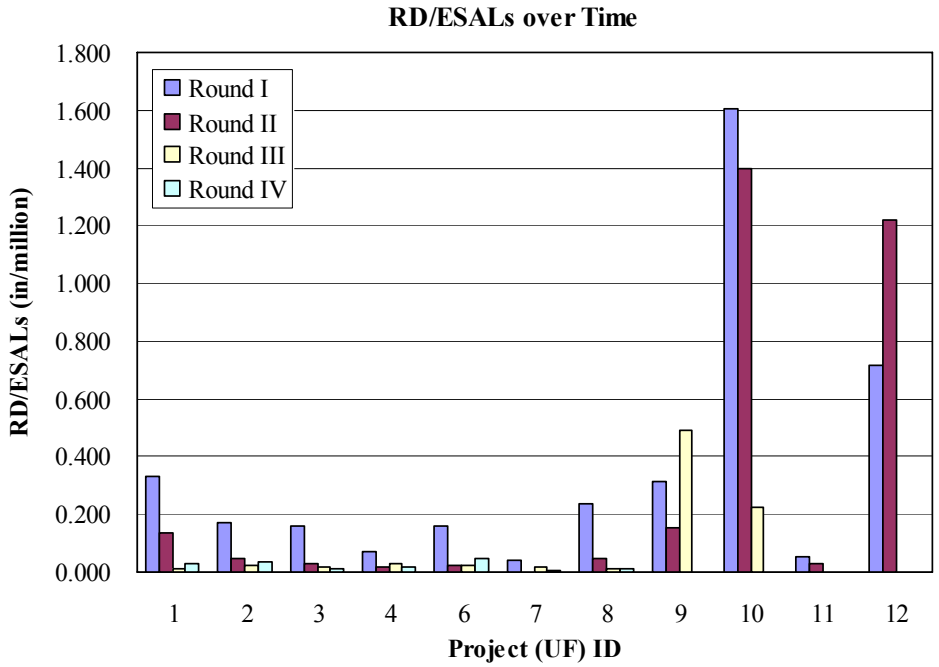

Figure 2-1 Change in RD/ESALs over time

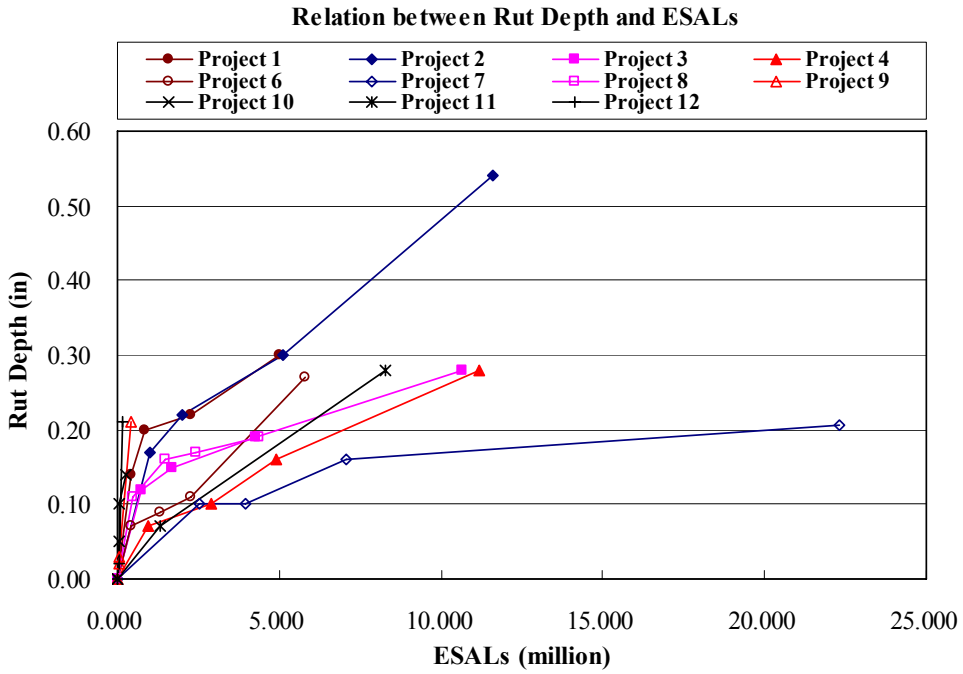

Figure 2-2 Rut depth as a function of ESALs

Figure 2-2 shows that the rate of increase in rut depth decreased significantly with increasing ESALs for Projects 3, 7, and 8. This appears to indicate that these mixtures and/or structures stabilized as they were further compacted by traffic. Projects 1, 2, 4, 6 and 11 also showed some reduction in the rate of increase in rut depth, but maintained a higher increase in rut depth than Project 3, 7, and 8. Finally, Projects 9, 10, and 12 exhibited and maintained a higher rate of increase in rut depth with ESALs. These low volume traffic facilities exhibited the worse rutting performance when normalized for traffic. Table 2-3 tabulates the relative rating in terms of rutting performance as defined by Rut Depth/ESALs.

Table 2-3 Rutting performance for Superpave projects

Category	Worse	Bad	Intermediate	Good	Better
Project (UF) ID	9, 10, 12	2, 6	1, 4, 11	3	7, 8

For most cases, the rut depth measured by the RSP was less than the rut depth measured by the TP. The results show that rut depth measured using the RSP was on average approximately three times less than the rut depth measured using the TP. Mehta et al. (2001) indicated that several issues, including effect of vehicle wander, effect of distance between the positions of the maximum rut depths, and effect of sensor spacing may explain the inaccuracy of rut depth measurements obtained from RSP. Figure 2-3 shows the discrepancy of rut depth measurement between the TP and the RSP for project 1 and 2.

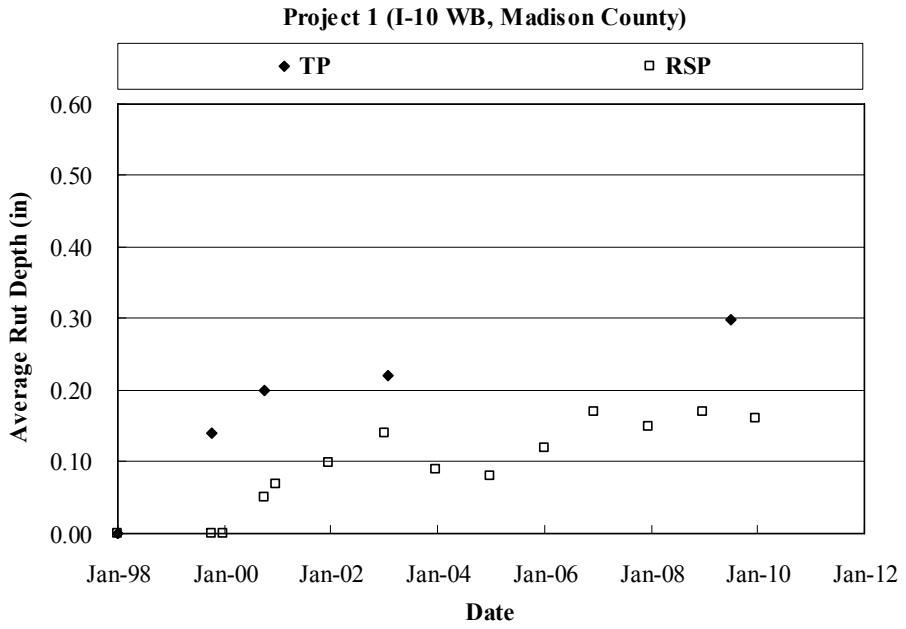

(a) Project 1

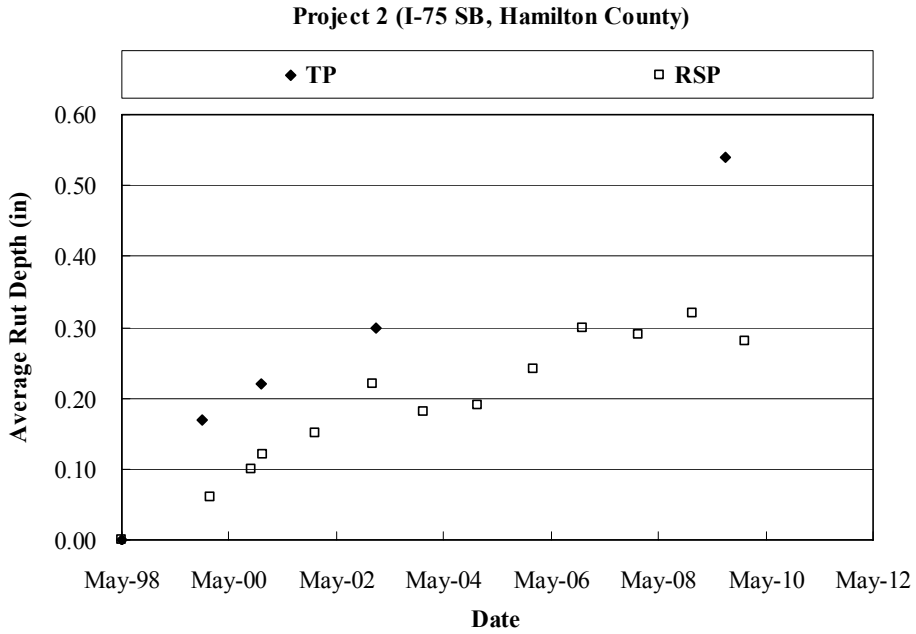

(b) Project 2

Figure 2-3 Rut depth measurement from TP and RSP for Project 1 and 2

2.2.3 Crack Rating

Crack rating has been widely used to evaluate cracking performance of asphalt pavement based on pavement condition survey (PCS) data. FDOT Flexible Pavement Condition Survey Handbook (June, 2009) designates the details of the crack rating system. In this method, cracking performance can be assessed as percent confined to wheel paths (CW) and percent outside of wheel paths (CO). A crack rating is a combination of CW and CO derived from established distress rating scales, and reported on a 0 - 10 point scale to the nearest integer value with 10 as the best condition. Crack type is reported as C = combination, B = block, and A = alligator. Table 2-4 represents the crack rating data provided by FDOT from construction through 2009 for the eleven Superpave project sections.

Table 2-4 Crack rating data

Project	Crack Rating											
(UF) ID	1998	1999	2000	2001	2002	2003	2004	2005	2006	2007	2008	2009
1	N/A	N/A	10.0	10.0	10.0	10.0	10.0	9.0	9.0	9.0	9.0	9.0
2	N/A	N/A	10.0	10.0	10.0	10.0	9.5	9.0	8.0	8.0	7.5	6.5
3	N/A	N/A	10.0	10.0	10.0	10.0	9.0	8.0	8.0	7.5	7.5	7.5
4	N/A	N/A	10.0	9.5	9.5	9.5	9.5	9.5	9.5	9.5	9.5	9.0
6	N/A	10.0	10.0	10.0	9.0	9.0	9.0	9.0	9.0	9.0	7.0	6.5
7	N/A	N/A	10.0	10.0	10.0	10.0	10.0	10.0	9.5	9.5	9.5	9.0
8	N/A	N/A	N/A	10.0	10.0	10.0	10.0	10.0	9.5	9.5	7.0	7.0
9	N/A	N/A	N/A	N/A	N/A	N/A	N/A	10.0	10.0	10.0	10.0	10.0
10	N/A	N/A	N/A	N/A	N/A	10.0	10.0	10.0	10.0	10.0	10.0	9.0
11	N/A	N/A	N/A	N/A	N/A	N/A	10.0	10.0	10.0	10.0	9.0	9.0
12	N/A	N/A	N/A	N/A	N/A	N/A	N/A	10.0	10.0	10.0	10.0	10.0

Note: 1. 10.0 Good, essentially no cracking / 0.0 Poor, high amount of cracking
2. FDOT classifies Crack Rating of < 6.5 as deficient

This information was specifically used to estimate the crack initiation time, which was required for calibration and validation of the top-down cracking performance prediction model described in Chapter 7. The crack initiation time for each project section was determined by

research team using a comprehensive approach based on the information obtained from comprehensive field investigations conducted by the UF research team and the crack rating history data from the pavement condition survey (PCS) performed by FDOT. Table 2-5 shows the crack initiation time and cracking status determined based on PCS data and independent field investigation by the UF research team for the Superpave project sections. Table 2-6 tabulates the relative rating of cracking performance for Superpave projects, and Figure 2-4 indicates the deterministic procedure used to estimate crack initiation time for Project 1 and 2.

Table 2-5 Crack initiation time and cracking status for Superpave projects

Project (UF ID)	Age (year)	PCS-based		Observed	Decision	
		Status	t_i (year)	Status	Status	t_i (year)
1	11	U	16 (P)	U	U	16 (P)
2	11	C	10	C	C	10
3	11	C*	9	U	C	9
4	11	U	28 (P)	C*	C	< 11
6	11	C	11	C	C	11
7	11	U	18 (P)	U	U	18 (P)
8	9	C	9	C	C	9
9	7	U	> 7	C*	C	< 7
10	7	U	10 (P)	C*	C	< 7
11	6	U	9 (P)	U	U	9 (P)
12	6	U	> 6 (P)	C*	C	< 6

Note: 1. U denotes “Uncracked” and C denotes “Cracked”
2. P denotes the value determined based on extrapolation
3. * denotes the final decision when an inconsistency occurred between our observation at coring time and the PCS data

Table 2-6 Cracking performance for Superpave projects

Category	Worse	Bad	Intermediate	Good	Better
Project (UF) ID	9, 10, 12	2, 4, 6	3, 8	11	1, 7

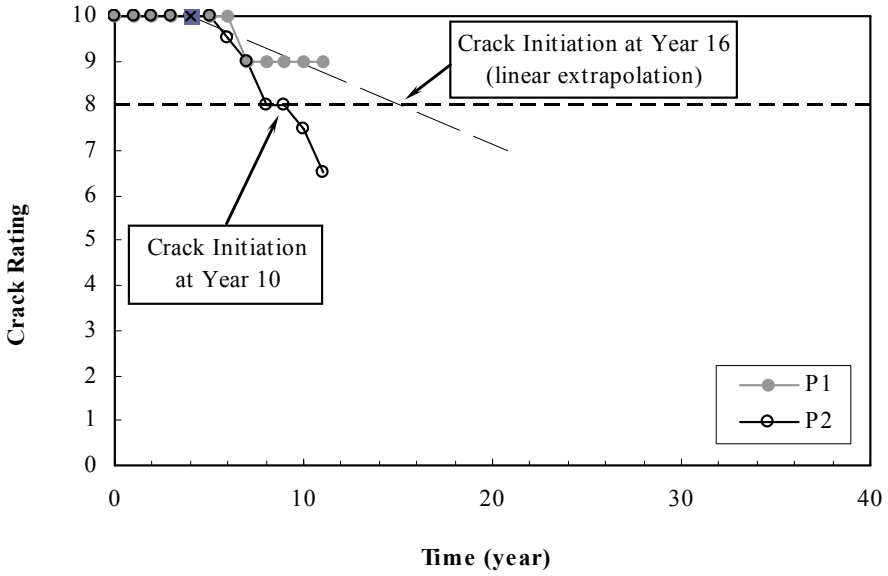

Figure 2-4. Determination of observed crack initiation time for Project 1 and 2

2.2.4 Roughness Data

Pavement roughness is one of the primary indicators of pavement performance. Most highway agencies, including Florida Department of Transportation (FDOT), have measured pavement roughness in units of international roughness index (IRI) and ride number (RN) that indicate the ride quality for flexible pavement.

IRI, which is the cumulative vertical movement of the wheel divided by the distance traveled, has been utilized by state agencies to evaluate pavement roughness. The evaluation of IRI is a mathematical process of the longitudinal pavement profile produced by the road surface profilograph (RSP). IRI is reported in units of inches per mile (in/mi) where the rating scale goes from 0 representing no roughness to infinity. Standard practice for computing IRI of roads from longitudinal profile measurements is designated and reported in ASTM E 1926 – 08. Table 2-7 shows the IRI rating scale used by FDOT.

Table 2-7 IRI rating scale used by FDOT

Rating Category	IRI (inches/mile)
Excellent	0 - 30
Good	30 - 75
Fair	75 - 135
Poor	135 - 200
Unacceptable	> 200

RN is also based on a mathematical calculation based on longitudinal profile measurements. RN is used to estimate the subjective ride quality and it is closely related to present serviceability index (PSI). RN is usually used by the FDOT's pavement condition survey to determine where pavement rehabilitation is needed. Rating scale of RN goes from 0 to 5 where a pavement with RN of 5 is considered as a perfect ride quality road. Standard practice for computing RN of roads from longitudinal profile measurements is designated and reported in ASTM E 1489 – 08. Table 2-8 represents typical rating scale of RN used in FDOT.

Table 2-8 RN rating scale used by FDOT

Rating Category	RN
Perfect	5.0
Good	4.0 - 5.0
Rehabilitation Needed	< 3.2

The international roughness index (IRI) and ride number (RN) through 2010 for the Superpave project sections were measured by FDOT as part of their annual pavement condition survey (PCS). Table 2-9 summarizes the latest measurement of IRI and RN for the eleven Superpave project sections. All data were obtained from the traffic lane of each project section which is consistent with other field data collected including coring, rut depth measurement, and FWD testing.

Table 2-9 IRI and RN for Superpave projects

Project (UF) ID	US Route	County	Date Measured	IRI (in/mile)	RN (in/mile)
1	I-10 WB	Madison	Jan, 2010	45	4.37
2	I-75 SB	Hamilton	Jan, 2010	59	4.05
3	I-75 SB	Hamilton	Jan, 2010	36	4.40
4	I-10 EB	Duval	Mar, 2010	50	4.22
6	US-301 SB	Marion	Aug, 2009	57	3.86
7	Turnpike NB	Palm Beach	Jan, 2010	54	4.24
8	I-10 WB	Leon	Jan, 2010	48	4.01
9	SR-121 SB	Alachua	Apr, 2010	52	4.11
10	SR-16 EB	Bradford	May, 2009	70	4.02
11	I-295 SB	Duval	Mar, 2010	53	3.88
12	SR-73 SB	Calhoun	Mar, 2010	62	4.10

Figure 2-5 and 2-6 represent the current value of IRI and RN for Superpave projects, respectively.

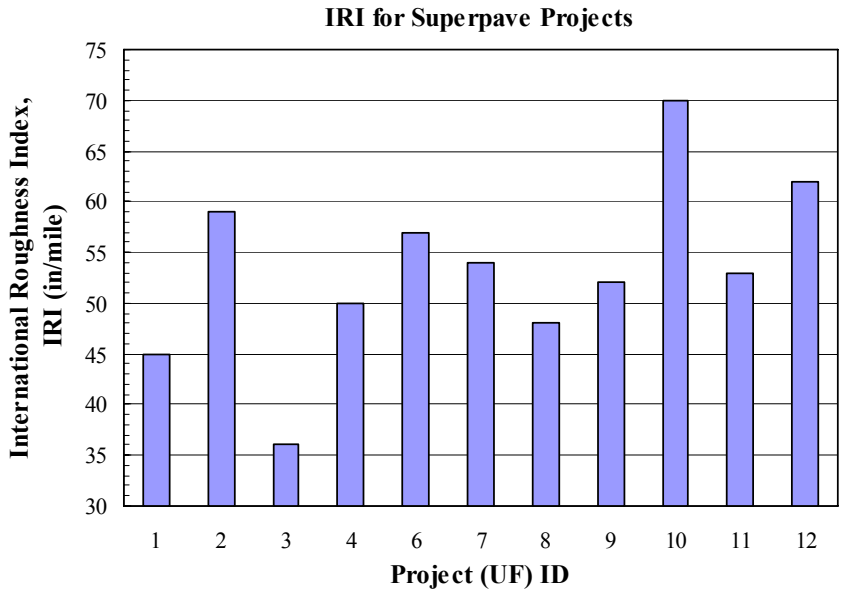

Figure 2-5 IRI for Superpave projects

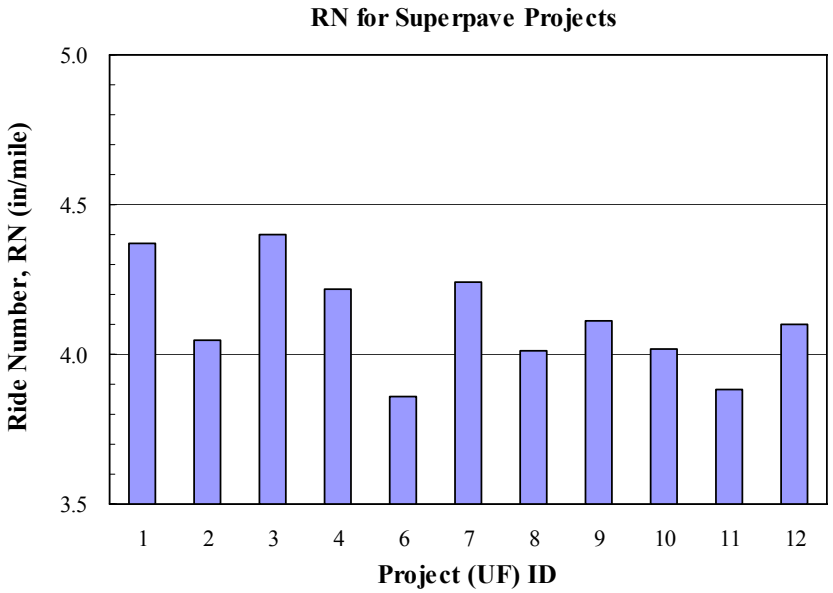

Figure 2-6 RN for Superpave projects

IRI for all Superpave project sections varied between 30 and 75 which falls within the "Good" rating category according to IRI rating scale used by FDOT. Specifically, Project 1 and 3 exhibited the lowest IRI values (best), while Project 2, 6, 10, and 12 exhibited the highest values (worst). All RN values were greater than 3.2 which make them acceptable based on FDOT's rating scale. Similarly with IRI, Project 1 and 3 indicate comparatively high RN values (best), while Project 2, 6, and 11 exhibited lower value of RN (worst).

2.2.5 Closure

The latest pavement condition survey (PCS) data for the eleven Superpave project sections was obtained and entered into the database, and used to evaluate the existing pavement condition. A thorough review of historical information for the PCS data was conducted to identify sections that exhibited any anomalous performance. A relative evaluation of pavement

condition in terms of structural deficiency and ride quality was performed for the Superpave Projects.

In terms of both rutting and cracking, Project 7 has exhibited the best performance. Project 1, 3, 8 and 11 have exhibited intermediate-good performance. Projects 2 and 6 have exhibited the intermediate-bad performance, while Project 9, 10 and 12 were the worst performing sections, even though these were among the youngest sections. The relatively poor performance of these latter sections appears to be related to moisture damage. More detailed analysis and results regarding mixture performance, particularly as related to the apparent moisture damage, will be introduced in the latter part of the report.

The coring plan, including the most appropriate coring location and number of cores required for purposes of this project, was finalized based on the findings from the review of the PCS data introduced. Results of individual field investigations are presented in the following section.

2.3 Field Investigations

2.3.1 Introduction

An independent visual inspection for the eleven Superpave project sections was conducted by the University of Florida research team for the purpose of:

- Check and identify the previous coring spots for the convenience of this phase coring operation.
- Obtain information regarding pavement condition by direct visual inspection to identify specific distress patterns in the field.
- Identify and evaluate any unusual conditions in the vicinity of each project section that may have affected pavement performance.

- Identify coring locations and the need for additional coring locations not evaluated in previous phases.

An intensive review of data gathered during field investigations was conducted to identify the most appropriate coring locations for purposes of the project. A line diagram of each project section was completed, which included information regarding changes in mixture type, any unusual features of the project sections, and performance difference along the entire project. The coring plan was finalized according to the findings from the review of summarized information in the line diagram, the review of existing database, and the evaluation of pavement condition survey (PCS) data. Table 2-10 shows the finalized coring plan with some detailed information for each of the Superpave monitoring projects.

Table 2-10 Finalized coring plan

Project (UF) ID	District	Coring Location	Remark
1	2	L5, L15	- L25: No performance difference
2	2	L5, L15, L25	
3	2	L5, L25	- L15: No performance difference - Consider the mix design change
4	2	L5, L15, L25, L18	- L18: Different performance (Good)
6	5	L5, L15, L25	
7	Turnpike	L5, L15	- L25: No performance difference
8	3	L15, L25, L22	- L5: No performance difference - L22: Different performance (Longitudinal wheel path crack)
9	2	L5, L15, L25	
10	2	L5, L15, L25	
11	2	L15, L25	- L5: No performance difference
12	3	L5, L15, L25, L10	- L10: Different performance (Good)

Note: L = Location

2.3.2 Summary of Field Investigation

Detailed descriptions of field investigation results for each project section are included in this sub-chapter. Overall performance and particular observations by visual inspection conducted in the field are included.

Project 1 generally exhibited good pavement condition throughout the entire project. A slight grooving was observed on the right side of traffic lane near the shoulder throughout this project.

Project 2 exhibited relatively bad pavement condition along the entire project. The surface course looked very coarse and rough. Longitudinal cracks were observed on the both right and left wheel paths throughout the entire project. Poor rutting performance was also evident throughout the project. The typical condition of Project 2 is shown in Figure 2-7.

Figure 2-7 Field investigation for Project 2 (I-75 SB, Hamilton County)

Project 3 exhibited good overall pavement condition throughout the entire project. A slight grooving, similar to that observed in Project 1, was observed on the right side of traffic lane near the shoulder throughout the length of this project.

Project 4 exhibited relatively poor pavement condition throughout the entire project. A lot of surface distresses were observed on the friction course. Friction course appeared to be segregated, very coarse graded and rough. Relatively severe longitudinal wheel path cracks also observed right before the Location 15, where evidence of pumping was even some soil particles start coming up due to pumping process. Figure 2-8 illustrates the longitudinal cracks typically observed throughout Project 4.

Figure 2-8 Field investigation for Project 4 (I-10 EB, Duval County)

Project 6 exhibited relatively poor pavement condition throughout the entire project. Surface course appeared very coarse and rough, and a lot of pop-out of surface material was observed. Both longitudinal and transverse cracks were observed and significant transverse cracking was observed in the passing lane. Figure 2-9 shows typical cracking observed on Project 6.

Figure 2-9 Field investigation for Project 6 (US-301 SB, Marion County)

Project 7 exhibited good overall pavement condition along the entire project. No cracks and good rutting performance were visually observed for this project.

Project 8 generally exhibited good pavement condition over the entire project. Slight grooving was observed on the right side of traffic lane near the shoulder throughout this project. Longitudinal wheel path cracks were observed in the traffic lane between the Location 22 and 24. Figure 2-10 illustrates the longitudinal cracks observed at Location 22 of Project 8.

Figure 2-10 Field investigation for Project 8 (I-10 WB, Leon County)

Project 9 exhibited generally good surface condition. However, some longitudinal wheel path cracks were found throughout the entire project. Evidence of moisture damage was identified for Project 9 through Project 12 during the inspection process of cores obtained. Figure 2-11 illustrates typical longitudinal wheel path cracking observed in Project 9.

Figure 2-11 Field investigation for Project 9 (SR-121 SB, Alachua County)

Similar to Project 9, Project 10 also exhibited good overall surface condition. No cracking or rutting was observed between Location 1 and Location 13. However, both longitudinal and transverse cracks were observed from Location 14 through the end of the project. Figure 2-12 show the cracks typically observed in these latter sections of Project 10.

Figure 2-12 Field investigation for Project 10 (SR-16 EB, Bradford County)

Project 11 generally exhibited good pavement condition throughout the entire project. However, some raveling and potholes were observed near the starting point of this project. Figure 2-13 show some surface distresses observed at the start of Project 11.

Figure 2-13 Field investigation for Project 11 (I-295 SB, Duval County)

Project 12 exhibited the transverse cracks at consistent intervals throughout the entire project. Some longitudinal cracks were also observed throughout this project. Figure 2-14 illustrates typical transverse cracks observed in Project 12.

Figure 2-14 Field investigation for Project 12 (SR-73 SB, Calhoun County)

2.3.3 Closure

An individual visual inspection for each Superpave project sections was conducted by the University of Florida research team. The relative evaluation of pavement condition was finalized based on the review of the PCS data combined with the independent field investigation. In addition, this information provided a great opportunity to identify the particular locations associated with unique trends or any anomalies that were likely to result in performance differences within a specific section. The data and observations were used to identify the final coring locations that were the most appropriate for the purposes of this study.

2.4 Field Data Collection and Evaluation

2.4.1 Introduction

One of the primary objectives of this project was to continue to obtain material properties, structural characteristics and performance data for the Superpave project sections, which constitute the extensive field data collection of research quality Superpave data on real world projects. The field data collection plan which is composed of sampling (coring), transverse profilograph test (TP), and falling weight deflectometer (FWD) was discussed and finalized based on the findings from review of the existing database, the evaluation of pavement condition survey (PCS) data, and independent field investigation by the UF research team. Specific plans and descriptions for coring, TP and FWD tests are presented in the following sections.

2.4.2 Sampling (Coring)

The coring locations and the number of cores per location were finalized based on the findings from the review of existing database, PCS data, and individual field inspection. Two to four locations per project were cored. Location 5, 15, and 25 were cored in each project because large quantities of original materials and plant mixture were sampled, tested, and stored during original construction at these three locations. In addition, coring locations associated with the important changes in mixture design, pavement structure, or performance differences within a particular project were also selected for coring.

Based on the proposed mixture testing plan, a minimum of 33 cores, including 18 cores for mixture property and composite specimen tension tests, 3 cores for binder recovery and testing, 3 supplementary cores for healing test and 6 extra cores were obtained from each coring location of interest. Therefore, at least 1089 cores were obtained for the eleven projects. Table 2-11 shows the proposed mixture testing plan and number of cores obtained per location.

Table 2-11 Initial mixture testing plan and number of cores per coring location

	Testing Plan	
Mixture Test	Superpave IDT for HMA at 10 ˚C and 20 ˚C	6
	Composite Specimen Tension Test at 10 ˚C and 20 ˚C	12
Additional Cores	Healing Test	3
	Binder Recovery and Binder Tests	6
	Extra Cores	6
Total Number of Cores Required	Total Number of Cores per Coring Location	33

Thirty wheel path (WP) cores and three between wheel path (BWP) cores were obtained from the traffic lane of each coring location. In addition, five to seven cores were acquired for the purpose of crack evaluation, including the determination of crack depth and the features of crack growth in the field. Figure 2-15 is a schematic of coring operation for each location, while Figure 2-16 shows the coring work for Project 8.

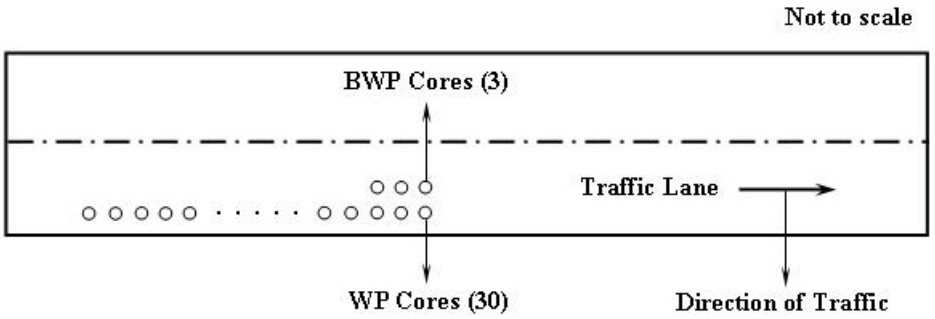

Figure 2-15 Schematic of coring operation for each location

Figure 2-16 Coring work for Project 8 (I-10 WB, Leon County)

2.4.3 Transverse Profilograph Measurements (TP)

Transverse profilograph is one of the most accurate devices to measure rut depth, especially for research purposes. Transverse profilograph is a relatively simple to operate apparatus that produces a chart displaying the cross section profile, from which wheel path ruts, imperfections and superelevations can be determined. A 8.5- by 14-inch chart records vertical deviations at full scale as sensed by a 3-inch-diameter wheel. Horizontal dimensions are recorded at 1 in = 1 ft scale along 13 ft length. A 14-ft steel box beam straightedge fitted with convenient handles, bubble level and leveling screws is used to carry the measuring wheel.

A transverse profile, which is a plot of the elevation across the width of the road, is developed from the transverse profilograph. The transverse profile provides the shape, the depth, and the lateral location of longitudinal pavement deformations. The beam was leveled to provide a horizontal datum, and a linear vertical displacement transducer was connected to a wheel below the beam. As the wheel was moved along the surface of pavement, the transducer was moved relative to the beam and the vertical displacement of the wheel was recorded on the paper.

In this research, transverse profilograph measurement was obtained for the eleven Superpave projects to determine the rut depth to evaluate the rut profile and the change in rut depth over time. In addition, further analysis was conducted to identify the source of rutting for each project, and rutting analysis software was developed to create a user-friendly option to interpret the data collected for a transverse profile. All details in terms of the analysis procedure and software development were included in Appendix A and B, respectively. Figure 2-17 illustrates the transverse profilograph test for project 9, and Figure 2-18 shows the variation of average rut depth over time along the length of the project section from the transverse profilograph for Projects 1 and 2.

Figure 2-17 Transverse profilograph test for Project 9 (SR-121 SB, Alachua County)

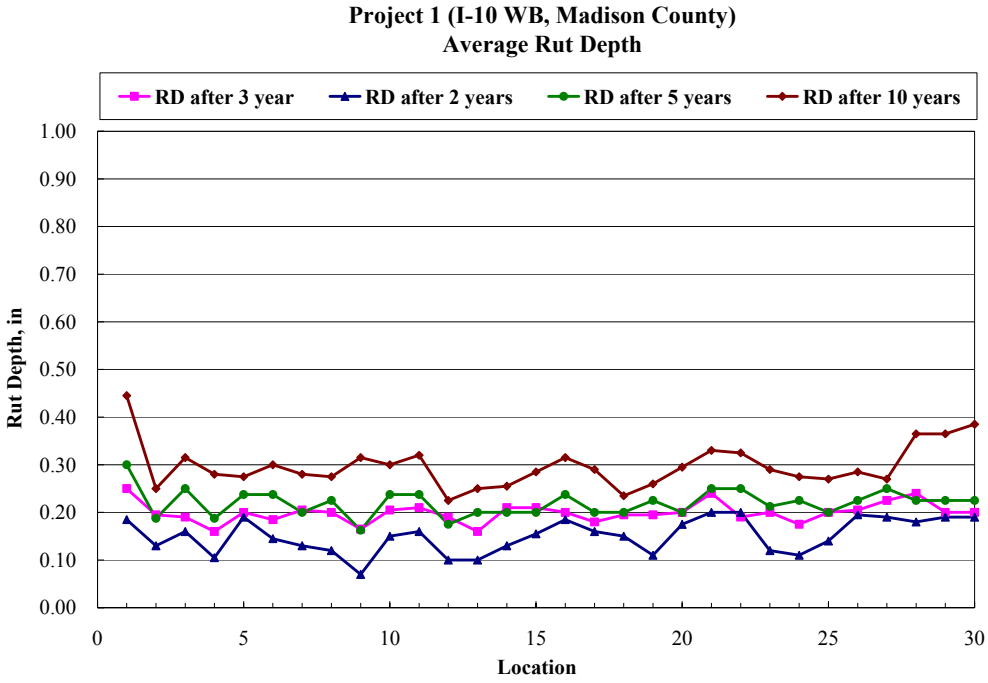

(a) Project 1

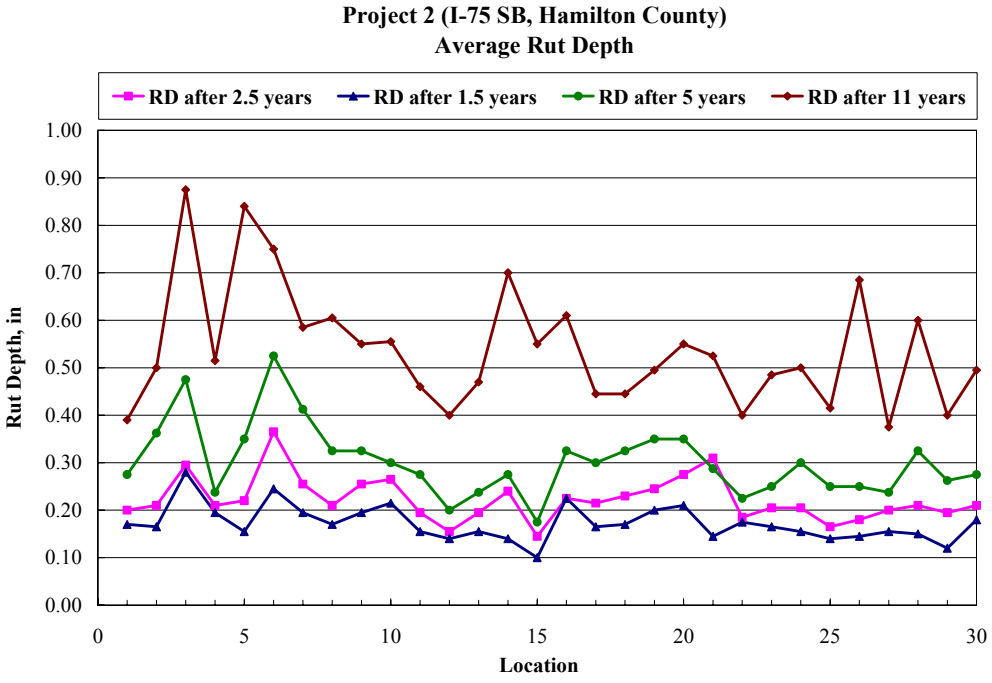

(b) Project 2

Figure 2-18 Variation of average rut depth over time for Project 1 and 2

2.4.4 Falling Weight Deflectometer Test (FWD)

The falling weight deflectometer test (FWD) which is a representative non-destructive testing device operating on the impulse loading principle has been widely used in pavement engineering to evaluate pavement structural condition. The FWD is a device capable of applying dynamic loads to the pavement surface, similar in magnitude and duration to a single heavy moving wheel load. The response of the pavement system to impulse loading is normally measured in terms of vertical deformation or deflection with a set of seven velocity transducers (geophones) placed at different radial distances from the center of the loading plate.

The FWD test was conducted by FDOT for all 30 locations of each project section. The data obtained was used to assess the structural condition and to determine the modulus of pavement layers for analysis. Figure 2-19 shows the FWD test being performed on project 9.

Figure 2-19 FWD test for Project 9 (SR-121 SB, Alachua County)

The test was performed twice at each location in the middle of the traffic lane, immediately after the previous coring location. The second data set was used for analysis. A 3000- to 4000-lb seating load and 9000-lb test load was used. Surface temperature and air

temperature were recorded. Seven deflection measurements were recorded at distances of 0 in, 8 in, 12 in, 18 in, 24 in, 36 in and 60 in from the center of the load. These deflections were designated as D_1, D_2, D_3, D_4, D_5, D_6, and D_7, respectively. Figure 2-20 represents the schematic of loading configuration, deflection basin and typical pavement structure.

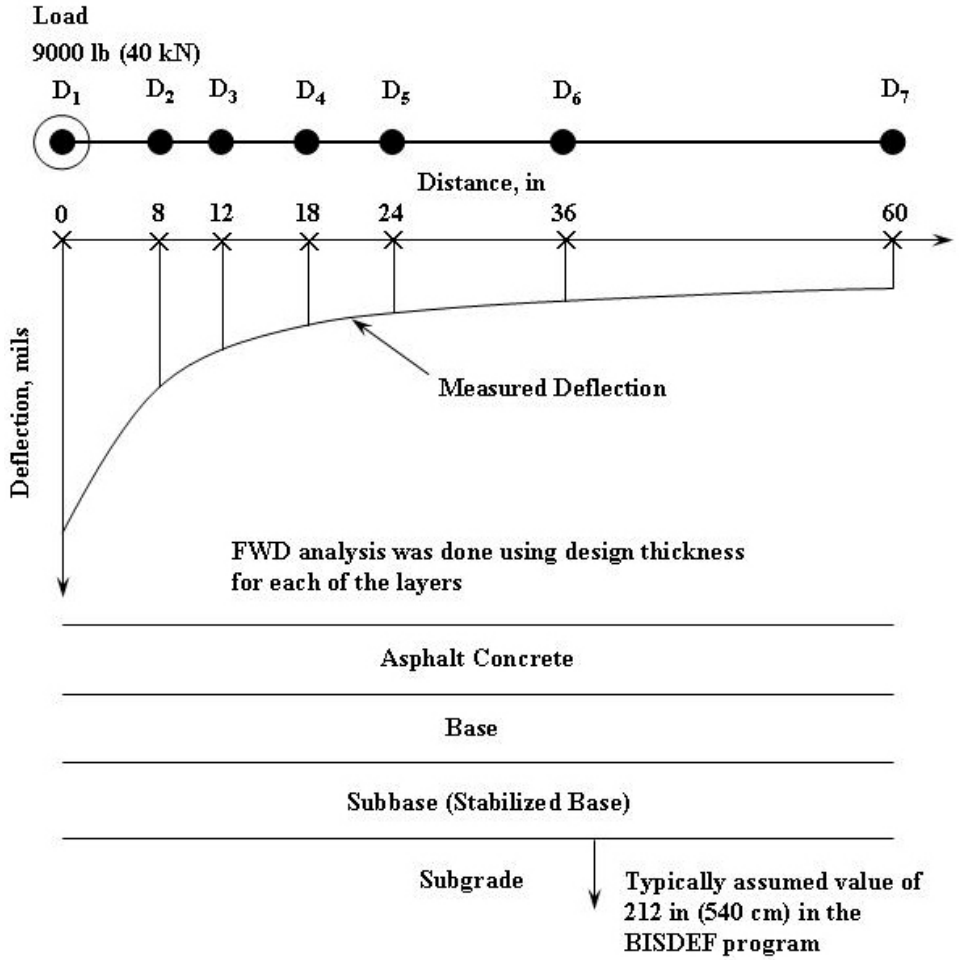

Figure 2-20 Schematic of loading configuration, deflection basin, and typical pavement structure

FWD test data from all 30 locations of each project section were analyzed based on the method suggested by Mehta and Roque (2003). The BISDEF computer program was used for backcalculation to calculate the layer modulus from the deflection basin measured by the FWD

test. Figure 2-21 represents the analysis procedure and interpretation of the FWD data used in this research.

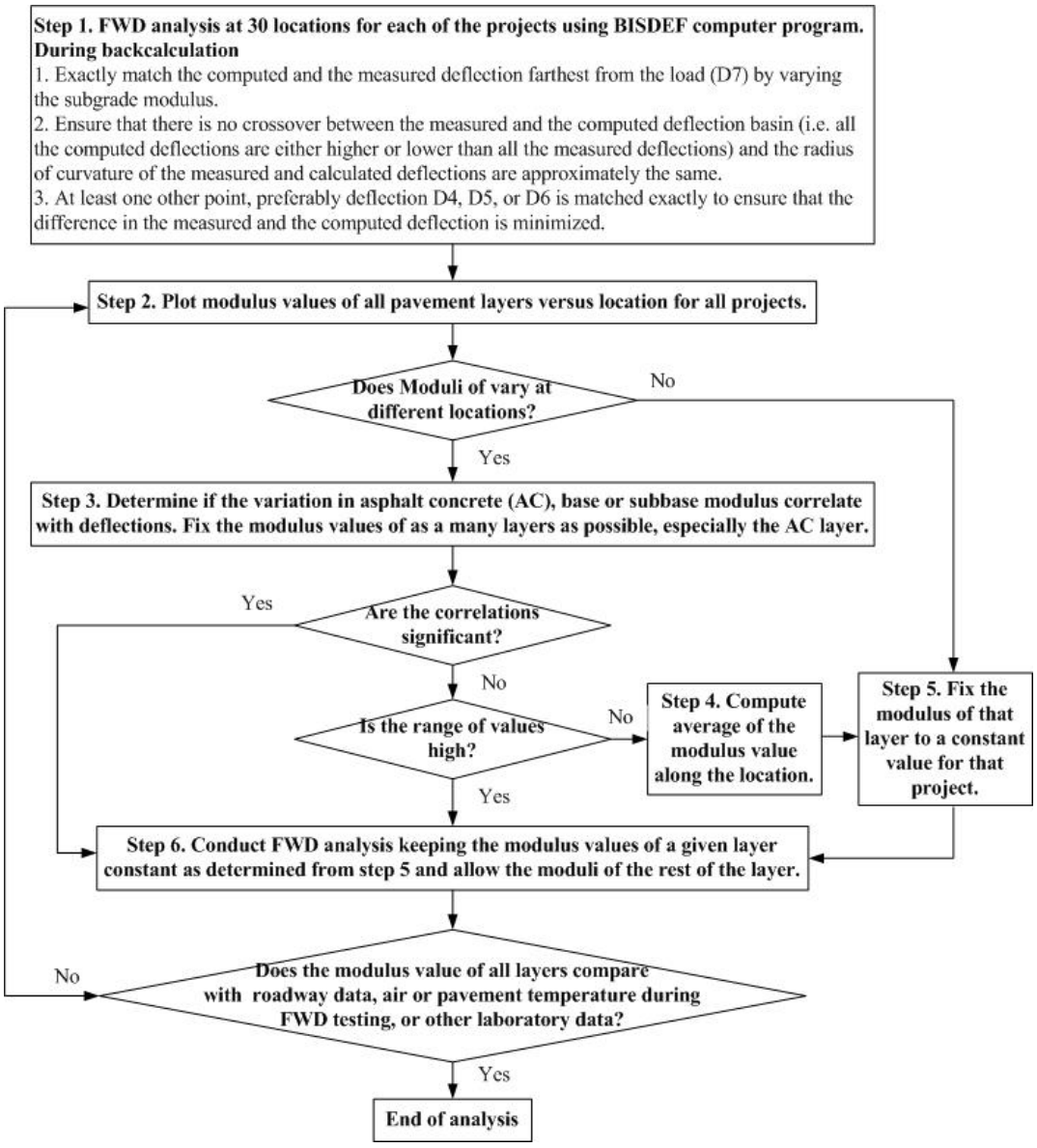

Figure 2-21 Analysis procedure of FWD test data

For each project, FWD tests were conducted during the same time of day with similar temperature conditions, in an area away from cracks or any visible damage. Therefore, the

asphalt concrete modulus was held constant along the project sections as the average value of all thirty locations obtained during the first iteration of the analysis procedure.

In most cases, it was observed that a high base modulus was accompanied with a low subbase modulus and vice-versa. From this tendency, it was determined that neither the base nor the subbase layers independently affected the deflection basin. Thus, they were combined and considered as one layer in the analysis. The details about the procedure for three steps of iteration to get the final modulus values used in this research are as follows.

- First Iteration
  - During the first iteration, backcalculation was done by using four layer system including asphalt concrete, base, subbase and subgrade.
- Second Iteration
  - During the second iteration, the asphalt concrete modulus was kept constant value using the average value of all thirty locations obtained during the first iteration.
  - Backcalculation was conducted by using four layer system including asphalt concrete, base, subbase and subgrade.
- Third Iteration
  - During the third iteration, the asphalt concrete modulus was kept constant value using the average value of all thirty locations obtained during the first iteration.
  - Base and subbase layer were combined and considered as one layer in the analysis.
  - Backcalculation was conducted by using three layer system including asphalt concrete, base/subbase and subgrade.

Table 2-12 summarizes the average calculated layer moduli for the eleven Superpave projects. Figure 2-22 shows the change of calculated layer moduli over time in terms of asphalt concrete, base/subbase, and subgrade for Project 1. It is noted that the asphalt moduli presented in Table 2-12 and Figure 2-22 (a) were not normalized to a standard temperature. Unbound layer moduli obtained from backcalculation were used as material inputs for performance model predictions described in Chapter 7.

Table 2-12 Layer moduli calculated using BISDEF computer program

Project (UF) ID	US Route	County	Date Measured	Layer Modulus, ksi		
				Asphalt Concrete	Base/ Subbase	Subgrade
1	I-10 WB	Madison	Jul, 2009	250	44.1	45.0
2	I-75 SB	Hamilton	Jun, 2009	350	74.9	35.6
3	I-75 SB	Hamilton	Jun, 2009	500	66.2	39.6
4	I-10 EB	Duval	Jun, 2009	390	50.7	30.3
6	US-301 SB	Marion	Jul, 2009	250	60.3	36.7
7	Turnpike NB	Palm Beach	Jul, 2009	480	67.7	31.0
8	I-10 WB	Leon	Jul, 2009	N/A	N/A	N/A
9	SR-121 SB	Alachua	May, 2009	350	51.0	23.1
10	SR-16 EB	Bradford	Jul, 2009	450	29.3	32.3
11	I-295 SB	Duval	Jun, 2009	200	65.9	31.9
12	SR-73 SB	Calhoun	Jul, 2009	270	47.8	21.6

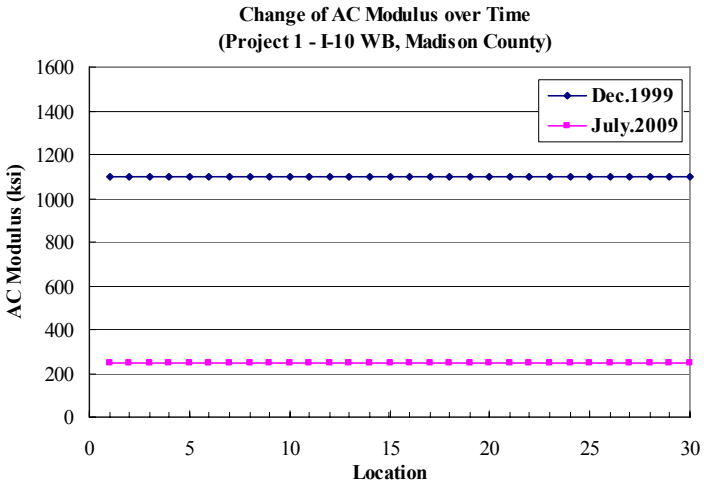

(a) AC modulus

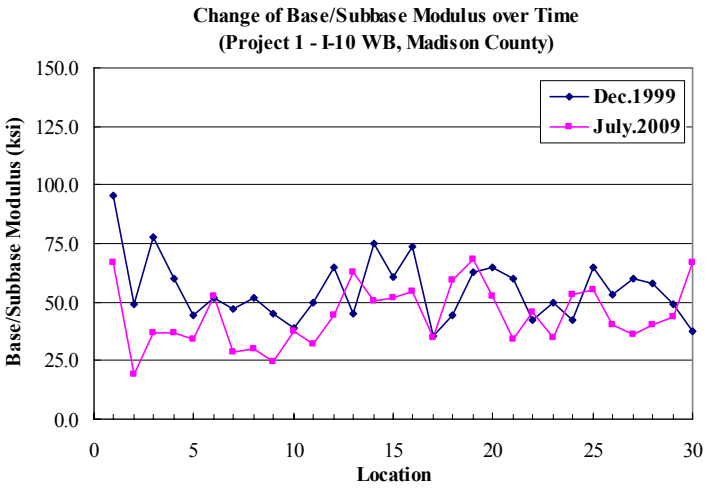

(b) Base/subbase modulus

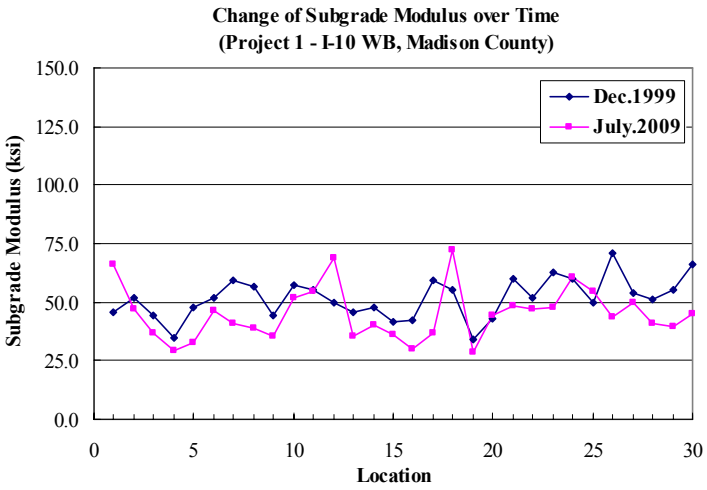

(c) Subgrade modulus

Figure 2-22 Change of calculated layer moduli over time for Project 1

2.4.5 Crack Evaluation on Field Cores

During the coring operation for each project, an additional 2 to 7 cores were obtained from locations of interests for the purpose of crack evaluation, including determination of crack type and actual crack depth to evaluate the features of crack growth in the field.

In most cases, top-down cracking was identified as the dominant crack type for the eleven Superpave projects. Actual crack depths measured from the cores varied from 0.40 to 3.30 in inches, which corresponded with approximately 10 % to 50 % of the total thickness of asphalt concrete layer. Transverse cracks that were evenly spaced along the length of the project section were observed in Project 12 (SR-73 SB, Calhoun County). The crack spacing was determined to be about 10 to 15 feet, which corresponds to spacing generally associated with thermal cracking. This type of crack is generally associated with volumetric contraction that occurs when temperature decreases in a cyclic manner or a one time drop. Figure 2-23 illustrates the crack evaluation procedure on the field cores obtained. Table 2-13 summarizes the crack type identified and crack depth measured from the cores for each project.

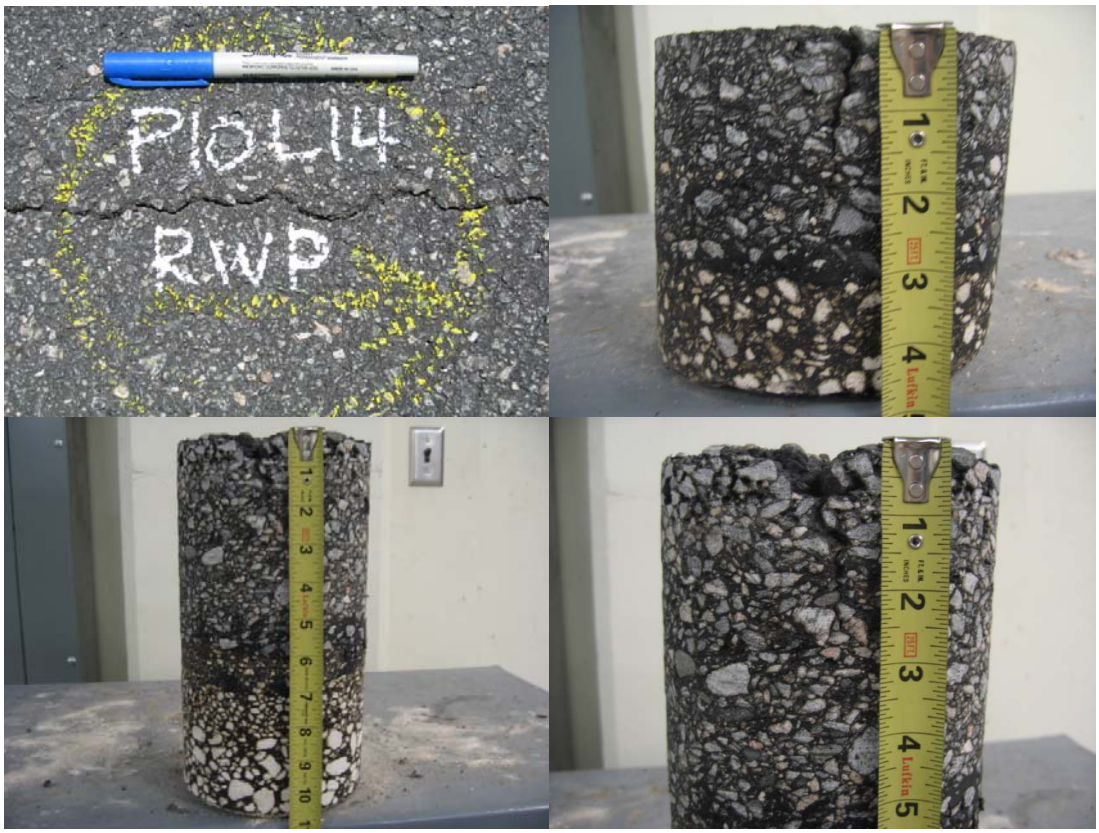

Figure 2-23 Crack evaluation procedure on field cores

Table 2-13 Crack evaluation results on the field cores

Project (UF ID)	Location	Source	Crack Type	Crack Depth (in)	AC Thickness (in)	Age at Coring Time (year)
2	5	LWP	Top-Down	2.75	7.40	11
	15	LWP	Top-Down	3.30	7.40	11
4	7	RWP	Top-Down	1.75	7.44	11
	8	RWP	Top-Down	1.75	7.44	11
	15	RWP	Top-Down	2.50	7.44	11
6	5	RWP	Bottom-Up	2.62	6.40	11
	15	RWP	Bottom-Up	2.03	6.40	11
		BWP	Top-Down	2.50	6.40	11
		TRANSVERSE	Whole-Layer	6.40	6.40	11
	25	RWP	Bottom-Up	3.25	6.40	11
7	5	RWP	Bottom-Up	1.72	6.74	11
8	22	LWP	Top-Down	2.50	6.14	9
9	1	LWP	Top-Down	1.50	5.50	7
	11	LWP	Top-Down	1.30	5.50	7
	14	LWP	Top-Down	2.00	5.50	7
	17	LWP	Top-Down	1.25	5.50	7
	25	LWP	Top-Down	0.40	5.50	7
	29	LWP	Top-Down	1.60	5.50	7
		RWP	Top-Down	1.50	5.50	7
10	5	RWP	Bottom-Up	2.00	7.75	7
	14	RWP	Top-Down	2.00	7.75	7
	22	RWP	Top-Down/Bottom-Up	1.50/2.70	7.75	7
		TRANSVERSE	Top-Down	1.75	7.75	7
	25	RWP	Bottom-Up	0.90	7.75	7
			Top-Down	1.00	7.75	7
	27	RWP	Top-Down	1.30	7.75	7
11	15	RWP	Bottom-Up	2.10	7.75	6
12	5	TRANSVERSE	Top-Down/Bottom-Up	2.50/3.50	6.49	6
	10	RWP	Bottom-Up	3.00	6.49	6
	15	TRANSVERSE	Whole Layer	6.49	6.49	6
	25	RWP	Bottom-Up	2.10	6.49	6

Note: 1. LWP = Left Wheel Path, RWP = Right Wheel Path, and BWP = Between Wheel Path
2. All bottom-up cracks were observed only in the old AC layer.

During the inspection process of the cores obtained, evidence of moisture damage was observed for Projects 9, 10, 11, and 12. Figure 2-24 illustrates typical observations for cores obtained from these Superpave projects. Additional details related to the apparent moisture damage observed are included in Chapter 4.

Figure 2-24 Visual inspection for cores obtained from the moisture-damaged projects

2.4.6 Closure

Field data collection was completed for this phase of Superpave monitoring project including sampling (coring), transverse profilograph test (TP), and falling weight deflectometer test (FWD). A thorough analysis of data obtained from the field was conducted. Crack evaluation on the field cores was conducted and top-down cracking was determined to be the dominant crack type for the eleven Superpave projects. All the data described in this chapter formed the basis of further analyses performed to achieve the goals of this research.

CHAPTER 3
BINDER RECOVERY AND BINDER TESTS

3.1 Introduction

Binder characterization and its relationship with pavement performance is one of the important issues for the development of performance based specification. Asphalt binders are commonly characterized by their physical properties, which may help describe how it will perform as a constituent in HMA pavement and its effect on field performance. Since most existing mixture property and aging relationships require binder properties as input, it is extremely important to characterize key asphalt binder properties and to identify how these properties change in the field throughout the pavement life.

Asphalt binder recoveries and binder tests were conducted for cores obtained from the eleven Superpave projects, including top and bottom layers identified as Superpave layers A and B, respectively. Cores for binder recovery were obtained from between wheel path (BWP) and within the wheel path (WP) of every coring location. Binder tests included penetration test at 25 ˚C and viscosity test at 60 ˚C for all project sections as a minimum. Additional binder tests, including dynamic shear rheometer (DSR) test, bending beam rheometer (BBR) test, and multiple stress creep recovery (MSCR) test were performed at selected locations for all projects. All tests were performed according to FDOT test methods. Binder test results indicate the properties for around six to eleven years of aging in the field. The binder testing plan is summarized below, while Table 3-1 represents the asphalt binder used on the eleven Superpave projects.

- Penetration test at 25 °C (77 °F)

- Viscosity test at 60 °C (140 °F)
- Dynamic shear rheometer (DSR) test: As PAV DSR, test was performed by using 8mm spindle at the intermediate temperature, 25 °C (77 °F)
- Bending beam rheometer (BBR) test: As PAV BBR, test was performed at the PG grade temperature per original specification, -12 °C (10.4 °F)
- Multiple stress creep recovery (MSCR) test: As PAV MSCR, test was performed by using 8mm spindle at 64 °C (147.2 °F) indicating the environmental grade for the State of Florida.

Table 3-1 Asphalt binder used on projects

Project	1	2	3	4	6	7	8	9	10	11	12
Layer A	AC-30	AC-20	AC-30	AC-30	AC-20	AC-20	PG76-22	ARB-5	ARB-5	PG76-22	ARB-5
Layer B	AC-30	AC-20	AC-30	AC-30	AC-20	AC-20	PG76-22	PG64-22	PG64-22	PG64-22	PG64-22

3.2 Binder Recovery

Asphalt recovery was performed by using the solvent extraction method for cut cores obtained from the eleven Superpave projects, including Superpave top and bottom layers which are denoted as layer A and B, respectively. For each coring location, six cut cores including three wheel path (WP) and three between wheel path (BWP) cores were used for binder recovery. Trichloroethylene (TCE) was used as a solvent for binder recovery and the test procedure was carefully followed to minimize any additional aging of the binder during the binder recovery operation according to FDOT test methods.

3.3 Penetration Test

The penetration test is one of the oldest and simplest empirical tests used to measure the consistency of asphalt binder. In general, penetration test is performed at 25 ˚C which is considered approximately representative value of average service temperature for asphalt pavement. The depth of penetration is measured in units of 0.1 mm and reported in penetration units. For example, if the penetration depth of the needle is 8 mm, the penetration number of asphalt binder is 80. The description and practice of standard penetration test method is designated and reported in AASHTO T 49 and ASTM D 5. Penetration tests were conducted at 25 ˚C. Figure 3-1 represents penetration test results from binder recovered for the eleven Superpave projects.

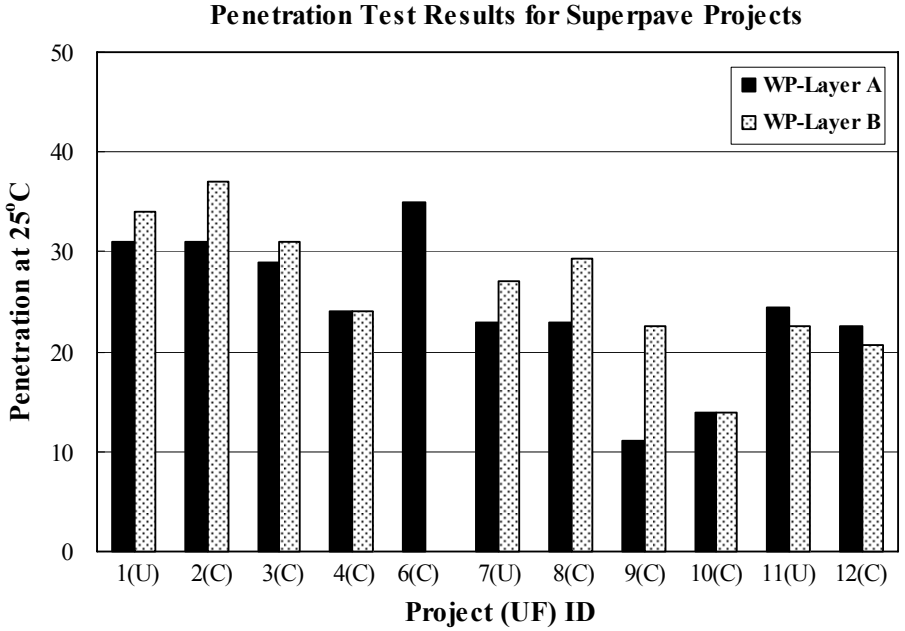

Note: (C) = Cracked, (U) = Uncracked
Figure 3-1 Penetration test results for Superpave projects

Results show that penetration measured for binder extracted from top layer denoted as layer A generally has lower value than for binder obtained from bottom layer denoted as layer B. This was expected because the effect of oxidative aging for top layer is generally more severe than bottom layer. Binders obtained from top layer of Project 9 and 10, which are rubber modified binder (ARB-5) exhibited especially lower penetration.

3.4 Viscosity Test

Viscosity represents the resistance to flow of a fluid and it can be simply defined as the ratio of shear stress to shear rate. As opposed to other empirical tests including penetration test, viscosity is a fundamental property. However, viscosity is generally measured at only one temperature, so it does not cover the full range of construction and service conditions.

Viscosity test is usually performed at 60 ˚C which is approximately considered to be representative of the maximum in-service surface temperature of asphalt pavement. The description and practice of standard absolute viscosity test method is described in AASHTO T 202 and ASTM D 2171. Figure 3-2 exhibits current viscosity measured from extracted binder and Figure 3-3 shows the change in viscosity over time for the eleven Superpave projects.

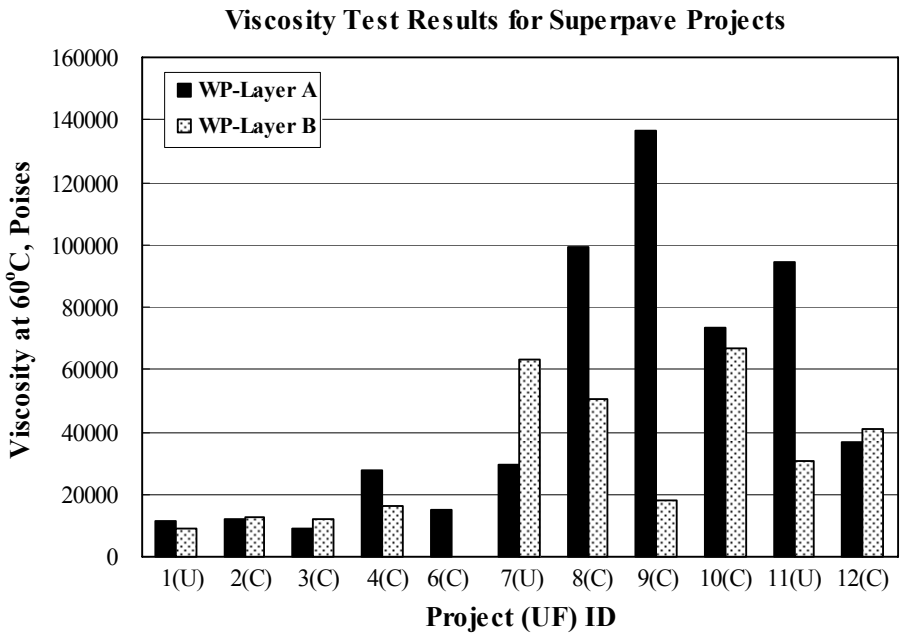

Note: (C) = Cracked, (U) = Uncracked
Figure 3-2 Viscosity test results for Superpave projects

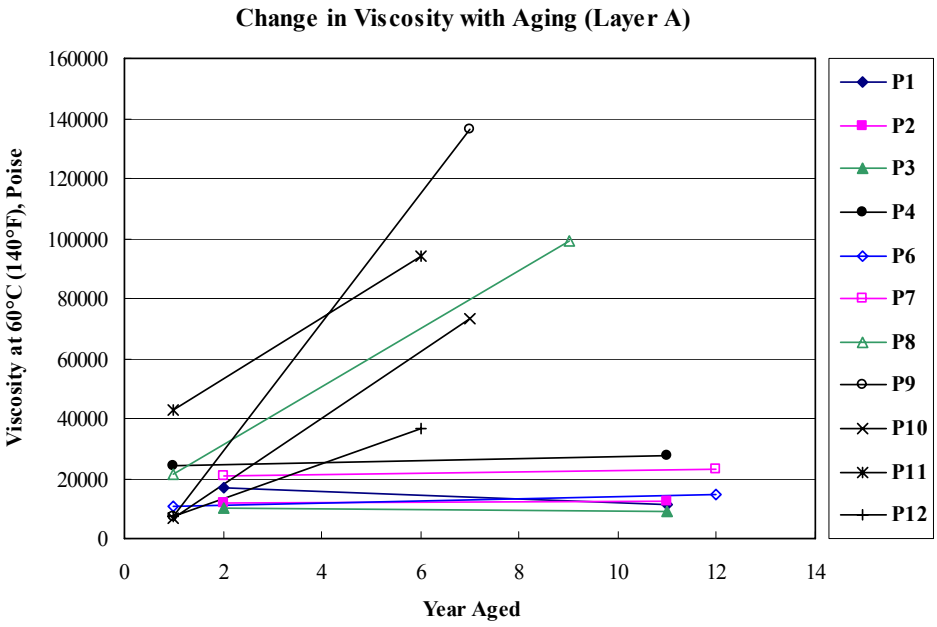

(a) Layer A

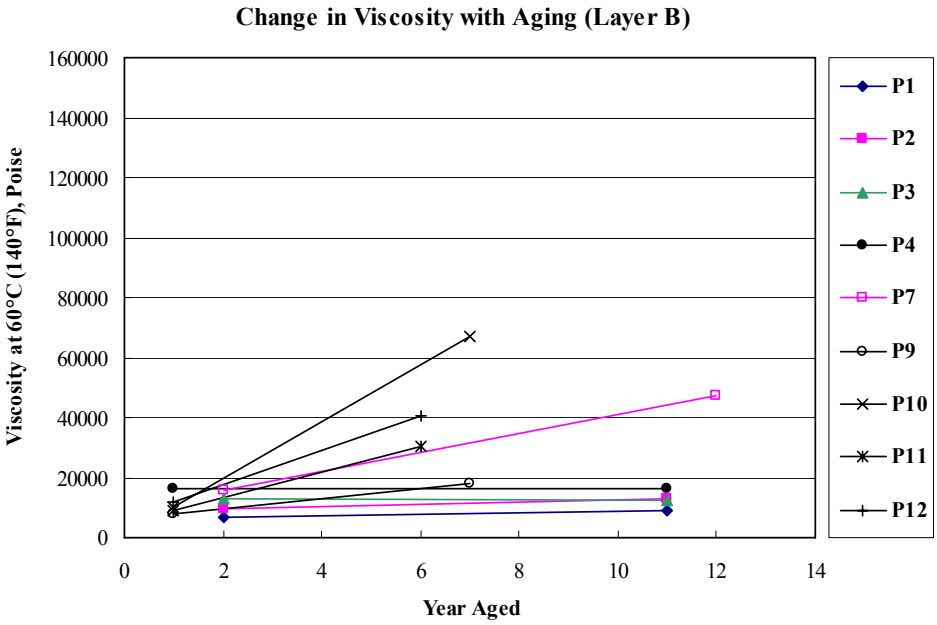

(b) Layer B

Note: (C) = Cracked, (U) = Uncracked
Figure 3-3 Change in viscosity with aging for Superpave projects

Due to more severe effect of oxidative aging caused by higher surface temperature, the top layer shows higher viscosity as well as higher rate of increase in viscosity than the bottom layer. Specifically, top layer (Layer A) of Project 8 through 12 which include polymer modified (PG76-22) and rubber modified binder (ARB-5) sections indicate higher viscosity with around six to nine years of aging in the field. Also, as indicated in Figure 3-3 (a), these sections show higher rate of increase in viscosity with aging.

3.5 Dynamic Shear Rheometer Test (DSR)

The dynamic shear rheometer (DSR) test is used in the Superpave system to characterize the viscous and elastic behavior of asphalt binder at intermediate and high service temperatures.

The DSR measures the complex shear modulus G^* and phase angle δ of asphalt binder to determine the characteristics of elastic and viscous components at pavement service temperatures. Specifically, G^* and δ measured are utilized as the indicators to predict two HMA distresses: rutting and fatigue cracking. The description and practice of standard DSR test method is designated and reported in AASHTO TP 5. In the Superpave asphalt binder specification, two parameters have been chosen ($G^*/\sin\delta$, and $G^*\cdot\sin\delta$) for evaluation of rutting and fatigue cracking, respectively.

Since eleven Superpave projects investigated have six to eleven years of service period from the construction, all recovered binders obtained were considered as PAV aged binders. As the DSR test for PAV aged binder, samples were tested by using 8mm spindle at intermediate temperature determined based on the PG grade of original binder used. Figure 3-4 represents the parameter $G^*\cdot\sin\delta$ for all Superpave projects.

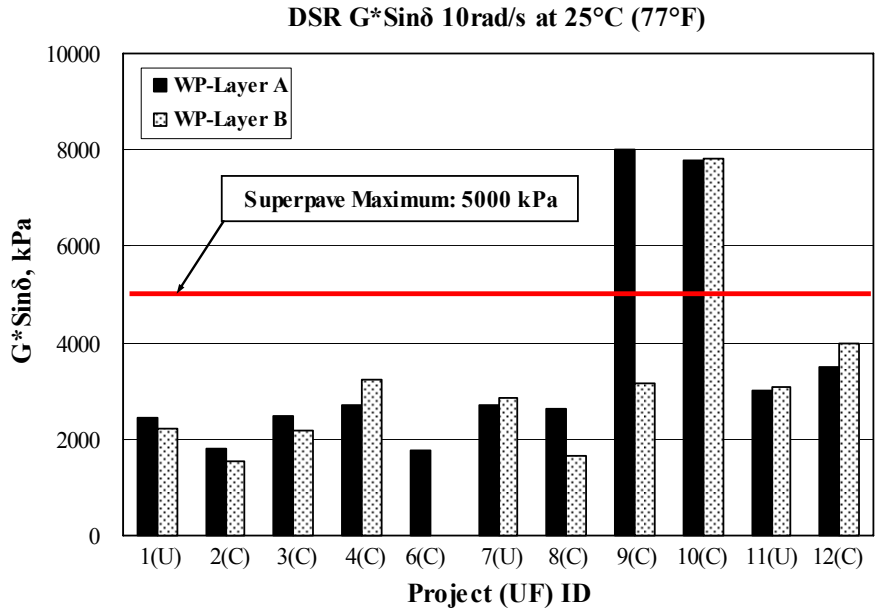

Note: (C) = Cracked, (U) = Uncracked
Figure 3-4 $G^*\cdot\sin\delta$, 10 rad/sec at 25 °C (77 °F) for Superpave projects

Figure 3-4 shows that all binders met the Superpave specification requirement for a maximum $G^*\cdot\sin\delta$ of 5000 kPa except for the top layer of Project 9 (ARB-5) and the top and bottom layer of Project 10 (Top: ARB-5. Bottom: PG64-22). $G^*\cdot\sin\delta$ is typically considered as an indicator of resistance to fatigue cracking because it indicates an amount of energy dissipated meaning that higher $G^*\cdot\sin\delta$ is related to higher energy loss. However, based on the results shown in Figure 3-4, and considering the cracking performance, it appears questionable whether the parameter $G^*\cdot\sin\delta$ is consistently correlated with cracking performance of mixtures.

3.6 Bending Beam Rheometer Test (BBR)

The bending beam rheometer (BBR) test is used in the Superpave system to determine the propensity of asphalt binders to thermal cracking at low temperatures. The BBR calculates the creep stiffness of asphalt binder (S(t)) and the rate of change of the stiffness (m-value). The creep stiffness (S(t)) is related to the thermal stresses developed in the HMA pavement as a result of thermal contraction, while the slope of the stiffness curve, m-value, is associated with the ability of HMA pavement to relieve thermal stresses. In other words, m-value is an indicator of the binder's ability to relax stresses by asphalt binder flow. The Superpave binder specification requires a maximum limit of creep stiffness and the minimum limit of m-value. The description and practice of standard BBR test method is designated and reported in AASHTO TP 1.

The BBR tests for PAV aged binder samples were tested at PG grade temperature according to their original specification. Figure 3-5 and 3-6 represent the parameters S(t) and m-value as a result of the BBR testing for all Superpave project sections, respectively.

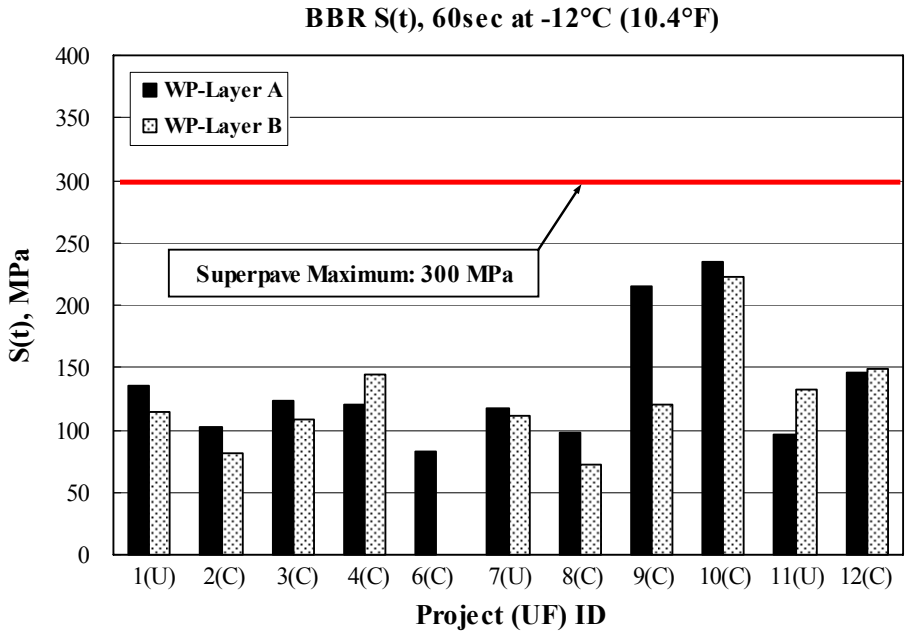

Note: (C) = Cracked, (U) = Uncracked
Figure 3-5 S(t), 60 seconds loading time at -12 °C (10.4 °F) for Superpave projects

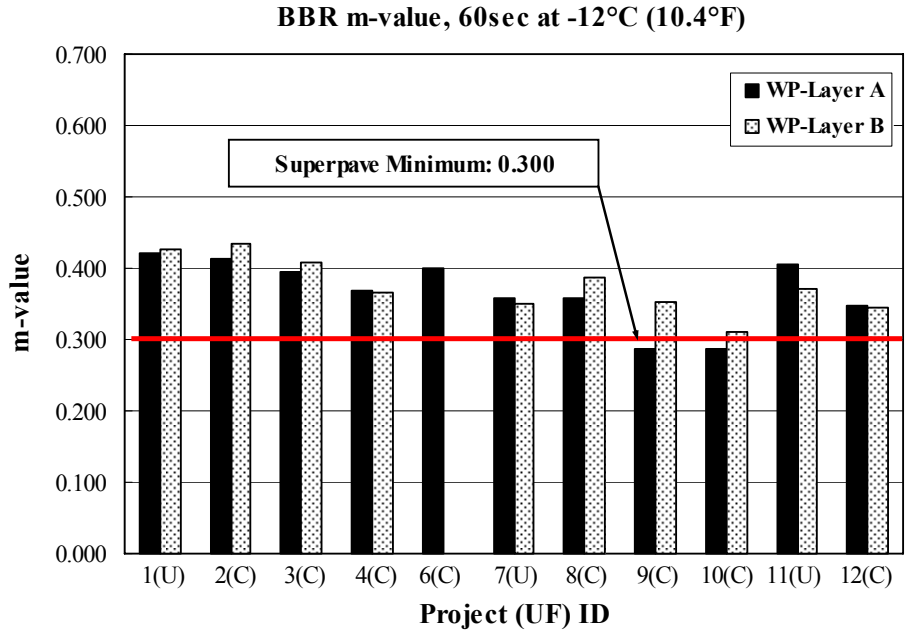

Note: (C) = Cracked, (U) = Uncracked
Figure 3-6 m-value, 60 seconds loading time at -12 °C (10.4 °F) for Superpave projects

Figure 3-5 shows that all binders met the Superpave specification requirement for a maximum S(t) of 300 MPa. Figure 3-6 indicates that all binders also met the Superpave specification requirement for a minimum m-value of 0.3 except for the top layers of Project 9 (ARB-5) and Project 10 (ARB-5). The BBR test results including S(t) and m-value are typically evaluated to determine the propensity of binder for thermal cracking. However, based on the results shown by Figure 3-5 and 3-6, it appears also questionable whether the parameters S(t) and m-value are consistently correlated with cracking performance of mixtures.

3.7 Multiple Stress Creep Recovery Test (MSCR)

The multiple stress creep recovery (MSCR) test is used to identify the presence of elastic response in the asphalt binder and the change of elastic response under shear creep and recovery using two different stress levels at a specified temperature. In general, the percent recovery of asphalt binders in the MSCR test is affected by the type and amount of polymer used in the polymer modified asphalt binder. Thus, it can be used as an indicator for determining whether polymer was utilized. In addition, non-recoverable creep compliance has been used as an indicator of the asphalt binder's resistance to permanent deformation under repeated load. D'Angelo et al. (2009) found that rutting is typically reduced by half as the non-recoverable creep compliance is reduced by half.

The description and practice of standard MSCR test method is designated and reported in AASHTO TP 70-07 and ASTM D 7405. The MSCR test was conducted by using an 8mm spindle at the environmental grade temperature (64 °C) for the State of Florida. Figure 3-7 and 3-8 represent the MSCR test results including average recovery and non-recoverable compliance for all Superpave project sections, respectively.

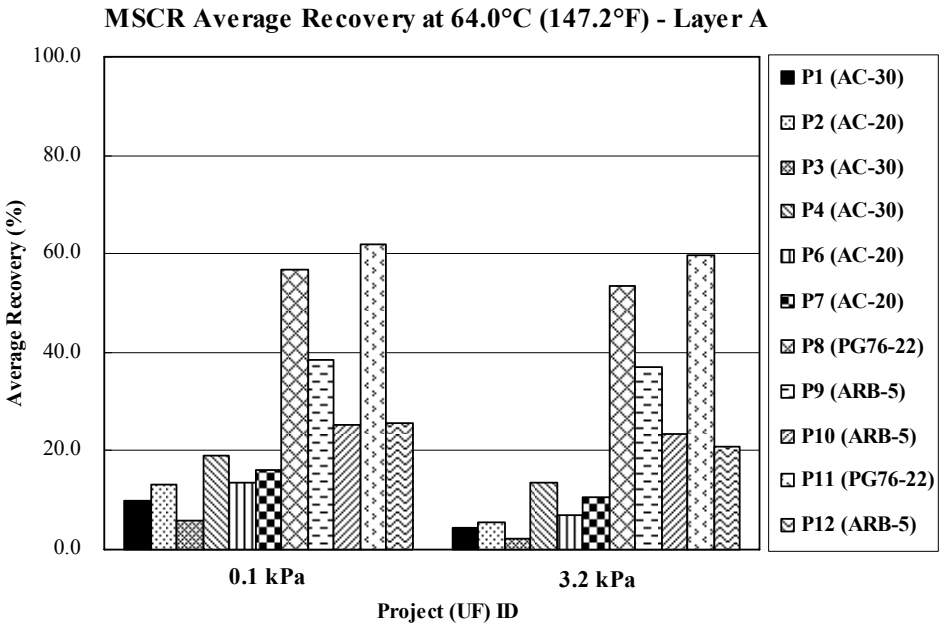

(a) Layer A

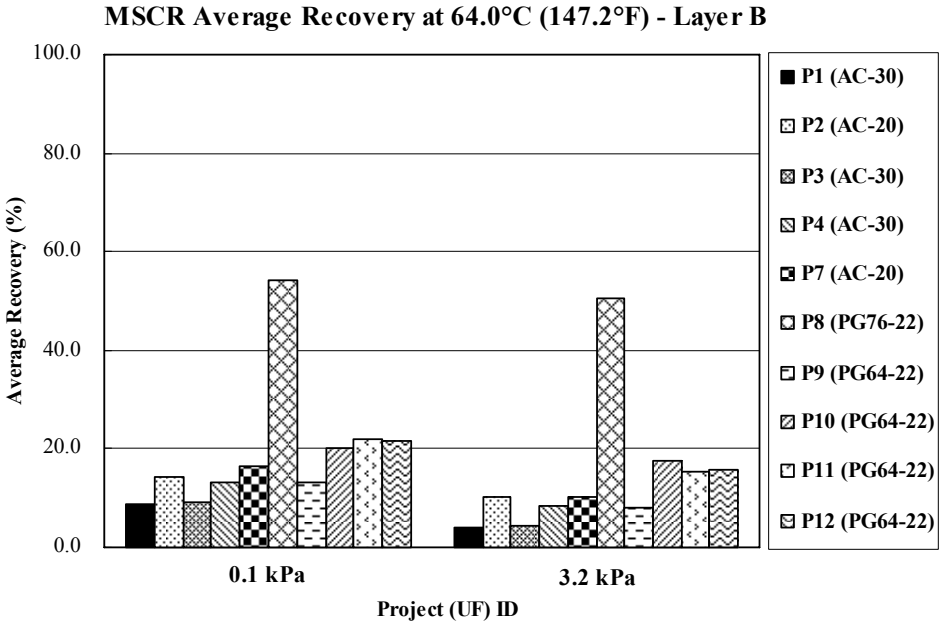

(b) Layer B

Figure 3-7 MSCR average recovery at 64 °C (147.2 °F) for Superpave projects

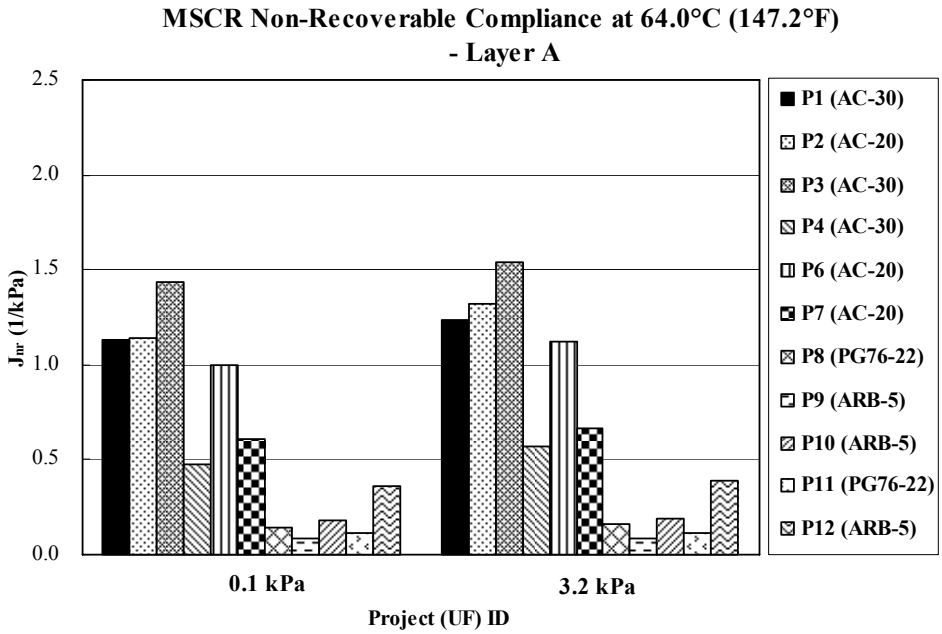

(a) Layer A

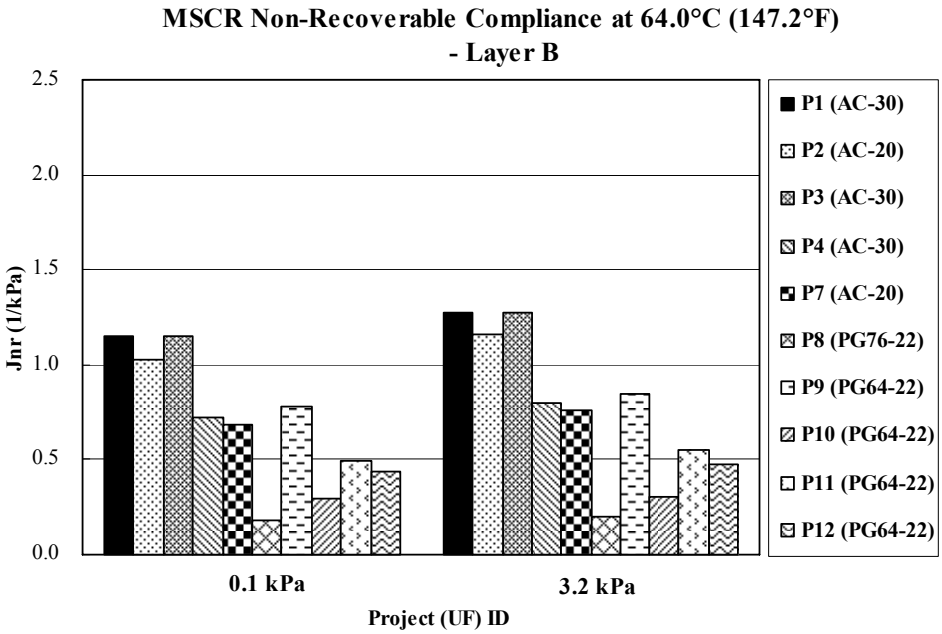

(b) Layer B

Figure 3-8 MSCR nonrecoverable compliance at 64 °C (147.2 °F) for Superpave projects

Figure 3-7 clearly shows that MSCR average percent recovery can distinguish the presence of polymers in asphalt binders. In general, percent recovery of polymer modified binders is greater than base binders including AC-20, AC-30, and PG64-22 for both stress levels. Rubber modified binders also show relatively high percent recovery than base binders. Since the percent recovery indicates the elastic response of asphalt binder, polymer modified binders (PG76-22) appear to exhibit higher elastic response and less sensitivity to change of stress level. Based on Figure 3-8, polymer and rubber modified binders normally show lower non-recoverable compliance than base binders for both stress levels. According to D'Angelo et al. (2009), nonrecoverable compliance can be used for evaluating the rutting resistance of asphalt binder. However, on the basis of the results analyzed, it seems questionable whether it is consistently correlated with rutting performance of mixtures in the field.

3.8 Closure

Asphalt binders were recovered from field cores and tested for the eleven Superpave projects. Test results from binders obtained were considered as comparable to PAV condition, since pavement ages ranged between six and twelve years in the field. Most binders met the Superpave specification requirements for DSR and BBR test results. However, it appears questionable whether the parameters from binder tests are consistently correlated with cracking or rutting performance of asphalt mixtures.

CHAPTER 4
IMPLEMENTATION OF MIXTURE TESTS ON FIELD CORES FOR SUPERPAVE MIXTURES IN FLORIDA

4.1 Introduction

Mixture testing plan on cores obtained from the eleven Superpave projects was formulated and finalized. Three types of mixture tests were in the initial mixture testing plan, including the Superpave IDT test, healing test, and composite specimen tension test. However, because the progress of FDOT research being performed at the UF on healing test and composite specimen tension test is still ongoing, these tests have not been performed in this study.

Superpave IDT tests were performed on both top and bottom layers, denoted as layer A and Layer B at 10 °C and 20 °C to determine mixture properties including modulus, creep compliance, strength, failure strain, and fracture energy and to identify the change in key mixture properties as a function of age in the field. A total of 342 specimens were prepared and tested using the Superpave IDT.

The information obtained was also very useful in the establishment of reasonable and effective mixture design guidelines and criteria, performance-related laboratory properties and parameters, identification of material properties and prediction model evaluation, and for calibration and validation of pavement performance prediction models. A comprehensive analysis was conducted of test data collected to identify the changes in important mixture properties as a function of age and environment for Superpave sections. HMA fracture mechanics model was used to analyze test results. Table 4-1 represents the finalized mixture testing plan on field cores.

Table 4-1 Mixture testing plan

Project (UF) ID	Location	Layer	Source	Test Temperature	Number of Replicates per Temperature
1 - 12	All locations cored for the Phase II Superpave Projects Monitoring	A and B	WP	10 and 20 °C	3

Note: WP = Wheel Path

4.2 Test Specimen Preparation

Specimens were prepared for laboratory testing using field cores obtained from the eleven Superpave project sections. All cores obtained were brought back to the University of Florida laboratory for processing. Two test specimens were obtained from each core including Superpave top and bottom layers denoted by layer A and layer B. Specific gravity (G_{mb}) test was conducted on each cut specimen and air voids were calculated using the G_{mb} and original (first time of coring) maximum specific gravity (G_{mm}). It should be noted that G_{mm} could change with time, especially for moisture-damaged projects. For moisture-damaged projects, air voids determined using original G_{mm} are probably conservatively low (i.e. true air voids of moisture-damaged projects are likely higher than air voids calculated using original G_{mm}). Cores of similar air voids were grouped for specific tests including Superpave IDT tests, healing test, binder recovery and binder tests, respectively.

4.2.1 Measuring, Cataloguing, and Inspecting

Each core obtained was cleaned and the layer of each different asphalt mixture was properly identified, measured, and catalogued with appropriate markings to prevent any confusion. For quality control purposes, cores were inspected and compared to construction information to verify the presence of different mixtures and thicknesses. Figure 4-1 shows the

cross-section layout of typical cores and Figure 4-2 represents the measuring, cataloguing, and inspecting work for Project 9.

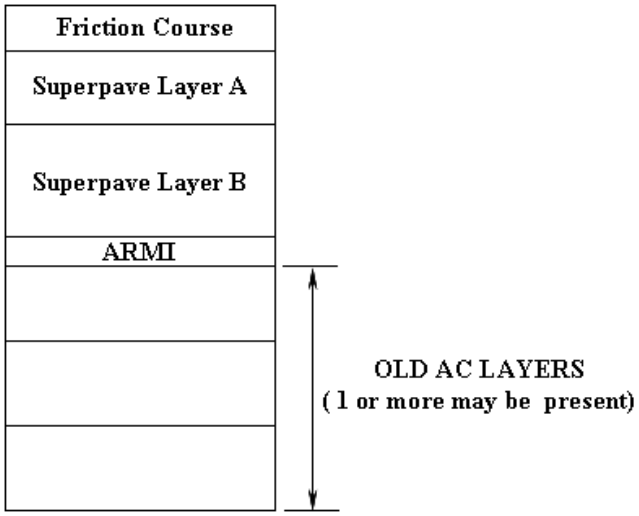

Figure 4-1 Cross-section layout of typical core

Figure 4-2 Measuring, cataloguing, and inspecting work for Project 9 (SR-121 SB, Alachua County)

4.2.2 Cutting

Once the data was properly logged and verified, the core was sliced to obtain test specimens for Superpave top and bottom layers denoted as layer A and B for testing purposes. A cutting device, which has a diamond cutting saw and a special attachment to hold the cores, was used to slice the cores into specimens of desired thickness. Because the saw uses water to keep the blade wet, the cut specimens were placed in the humidity chamber for at least two days to negate the moisture effects in testing. Figure 4-3 shows the cutting machine used in this research and Figure 4-4 represents the cut specimens prepared for Superpave IDT test.

Figure 4-3 Cutting machine used in this research

Figure 4-4 Cut specimens for Superpave IDT test

4.2.3 Gage Points Attachment

Gage points were attached to the specimens using a steel template, a vacuum pump setup, and a strong adhesive. Four gage points (5/16 inch diameter by 1/8 inch thick) were placed with epoxy on each side of the specimens at distance of 19 mm (0.75 in.) from the center, along the vertical and horizontal axes. During this process, the loading axis previously marked on the specimens was checked and clarified. This procedure helped for the placement of specimen in the testing chamber and assured proper loading of the specimen. Figure 4-5 shows the gage point attachment procedure.

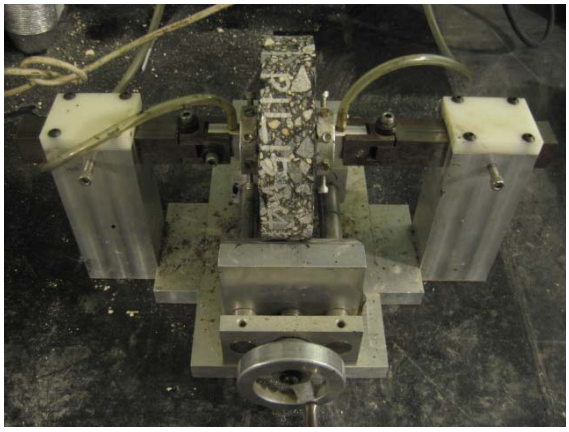

Figure 4-5 Gage points attachment

4.3 Test Procedure

One set of Superpave IDT tests including resilient modulus, creep compliance, and strength test were performed on each specimen for the eleven Superpave projects to determine modulus, creep compliance, strength, failure strain, and fracture energy at 10 °C and 20 °C. These test results provide the properties to identify changes in key mixture properties over time with aging environment in the field. In addition, as it mentioned previously, this information was also critical to identify material properties and prediction model evaluation, and to calibrate and validate the pavement performance prediction models. The material testing system (MTS) used for this study, and test configuration of Superpave IDT test set-up are shown in Figure 4-6.

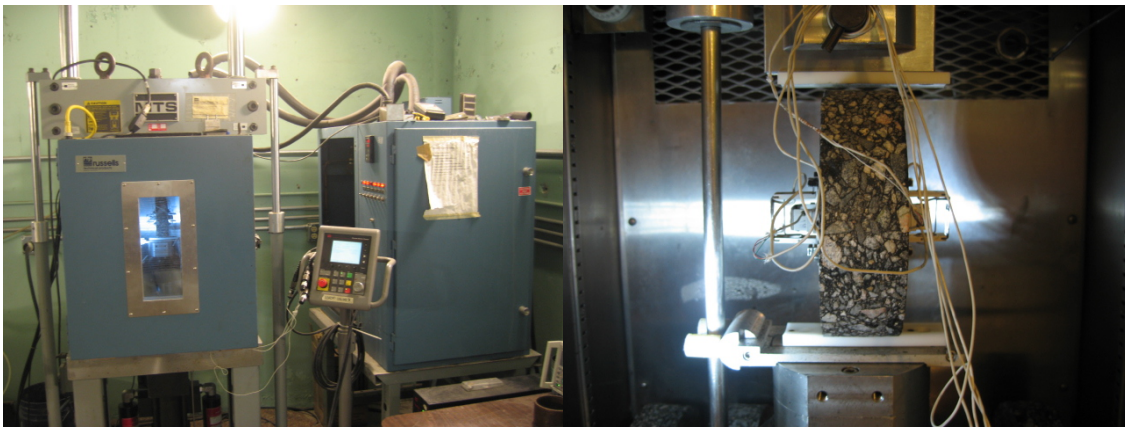

Figure 4-6 Superpave IDT tests

4.3.1 Resilient Modulus Test

The resilient modulus is defined as the ratio of the applied stress to the recoverable strain when repeated loads are applied. The test was conducted according to the system developed by Roque et al. (1997) to determine the resilient modulus and the Poisson's ratio. The resilient modulus test was performed in a load controlled mode by applying a repeated haversine

waveform load to the specimen for a 0.1 second followed by a rest period of 0.9 seconds. The load was selected to keep the horizontal resilient deformations within the linear viscoelastic range, where horizontal deformations are typically between 100 to 180 micro-inches during the test.

The resilient modulus and Poisson's ratio can be calculated by the following equations, which were developed based on three dimensional finite element analysis by Roque and Buttlar (1992). The equation is incorporated in the Superpave Indirect Tension Test at Low Temperatures (ITLT) computer program, which was developed by Roque et al. (1997).

$$M_R = \frac{P \times GL}{\Delta H \times t \times D \times C_{cmpl}} \tag{4-1}$$

$$\nu = -0.1 + 1.480 \times (X/Y)^2 - 0.778 \times (t/D)^2 \times (X/Y)^2 \tag{4-2}$$

Where, M_R = Resilient modulus, P = Maximum load, GL = Gage length, ΔH = Horizontal deformation, t = Thickness, D = Diameter, $C_{cmpl} = 0.6354 \times (X/Y)^{-1} - 0.332$, ν = Poisson's ratio, and (X/Y) = Ratio of horizontal to vertical deformation.

4.3.2 Creep Test

Creep compliance is a function of time-dependent strain over stress. The creep compliance curve was originally developed to predict thermally induced stress in asphalt pavement. However, it can also be used to evaluate the rate of damage accumulation of asphalt mixture. As shown in Figure 4-7, D_0, D_1, and m-value are mixture parameters obtained from creep compliance tests. Although D_1 and m-value are related to each other, D_1 is more related to the initial portion of the creep compliance curve, while m-value is more related to the longer-term portion of the creep compliance curve.

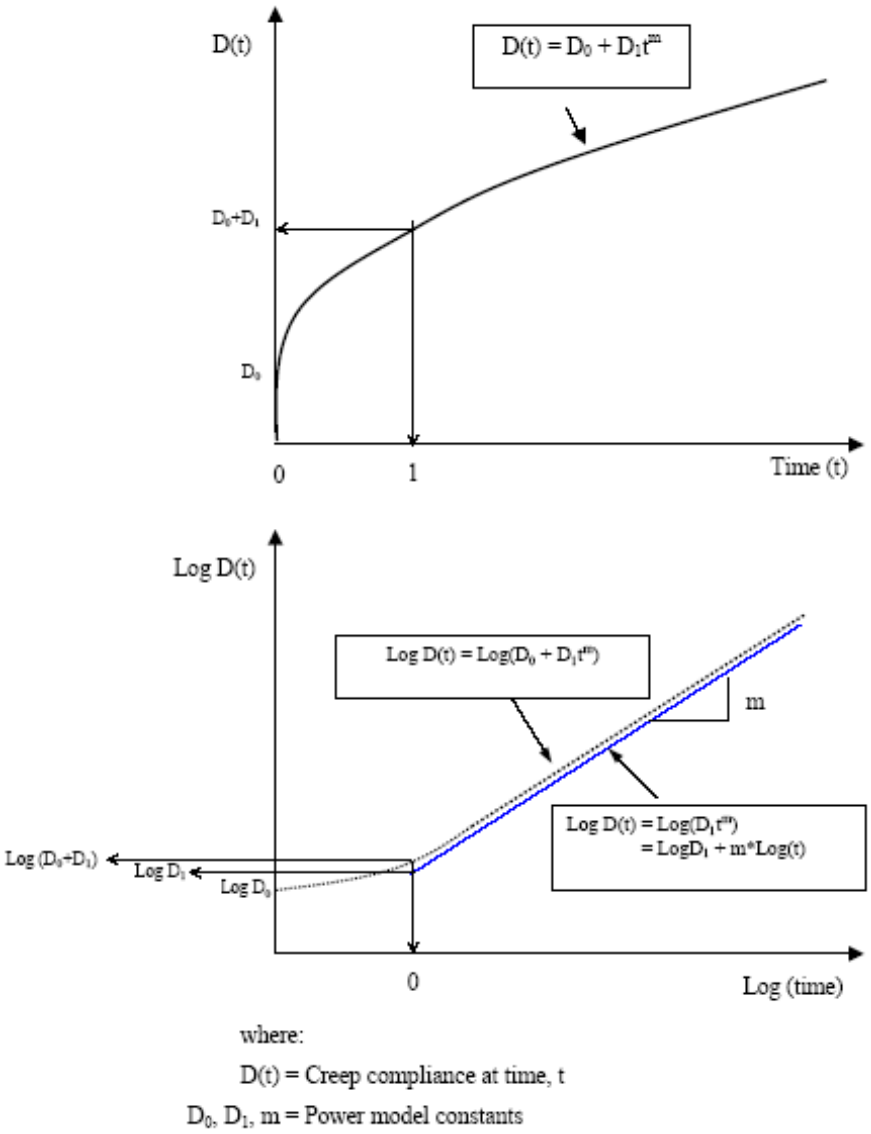

Figure 4-7 Power model of creep compliance

The creep test was performed in the load controlled mode by applying a static load in the form of a step function to the specimen and then holding it for 1000 seconds. The magnitude of load applied was selected to maintain the accumulated horizontal deformations in the linear viscoelastic range, which is below the total horizontal deformation of 750 micro-inches. Although the range of horizontal deformation at 100 seconds can vary depending upon test

temperature, specimen type, and the level of aging, a horizontal deformation of 100 to 130 micro-inches at 100 seconds is generally considered to be acceptable.

The Superpave Indirect Tension Test at Low Temperatures (ITLT) computer program was used to determine creep properties of the mixtures by analyzing the load and deformation data. Creep compliance and Poisson's ratio are computed by the following equations.

$$D(t) = \frac{\Delta H \times t \times D \times C_{cmpl}}{P \times GL} \tag{4-3}$$

$$\nu = -0.1 + 1.480 \times (X/Y)^2 - 0.778 \times (t/D)^2 \times (X/Y)^2 \tag{4-4}$$

Where, D(t) = Creep compliance at time t (1/psi), ΔH, t, D, C_{cmpl}, GL, ν, P, and (X/Y) are same as described above.

4.3.3 Tensile Strength Test

Failure limits including tensile strength, failure strain, and fracture energy were determined from strength test. These properties can be used for estimating the cracking resistance of the asphalt mixtures. The strength test was conducted in a displacement controlled mode by applying a constant rate of displacement of 50 mm/min until the specimen failed. The maximum tensile strength is calculated as the following equation.

$$S_t = \frac{2 \times P \times C_{sx}}{\pi \times b \times D} \tag{4-5}$$

Where, S_t = Maximum indirect tensile strength, P = Failure load at first crack, C_{sx} = 0.948 – 0.01114 × (b/D) – 0.2693 × ν +1.436(b/D) × ν, b = Thickness, D = Diameter, and ν = Poisson's ratio.

Fracture energy and dissipated creep strain energy can be determined from the strength test and the resilient modulus test. Fracture energy is the total energy necessary to induce fracture. Dissipated creep strain energy (DCSE) is the absorbed energy that damages the specimen, and dissipated creep strain energy to failure is the absorbed energy to fracture ($DCSE_f$). As shown in the Figure 4-8, fracture energy and $DCSE_f$ can be determined as described below. The ITLT program also calculates fracture energy automatically.

$$M_R = \frac{S_t}{\varepsilon_f - \varepsilon_0} \Rightarrow \varepsilon_0 = \frac{M_R \varepsilon_f - S_t}{M_R} \tag{4-6}$$

$$Elastic\ Energy\,(EE) = \frac{1}{2} S_t (\varepsilon_f - \varepsilon_0) \tag{4-7}$$

$$Fracture\ Energy\,(FE) = \int_0^{\varepsilon_f} S(\varepsilon) d\varepsilon \tag{4-8}$$

$$Dissipated\ Creep\ Strain\ Energy\,(DCSE_f) = FE - EE \tag{4-9}$$

Where, S_t = Tensile strength, and ε_f = Failure strain.

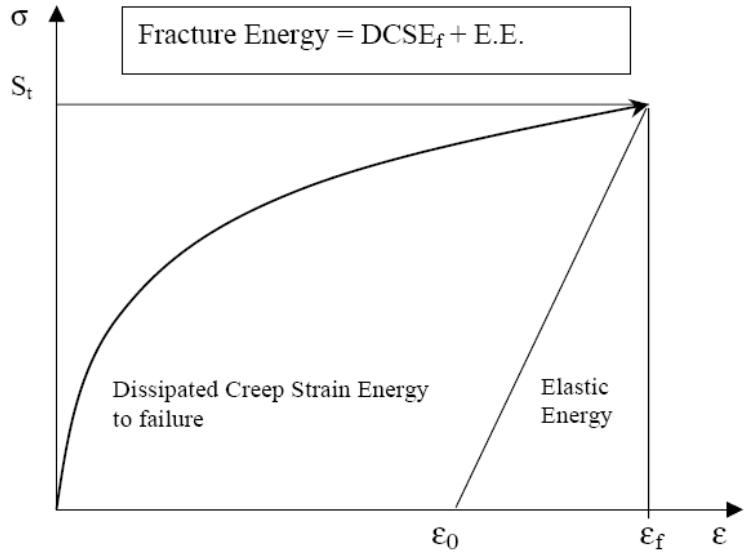

Figure 4-8 Determination of fracture energy and dissipated creep strain energy to failure

In addition, a parameter, Energy Ratio (ER), which represents the asphalt mixture's potential for top-down cracking was recently developed by Roque et al. (2004). This parameter allows the evaluation of cracking performance on different pavement structures by incorporating the effects of mixture properties and pavement structural characteristics. The energy ratio is expressed in the equation shown below. The ITLT program calculates energy ratio automatically.

$$ER = \frac{DCSE_f}{DCSE_{\min}} = \frac{a \times DCSE_f}{m^{2.98} \times D_1} \quad (4\text{-}10)$$

Where, $DCSE_f$ = Dissipated creep strain energy (in KJ/m^3), $DCSE_{min}$ = Minimum dissipated creep strain energy for adequate cracking performance (in KJ/m^3), D_1 and m = Creep parameters, $a = 0.0299\sigma^{-3.1}(6.36 - S_t) + 2.46 \times 10^{-8}$ in which, σ = Tensile stress of asphalt layer (in psi), and S_t = Tensile strength (in MPa).

4.4 Superpave IDT Test Results

The test results obtained from Superpave IDT were obtained using the ITLT computer program developed at the University of Florida. A comprehensive analysis of test results was conducted to identify the trend of changes in key mixture properties including fracture energy, creep rate, resilient modulus, creep compliance, tensile strength, and failure strain as a function of age and environment for the eleven Superpave projects. Table 4-2 summarizes the mixture information for the Superpave Projects evaluated.

Table 4-2 Mixture information for 11 Superpave projects

Project (UF) ID	Year Aged	Binder Type		Mixture Type		Traffic Level
		Top	Bottom	Top	Bottom	
1	11	AC-30	AC-30	9.5C	19.0C	D/5
2	11	AC-20	AC-20	12.5C	19.0C	D/5
3	11	AC-30	AC-30	12.5C	19.0C	D/5
4	11	AC-30	AC-30	9.5C	19.0C	E/6
6	12	AC-20	N/A	12.5F	N/A	C/4
7	12	AC-20	AC-20	12.5F	12.5F	C/4
8	9	PG 76-22	PG 76-22	12.5C	12.5C	D/5
9	7	ARB-5	PG 64-22	FC-6	12.5F	C/4
10	7	ARB-5	PG 64-22	FC-6	12.5F	B/4
11	6	PG 76-22	PG 64-22	12.5C	12.5C	E/6
12	6	ARB-5	PG 64-22	FC-6	12.5F	C/4

Results of resilient modulus (M_R) which is a measure of elastic stiffness are presented in Figure 4-9. These include initial and current values of resilient modulus obtained from field cores indicating the trend in resilient modulus over time for the Superpave projects.

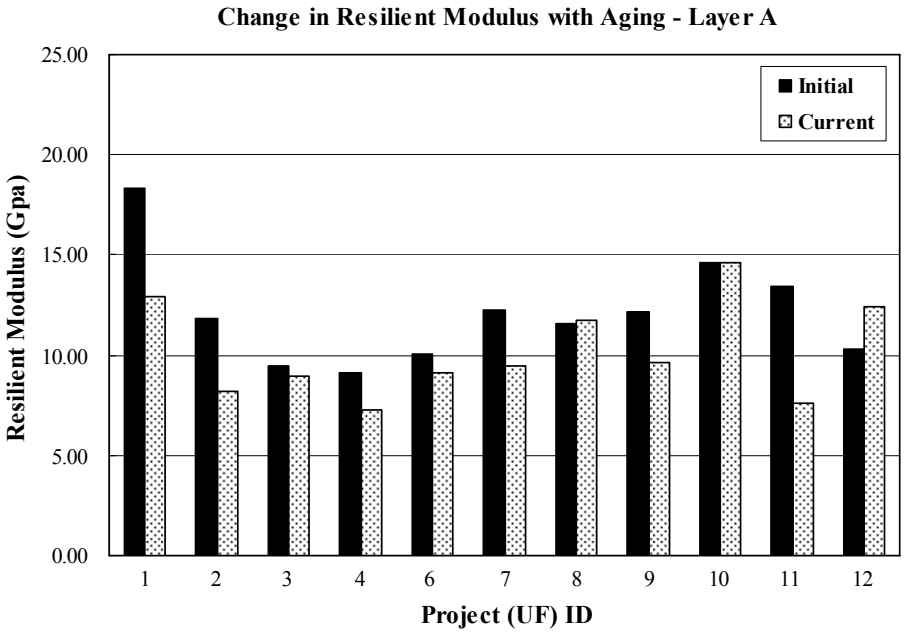

(a) Layer A

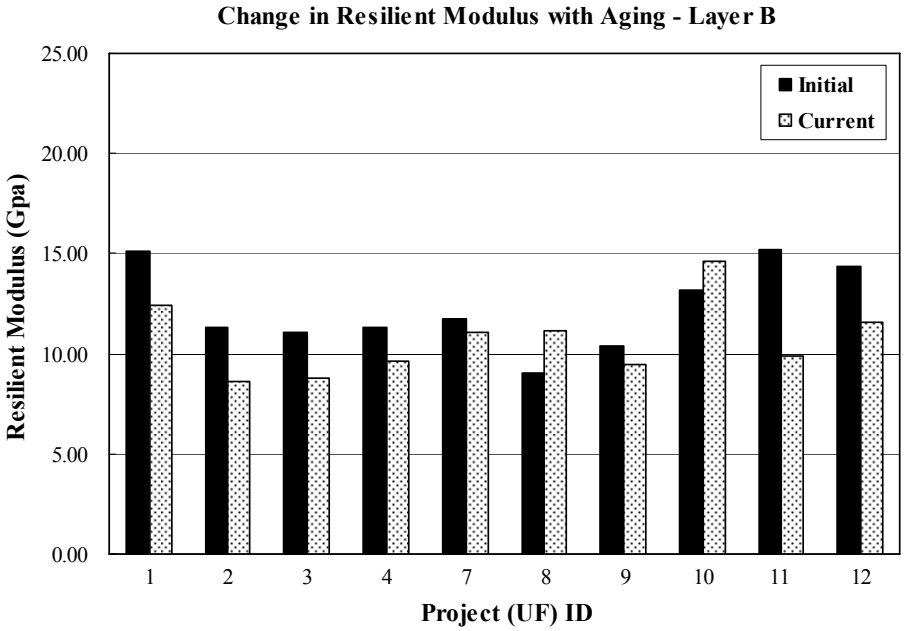

(b) Layer B

Figure 4-9 Change in resilient modulus over time

For most cases, resilient modulus decreased over time, which clearly indicates the presence of permanent damage and the existence of incomplete healing beyond after some level of aging. The top layer (Layer A) generally exhibited higher rates of reduction in resilient modulus than the bottom layer (Layer B). This reflects that the effect of permanent damage induced by traffic load is more severe for top layer than bottom layer.

Creep compliance results are shown in Figure 4-10. Creep compliance is related to the ability of a mixture to relax stresses. In general, higher creep compliance indicates that mixtures can relax stresses faster than mixtures with lower creep compliance, which is critical for evaluating thermal stresses. However, higher creep compliance may also be an indication of permanent damage, and the reduction in creep compliance is expected if there is no permanent damage effect.

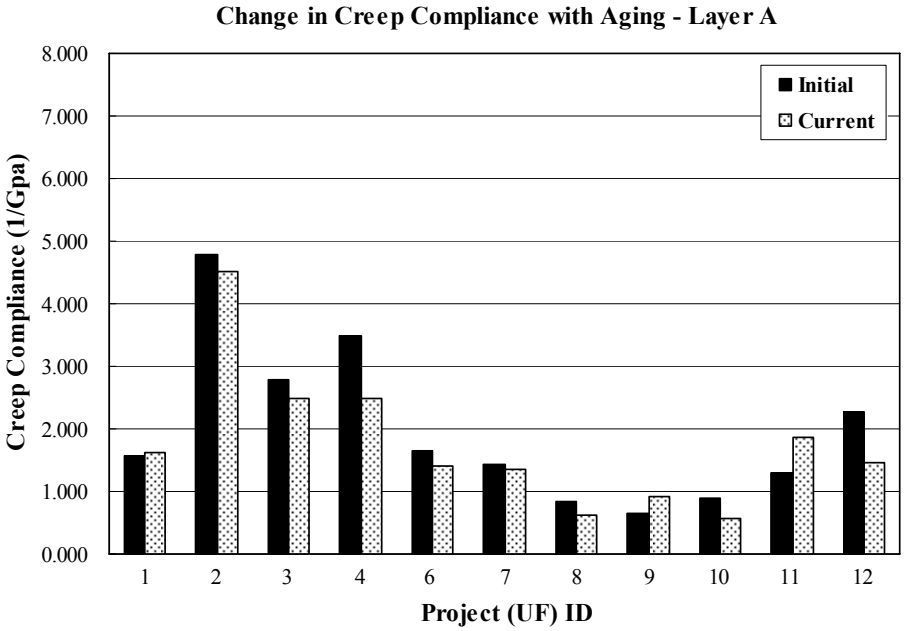

(a) Layer A

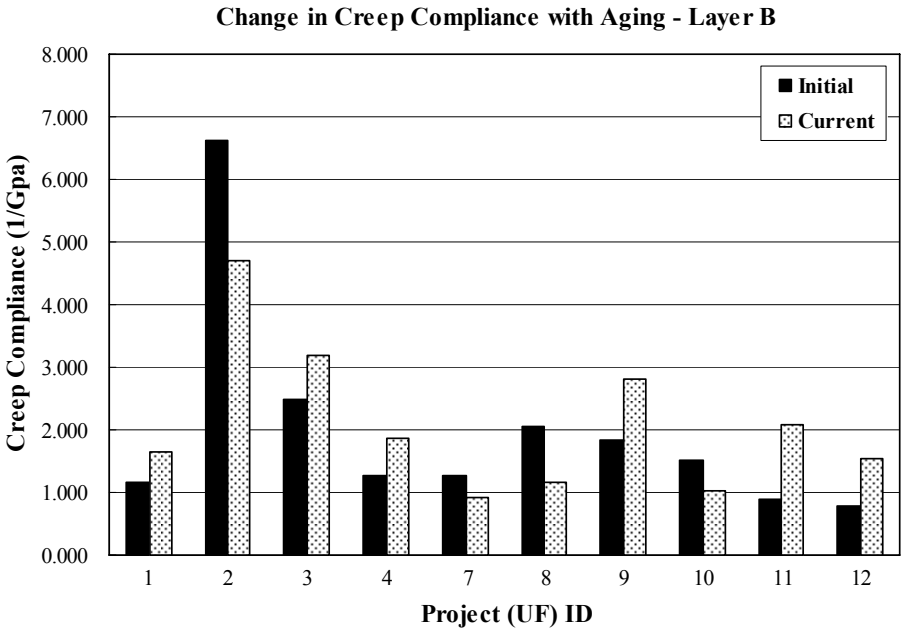

(b) Layer B

Figure 4-10 Change in creep compliance over time

Creep rate, or the rate of change of creep compliance, is related to rate of damage. Figure 4-11 shows the creep rate results. For mixtures not affected by moisture damage (Project 1 through 8), creep rate of the top and bottom layers generally decreased over time, which indicates that oxidative aging had a predominant effect on change in creep rate. However, for mixtures affected by moisture damage (Project 9 through 12), three cases (Layer B of Project 9, 10, and 12) show clear increase as well as two cases (Layer A of Project 9 and 11) exhibit slight increase of creep rate over time as opposed to the effect of oxidative aging, which indicates the effect of non-healable permanent damage induced by moisture. The other three cases exhibit clear decrease of creep rate over time.

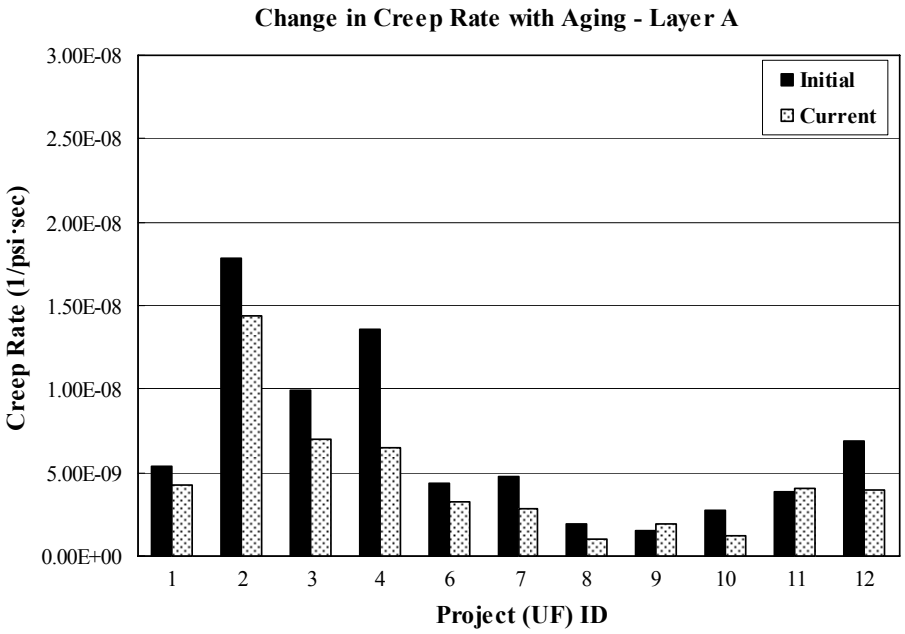

(a) Layer A

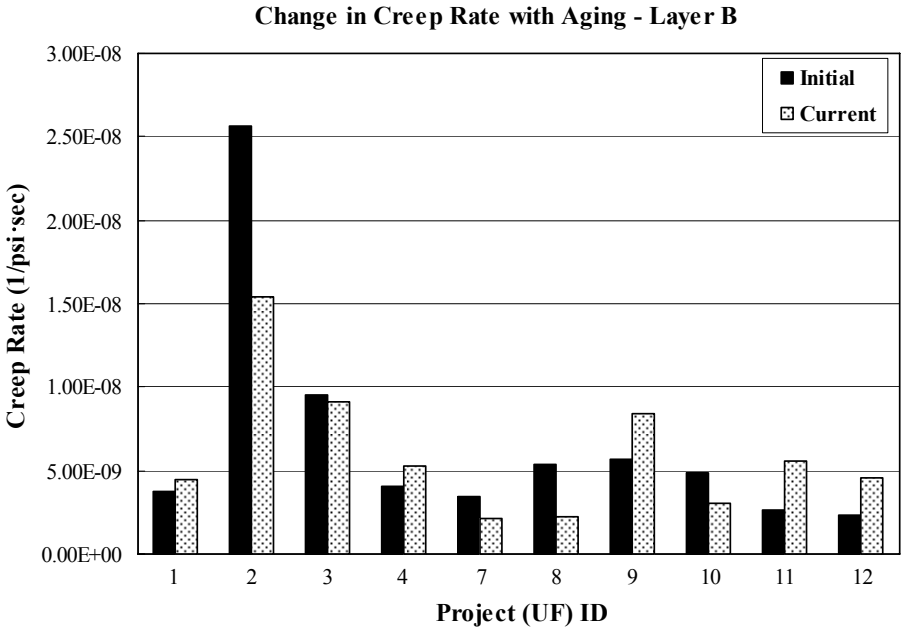

(b) Layer B

Figure 4-11 Change in creep rate over time

Tensile strength indicates the maximum tensile stress that the mixture can sustain before fracture. Figure 4-12 shows the tensile strength results, which exhibit a similar trend as the results of resilient modulus. It was also determined that tensile strength decreased over time, indicating the presence of permanent damage and the existence of incomplete healing after a certain level of aging.

The top and bottom layers of Project 8 exhibited a lower rate of reduction in tensile strength which appears to be related to the effect of polymer modification. However, the top layer of Project 11, which also used a polymer modified binder, exhibited an unusually high rate of reduction in tensile strength over time, which seems to be associated with the effect of moisture damage.

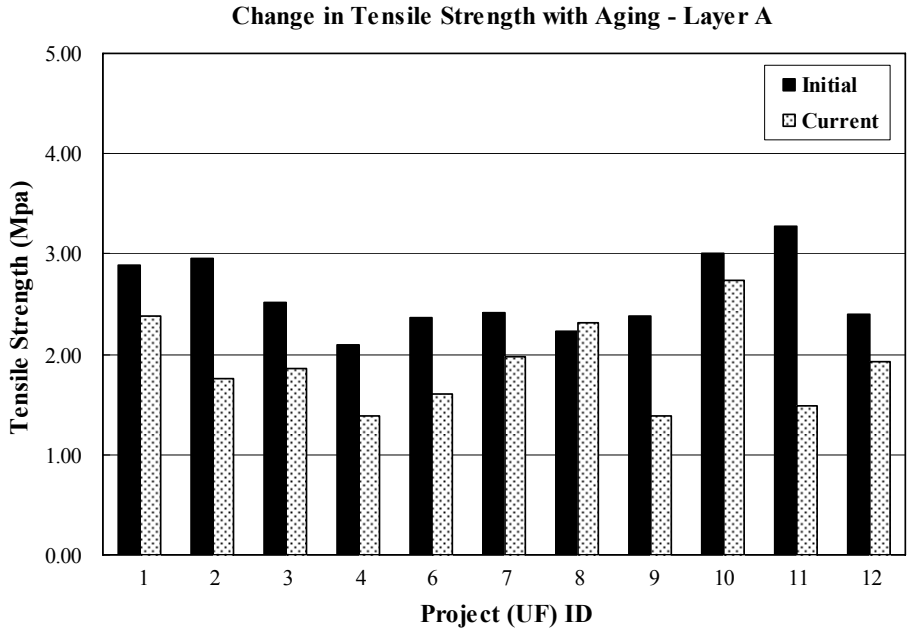

(a) Layer A

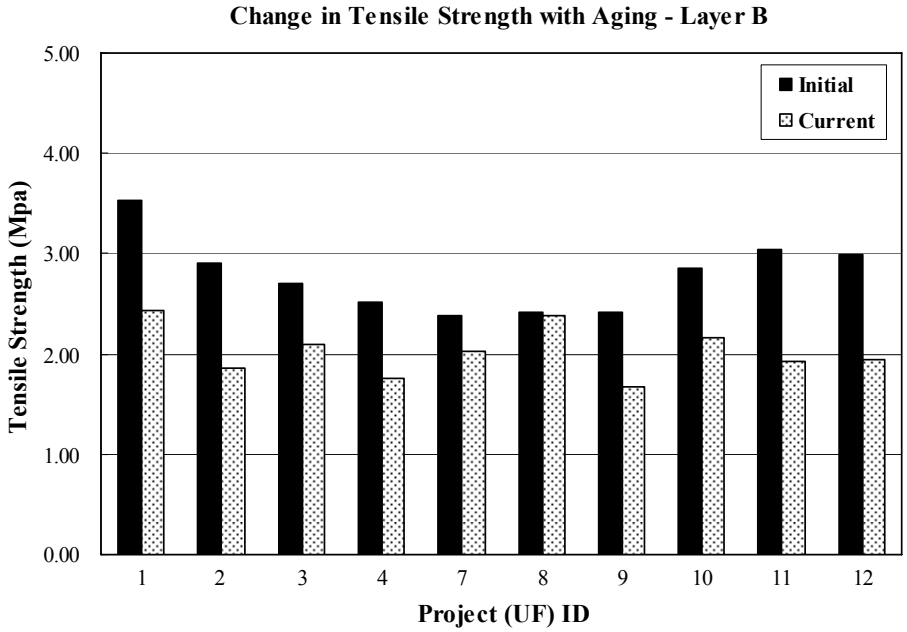

(b) Layer B

Figure 4-12 Change in tensile strength over time

Failure strain characterizes the brittleness of a mixture. This value is related to the severity of aging condition and the mixture susceptibility to aging, especially oxidative aging. Figure 4-13 shows initial (less than six months after construction) and current failure strain for the eleven Superpave projects. As expected, the rate of reduction in failure strain for top layer was generally greater than for the bottom layer. The top and bottom layers of Project 2 and the top layer of Project 6 exhibited the highest rate of reduction in failure strain of sections 1 to 8.

Projects 9 through 12, which showed evidence of moisture damage, also exhibited a high reduction in failure strain. High initial and current air voids as well as the increase in air voids over time caused by the moisture damage for these sections may have accelerated the effect of oxidative aging, so the mixture embrittled within a relatively short period of time.

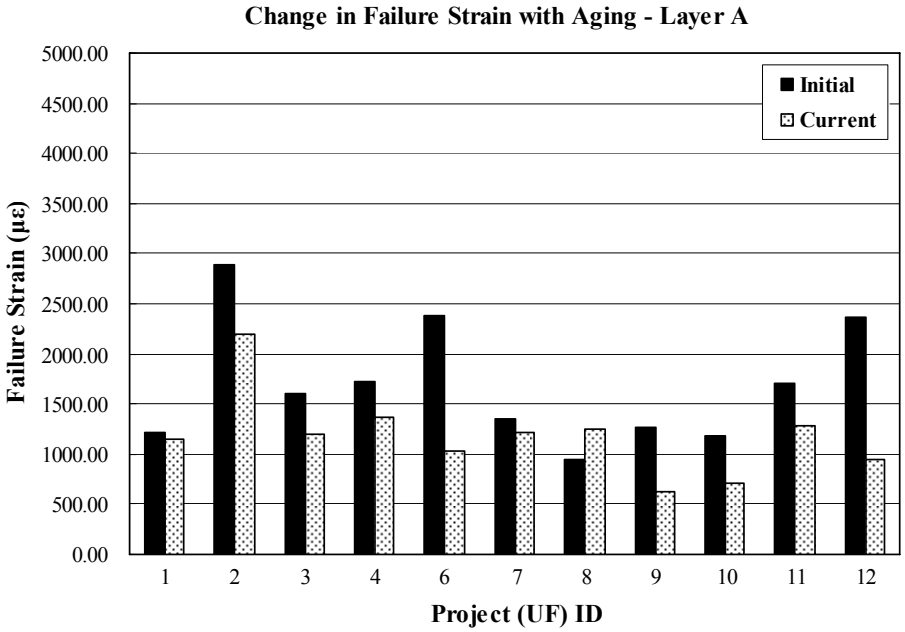

(a) Layer A

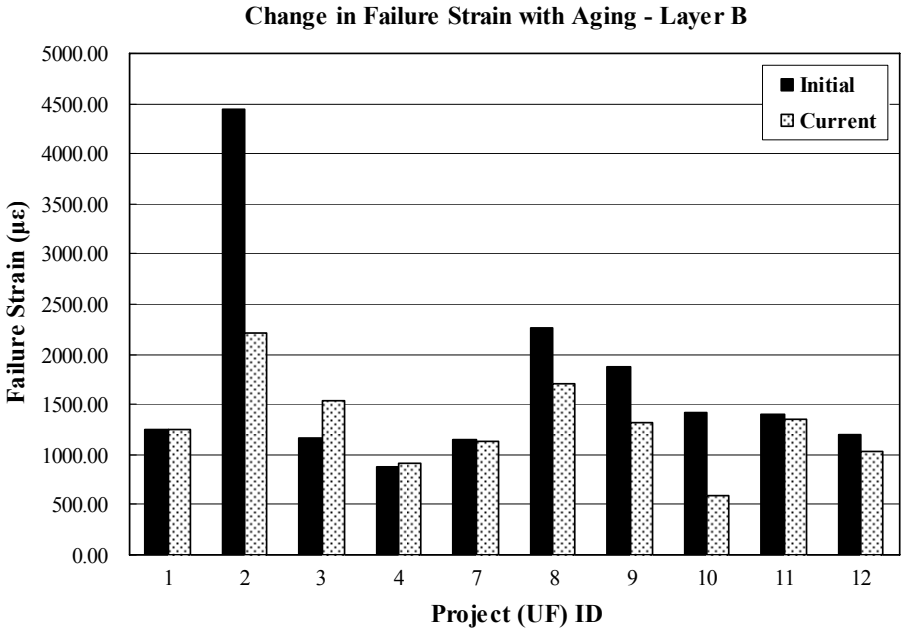

(b) Layer B

Figure 4-13 Change in failure strain over time

Fracture energy reflects the mixture's resistance to damage without fracturing. It has been identified as a good indicator of cracking performance of asphalt pavements having similar pavement structure, traffic and environmental condition. Fracture energy results for the eleven Superpave projects are presented in Figure 4-14. As expected, fracture energy has decreased over time. This observation was the basis for the fracture energy aging model introduced in the NCHRP Project 01-42A.

Based on the results shown in Figure 4-14, it seems clear that higher initial FE results in higher rate of reduction in FE with aging. Also, the top layers exhibited relatively higher rates of reduction in FE than the bottom layers for most projects. However, the rate of reduction in FE for projects showing evidence of moisture damage (Project 9, 10, 11 and 12) exhibited unusually high rates of reduction in FE regardless of the initial FE magnitude and layer depth.

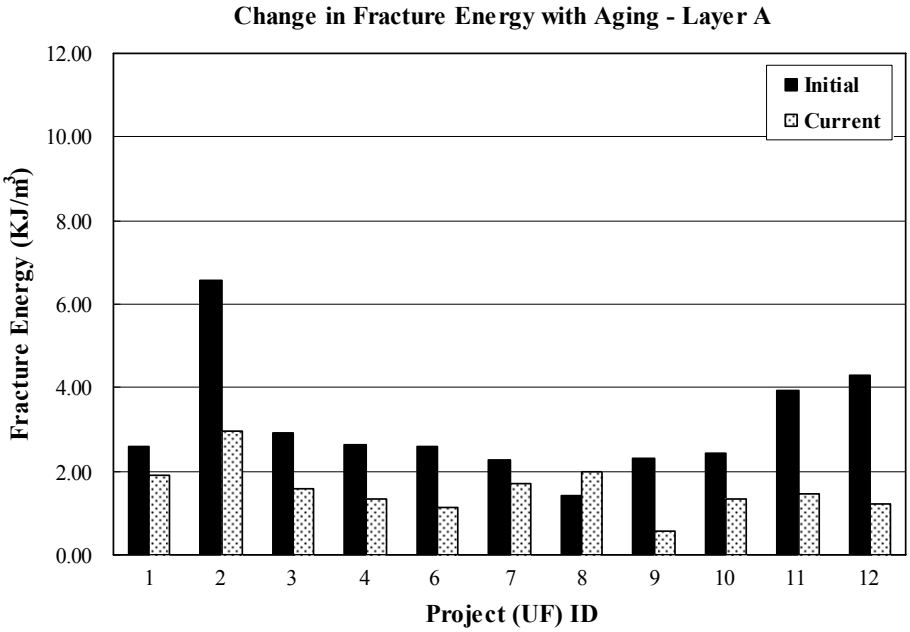

(a) Layer A

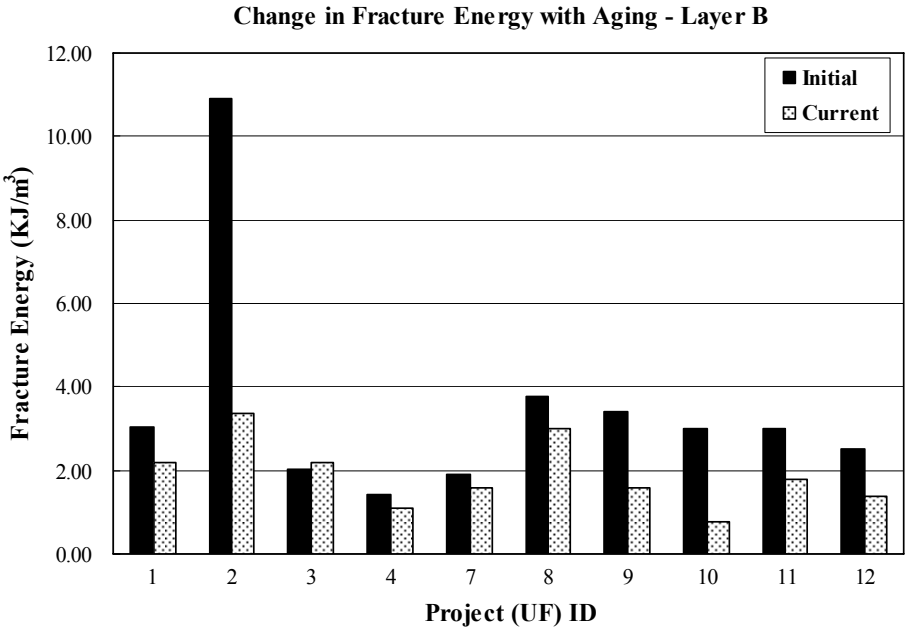

(b) Layer B

Figure 4-14 Change in fracture energy over time

4.5 Moisture-Damaged Projects

Moisture damage of asphalt mixture is a major distress mode that can result in significant costs for repair and rehabilitation. The effect of moisture on asphalt mixture involves various factors acting simultaneously including the effect of moisture susceptibility of asphalt mixture, stresses induced by traffic load, environmental condition, and moisture. Many researchers have tried to identify relationships between asphalt mixture properties and moisture (Schmidt and Graf, 1972; T. F. Fwa and C. B. Oh, 1995; Lottman, 1986). However, the mechanism and effect of moisture damage have not yet been fully identified or verified.

During the inspection process of the cores obtained, evidence of moisture damage was visually identified in the form of stripping for Project 9, 10, 11, and 12. Stripping was particularly prominent at the interface between top and bottom Superpave layers. These projects are relatively new pavements (six to seven years of age). Specifically, as shown in Table 4-10, use of granite aggregates was common to all moisture damaged projects. No moisture damage was observed for projects produced with limestone aggregate. Three of the four projects (Project 9, 10, and 12) had fine-graded mixtures with rubber modified binder (ARB-5) in the top layer and PG64-22 binder in the bottom layer. The fourth project had a coarse-graded mixture with SBS-modified binder in the top layer and PG64-22 binder in the bottom layer. Table 4-3 summarizes project information and the moisture damaged sections are highlighted.

Table 4-3 Project information for moisture-damaged projects

Project (UF) ID	Year Aged	Aggregate Type	Binder Type		Mixture Type		Traffic Level
			Top	Bottom	Top	Bottom	
1	11	Granite	AC-30	AC-30	9.5C	19.0C	D/5
2	11	Granite	AC-20	AC-20	12.5C	19.0C	D/5
3	11	Limestone	AC-30	AC-30	12.5C	19.0C	D/5
4	11	Limestone	AC-30	AC-30	9.5C	19.0C	E/6
6	12	Limestone	AC-20	N/A	12.5F	N/A	C/4
7	12	Limestone	AC-20	AC-20	12.5F	12.5F	C/4
8	9	Limestone	PG 76-22	PG 76-22	12.5C	12.5C	D/5
9	7	Granite	ARB-5	PG 64-22	FC-6	12.5F	C/4
10	7	Granite	ARB-5	PG 64-22	FC-6	12.5F	B/4
11	6	Granite	PG 76-22	PG 64-22	12.5C	12.5C	E/6
12	6	Granite	ARB-5	PG 64-22	FC-6	12.5F	C/4

Several unique trends were identified for moisture damaged sections with regard to the change in fracture energy and air voids over time. Relatively high initial and/or current air voids were measured on field cores obtained from layer A for Project 9 and 10. In some cases (Layer A of Project 9 and 11 and layer B of Project 9, 11, and 12), the air voids increased over time, which appears to be related to the displacement of material caused by moisture damage. Figure 4-15 shows the change in air voids for Superpave projects including layers A and B, respectively.

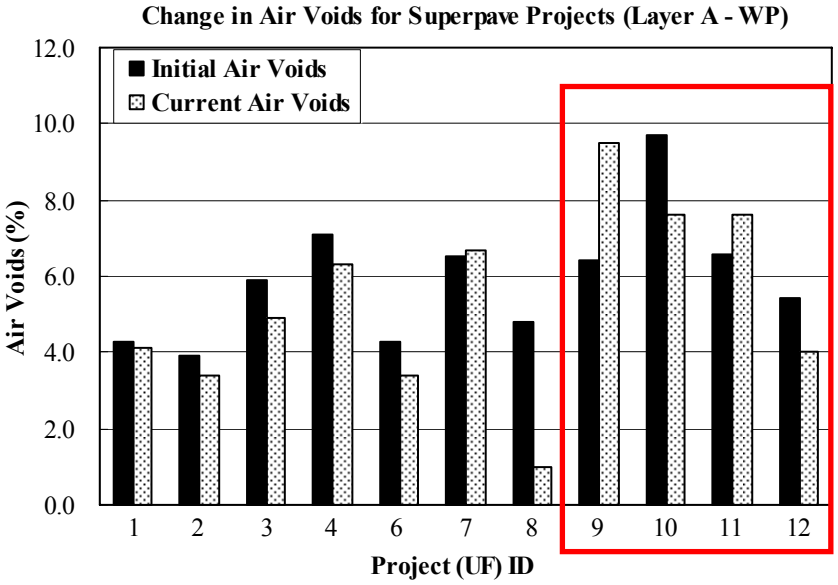

(a) Layer A

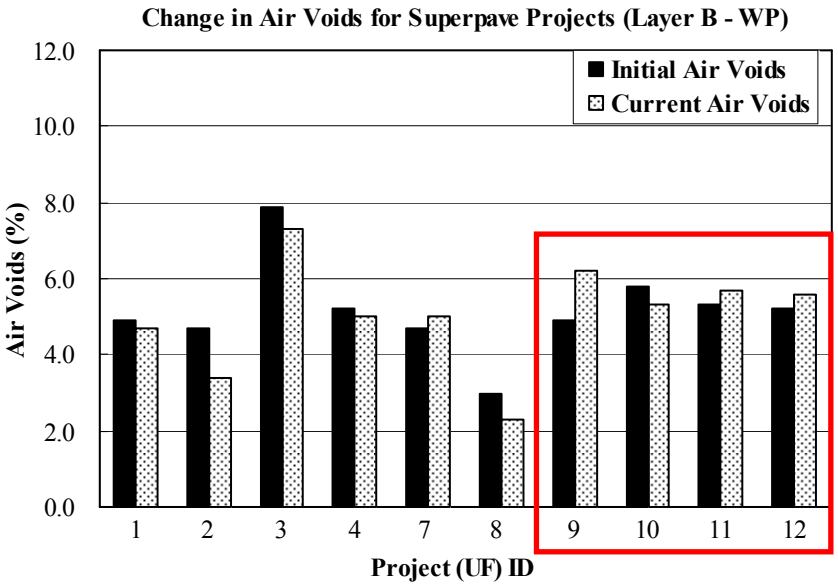

(b) Layer B

Note: "WP" denotes the "Wheel Path"
Figure 4-15 Change in air voids over time

In addition, as shown in Figure 4-16, much greater rate of reduction in normalized fracture energy was obtained for moisture damaged sections. Rate of reduction of normalized fracture energy over time was calculated to account for the difference in age between moisture damaged sections and other sections. Figure 4-16 shows the initial rate of reduction in normalized fracture energy for Superpave projects including layer A and B, respectively.

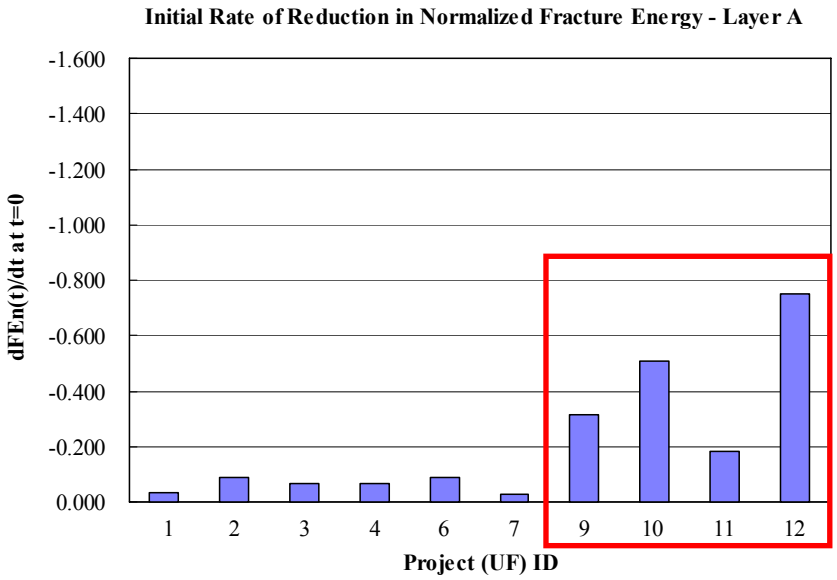

(a) Layer A

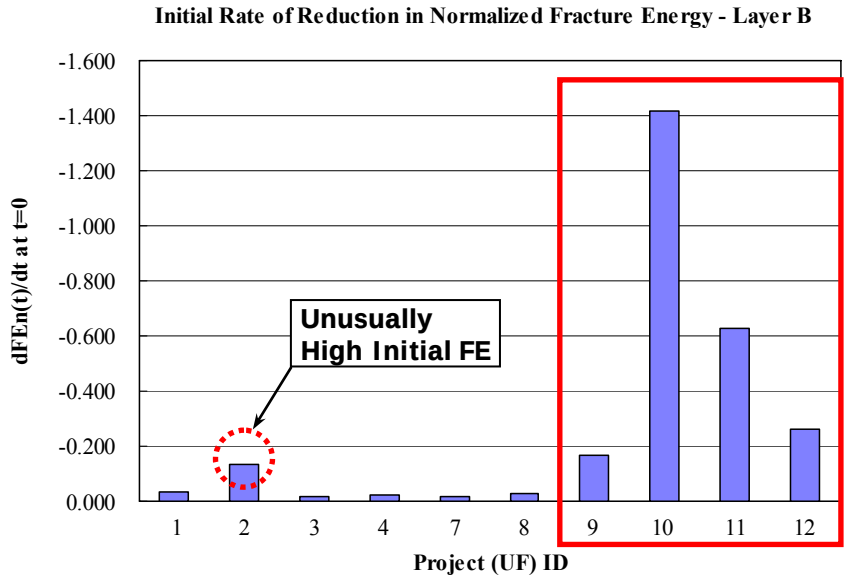

(b) Layer B

Note: $dFE_n(t)/dt$ at t=0 denotes the initial rate of reduction in normalized fracture energy
Figure 4-16 Initial rate of reduction in normalized fracture energy over time

Birgisson et al. (2004) indicated that the Energy Ratio (ER) can be used to evaluate the effect of moisture damage on changes in fracture resistance of asphalt mixtures. Figure 4-17 represents the initial rate of reduction in normalized ER for Superpave projects including layer A and B. Figure 4-17 clearly shows that a much greater reduction in normalized ER was observed in moisture damaged sections. In other words, the effect of moisture dramatically reduced the fracture resistance of asphalt mixtures, and the ER is capable of detecting the effect of moisture damage. Figure 4-17 clearly indicates that the ER is very sensitive to, and therefore able to capture the effects of moisture damage. As expected, high rate of reduction in normalized ER with aging was identified for moisture damaged sections.

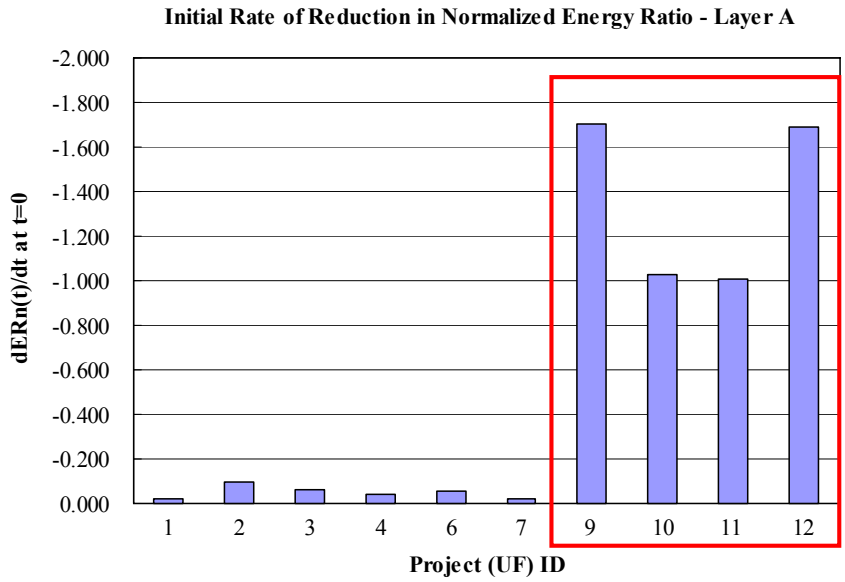

(a) Layer A

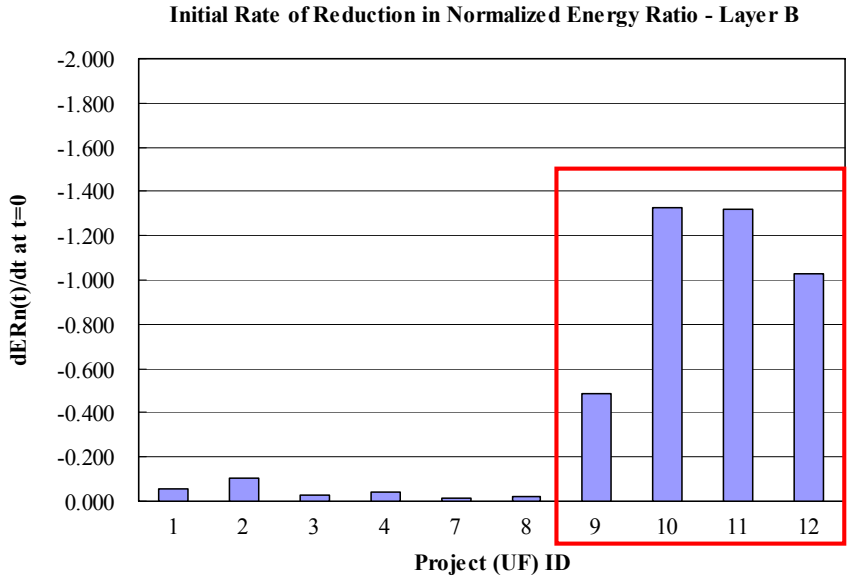

(b) Layer B

Note: $dER_n(t)/dt$ at t=0 denotes the initial rate of reduction in normalized energy ratio
Figure 4-17 Initial rate of reduction in normalized energy ratio over time

4.6 Closure

Mixture tests were performed on field cores using the Superpave IDT to determine key mixture properties and to identify the change in these properties as a function of age and environment in the field. Test results were analyzed for the eleven Superpave projects using the HMA fracture mechanics model. This information will be very useful to establish reasonable and effective mixture design guidelines, criteria, performance-related properties and parameters. It is also important for the identification of material property relations, material property prediction model evaluation, and for calibration and validation of pavement performance prediction models.

CHAPTER 5
EVALUATION OF FIELD MIXTURE PERFORMANCE USING DASR-IC (DOMINANT AGGREGATE SIZE RANGE-INTERSTITIAL COMPONENT) MODEL

5.1 Introduction

It is generally accepted that aggregate gradation is one of the most important factors that affect the properties and performance of asphalt mixtures. Having suitable gradation characteristics, including appropriate aggregate particle size distribution and resulting volumetric properties, is obviously an important component to ensure good field performance. Therefore, aggregate related parameters were studied to identify their effect on observed field performance of asphalt mixtures used in the Superpave projects.

Although many different parameters, including film thickness and other volumetric parameters, have been extensively evaluated to assess their effect on mixture performance, consensus has not been reached regarding rational design guidelines, especially as related to the selection of the best aggregate blend to achieve optimal performance.

Previous work conducted by the University of Florida has concluded that two gradation parameters, DASR porosity and disruption factor (DF), appear to be good tools for evaluating potential mixture performance (Roque et al., 2006; Guarin, 2009). Two other parameters, effective film thickness (EFT) and ratio between coarse portion of fine aggregate and fine portion of fine aggregate (CFA/FFA), were identified in this study to better capture the effects of the interstitial component (IC) on mixture properties and expected performance. The Dominant Aggregate Size Range – Interstitial Component (DASR-IC) Model has been developed based on

the parameters introduced above named as the DASR-IC parameters to describe the characteristics of gradation and resulting volumetric properties of asphalt mixtures.

This chapter will deal with the evaluation of mixture performance mainly on the basis of the DASR-IC model formed, including the gradation parameters developed and any other component material properties and characteristics, to determine whether any clear patterns emerge between these factors and performance for the different Superpave mixtures in Florida. This evaluation also served as a quality check on the input data to be included in the performance model prediction and identification of material property relations by identifying the performance differences that may have been caused by anomalies in any of these factors.

5.2 Characterization of Mixture Gradation (DASR-IC Model)

Recent research conducted by the UF research team has concluded that gradation characteristics of mixture can be expressed by separating the gradation into two major components: Dominant Aggregate Size Range (DASR) and Interstitial Component (IC). It has also been shown that parameters describing the characteristics of these components, which are determined based on packing theory and particle size distributions, seem to be well correlated to mixture performance. The work has clearly shown that characteristics of both the coarse (DASR) and fine (IC) portion of mixture gradation play a major role on mixture performance. A new parameter associated with the IC called the Disruption Factor (DF) was developed as part of this study to determine the potential effect of the finer portion of the mixture's gradation.

The following gradation DASR-IC model parameters were used in this study: DASR porosity, Disruption Factor (DF), Effective Film Thickness (EFT), and CFA/FFA. These parameters address the following three aspects of gradation, particularly as related to the characteristics of the IC:

- Volumetric distribution of IC: DASR porosity and Disruption Factor
- Property(Stiffness) of IC: Effective Film Thickness
- Composition of IC: CFA/FFA

Detailed descriptions of DASR-IC model components with regard to the definition and calculation procedure of each gradation parameters assigned are included in the next part of report.

5.2.1 Dominant Aggregate Size Range (DASR)

The concept and theoretical development of DASR which is defined as the interactive range of particle sizes that forms the dominant structural network of aggregate was introduced by Roque et al. (2006). According to the DASR approach, there is an interactive range of particle sizes that primarily contribute to aggregate interlocking in asphalt mixtures. Particle sizes interacting with each other will form the primary structure to resist deformation and fracture. Particle sizes smaller than the DASR will serve to fill the voids between DASR particles, called interstitial volume. The IC particles combined with binder form a secondary structure to help resist deformation and fracture, and it is the primary source of adhesion and resistance to tension. Particle sizes larger than the DASR will simply float in the DASR matrix and will not play a major role in the aggregate structure.

The DASR, which is determined by conducting particle interaction analysis based on packing theory, can be composed of one size or multiple sizes based on the interaction analysis. It has been concluded that the DASR should be composed of coarse enough particles, and that all

contiguous particle sizes determined to be interactive can be considered as a part of the DASR. The schematic of this concept for three different types of mixture is illustrated in Figure 5-1.

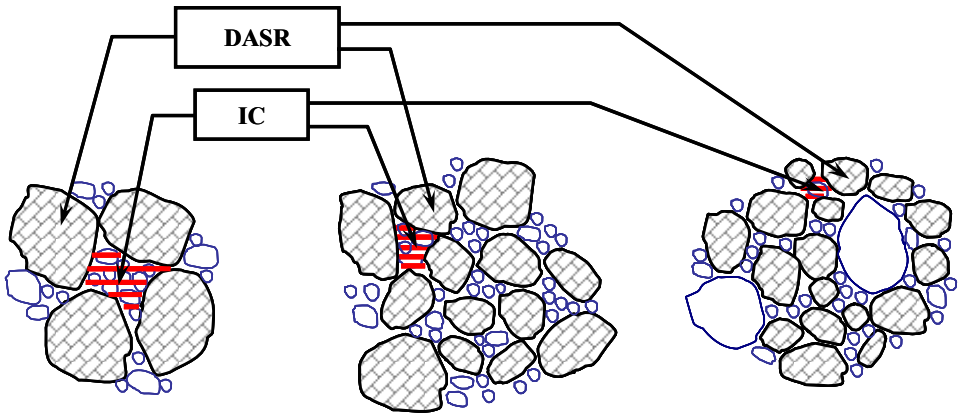

(a) SMA Mixture (b) Coarse Dense Mixture (c) Fine Dense Mixture

Figure 5-1 DASR and IC for three different types of mixture

5.2.2 DASR Porosity

Porosity has been widely used in the field of soil mechanics as a dimensionless parameter that indicates the relative ratio of voids to total volume. It has been determined that the porosity of granular materials should be no greater than 50 % for particles to have contact with each other (i.e. to be interactive). Thus, porosity can be used as a criterion to ensure contact between DASR particles within the asphalt mixture to provide adequate interlocking and resistance to deformation and fracture.

The basic principles related to the calculation of DASR porosity are as follows. The VMA of asphalt mixtures, which indicates the volume of available space between aggregates in a compacted mixture, is comparable to volume of voids in soil. Porosity can be calculated for any DASR by assuming that a mixture has a certain effective asphalt content and air voids (i.e.

VMA) for a given gradation. Finally, DASR porosity can be calculated by subtracting the volume of particles bigger than DASR from the total volume of mixture as shown in Figure 5-2.

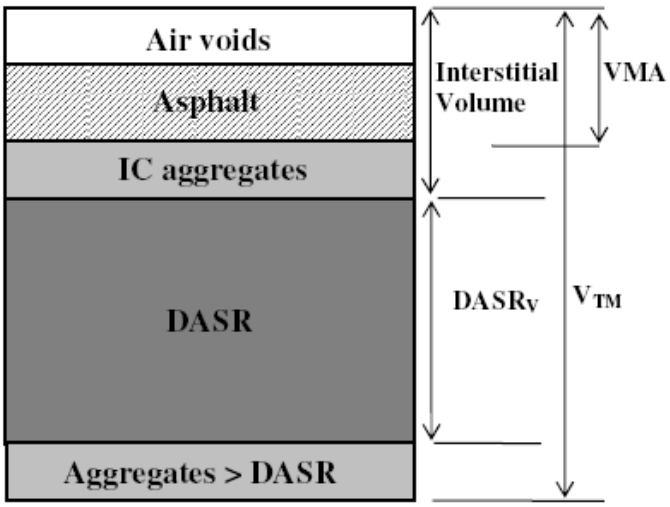

Figure 5-2 Mixture components for calculation of DASR porosity

The equations for calculating the DASR porosity are shown below.

$$V_{T(DASR)} = V_{TM} - V_{AGG>DASR} \tag{5-1}$$

$$V_{V(DASR)} = V_{ICAGG} + VMA \tag{5-2}$$

$$\eta_{DASR} = \frac{V_{V(DASR)}}{V_{T(DASR)}} = \frac{V_{ICAGG} + VMA}{V_{TM} - V_{AGG>DASR}} \tag{5-3}$$

Where, η_{DASR} = DASR porosity, $V_{V(DASR)}$ = Volume of voids within DASR, $V_{T(DASR)}$ = Total volume available for DASR particles, V_{ICAGG} = Volume of IC aggregates, VMA = Voids in Mineral Aggregate, V_{TM} = Total volume of mixture, and $V_{AGG>DASR}$ = Volume of particles bigger than DASR.

A maximum porosity of 50 % was selected as a criterion for the evaluation of asphalt mixture. DASR porosity should be less than 50 % for particles to be in a contact with each other. Prior work has indicated that DASR porosity should also be greater than a certain value in order to have good mixture performance.

5.2.3 Interstitial Component (IC) of Mixture Gradation

As illustrated in Figure 5-1, interstitial component is the material including asphalt, aggregate, and air voids that exists within the interstices of the DASR, and the volume of this material is considered as the interstitial volume (IV). Previous work conducted by the UF research team has concluded that the properties and characteristics of the IC will strongly influence the rutting and cracking resistance of asphalt mixtures.

The IC should fill the voids within the aggregates larger than the IC without disrupting the DASR structure. As the DASR-IC Model assumes that the particles bigger than the DASR are floating in the DASR structure, it would be reasonable to accept that the effect of the DASR voids structure could be utilized to evaluate the total voids structure for the IC including the particles bigger than the DASR. Information on the IC characteristics is fundamental to understand and predict how the IC will fit into the IV and consequently to determine whether the DASR structure would be disrupted by the IC. This is important because it will define if the DASR system is disrupted by the IC. Another parameter, disruption factor (DF), which will be introduced in the next part of this chapter, was identified for this purpose. The characteristics of the IC are expected to have a strong influence on key mixture properties including fracture energy and creep rate as well as their trend of change with aging. Therefore, it was expected that DF and other IC parameters would correlate well with the mixture performance including rutting

and cracking. It was also hypothesized that IC parameters would be useful to predict mixture properties and their changes with aging.

5.2.4 Disruption Factor (DF)

A new parameter called the Disruption Factor (DF) was conceived and developed as a part of this study to determine the potential of the finer portion of the mixture's gradation to disrupt the DASR structure. It has been shown in laboratory studies that the DF can effectively evaluate the potential of IC particles to disrupt the DASR structure. DF can be calculated by using the following equation.

$$DF = \frac{Volume\,of\ \ potentially\,distuptive\,IC\ particles}{Volume\,of\ \ DASR\,voids} \tag{5-4}$$

The range of potentially disruptive IC particles includes both IC particles bigger than the volume of DASR voids and smaller than the smallest DASR particle size. Volume of potentially disruptive IC can be calculated using the following equation.

$$Volume\,of\ \ potentially\,disruptive\,IC\ particles = \frac{Weight\,of\ \ potentially\,disruptive\,IC\ particles}{G_{sb}} \tag{5-5}$$

Where, G_{sb} = Bulk specific gravity of the overall combined aggregate blend.

The number of DASR particles can be calculated by using the equation (5-6) on the basis of the density of DASR particles, G_{sb}, and the volume of the weighted average DASR particle size by assuming spheres.

$$Number\ of\ DASR\ particles = \frac{Weight\ of\ DASR\ particles}{Volume\ of\ weighted\ average\ DASR\ particle \times G_{sb}} \quad (5\text{-}6)$$

DASR void size and number of voids can be estimated based on DASR packing and number of DASR particles, then DASR void volume can be calculated as a function of DASR void size using equation (5-7). Table 5-1 tabulates the average void size based on Bailey Method.

$$Volume\ of\ DASR\ voids = Number\ of\ DASR\ voids \times DASR\ void\ volume \quad (5\text{-}7)$$

Table 5-1 Average void size based on Bailey method

Smallest DASR particle size		0.22 × sieve size	Average voids size	
Sieve size (in)	Sieve size (mm)		Sieve size (in)	Sieve size (mm)
3/8”	9.500	2.09	#8	2.360
#4	4.750	1.045	#16	1.180
#8	2.360	0.519	#30	0.600
#16	1.180	0.260	#50	0.300

Roque et al. (2009) identified the existence of an optimal DF range to attain better rutting and cracking performance of asphalt mixture. Figure 5-3 is a conceptual figure representing the configuration for different DF values including the case of low, optimal, and high DF values.

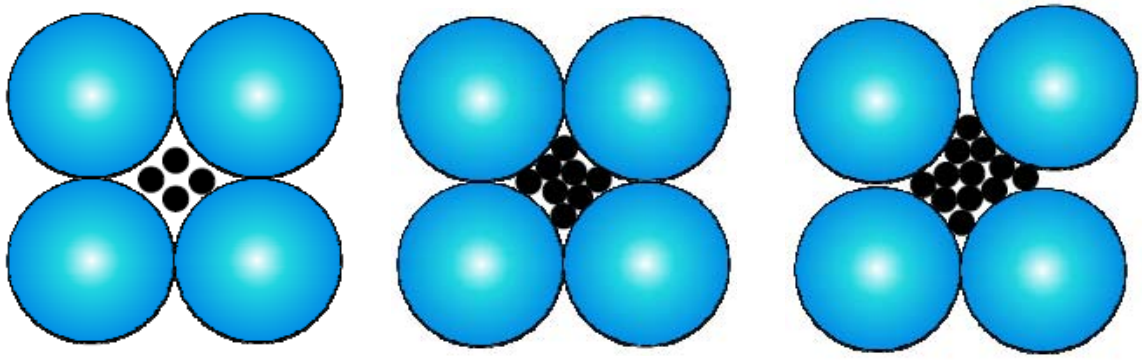

(a) DF < Optimal DF Range (b) DF = Optimal DF Range (c) DF > Optimal DF Range

Figure 5-3 Configurations of different DF values

According to the DF approach, the IC aggregates would not be involved in transmitting load between the DASR aggregates if the DF is too low. Consequently, the DASR structure would not take the potential advantage that could be provided by IC particles. In the case of high DF, mixture performance would be negatively affected because the DASR structure would be disrupted by the IC aggregates. Lastly, if the DF is in the optimal range, better mixture performance would be expected because the IC aggregates will be involved in resisting shear stresses for the DASR structure. Therefore, the DF appears to be one good indicator to describe the IC characteristics with respect to the volumetric distribution of IC, and a link between the DF and material properties which are related to the performance of asphalt mixtures was expected.

5.2.5 Effective Film Thickness (EFT)

Film thickness of asphalt mixture has been used to help explain aging phenomena and many researchers attempted to evaluate the relationship between the film thickness and mixture performance. Kandhal and Chakraborty (1996) have showed that this parameter can be utilized as an indicator to characterize the durability and fatigue resistance of asphalt mixtures using various types of mixtures with different range of film thicknesses. However, it is still controversial with regard to its application in mix design of HMA. The Superpave system does not include any requirements or guidelines regarding film thickness.

Typically, apparent film thickness (or standard film thickness) which is calculated by dividing the effective binder volume by the specific surface of the aggregate has been used for film thickness analysis. However, many researchers have been opposed to this term because "film thickness" does not really exist in asphalt mixture. Nukunya et al. (2001) introduced a new concept of effective film thickness (EFT) which can be calculated by using the effective volumetric properties of asphalt mixture. They concluded that the effective volumetric properties

including the EFT seem to effectively evaluate and control the aging effect and mixture properties.

In this study, the EFT has been selected as one parameter to act as a surrogate to the stiffness of the interstitial component. The EFT can be calculated by using the following equation.

$$EFT\,(microns) = \frac{V_{be}}{SA \cdot W_T \cdot PF_{AGG}} = \left[\frac{Pb - (Abs/100) \cdot P_{AGG}}{SA \cdot PF_{AGG} \cdot Gb}\right] \times 1000 \quad (5\text{-}8)$$

Where, V_{be} = Effective volume of asphalt binder, SA = Surface area of fine aggregate, W_T = Total weight of mixture, PF_{AGG} = Percent fine aggregate by mass of total mixture, P_b = Asphalt content percent by mass of total mixture, Abs = Absorption, P_{AGG} = Percent aggregate by mass of total mixture, and G_b = Specific gravity of asphalt binder.

5.2.5.1 Film Thickness Effect

Adequate interstitial volume is important for mixtures to have sufficient strain tolerance, which can be controlled by having an acceptable range of effective film thickness (EFT). EFT of asphalt mixtures is related to the behavior of the IC. The fineness of the IC aggregate is the primary factor controlling the EFT.

Two parameters related to the IC behavior were evaluated: effective film thickness (EFT) and effective binder content (EAC). In addition, these parameters were used to establish prediction models for properties of asphalt mixtures. EAC and EFT are associated with the time-dependent response and brittleness of asphalt mixture. For example, higher EFT results in higher creep rate and higher fracture energy. Figure 5-4 shows a schematic that conceptually illustrates how EFT affects mixture properties for two cases which have same component materials.

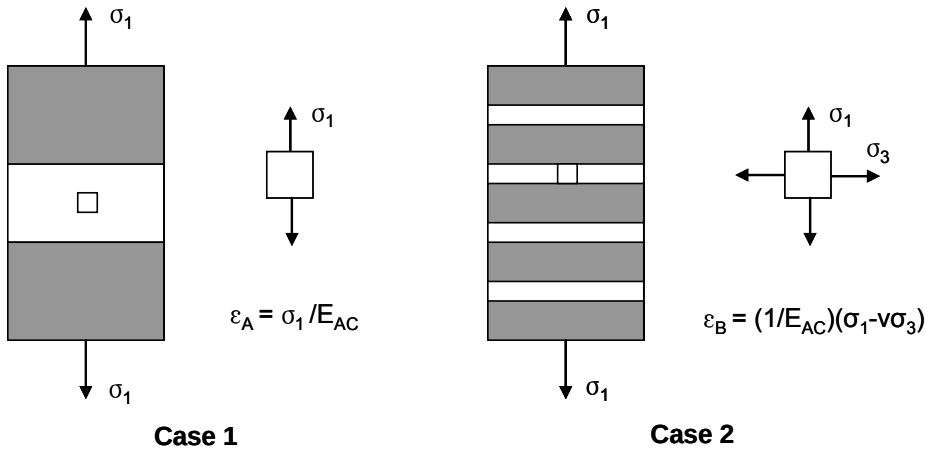

Note: Then $\varepsilon_A > \varepsilon_B$, therefore, $E_A < E_B$
Figure 5-4 Conceptual drawing of film thickness effect

The white color portion of Figure 5-4 represents the asphalt binder part, while the gray color portion represents the aggregate. In the case of thicker effective film thickness represented by case 1, it is expected that material will tolerate higher strain (less brittle) than the thinner effective film thickness (Case 2), that will tolerate less strain and failed in a brittle manner.

5.2.6 CFA/FFA

Preliminary analyses performed by the research team indicated that the fineness of fine aggregate portion was strongly related to the effective film thickness. Therefore, a new parameter CFA/FFA, which is the ratio between coarse portion of the IC and fine portion of the IC, was introduced to characterize the composition of interstitial component of mixture gradation. The CFA/FFA was used as an indicator to represent the fineness of the IC. It was hypothesized that CFA/FFA was related to the creep response or time-dependent response of asphalt mixture. Figure 5-5 describes the basic principles of determining the CFA/FFA.

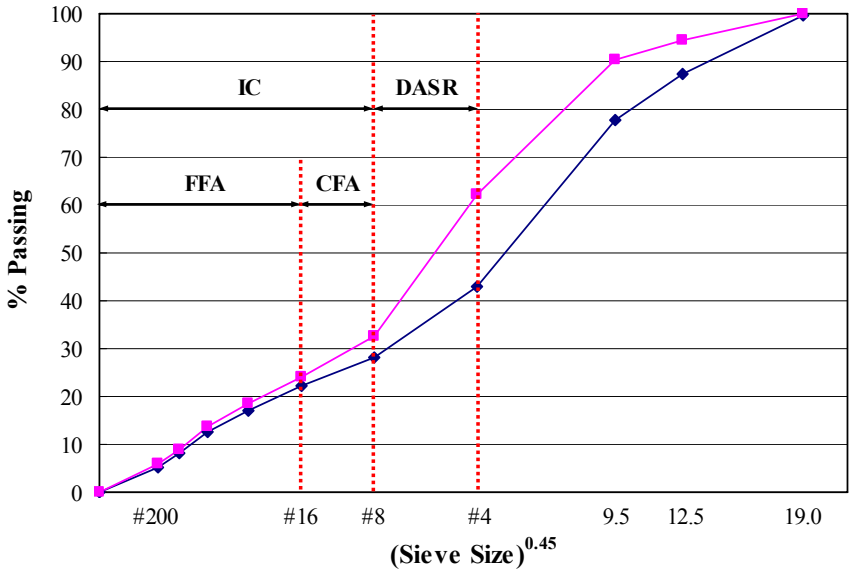

Figure 5-5 Determination of CFA/FFA

5.3 Gradation Analysis Results for Superpave Projects

Gradation Analysis was conducted for all mixtures from the eleven Superpave projects using the in-place gradations. All mixtures analyzed include top and bottom layers denoted as layers A and B. Table 5-2 shows the mixture information of Superpave projects analyzed.

Table 5-2 Mixture information of Superpave projects

Project (UF) ID	Aggregate Type	Binder Type		Mixture Type*	
		Top	Bottom	Top	Bottom
1	Granite	AC-30	AC-30	9.5C	19.0C
2	Granite	AC-20	AC-20	12.5C	19.0C
3	Limestone	AC-30	AC-30	12.5C	19.0C
4	Limestone	AC-30	AC-30	9.5C	19.0C
6	Limestone	AC-20	N/A	12.5F	N/A
7	Limestone	AC-20	AC-20	12.5F	12.5F
8	Limestone	PG 76-22	PG 76-22	12.5C	12.5C
9	Granite	ARB-5	PG 64-22	FC-6	12.5F
10	Granite	ARB-5	PG 64-22	FC-6	12.5F
11	Granite	PG 76-22	PG 64-22	12.5C	12.5C
12	Granite	ARB-5	PG 64-22	FC-6	12.5F

* Mixture Type: C = Coarse mixtures, F = Fine mixtures, N/A = Not applicable

Gradation parameters, including the DASR porosity, DF, EFT, and CFA/FFA were calculated by using the in-place gradation and mixture volumetric properties for each project. Table 5-3 and 5-4 summarize all gradation parameters calculated, and DASR for Superpave projects layer A and B, respectively. Detailed descriptions of gradation analysis results for each project are included in below, including a brief introduction of material composition used for each layer, gradation characteristics, evaluation of gradation parameters calculated and material property characteristics.

Table 5-3 Gradation parameters calculated for Superpave projects – Layer A

Project (UF) ID	DASR (mm)	DASR Porosity (%)	DF	EFT (Microns)	CFA/FFA
1	4.75 – 1.18	48.0	0.64	19.5	0.31
2	4.75	60.2	1.02	37.1	0.60
3	4.75 – 2.36	43.8	0.52	23.5	0.35
4	4.75 – 2.36	47.5	0.56	32.5	0.46
6	4.75 – 1.18	56.2	0.92	13.7	0.29
7	9.5 – 1.18	50.2	0.86	12.7	0.30
8	4.75 – 2.36	48.8	0.60	28.3	0.42
9	4.75 – 1.18	51.0	0.69	15.2	0.29
10	9.5 – 1.18	50.3	0.71	14.4	0.31
11	4.75 – 1.18	40.6	0.56	24.8	0.39
12	4.75 – 1.18	61.3	0.76	30.4	0.24

Table 5-4 Gradation parameters calculated for Superpave projects – Layer B

Project (UF) ID	DASR (mm)	DASR Porosity (%)	DF	EFT (Microns)	CFA/FFA
1	4.75 – 2.36	46.0	0.51	26.9	0.30
2	4.75	60.2	1.05	45.4	0.70
3	4.75 – 1.18	35.0	0.43	25.6	0.38
4	4.75 – 2.36	41.9	0.28	36.7	0.36
6	N/A	N/A	N/A	N/A	N/A
7	9.5 – 1.18	49.1	0.95	14.3	0.29
8	4.75 – 2.36	43.8	0.57	26.1	0.36
9	4.75 – 1.18	53.2	0.70	15.7	0.24
10	4.75 – 1.18	69.3	1.09	18.7	0.33
11	4.75 – 1.18	37.9	0.51	22.8	0.34
12	4.75 – 1.18	50.9	0.70	17.4	0.26

Project 1 was constructed with two layers of asphalt mixture. Layer A was composed of 9.5 mm coarse-graded Superpave mixture using granite aggregate, and Layer B was 19.0 mm coarse-graded Superpave mixture also using granite aggregate. AC-30 binder was used for both Layers A and B. According to the gradation analysis results, both Layers A and B of Project 1 exhibited continuous gradation pattern with good interaction within the DASR structure. All gradation parameters were within the acceptable range. Mixture test results indicated that initial fracture energy and creep rate were in a range associated with good-performing mixtures.

Project 2 was constructed using two coarse-graded Superpave mixtures comprised of 12.5 mm and 19.0 mm for Layers A and B, respectively. Granite aggregate was used with AC-20 binder for both layers. Project 2 had the highest amount of RAP (35 % for both layers) among all Superpave projects evaluated. Both Layers A and B of Project 2 exhibited high values of DASR porosity and DF with poor interaction within the DASR structure. In addition, uncommonly high effective film thickness and CFA/FFA were identified for both layers. It appears that the gradation characteristics mentioned above result in the unusually high initial fracture energy and creep rate measured by mixture tests.

Project 3 was constructed with two coarse-graded Superpave mixtures composed of 12.5 mm and 19.0 mm for Layers A and B, respectively. Limestone aggregate was used along with AC-30 binder for both layers. As with Project 1, Project 3 also exhibited a continuous gradation with good interaction within the DASR structure. Gradation parameters for Layer A were within the acceptable range. Mixture test results indicated that initial fracture energy and creep rate were in a range associated with good-performing mixtures. However, relatively low DASR porosity and DF was identified for Layer B, which appears to explain the lower initial fracture energy of Layer B.

Project 4 was constructed with two coarse-graded Superpave mixtures, including 9.5 mm and 19.0 mm for Layers A and B, respectively. Limestone aggregate was used with AC-30 binder for both layers. Layers A and B of Project 4 exhibited different gradation analysis results and initial mixture property magnitude. Layer A had an acceptable DASR porosity and DF, but also had unusually high effective film thickness (EFT), CFA/FFA and effective asphalt content (EAC). Layer A exhibited relatively high initial creep rate, which appears to be associated with the high EFT and CFA/FFA along with the high EAC. Layer B had an acceptable range of DASR porosity, but had a low DF, indicating that the IC aggregates would not be involved in transmitting load between the DASR aggregates. Therefore, it appears that the low DF is primarily responsible for the unusually low initial fracture energy for this layer.

Project 6 was constructed with one layer (Layer A) of Superpave mixture. A 12.5 mm fine-graded mixture was used along with AC-20 asphalt binder. Limestone aggregate was used with 20 % of RAP for this section. Based on the gradation analysis results, Project 6 had high DASR porosity and relatively high DF, indicating potentially poor mixture performance. In fact,

relatively poor field performance for both rutting and cracking has been identified based on the PCS data and field investigation.

Project 7 was constructed with two fine-graded Superpave mixtures composed of 12.5 mm for both Layers A and B. Limestone aggregate and 20 % RAP was used with AC-20 binder for both layers. Both Layers A and B of Project 7 exhibited continuous gradations with good interaction within the DASR structure. Results of gradation analysis exhibited marginal DASR porosity with DF within the acceptable range. Acceptable values of initial fracture energy and creep rate magnitude were determined from mixture tests.

Project 8 was constructed with two coarse-graded Superpave mixtures, including 12.5 mm for both Layers A and B. Limestone aggregate was used along with an SBS modified binder. Both Layers exhibited continuous gradations with good interaction within the DASR structure. According to the gradation analysis results, marginal DASR porosity with DF within the acceptable range was observed for both Layers. Project 8 mixtures exhibited relatively high EFT and CFA/FFA which may be associated with high damage rates. However, mixture test results indicated that initial creep rate magnitude was within range considered acceptable. This was probably due to the beneficial effect of polymer modification. More details regarding material property relations will be introduced in Chapter 6.

Project 9 through 12 were categorized as unusual projects from the standpoint of gradation effects and material property relations because evidence of moisture damage was observed. Results of gradation analysis for these sections are included in the Table 5-3 and 5-4. Also, results of performance evaluation for both cracking and rutting are included along with normal projects. However, moisture damaged sections have to be dealt with differently from

other sections for the performance evaluation. Therefore, moisture damaged sections, Project 9, 10, 11 and 12, were excluded from performance evaluation in this study.

5.4 Effect of Gradation Characteristics on Mixture Performance

Seven Superpave project sections in Florida were evaluated to identify effects of gradation characteristics on field performance, including cracking and rutting. Field rutting and cracking performance data were collected as indicated in Chapter 2. Also, the results of gradation analysis, including DASR porosity, DF, EFT, and CFA/FFA, were used as gradation parameters for the evaluation.

5.4.1 Field Performance: Rutting

A comprehensive monitoring of field rutting performance was conducted for Superpave projects from construction throughout the pavement's life. Field rut depth measured from transverse profilograph was used for the evaluation. As the indicator of rutting performance evaluation, the results are presented in terms of rut depth per ESALs (inch/ESALs$\times 10^6$) to normalize the effect of traffic volume between the different project sections. In addition, the rut depth/ESALs at 2 years values were used for analysis in order to account for the fact that the rate of rutting generally decreases with time. Figure 5-6 shows the rut depth/ESALs at 2 years for the Superpave projects evaluated.

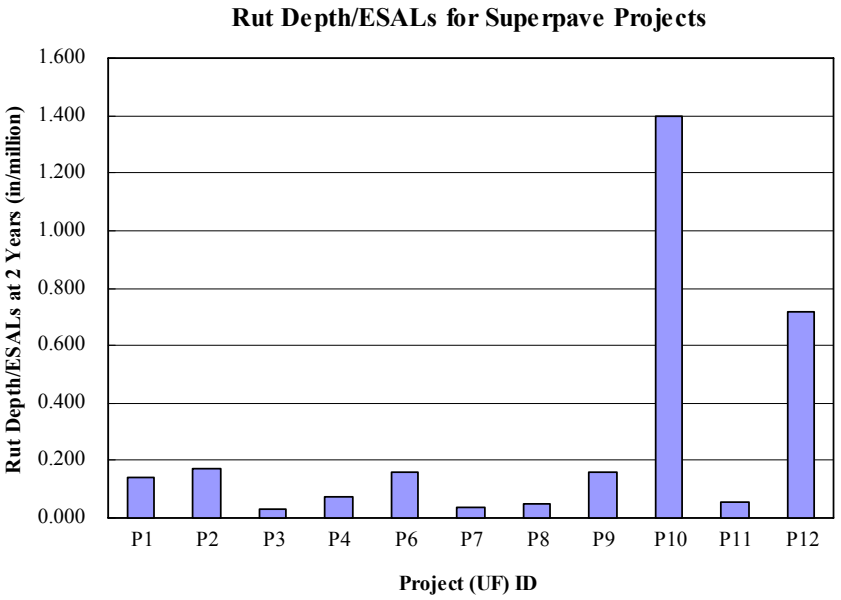

Figure 5-6 Rut Depth/ESALs for Superpave projects

All project sections were divided into three groups based on the range of DASR porosity and DF calculated for performance evaluation. According to the reference ranges introduced in prior research, projects with DASR porosity less than 48 % were categorized as “Good” sections. Projects with DASR porosity between 48 % and 52 % were grouped as “Marginal” and projects with DASR porosity greater than 52 % were considered “Bad.”

For the DF, projects with DF less than 0.60 were grouped as “Low,” and projects with DF greater than 0.90 were grouped as “High.” Projects with DF between 0.60 and 0.90 were categorized as “Good.” Figure 5-7 and 5-8 show the rut depth/ESALs for three groups of mixtures analyzed using two gradation parameters, DASR porosity and DF, respectively.

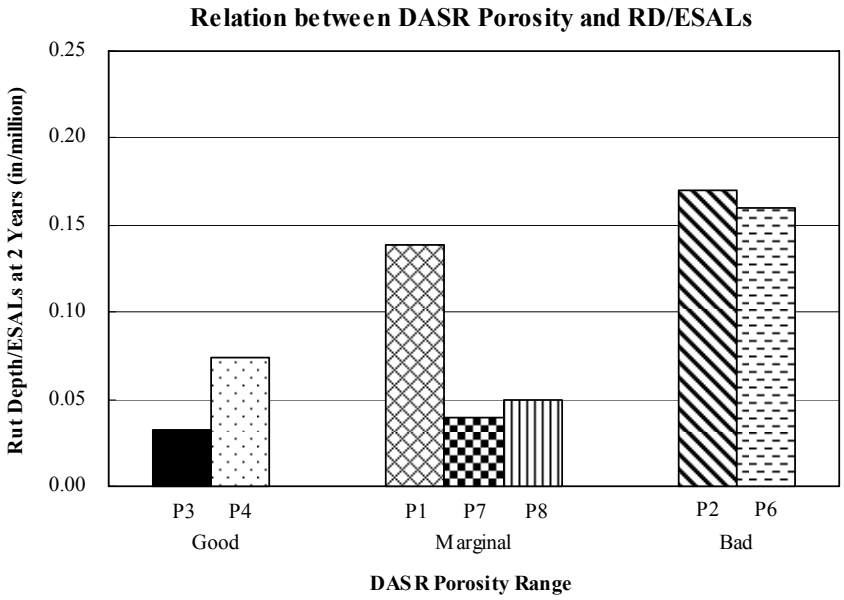

(a) Normal projects

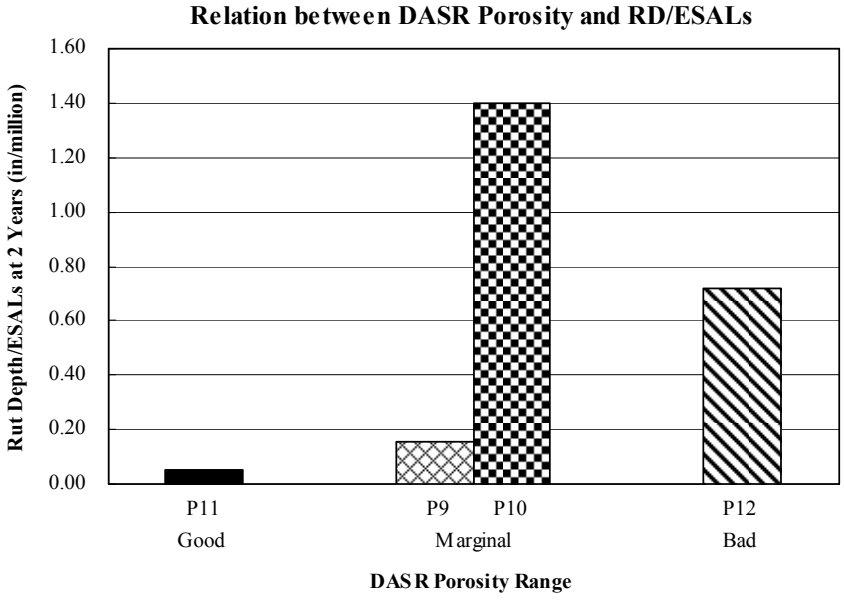

(b) Moisture-damaged projects

Figure 5-7 Rut Depth/ESALs for different groups of DASR porosity

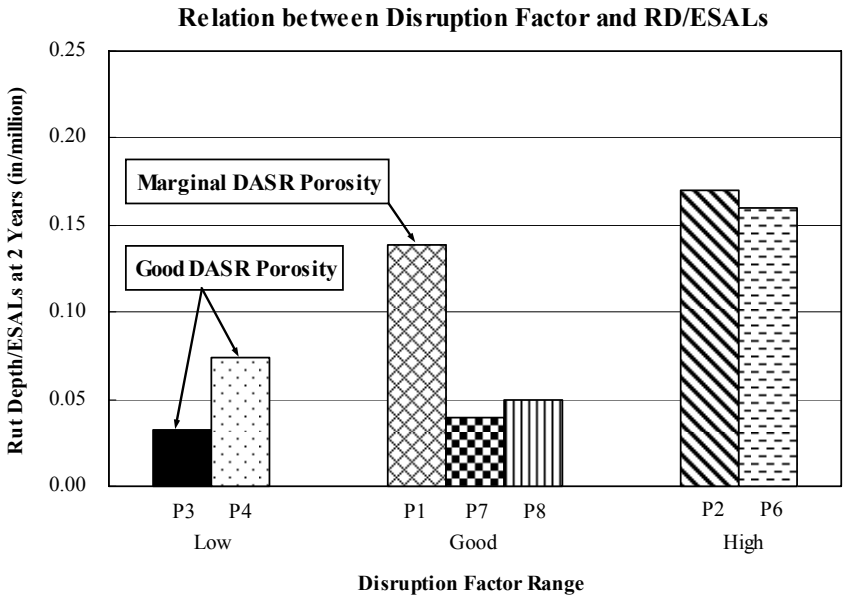

(a) Normal projects

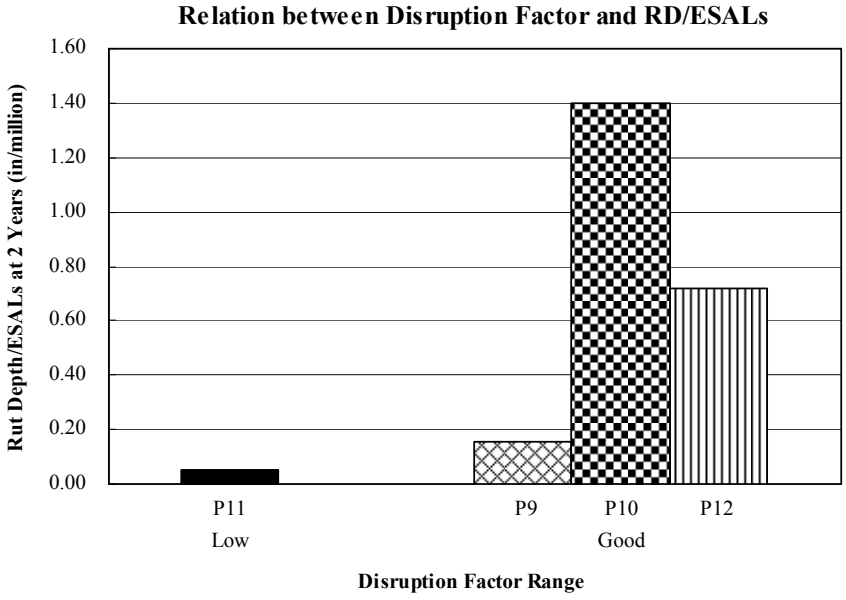

(b) Moisture-damaged projects

Figure 5-8 Rut Depth/ESALs for different groups of disruption factor

Figure 5-7 clearly indicates that the mixtures with good DASR porosity exhibited much lower rut depth/ESALs, which reflects good field rutting performance, than mixtures with high DASR porosity. For mixtures with marginal DASR porosity, it was noted that the mixtures could exhibit either good or bad rutting performance.

Based on the Figure 5-8, the range of DF appears to be correlated with DASR porosity. Mixtures with good range of DF exhibited lower rut depth/ESALs, which indicate the good rutting performance, except for Project 1. However, Project 1 had marginal DASR porosity, which appeared to result in relatively bad performance. Mixtures with high DF clearly exhibited high rut depth/ESALs.

However, Projects 3 and 4 exhibited good rutting performance, even though the DF was relatively low. Gradation analysis results indicate that these two sections had good DASR porosity with good interaction within the DASR structure. In summary, the characteristics of the coarse aggregate structure as reflected by the DASR porosity, appears to play a more significant role than the DF on rutting performance in the field. Therefore, a DASR porosity criterion appears to provide an effective tool that can accurately distinguish the relative field rutting performance of Superpave mixtures.

5.4.2 Field Performance: Cracking

Field cracking performance was also monitored for the Superpave projects from construction throughout the pavement's life. As the indicator of cracking performance evaluation, crack initiation time for each project was estimated by the process described in Chapter 2, which was based on data obtained from comprehensive field investigation conducted by the UF research team, and the crack rating history data from the pavement condition survey (PCS)

performed by the FDOT. Figure 5-9 represents the crack initiation time determined for the Superpave projects evaluated.

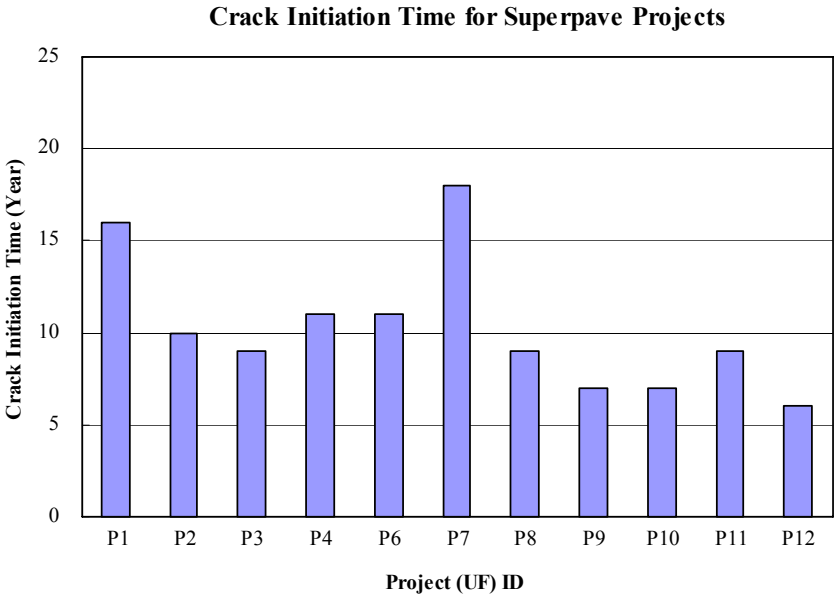

Figure 5-9 Crack initiation time for Superpave projects

As introduced in the rutting performance evaluation, all project sections were divided into three groups based on the range of DASR porosity and DF calculated for performance evaluation using the reference ranges introduced in prior research. Figure 5-10 and 5-11 show the crack initiation time for three groups of mixtures analyzed using the two gradation parameters, DASR porosity and DF, respectively.

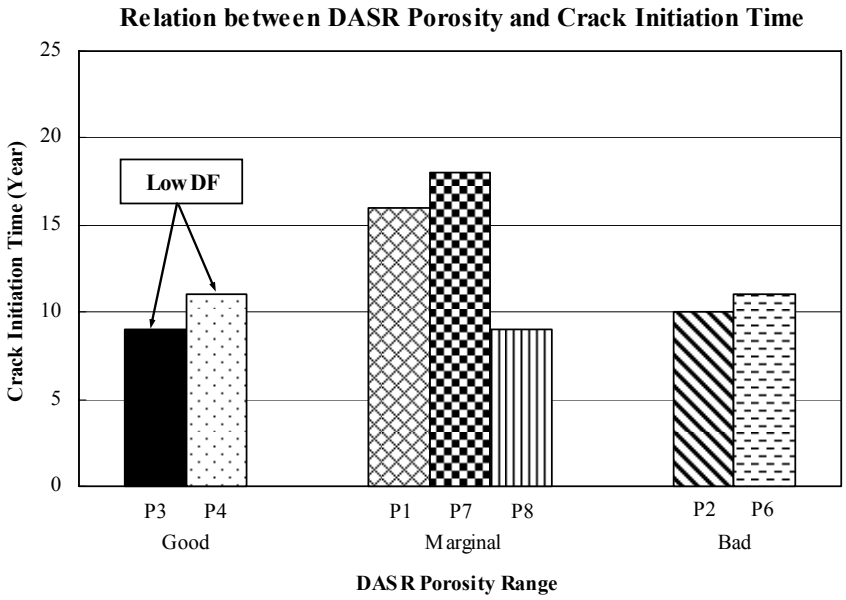

(a) Normal projects

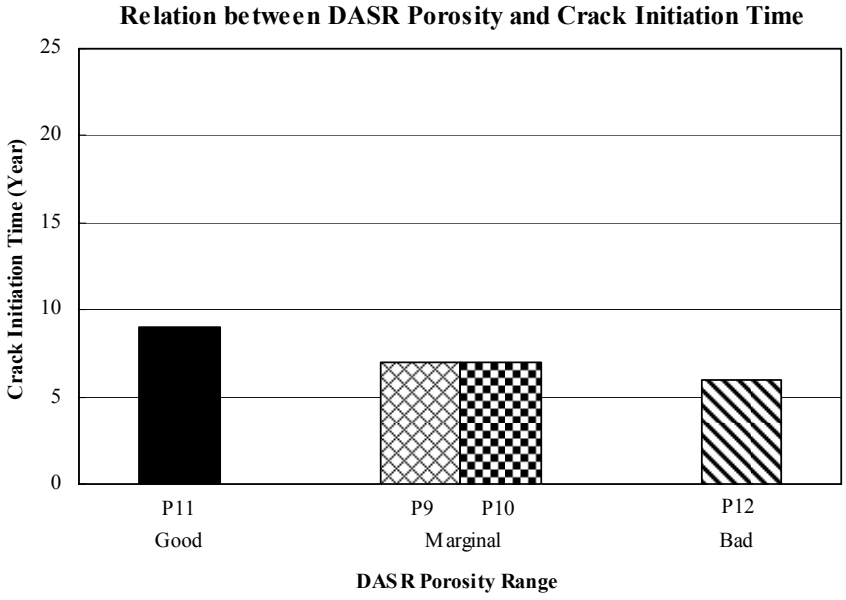

(b) Moisture-damaged projects

Figure 5-10 Crack initiation time for different groups of DASR porosity

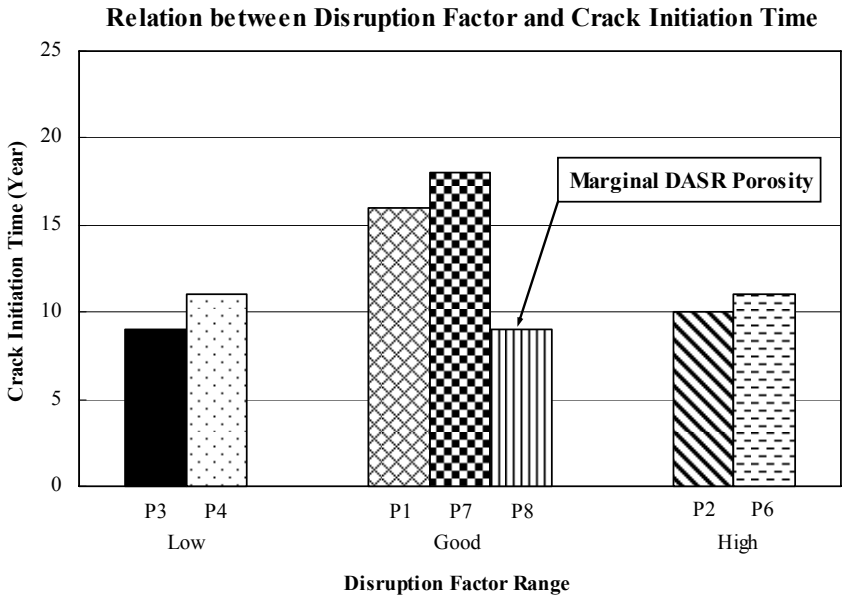

(a) Normal projects

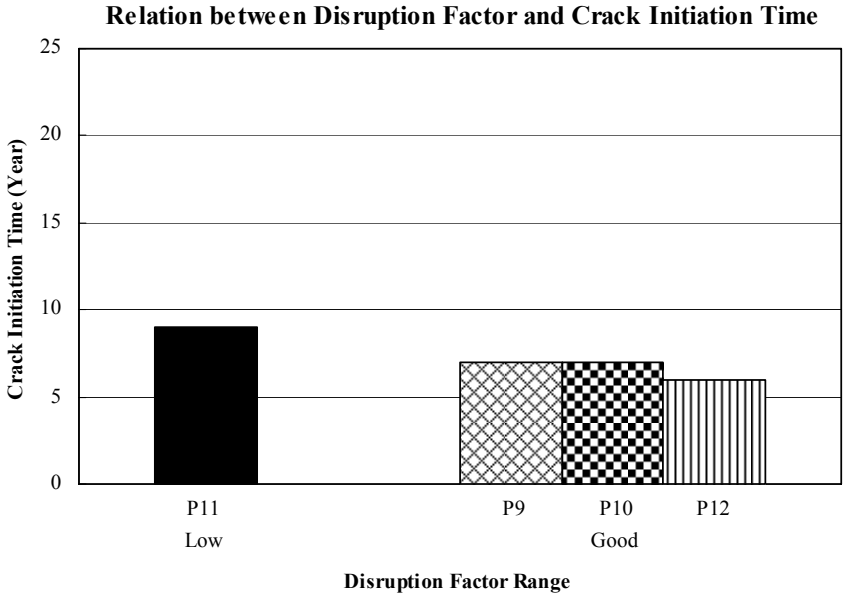

(b) Moisture-damaged projects

Figure 5-11 Crack initiation time for different groups of disruption factor

Based on the results in Figure 5-10 and 5-11, the mixtures with good range of DF exhibited relatively longer times to crack initiation, except the Project 8, which had marginal DASR porosity. It is expected that the effect of marginal DASR porosity is probably associated with earlier crack initiation time for Project 8. The mixtures with the either low or high DF represent shorter crack initiation time.

On the basis of field cracking performance evaluation, the existence of an acceptable range of DF was identified to achieve better performance. The DASR porosity alone does not appear to clearly differentiate field cracking performance. It appears that the DF criterion combined with DASR porosity criterion may effectively distinguish the relative field cracking performance of Superpave mixtures.

5.5 Closure

A comprehensive monitoring and evaluation of field performance, including rutting and cracking, were conducted for Superpave project sections from construction throughout the pavement's life to identify effective and realistic performance-based specifications in Florida. The performance evaluation was conducted based on gradation parameters developed and performance indicators were obtained from the field performance monitoring of Superpave projects. The results of evaluation indicate that the DASR porosity criterion appear to accurately distinguish the relative field rutting performance. In addition, it appears that the DF criterion combined with DASR porosity criterion may effectively be used as a performance-related design parameter in order to evaluate the relative field cracking performance for Superpave mixtures.

CHAPTER 6
IDENTIFICATION OF MATERIAL PROPERTY RELATIONS AND MODEL DEVELOPMENT

6.1 Introduction

The current lack of material property models that can accurately describe the changes in material properties over time in the field condition is probably the greatest deficiency in our ability to accurately predict pavement performance. Therefore, there is a need to evaluate existing material property models, and develop and evaluate improved models for use in the prediction of pavement performance. The Superpave monitoring projects provided us with the unique opportunity to have material property data throughout pavement life, and to evaluate material property models using the historic data.

Previous research has shown that fracture energy limit (FE), which is associated with mixture's tolerance to damage, and creep rate (CR), which is related to the rate of damage accumulation in the mixture, are key material properties that affect cracking performance of asphalt pavement (Zhang et al., 2001). Therefore, the following two material property models were selected in this evaluation (Section 6.2), which are part of the HMA-FM-E model developed during the completion of NCHRP Project 01-42A (Roque et al., 2010).

- AC stiffness (creep compliance) aging sub-model
- Fracture energy limit aging sub-model

The Superpave historic data that were used in the evaluation was presented in Chapter 4. Based on the evaluation results, improved material property relations were identified (Section

6.3), which led to the development of improved models to predict mixture properties as a function of age subjected to field conditions (Section 6.4). Finally, recommendations were presented for further refinement and evaluations of material property models in future work (Section 6.5).

6.2 Material Property Models in the HMA-FM-E Model: A Revisit

Two material property models, i.e., AC stiffness aging model and fracture energy limit aging model, were revisited in this section. First, following a brief description of each model, predicted changes in material properties over time by each model were compared to the general trend observed from the historic data (as presented in Chapter 4). Then, modifications that were necessary to improve the existing models were proposed to further narrow the differences between predictions and reality.

6.2.1 AC Stiffness Aging Sub-Model

The AC stiffness aging sub-model was developed on the basis of the global binder aging model (Mirza and Witczak, 1995) and dynamic modulus model (Witczak and Fonseca, 1996) at a loading time of 0.1 seconds. In this model, the following empirical equation was identified to consider the aging effect on mixture stiffness (S),

$$S = \left|E^*\right|_0 \frac{\log \eta_t}{\log \eta_0} \tag{6-1}$$

Where $|E^*|_0$ represents the unaged mixture stiffness, η_t and η_0 correspond to the aged and unaged binder viscosities at 10 °C, respectively. The general trend for predicted change in mixture stiffness at surface as a function of age is presented in Figure 6-1. As shown, the

stiffness S(t) increases with age at a decreasing rate, where S_0 is the initial value and S_{max} is the maximum value after being aged for a sufficiently long time.

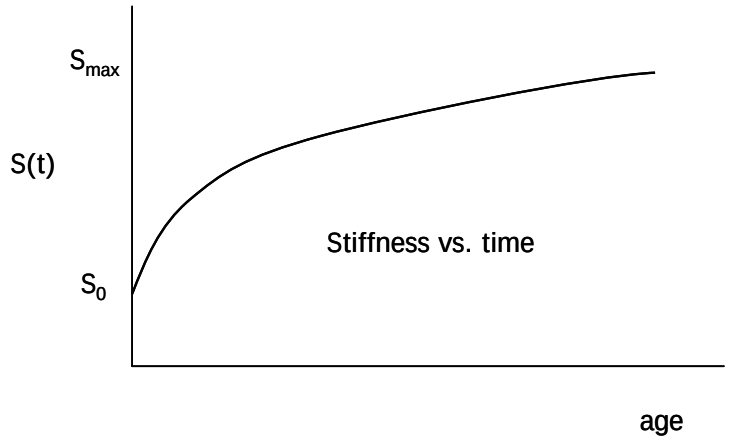

Figure 6-1 Schematic plot for AC stiffness at surface vs. age

Using the AC stiffness aging model, creep compliance values at 1, 2, 5, 10, 20, 50, 100, 200, 500, and 1000 seconds for three temperatures (i.e., 0, 10, and 20 °C) were obtained by taking inverse of the AC stiffness values at the corresponding time for each of the temperatures, which resulted in three 1000-second creep compliance curves. Then, these isothermal creep compliance curves were used to generate master curve and determine creep rate of the master curve (Buttlar et al., 1998). The general trend for the predicted creep rate aging curve is presented in Figure 6-2, which shows that the creep rate decreases with age at a decreasing rate.

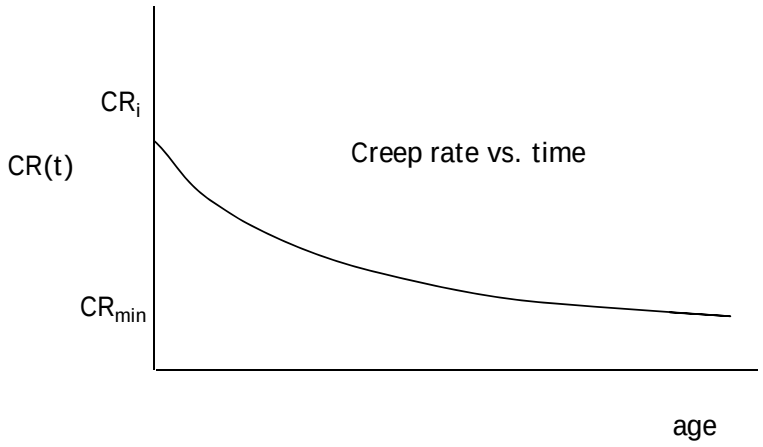

Figure 6-2 Schematic plot for creep rate vs. age

The prediction in Figure 6-1 is generally consistent with our observations from resilient modulus data for the early stage of pavement life. However, it is different from the historic data at the later stage of pavement life, during which it was found that the modulus actually decreases with age (see Figure 4-9). It appears that oxidative aging alone is not sufficient to account for the change in AC stiffness over time. Effects of the other factors on AC stiffness, such as load-induced damage, moisture-related damage, and healing potential, need to be considered for more accurate prediction. Once the existing AC stiffness aging model is modified by incorporating the aforementioned key factors, it is expected that creep rate aging curve will be affected accordingly, because as mentioned before the determination of creep rate is dependent on the AC stiffness.

6.2.2 Fracture Energy Limit Aging Sub-Model

The fracture energy limit surface aging sub-model developed as part of the HMA-FM-E model is expressed in the following form:

$$FE_f(t) = FE_i - (FE_i - FE_{\min}) \cdot [S_n(t)]^{k1} \quad (6\text{-}2)$$

Where FE_i is the initial fracture energy and FE_{min} is the minimum value of FE limit after a sufficiently long aging period t_{inf}. FE_{min} was determined based on experience (field specimens) to be 0.2 kJ/m^3, and t_{inf} was chosen as 50 years. k_1 is an aging parameter determined through field calibration (Roque et al., 2010). $S_n(t)$ is the normalized change in stiffness (with respect to its initial value) at the surface of the AC layer, and is expressed as,

$$S_n(t) = \frac{S(t) - S_0}{S_{\max} - S_0} \quad (6\text{-}3)$$

Where S(t), S_0, and S_{max} were defined when describing Figure 6-1. Figure 6-3 shows that $S_n(t)$ generally increases with age at a decreasing rate. It can also be seen that $S_n(t)$ varies between zero and one.

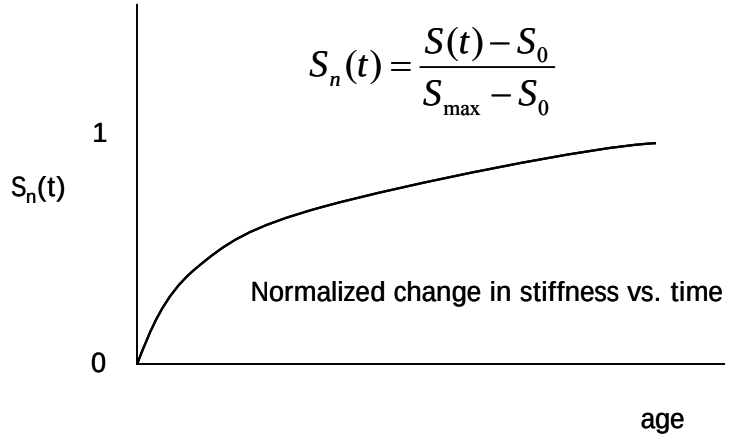

Figure 6-3 Schematic plot for normalized change in AC stiffness vs. age

The trend for predicted change in FE limit at surface as a function of age is presented in Figure 6-4. As shown, overall the FE limit decreases with age at a decreasing rate. The

prediction generally agrees with our observations from measured FE limit data. However, the effects of load induced damage, moisture-related damage, and healing potential on FE limit, which were not considered in the existing model, could accelerate its degradation at the later stage of pavement life (see Figure 4-16). So, it is necessary to take these factors into account to improve the accuracy of the model. Besides, it is noted that the input for initial fracture energy in the existing model relies on measurements from field cores. In other words, no model is available for prediction of initial fracture energy.

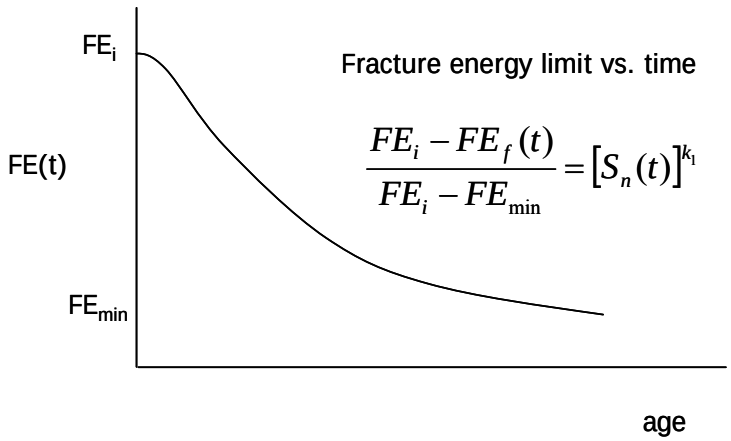

Figure 6-4 Schematic plot for FE limit vs. age

6.3 Identification of Material Property Relations

Identification of appropriate material property relations for key mixture properties is important for accurate prediction of pavement performance. Based on the discussion in the prior section, the existing material property models for AC stiffness, CR, and FE developed as part of the HMA-FM-E model are capable of predicting changes in these mixture properties due to oxidative aging. However, they are subjected to several deficiencies as described below:

- Oxidative aging was considered as the only factor responsible for changes in these material properties. Other factors such as load induced damage, moisture-related damage and healing that could also affect these material properties, especially in the later stage of pavement life, were not considered.
- Determination of creep rate as a function of age was directly based on the current AC stiffness aging model using a simple inverse relation. As expected, the accuracy of the creep rate predictions is not very high, although the overall trend of the creep rate aging curve is generally correct. So, measured creep rate from field cores was needed to improve the accuracy of model prediction.
- In the existing FE model, the input for initial fracture energy relies on measurements from field cores.

Therefore, there is a need to improve the existing models by incorporating effects of load induced damage, moisture-related damage and healing on changes in these mixture properties over time in the field. Also, there is clearly a need to develop models for prediction of initial FE and CR, so that accurate model predictions can be achieved without relying on measurements from cores. As illustrated in Figure 6-5, two types of material property relations were considered for further improvement and/or development to meet these needs:

- Material property relation I: This set of relations was conceived to relate mixture characteristics and component properties to initial mixture properties (i.e., initial FE and CR).
- Material property relation II: This set of relation was conceived to improve the models for prediction of changes in mixture properties over time by taking into

account key factors such as load induced damage, moisture-related damage, oxidative aging and healing.

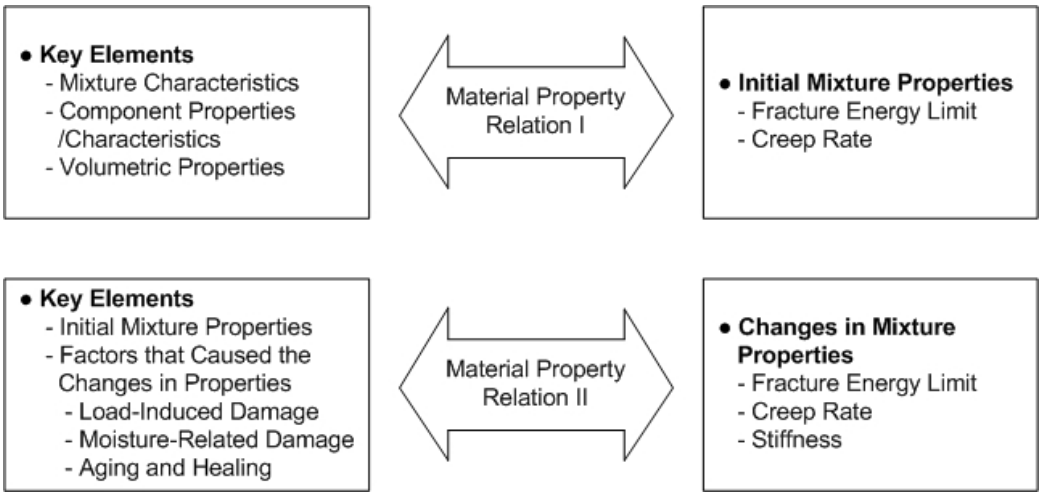

Figure 6-5 Two types of material property relations

It should be noted that mixture characteristics considered in this study included four DASR-IC parameters, i.e., DASR porosity, DF, CFA/FFA, and EFT. A brief description for the definition and procedures to calculate each of these parameters was presented in Chapter 5. Component properties/characteristics covered binder properties (e.g., binder viscosity) and aggregate characteristics (e.g., aggregate type).

6.4 Development of Material Property Prediction Model

In Chapter 5, DASR-IC parameters including DASR porosity, DF, CFA/FFA, and EFT, were determined using field data from Superpave monitoring projects. In other words, these parameters were calculated based on in-place gradation and volumetric properties. Also, comprehensive analyses were conducted to evaluate field mixture performance using these

parameters. Based on the analyses performed, an acceptable range (or reference range) of each parameter was recommended for optimal mixture property/performance and is presented as follows:

- DASR porosity (%): 38 – 52 (48 – 52: Marginal DASR porosity)
- DF (for cubical DASR structure): 0.50 – 0.95
- EFT (microns): 12.5 – 25.0
- CFA/FFA: 0.28 – 0.36

In this chapter, further analyses were undertaken to identify whether any distinctive relation/pattern exists between key mixture properties including FEL and CR, and DASR-IC parameters within the recommended range. Due to the limited data obtained in this research, the goal of this part of the study was limited to developing rudimentary (or place-holder) relationships. Figure 6-6 shows the flowchart for development of the material property models.

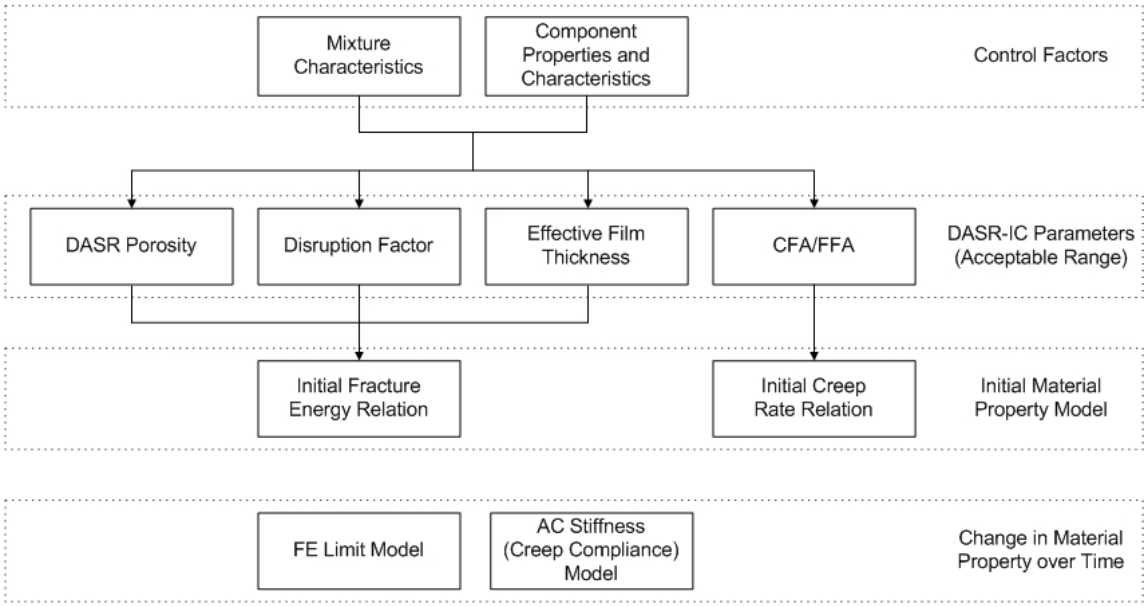

Figure 6-6 Flowchart for development of material property models

6.4.1 Models for Initial Material Properties

Initial material property is one of the key parameters that govern the change in the material property over time. For example, the trend of fracture energy limit aging curve is controlled by its initial fracture energy limit such that a larger initial FEL generally results in a larger initial reduction rate in the FEL aging curve (Roque et al., 2010). Therefore, models for initial material property are important for accurate prediction of changes in the material properties over time and for accurate prediction of overall pavement performance.

Two models for initial material properties were developed during this research, which are presented in the sub-sections that follow. It is noted that initial material property data used for this development were determined based on measured properties of cores obtained from Phases I and II of the Superpave Monitoring Project (see Chapter 4).

6.4.1.1 Initial Fracture Energy Relation

As mentioned earlier, the initial fracture energy FE_i is one key parameter that governs the trend of FE limit aging curve. Based on analyses of mixture characteristics and component properties and the results of mixture testing, the relationships between initial fracture energy and DASR-IC parameters were identified. Figures 6-7 through 6-9 present the relations identified between initial fracture energy and each of the DASR-IC parameters including DASR, DF, and EFT, respectively.

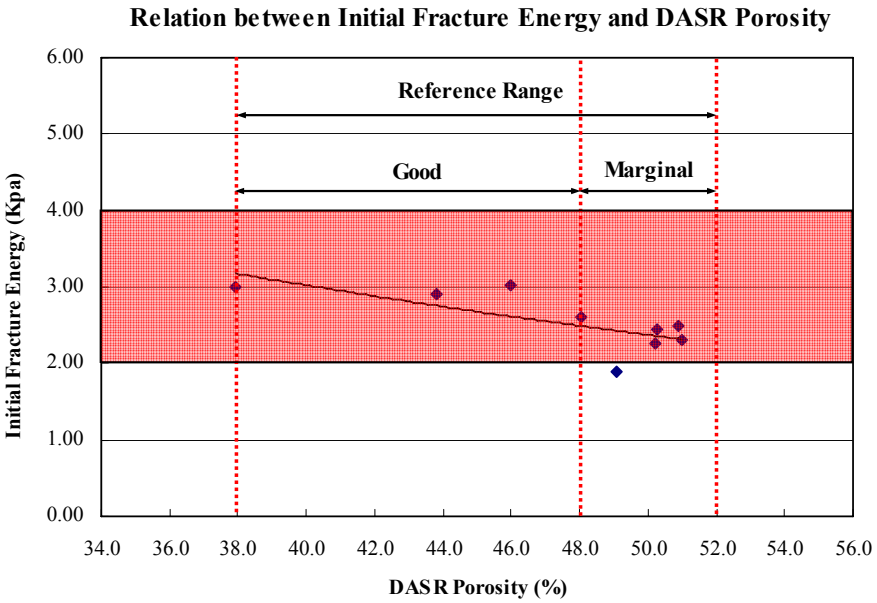

Figure 6-7 Relation between initial fracture energy and DASR porosity

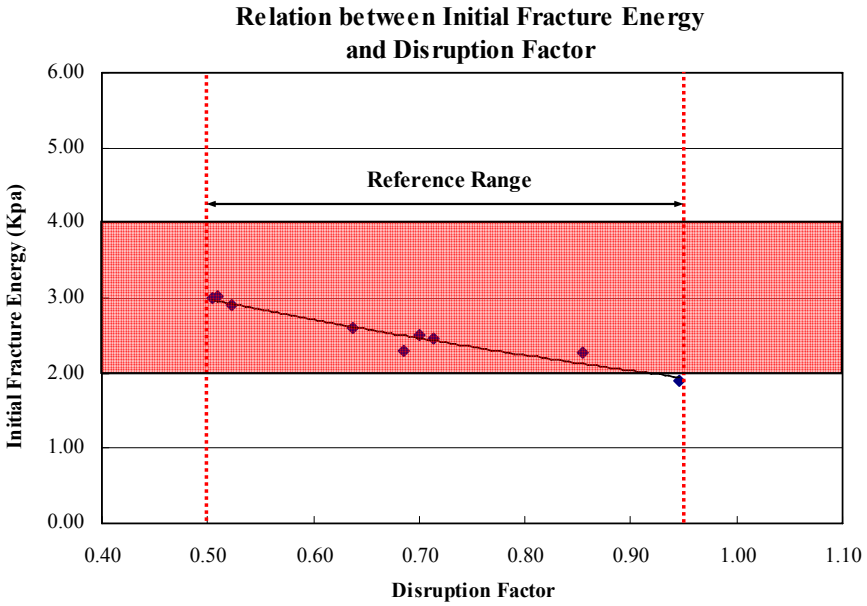

Figure 6-8 Relation between initial fracture energy and disruption factor

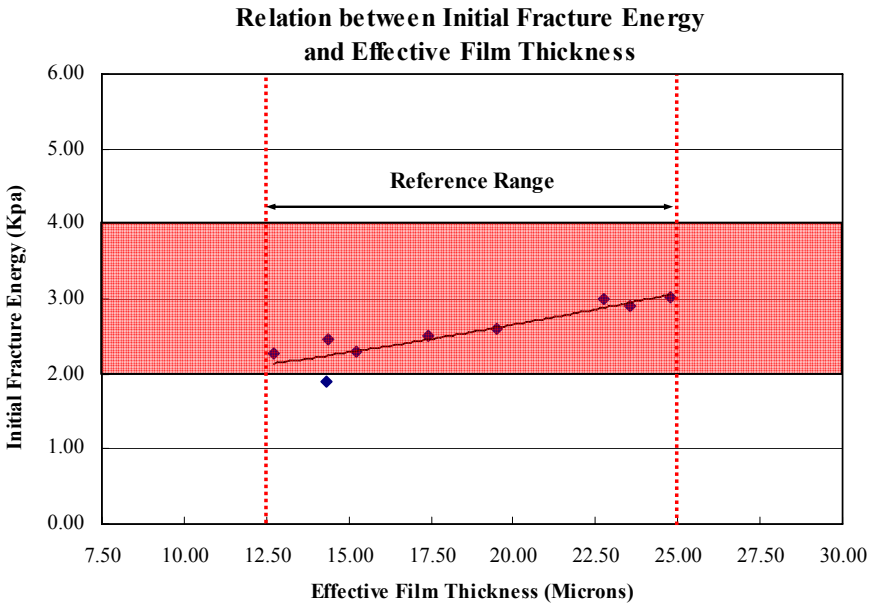

Figure 6-9 Relation between initial fracture energy and effective film thickness

As shown, the initial fracture energy generally decreases with increasing DASR porosity and disruption factor (DF). Also, it can be seen that the initial fracture energy increases with increasing effective film thickness (EFT). As a result, it was identified that there are unique relationships between initial fracture energy and each individual DASR-IC parameters, which control characteristics of mixture, particularly characteristics of the interstitial component (IC) of mixture. It is noted that this trend appears to hold only when DASR porosity, DF, and EFT are within the ranges considered to be acceptable based on findings presented in Chapter 5.

Based on the identified relations between initial fracture energy and three individual parameters, i.e., a proportional relation between initial fracture energy and EFT, and inversely proportional relations between initial fracture energy and DASR porosity and DF, respectively, an empirical relation was further conceived to relate initial fracture energy to all three parameters, which resulted in the following equation,

$$FE_i = a \cdot \frac{EFT^b}{DASR^c \cdot DF^d} \tag{6-4}$$

Where, FE_i is initial fracture energy, DASR denotes DASR porosity, and a, b, c, and d are fitting parameters. Taking the logarithm on both sides of Equation (6.4), it becomes,

$$\log FE_i = a + b \cdot \log(EFT) - c \cdot \log(DASR) - d \cdot \log(DF) \tag{6-5}$$

With a simple manipulation, the initial FE equation can be obtained and expressed as below,

$$FE_i = 10^{a+b\cdot\log(EFT)-c\cdot\log(DASR)-d\cdot\log(DF)} \tag{6-6}$$

Figure 6-10 shows the predicted initial fracture energy using the predictive equation developed compared to the measured values from the field cores. As shown, all data points in the figure are close to the line of equality, which indicates that the predictions generally agree well with the measured values.

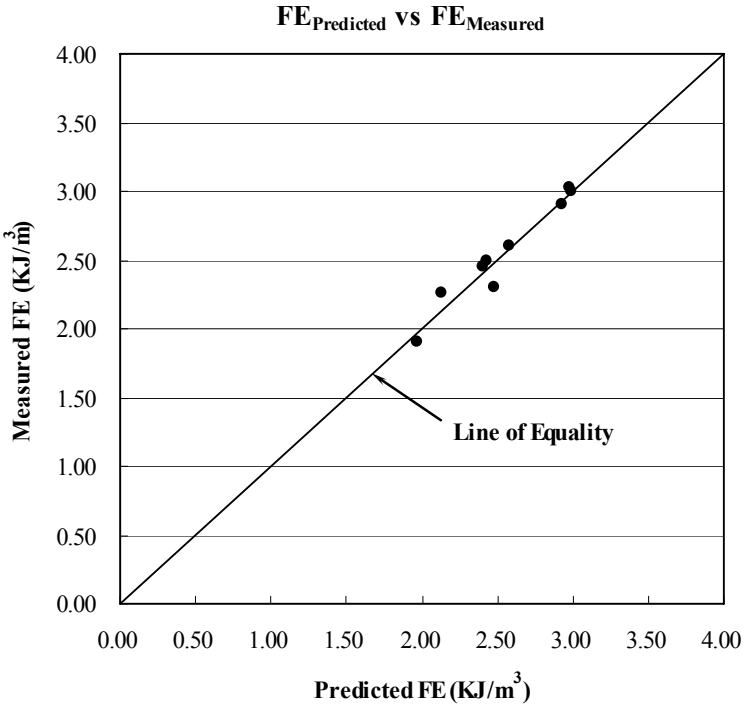

Figure 6-10 Predicted vs. measured initial fracture energy

6.4.1.2 Initial Creep Rate Relation

Initial Creep Rate and DASR-IC Parameters:

Creep rate, also called the rate of creep compliance, is related to rate of damage, which is considered to be a good indicator for evaluating the cracking performance of asphalt pavement. Attempts were made to identify the relation between initial creep rate and each of the DASR-IC parameters including DASR porosity, DF, and EFT. However, no distinctive relation or pattern was identified from the analysis using these three parameters initially assigned (see Figures 6-11 to 6-13). In other words, none of these three is capable of defining a clear relation with the initial creep rate. It is noted that in these figures, the term "Good" denotes good mixtures for which all DASR-IC parameters are within the ranges considered to be acceptable, the term "Bad" denotes bad mixtures for which at least one of the DASR-IC parameters is not within the ranges

considered to be acceptable, and the term “Modified” denotes mixtures with polymer modification.

However, prior research conducted at the University of Florida has shown that creep rate can be controlled by parameters obtained using the DASR-IC model, including properties and characteristics of IC (Roque et al, 2006; Guarin, 2009). It was expected that other DASR-IC parameters can be identified to uniquely define the initial creep rate relation.

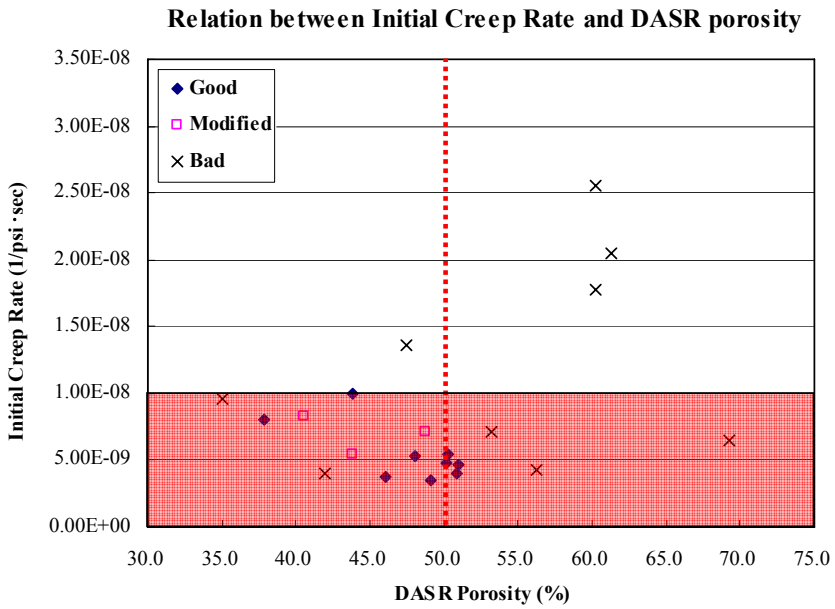

Figure 6-11 Relation between initial creep rate and DASR porosity

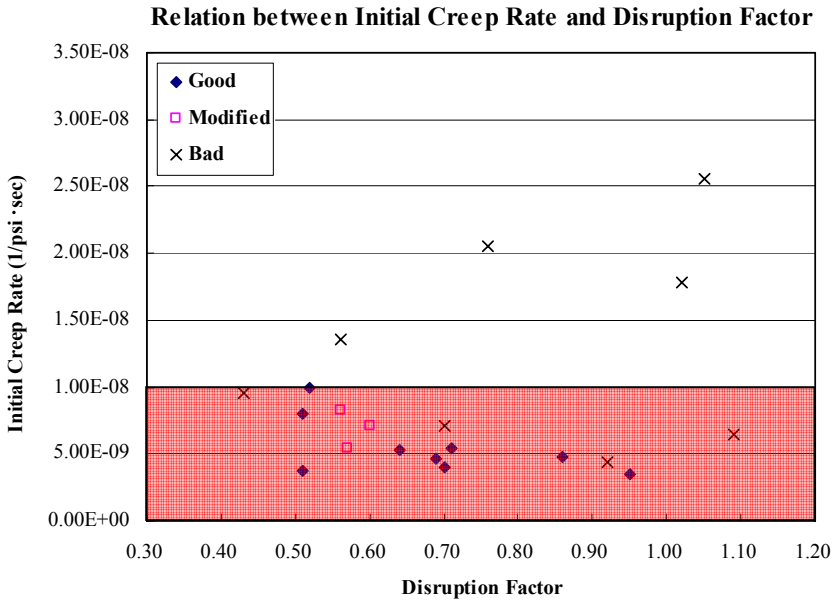

Figure 6-12 Relation between initial creep rate and DF

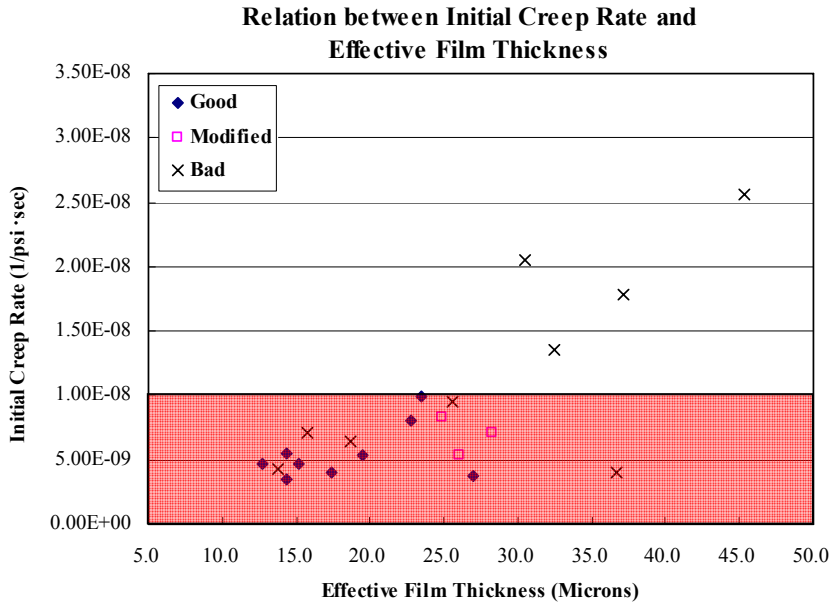

Figure 6-13 Relation between initial creep rate and EFT

In general, DASR-IC parameters, which indicate the property and distribution of interstitial component, govern creep behavior of the mixture as indicated by effective film thickness and effective asphalt content. For example, DASR porosity can be used to control effective asphalt content (i.e., higher DASR porosity will result in greater effective asphalt content). Interstitial component, which represents the finer portion of mixture gradation can be used to control effective film thickness (i.e., coarser IC will result in higher effective film thickness).

Preliminary analyses performed by the research team showed that the ratio between coarse portion and fine portion of fine aggregate (CFA/FFA), which is associated with effective film thickness, is strongly related to initial creep rate of mixture. Therefore, this new parameter indicating the composition of interstitial component was used to identify the initial creep rate relation. Based on the calculation of CFA/FFA and the results of mixture testing, the relation between initial creep rate and CFA/FFA was identified and is presented in Figure 6-14. It is clear that CFA/FFA is better than effective film thickness in terms of defining a distinctive relation with initial creep rate (see also Figure 6-13), because CFA/FFA involves the effect of interaction between particles in the interstitial component structure.

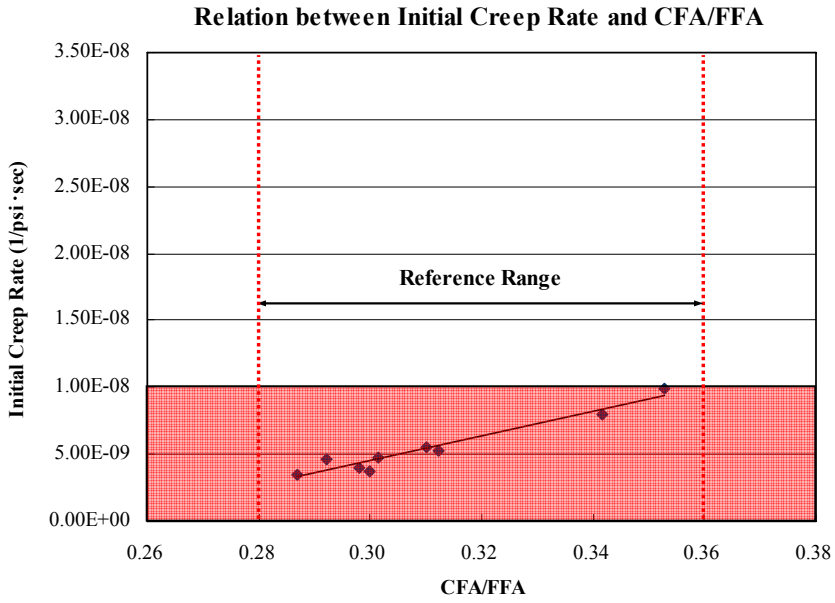

(a) "Good" Mixtures

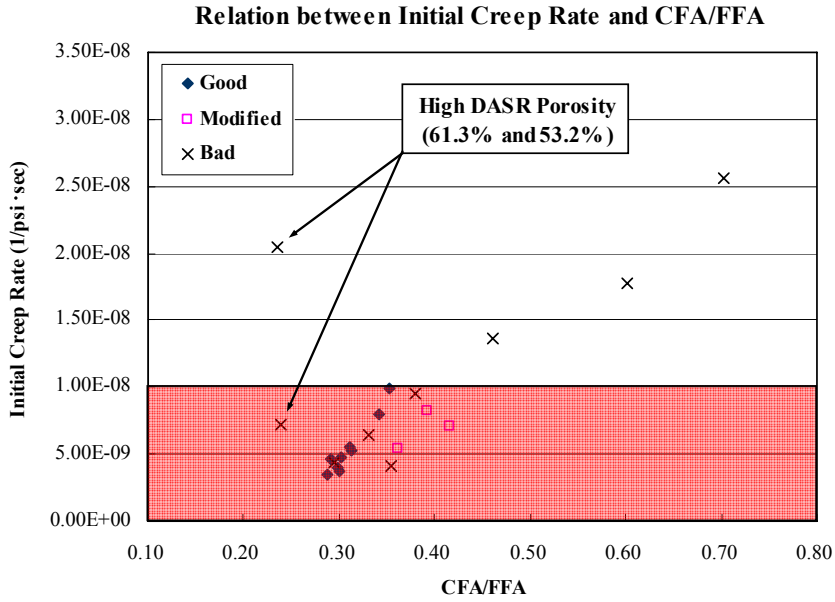

(b) All mixtures

Figure 6-14 Relation between initial creep rate and CFA/FFA

It can also be seen from Figure 6-14 that initial creep rate generally increases with increasing CFA/FFA. As for the initial fracture energy relations, it is noted that this relation appears to hold only when CFA/FFA are within the range considered to be acceptable based on findings presented in Chapter 5.

In addition, it was found that the initial creep rate relation can be extended for mixtures with polymer modified binder. As shown in Figure 6-15, the continuous line represents the initial creep rate relation for mixtures with unmodified binder, while the dashed line represents the relation for mixtures with polymer modified binder. As expected, initial creep rate is reduced due to polymer modification, as indicated by the relative positions between the continuous and dashed lines. This observation is consistent with our finding from prior research (Kim et al., 2003) that the polymer modification generally helps to reduce the damage rate of asphalt mixture.

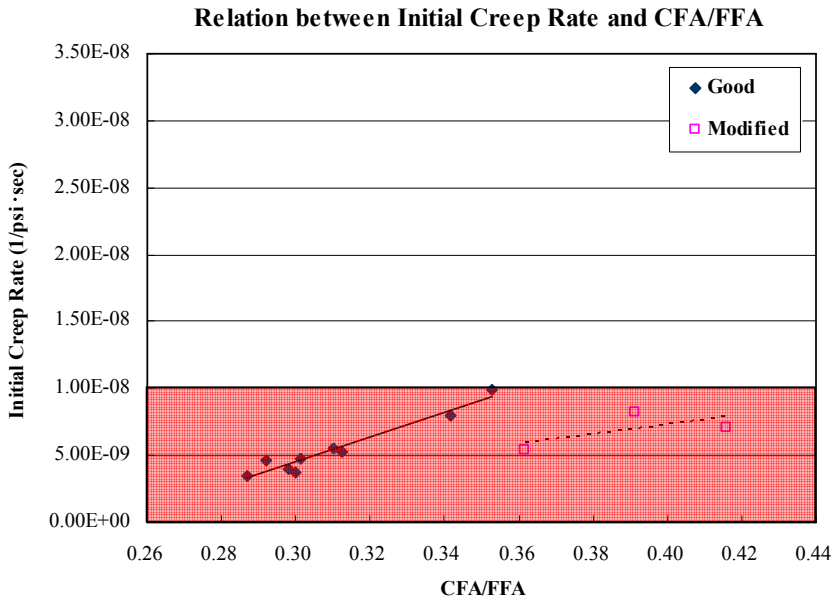

Figure 6-15 Effect of polymer modification on initial creep rate relation

Initial Creep Rate and Binder Properties:

Additional analyses were conducted to identify whether any clear pattern emerges between initial creep rate and any of the parameters for binder properties, including viscosity, effective asphalt content, $G^{*}\cdot\sin\delta$, MSCR average recovery and non-recoverable creep compliance. Figures 6-16 through 6-20 present the relations between initial creep rate and each of the parameters evaluated, respectively.

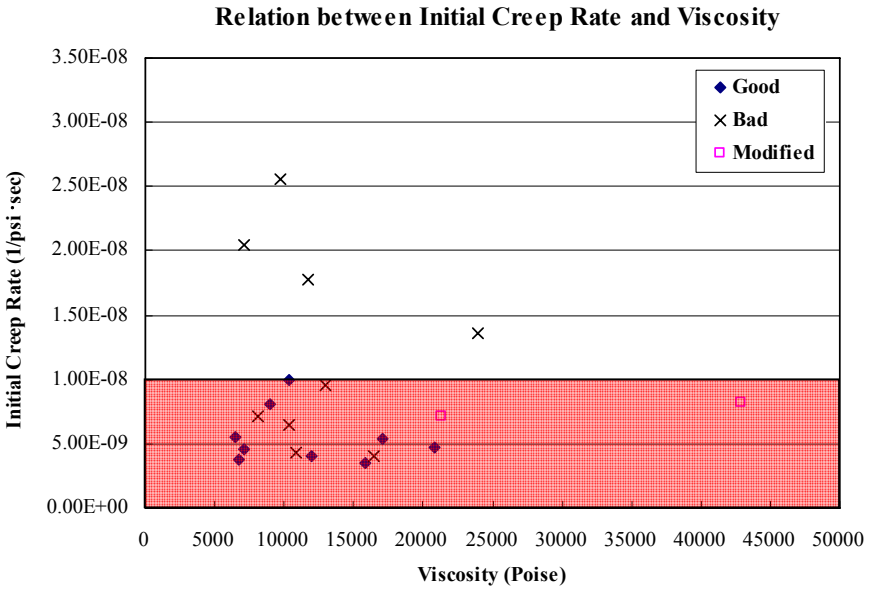

Figure 6-16 Relation between initial creep rate and viscosity

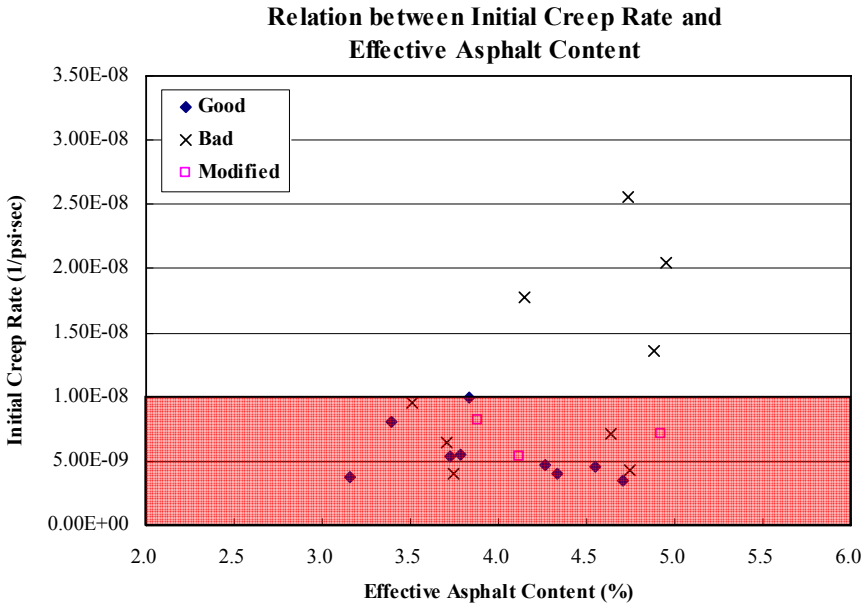

Figure 6-17 Relation between initial creep rate and effective asphalt content

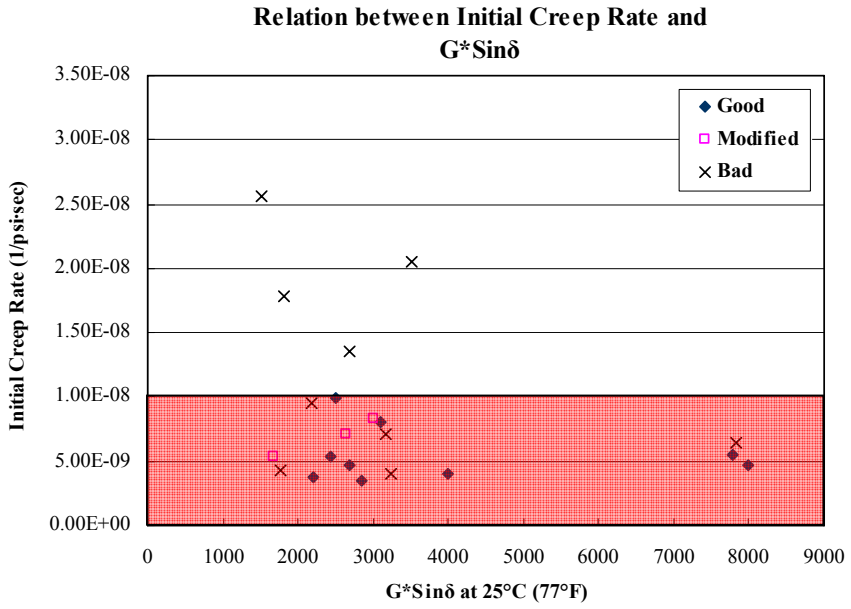

Figure 6-18 Relation between initial creep rate and $G^{*}\cdot\sin\delta$

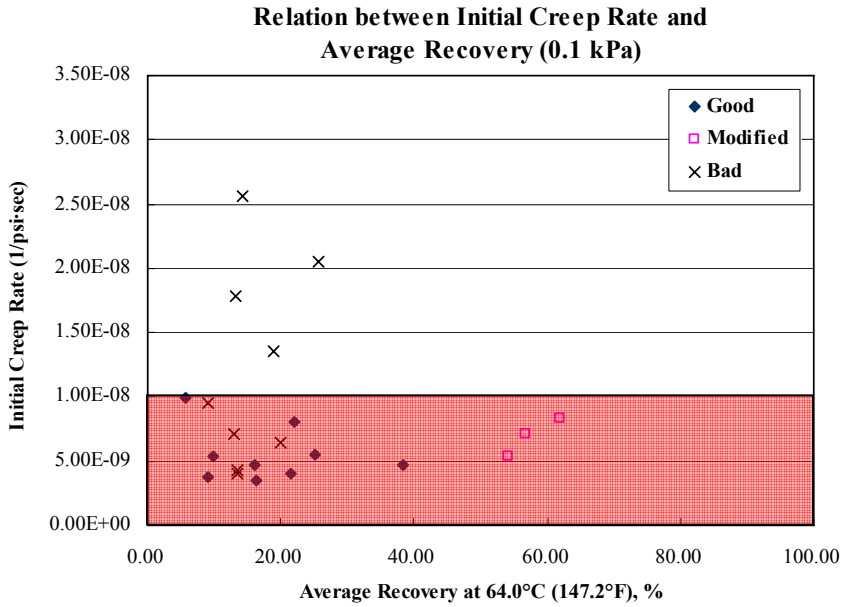

Figure 6-19 Relation between initial creep rate and MSCR average recovery (0.1 kPa)

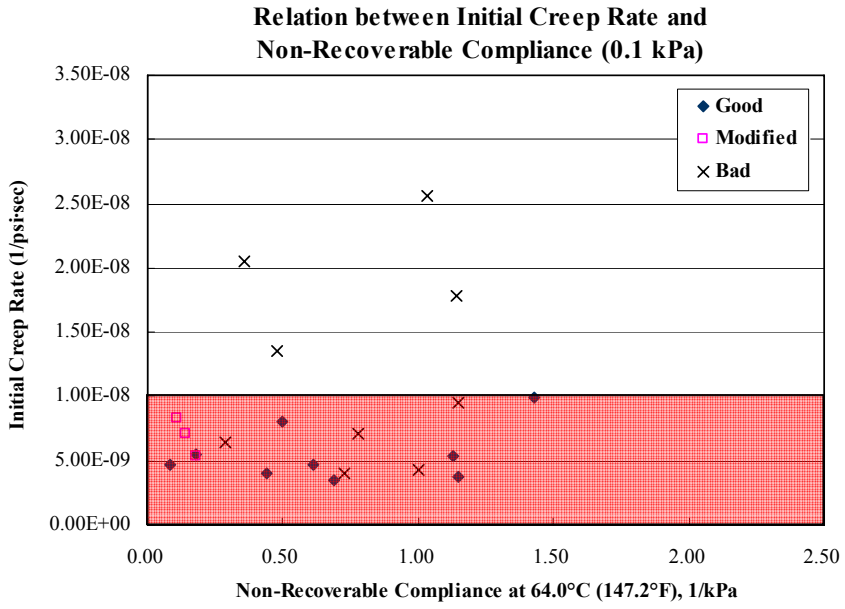

Figure 6-20 Relation between initial creep rate and MSCR nonrecoverable compliance (0.1 kPa)

According to the analysis results, it appeared that none of these parameters for binder properties is capable of defining a clear relation with the initial creep rate. However, it has been identified that "Good" and "Modified" mixtures showed relatively lower initial creep rate than "bad" mixtures. A range for initial creep rate that included all "Good" and "Modified" mixtures is highlighted in Figures 6-16 through 6-20. This clearly indicates that once all DASR-IC parameters (including DASR porosity, DF, EFT, and CFA/FFA) are within the ranges considered to be acceptable, mixtures will have relatively low initial creep rates which could result in better crack performance, regardless of binder properties. Therefore, it is important for mixtures to have all DASR-IC parameters within the defined acceptable ranges, since mixture characteristics and component properties are dominant factors to control the initial creep rate.

6.4.2 Models for Changes in Material Properties

The identification of appropriate trends with respect to the changes in key material properties (e.g., fracture energy limit and creep rate) over time is important for accurate prediction of cracking performance of asphalt mixtures. As discussed earlier in this chapter, the current lack of material property models of this type is probably the greatest deficiency in our ability to accurately predict pavement performance. Possible goals to develop improved material property models are presented as follows.

- Adjust the change in material property based on the change in IC characteristics.
- Adjust the change in material property by inclusion of the effects of non-healable permanent damage related to traffic load and moisture (environment).

However, due to the limited data available to this research, the scope of this part of study was limited to recommendation of new concept for modification based on the evaluation of several candidate models conducted in Section 6.2, including:

- AC stiffness (creep compliance) aging model
- Fracture energy limit aging model

It is expected that the results of two ongoing research projects sponsored by FDOT, including "Development of A Test Method that will Allow Evaluation and Quantification of The Effects of Healing on An Asphalt Mixture", and "Effects of Laboratory Heating, Cyclic Pore Pressure, and Cyclic Loading on Fracture Properties of Asphalt Mixture" will be of great benefit in helping to meet the final goal of this task.

6.4.2.1 AC Stiffness Model

As mentioned before, the existing model shown in Figure 6-1 indicates that the AC stiffness is continuously increasing with time. However, this trend does not coincide with the results of prior laboratory, field, and accelerated pavement testing (APT) research, which indicated that the stiffness generally reduces with time after a certain age. Therefore, a new concept was proposed and modification of the existing model was conceived to appropriately describe the known trend of this property. Figure 6-21 describes the proposed modification including the effect of the non-healable permanent damage related to load and moisture on the change in AC stiffness with time.

As shown in Figure 6-21, there is a critical time denoted as t_d which separates pavement life into two stages. In the early stage denoted as Stage I, there is no effect of non-healable permanent damage (related to load and moisture) on changes in AC stiffness. For Stage I, the

trend of change in AC stiffness is mainly controlled by oxidative aging rather than non-healable permanent damage related to load and moisture. This indicates that healing process is a dominant factor as compared to damage process in governing the trend of change in material property in this stage.

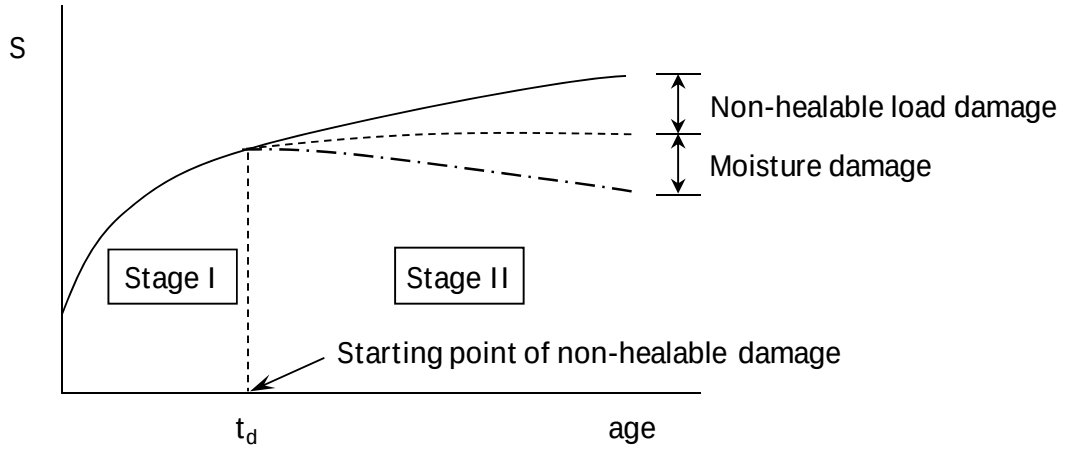

Figure 6-21 Proposed AC stiffness model

As also shown in the figure, the non-healable permanent damage process takes control in Stage II. The non-healable permanent damage included load-induced and moisture-related damage, which tends to reduce the AC stiffness after the critical time. Clearly, determination of t_d is the first task in finalizing the proposed AC stiffness model. The next challenge is how to quantify the effect of load induced and moisture-related damage on AC stiffness after the critical time.

6.4.2.2 Fracture Energy Limit Model

The fracture energy limit aging model developed as part of the NCHRP Project 01-42A showed that the FE limit generally decreases with aging, and eventually reaches some minimum

value after a sufficiently long time (see Figure 6-4). However, the results of prior laboratory, field, and APT research did not coincide with the trend introduced in the existing model. Therefore, modification of the existing model was conceived to reasonably describe the observed trend of this property.

Figure 6-22 presents the proposed modification including the effect of the non-healable permanent damage related to load and moisture on the change in fracture energy limit with time. Since the fracture energy limit in the existing model was associated with the AC stiffness in a normalized form (see Equation 6-2), the proposed modifications for the existing fracture energy limit model (see Figure 6-22 (b)) are related to the modified AC stiffness model (Figure 6-22 (a)).

As shown in Figure 6-22, the pavement life was separated into two stages by the critical time t_d: In Stage I when mixture healing potential is high, it was assumed that there is no permanent damage induced by load and moisture. So, the existing relation for surface AC stiffness S(t), which accounts for the change in AC stiffness due to only oxidative aging, was used for determination of the normalized change in stiffness $S_n(t)$. As a result, the existing relation for fracture energy limit can be used for this part of the model.

However, during Stage II when the time is greater than t_d, a modified relation for surface AC stiffness, termed $S_d(t)$, is required to consider the permanent damage effect on the change in AC stiffness with time (see Figure 6-22(a)). As a result, the normalized change in the modified AC stiffness can be expressed using the following equation.

$$S_{dn}(t) = \frac{S_{d0} - S_d(t)}{S_{d0} - S_{d\min}} \tag{6-7}$$

Where, $S_{dn}(t)$ is the normalized change in stiffness $S_d(t)$ defined for Stage II, and S_{d0} and S_{dmin} are stiffness values when $S_d(t)$ is at $t = t_d$ and $t = 50$ years, respectively. Then, the modified

FE limit aging function was introduced for Stage II by relating the normalized change in FE limit to the normalized change in stiffness $S_d(t)$ by a power of k_2, which is expressed in the following equation.

$$\frac{FE_{d0} - FE_d(t)}{FE_{d0} - FE_{\min}} = \left[S_{dn}(t)\right]^{k_2} \tag{6-8}$$

Where, $FE_d(t)$ is the fracture energy limit function defined for Stage II, FE_{d0} is the value when $FE_d(t)$ is at $t = t_d$, k_2 is aging parameter for Stage II, FE_{min} denotes minimum FE, and $S_{dn}(t)$ was defined in Equation (6-7).

It can also be seen from Figure 6-22, due to the incorporation of the permanent damage effect, the modified fracture energy limit function (Stage II) has a higher rate of reduction in fracture energy over time than the existing function. The modified trend is consistent with the results of the change in FE over time actually measured from field cores.

In the case of the proposed fracture energy function, it is important to determine the critical time t_d, which indicates the point when permanent damage starts to affect the change in fracture energy with time. Also, it is required to quantify the effect of non-healable permanent damage due to load and moisture, in addition to the effect of oxidative aging after the critical time.

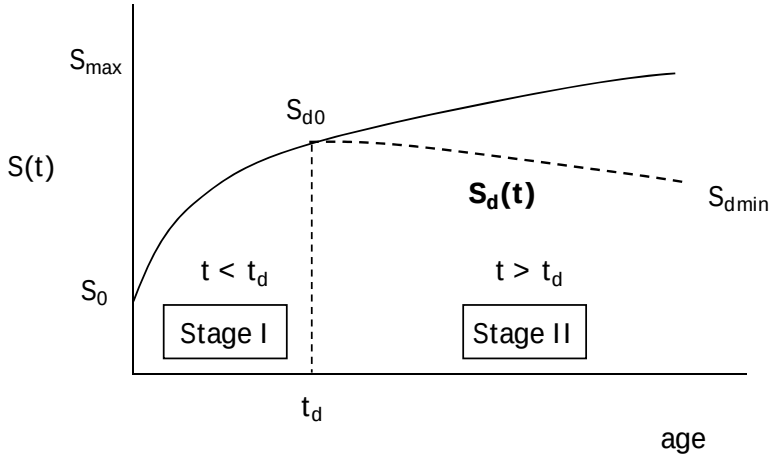

1) For $t < t_d$ (Stage I)

$$S_n(t) = \frac{S(t) - S_0}{S_{\max} - S_0}$$

2) For $t > t_d$ (Stage II)

$$S_{dn}(t) = \frac{S_{d0} - S_d(t)}{S_{d0} - S_{d\min}}$$

(a) Change in AC stiffness over time

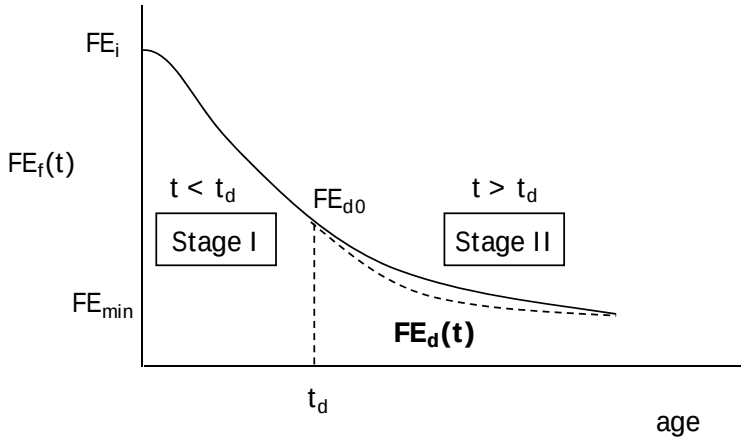

1) For $t < t_d$ (Stage I)

$$\frac{FE_i - FE_f(t)}{FE_i - FE_{\min}} = \left[S_n(t)\right]^{k_1}$$

2) For $t > t_d$ (Stage II)

$$\frac{FE_{d0} - FE_d(t)}{FE_{d0} - FE_{\min}} = \left[S_{dn}(t)\right]^{k_2}$$

(b) Change in FE limit over time

Figure 6-22 Proposed FE limit model

6.5 Closure

Material property relations were identified using material properties measured from field cores over time and assigned DASR-IC parameters calculated from analysis of mixture characteristics and component properties. Unique relationships were identified between DASR-IC parameters which characterize the interstitial component (IC) of the mixture and initial

mixture properties (i.e., fracture energy limit and creep rate). It is noted that these relations appear to hold only when all DASR-IC parameters are within the ranges considered to be acceptable. Mixtures having DASR-IC parameters within the acceptable range were shown to have more consistent and predictable properties, and better performance than those having DASR-IC parameters beyond the acceptable range. In addition, based on evaluation of existing material property aging models, a new concept and modifications were proposed to improve these models for more accurate prediction of changes in material properties over time. Due to the limited data available to this research, a full model could not be developed. Nevertheless, procedures to continue and complete the development of the improved models were recommended for future work.

CHAPTER 7
PERFORMANCE MODEL PREDICTIONS AND EVALUATION FOR SUPERPAVE MIXTURES IN FLORIDA

7.1 Introduction

The primary purpose of this chapter is the evaluation of existing pavement performance models in terms of their capability of predicting cracking performance of Superpave mixtures in Florida. Four candidate tools for pavement performance prediction were selected based on availability and on the best knowledge of the research team:

- Enhanced HMA Fracture Mechanics-Based Model (HMA-FM-E)
- Mechanistic-Empirical Pavement Design Guide (MEPDG) Program
- Perpetual Pavement Design (PerRoad) Program
- Energy Ratio-Based Model (ER Model)

Prediction efforts using each of these tools are presented in Sections 7.2 to 7.5, including a brief introduction to each tool, its input module, and prediction results for ten Superpave projects (1 to 4, 6, 7 and 9 to 12). Project 5 was overlaid before coring was started (i.e. no field cores were obtained), and Project 8 has a Portland cement concrete base. Therefore, these two projects were not included in this part of the study. In Section 7.6, the prediction results in terms of bottom-up cracking and top-down cracking were compared separately to the observed pavement performance data (see Chapter 2), which led to conclusions and recommendations regarding the quality and use of different models for pavement cracking performance prediction in Florida in Section 7.7.

It should be noted that the following conditions were enforced among all prediction tools to achieve fair comparisons of prediction results, based on which reasonable conclusions could be made:

- ESAL approach instead of the load spectra approach
- Constant granular base (GB) and subgrade (SG) moduli without considering moisture effect
- Deterministic analysis as opposed to probabilistic analysis

7.2 Enhanced HMA Fracture Mechanics Based Model (HMA-FM-E)

7.2.1 Introduction

The HMA-FM-E model was developed by the UF research team as part of the NCHRP Project 01-42A to predict top-down cracking performance in HMA layers. As indicated by the name, the model is an enhanced version of the existing HMA-FM model, which is the result of the continuous efforts of the UF team over the past years (Zhang et al., 2001, Roque et al., 2002, 2004, Sangpetngam et al., 2003, 2004, Kim et al., 2008). During the course of the NCHRP project, the enhanced performance model was formed by developing and incorporating into the existing model appropriate sub-models that account for effects of aging, healing, and transverse thermal stresses on top-down cracking performance. Furthermore, the enhanced model was calibrated and validated using data from Florida field sections (Roque et al., 2010).

The enhanced top-down cracking performance model has four major components, as shown in the general model framework presented in Figure 7-1, including

- The load response and load-associated damage sub-models that are used to predict step-wise load induced damage.

- The thermal response and thermal-associated damage sub-models that are used to predict thermally induced damage.
- The damage recovery and accumulation process that is used to accumulate damage after taking into account healing effect. Once the accumulated damage reaches the threshold, a crack will initiate or propagate.
- The mixture properties sub-models that were devised to account for changes in mixture damage, fracture, and healing properties due to aging.

Details for each component are described elsewhere (Roque et al., 2010, Zou and Roque, 2011) and were not included in this report.

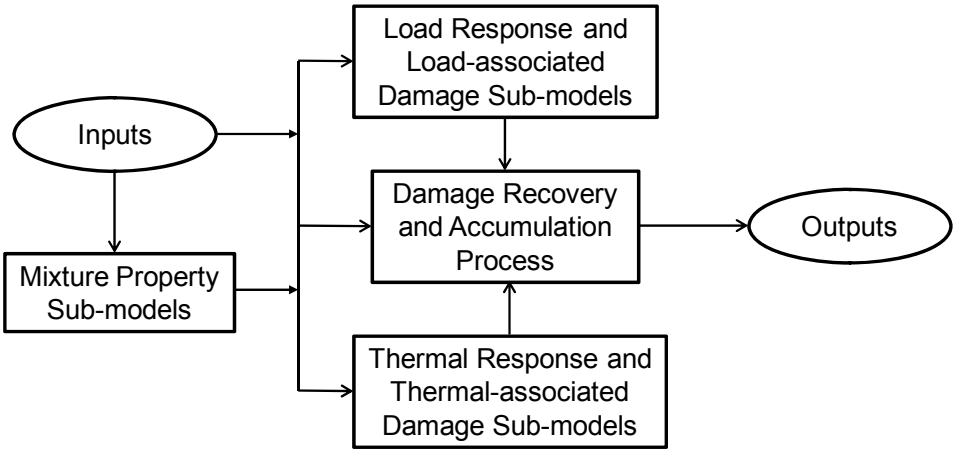

Figure 7-1 General framework of the HMA-FM-E model

The enhanced model was used to predict top-down cracking performance in HMA layers for all ten Superpave projects. The remaining parts of this section present the input module for the HMA-FM-E model, followed by model prediction results.

7.2.2 Input Module

The inputs for the HMA-FM-E model are divided into six categories, including traffic, climate, structure, mixture damage and fracture property, mixture healing property, and analysis type, as shown in Table 7-1. Data characteristics for each input category are described as follows (see also Table 7-1).

- Traffic: The traffic volume (in terms of million ESALs per year) for the year of field evaluation for each project was taken as the base value and applied to the corresponding pavement section for the entire simulation period, without considering annual traffic growth.
- Climate: Hourly temperature variation at different depths in the asphalt concrete (AC) layer for one typical year in Melrose, FL was used for all projects for the entire simulation period. The annual change in temperature was not considered.
- Structure: A three-layer pavement structure was selected for the simulation. Thickness for AC and Base were obtained from design values. Modulus for Base and Subgrade were determined based on back-analysis of FWD data obtained at the time of field evaluation. The changes in Base and Subgrade moduli due to moisture variation in the unbound materials were not considered. AC layer modulus was predicted using the AC stiffness aging sub-model which requires gradation, binder type, and volumetric information measured at the unaged condition. In other words, the change in AC modulus due to aging was taken into account for the entire simulation period.
- AC damage and fracture property: AC damage and fracture properties including creep rate, fracture energy limit (FE_f), etc., were predicted using mixture property

aging sub-models, taking into account the measured properties from field cores obtained at the time of field evaluation.

- AC healing property: AC healing potential was predicted using the maximum healing potential aging sub-model.
- Analysis type: Deterministic analyses were conducted for all projects.

Table 7-1 Summary of input data characteristics for the HMA-FM-E model

Inputs	Description
Traffic	Multi-year data: - Based on current ESALs/Year as measured (No growth is counted)
Climate	Multi-year data: Based on typical one-year data in Melrose, FL
Structure	- Three-layer - AC modulus (multi-year data) predicted from initial data: Gradation, binder type, volumetric information (for AC stiffness model) - GB, SG moduli (current data) obtained from FWD data (No moisture effect)
AC damage and fracture property	Multi-year data: - Predicted using mixture property aging sub-models - Adjusted based on current data from IDT tests
AC healing property	Multi-year data: - Predicted using the maximum healing potential aging sub-model
Analysis Type	- Deterministic analysis

7.2.3 Model Prediction Results

The predicted relative crack depth (CD_r), crack amount (CA) and crack status for top-down cracking for each Superpave section are presented in Table 7-2. It shows that at the time of field evaluation, two out of the ten sections (Projects 3 and 4) have reached CA_{max} (failure), two (Projects 6 and 7) started to crack, three (Projects 2, 9, 11) did not but were about to crack, and three (Projects 1, 10 and 12) were far from crack initiation.

Table 7-2 Predicted top-down cracking performance using HMA-FM-E model

Project (UF) ID	Time of Evaluation (Year)	Enhanced HMA-FM-Based Model Prediction Top-Down Cracking				
		CD_r (%)	CA (ft/100 ft)	CA_i (ft/100 ft)	t_i (Year)	Status
1	11	2.2	14.5	22.2	16.9	U
2	11	2.9	19.2	22.3	12.8	U
3	11	50.0	330.0	17.1	6.9	C
4	11	50.0	330.0	22.2	5.9	C
6	11	10.7	70.5	25.8	9.5	C
7	11	8.2	54.3	24.5	10.0	C
9	7	4.1	27.4	30.0	7.7	U
10	7	1.5	10.1	21.3	14.7	U
11	6	2.8	18.8	21.3	6.8	U
12	6	1.5	9.7	25.4	15.8	U

Note:
1. CD_r denotes relative crack depth (in %), defined as crack depth over AC layer thickness
2. For CD_r = 50 %, the maximum crack amount (CA_{max}) is 330 ft/100 ft

Figure 7-2 (a) to (c) shows the predicted development of top-down crack amount over time. As shown, project sections 3, 4, and 11 had the worst cracking performance with shorter crack initiation time (t_i) and higher average crack growth rate (G_t) than rest of the sections, while Sections 1, 10, and 12 had the best performance.

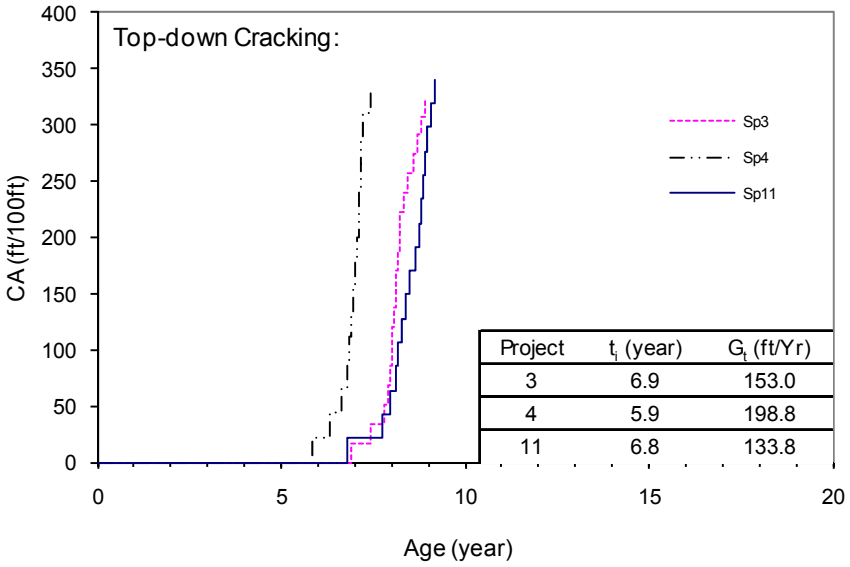

(a) Bad performance sections

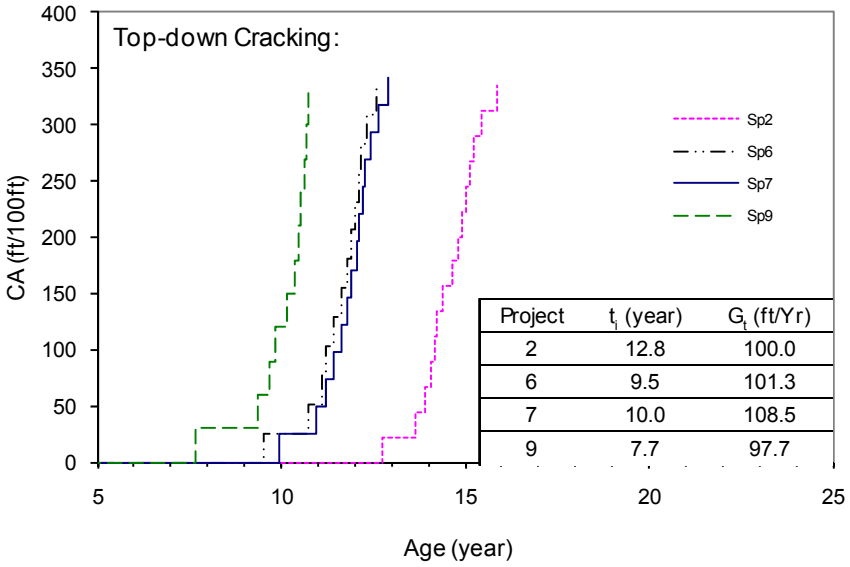

(b) Intermediate performance sections

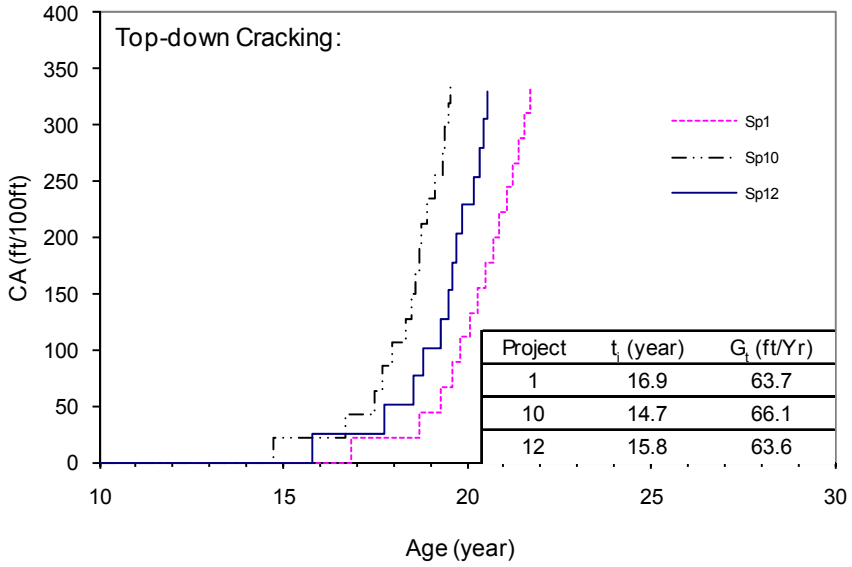

(c) Good performance sections

Figure 7-2 Predicted crack amount increase over time using HMA-FM-E model

7.3 Mechanistic-Empirical Pavement Design Guide (MEPDG) Program

7.3.1 Introduction

The MEPDG program/software was developed under NCHRP Project 01-37A as part of the 2002 design guide for use in the design of new and rehabilitated pavement structures, including both flexible and rigid pavements (ERES Consultants, 2004). It has been (and is being) continuously improved over the years through a series of projects that followed. The 1.1 version (released in Sep., 2009) was adopted for this study, which is available from the design guide website.

In this study, the MEPDG program was used to predict cracking performance (both bottom-up and top-down cracking) for the Superpave flexible pavement sections. In other words, the bottom-up and top-down cracking models of the MEPDG program were adopted to undertake the prediction tasks. The cracking models were calibrated based on three large-scale

pavement experiments, including the Minnesota Road Research (MnRoad) Project, the WesTrack Project, and the Long-Term Pavement Performance (LTPP) Program. A general flowchart of the cracking models is presented in Figure 7-3, which includes three major components: a response sub-model, a damage sub-model, and a damage-crack amount relationship. Details for each component are described elsewhere (El-Basyouny and Witczak, 2005a, 2005b) and were not included in this report.

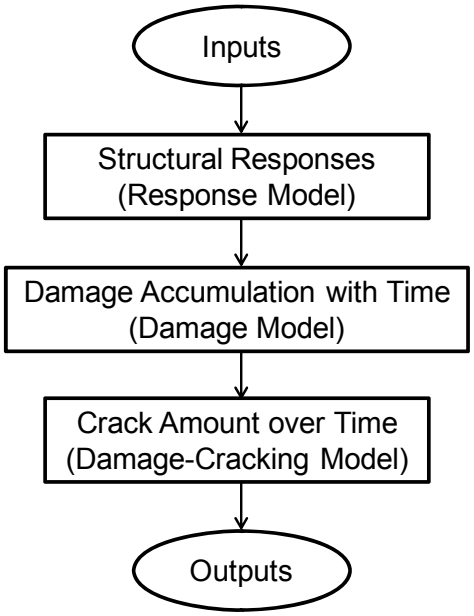

Figure 7-3 General flowchart for the cracking models in MEPDG program

The remaining parts of this section present the input module for the cracking models in the MEPDG, followed by model prediction results.

7.3.2 Input Module

The inputs for the MEPDG program are divided into four categories, including traffic, climate, structure, and analysis type, as shown in Table 7-3. Data characteristics for each input category are described as follows (see also Table 7-3).

- Traffic: The traffic volume (in terms of million ESALs per year) for the year of field evaluation for each project was taken as the base value and applied to the corresponding pavement section for the entire simulation period, without considering annual traffic growth.
- Climate: For any given location (i.e., latitude and longitude of any pavement section), the MEPDG program allows interpolating and generating climatic data based on available data of nearby weather stations. The interpolated/weighted data were used to predict temperature variation at different depths in the AC layer of all Superpave sections.
- Structure: A three-layer pavement structure was selected for the simulation. Thickness for AC and Base were obtained from design values. Modulus for Base and Subgrade were determined based on back-analysis of FWD data obtained at the time of field evaluation. The change in Base and Subgrade moduli due to moisture variation in the unbound materials was not considered. AC layer modulus was predicted using the dynamic modulus sub-model which requires gradation, binder type, and volumetric information measured at the unaged condition. The change in AC modulus due to aging was taken into account for the entire simulation period.
- Analysis type: Deterministic analyses were conducted for all projects.

Table 7-3 Summary of input data characteristics for the MEPDG

Inputs	Description
Traffic	Multi-year data: - Based on current ESALs/Year as measured (No growth is counted)
Climate	Multi-year data: - Weighted data from weather stations near the site
Structure	- Three-layer - AC modulus (multi-year data) predicted from initial data: Gradation, binder type, volumetric information (for dynamic modulus model) - GB, SG moduli (current data) obtained from FWD data (No moisture effect)
Analysis Type	- Deterministic analysis

7.3.3 Model Prediction Results

Predicted results using the bottom-up cracking and top-down cracking models in the MEPDG are presented separately as follows:

7.3.3.1 Prediction Using the BUC Model

Table 7-4 presents the predicted damage (D), crack amount (CA) and crack status for bottom-up cracking for each Superpave section. It shows that at the time of evaluation, CA in any section did not reach the amount for crack initiation (CA_i), so the predicted crack status is uncracked (denoted as ″U″) for all sections. It can also be seen that one out of ten sections (i.e., Project 7) which has the largest CA was about to crack at the time of evaluation.

Table 7-4 Predicted bottom-up cracking using the MEPDG

Project (UF) ID	Time of Evaluation (Year)	MEPDG Prediction				
		Bottom-Up Cracking				
		D (%)	CA (%)	CA_i (%)	t_i (Year)	Status
1	11	0.32	0.2	7.6	50+	U
2	11	0.36	0.2	7.6	50+	U
3	11	0.49	0.3	7.9	50+	U
4	11	3.74	2.8	7.6	31.5	U
6	11	0.40	0.2	7.3	50+	U
7	11	9.34	6.9	7.4	11.9	U
9	7	0.39	0.2	6.9	50+	U
10	7	1.51	1.1	7.7	50+	U
11	6	1.68	1.2	7.7	39.0	U
12	6	0.05	0.0	7.3	50+	U

Note:
1. CA denotes crack amount
2. For 100 % damage, the CA_{max} for BUC is 50 % (or 3000 ft^2/6000 ft^2)

It should be noted that the cracking models in MEPDG essentially only describe the crack initiation phase of pavement cracking in which the models accumulate damage to 100 %, and the crack propagation phase is taken into account through field calibration (i.e., by correlating damage to observed crack amount in the field). So, the CA_i is in fact not defined in the models. However, the introduction of CA_i into the cracking models was necessary because it can be used to estimate t_i, which was needed to compare to the field observation-based crack initiation time for model evaluation (Section 7.6). In this study, CA_i was determined to be the crack amount at 10 % damage based on work by Timm (2008) and engineering judgment of the research team.

Prediction of bottom-up cracking development over time for all ten Superpave sections is shown in Figure 7-4. Overall, the increase of crack amount over time is approximately linear. So, an average rate of increase in crack amount (G_r) was estimated for each project, which is the slope of each line in the Figure. It can be seen that four out of ten sections have a G_r greater than 0.1 % per year (Figure 7-4 (a)), and rest of the sections have a G_r less than 0.05 % per year

(Figure 7-4 (b) to (c)). Among all sections, Project 7 has the worst performance (with the largest G_r and the shortest t_i).

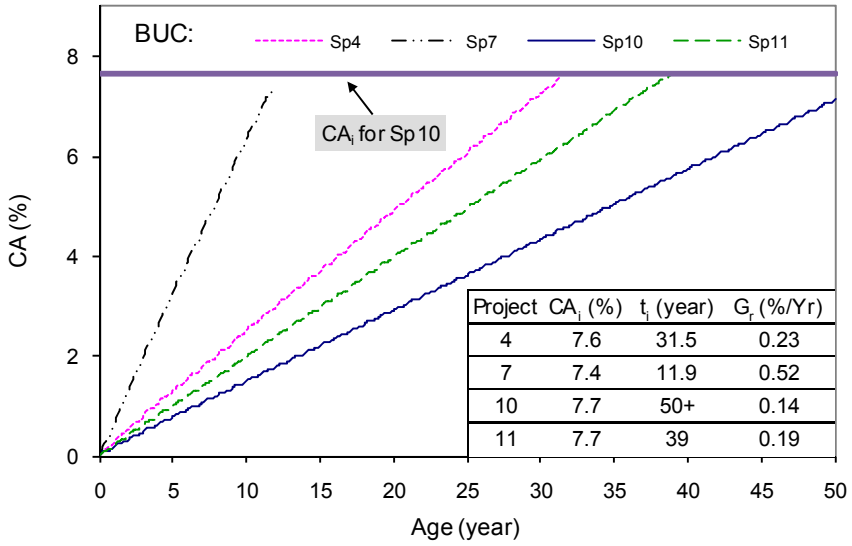

Project	CA_i (%)	t_i (year)	G_r (%/Yr)
4	7.6	31.5	0.23
7	7.4	11.9	0.52
10	7.7	50+	0.14
11	7.7	39	0.19

(a) Projects (4, 7, 10, and 11) with a G_r greater than 0.1 % per year

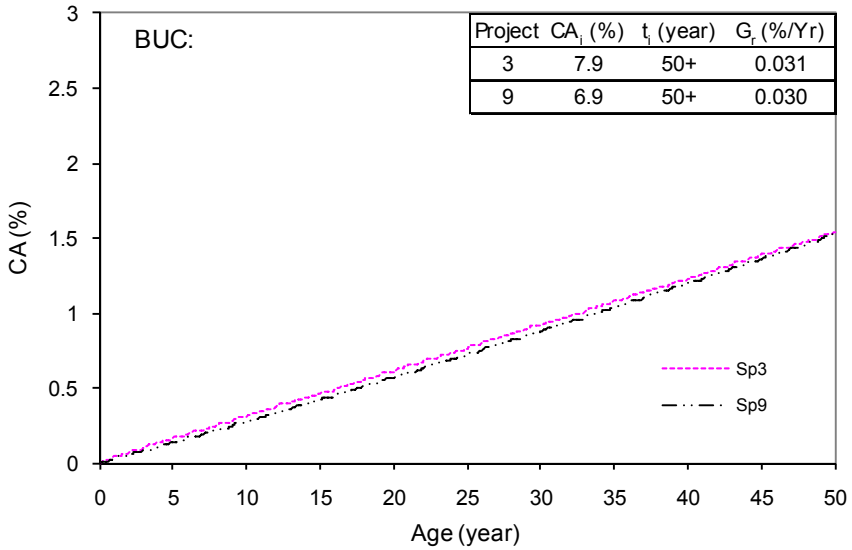

Project	CA_i (%)	t_i (year)	G_r (%/Yr)
3	7.9	50+	0.031
9	6.9	50+	0.030

(b) Projects (3 and 9) with a low G_r

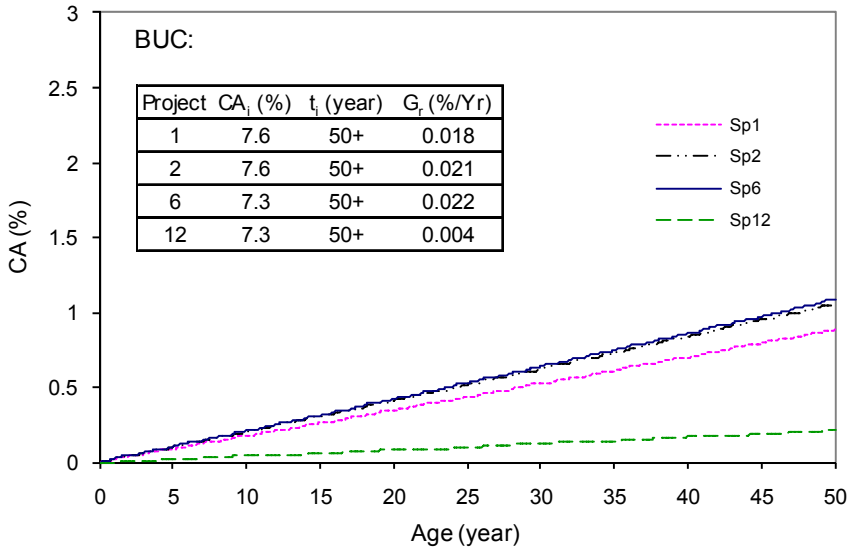

(c) Projects (1, 2, 6, and 12) with a lower G_r

Figure 7-4 Predicted increase of bottom-up crack amount over time using the MEPDG

7.3.3.2 Prediction Using the TDC Model

Table 7-5 presents the predicted damage (D), crack amount (CA) and crack status for top-down cracking for each Superpave section. It shows that at the time of evaluation, CA in Project 7 is greater than the CA_i, so the predicted crack status is cracked (denoted as ″C″) for this section. The rest of the sections are not cracked.

Table 7-5 Predicted top-down cracking using the MEPDG

Project (UF) ID	Time of Evaluation (Year)	MEPDG Prediction				
		Top-Down Cracking				
		D (%)	CA (ft/500ft)	CA_i (ft/500ft)	t_i (Year)	Status
1	11	0.81	0.7	29.3	50+	U
2	11	0.67	0.5	29.3	50+	U
3	11	1.18	1.2	29.3	50+	U
4	11	6.60	15.8	29.3	17.2	U
6	11	0.68	0.5	29.3	50+	U
7	11	14.20	49.1	29.3	7.3	C
9	7	0.42	0.2	29.3	50+	U
10	7	3.09	5.0	29.3	26.0	U
11	6	2.43	3.5	29.3	27.0	U
12	6	0.06	0.0	29.3	50+	U

Note:
1. For 100 % damage, the CA_{max} for TDC is 473 ft/500 ft (or 5000 ft/mile)

Prediction of top-down cracking development over time for all Superpave sections is presented in Figure 7-5. As shown, the increase of crack amount over time is nonlinear, which is clearly different from the linear relationship observed from bottom-up cracking predictions (see Figure 7-4). For convenience in comparison of performance among different sections, an average rate of increase in crack amount (G_r) was estimated for each project, which is the overall slope of each curve in Figure 7-5.

It can be seen that four out of ten sections have a G_r greater than 1 ft/Year (Figure 7-5 (a)), and the rest of the sections have a G_r less than 0.2 ft/Year (Figure 7-5 (b) to (c)). Among all sections, Project 7 has the worst performance (with the largest G_r and the shortest t_i).

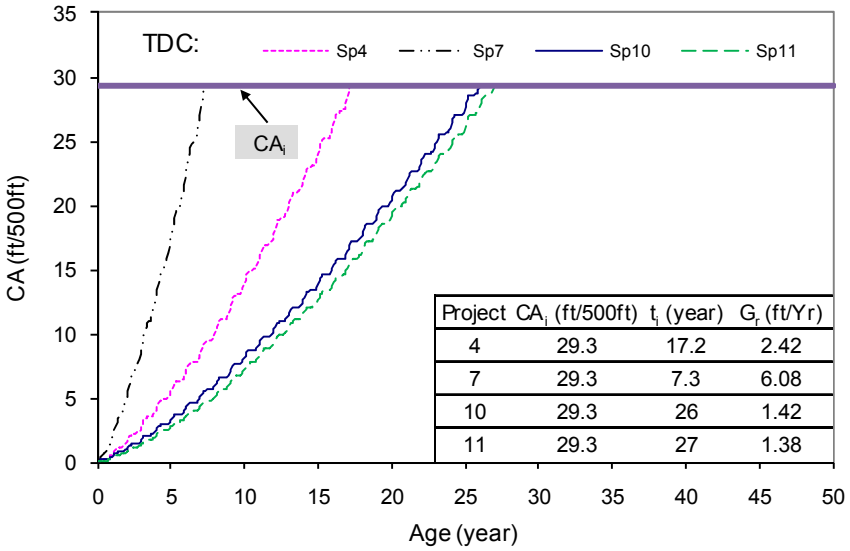

Project	CA_i (ft/500ft)	t_i (year)	G_r (ft/Yr)
4	29.3	17.2	2.42
7	29.3	7.3	6.08
10	29.3	26	1.42
11	29.3	27	1.38

(a) Projects (4, 7, 10, and 11) with a G_r greater than 1 ft per year

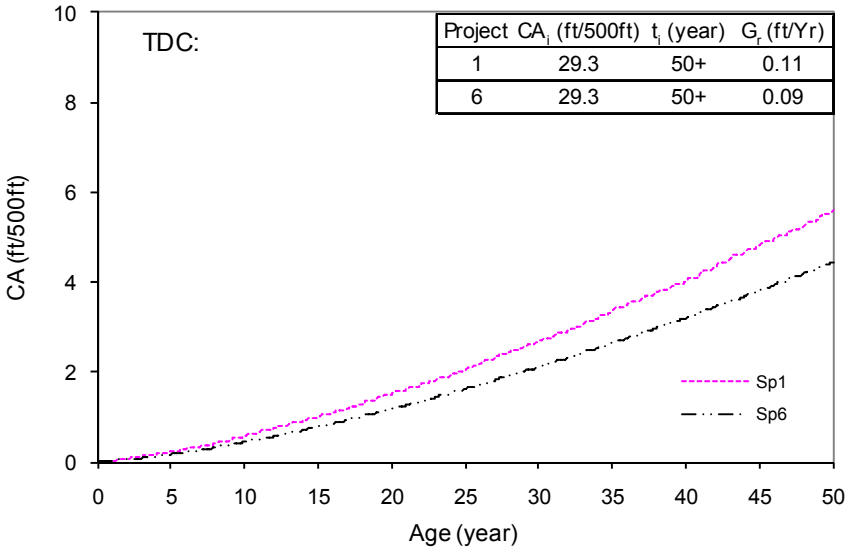

Project	CA_i (ft/500ft)	t_i (year)	G_r (ft/Yr)
1	29.3	50+	0.11
6	29.3	50+	0.09

(b) Projects (1 and 6) with a Low G_r

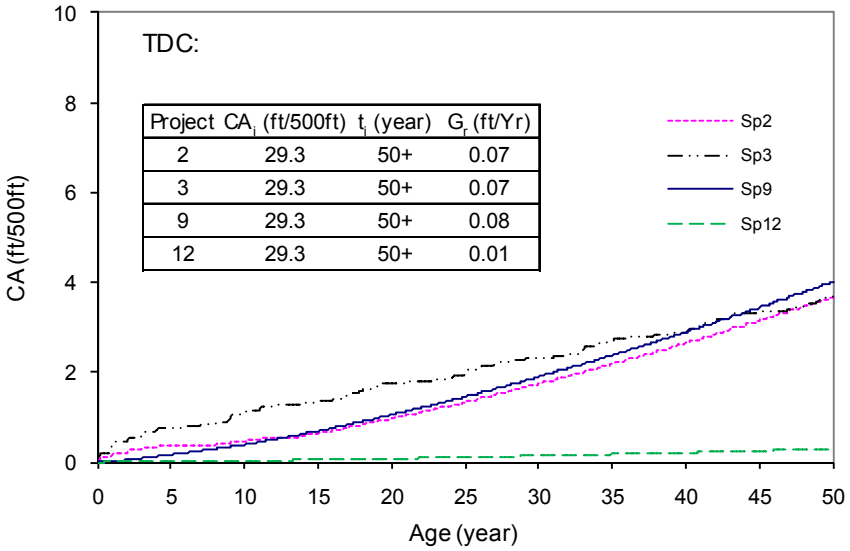

(c) Projects (2, 3, 9, and 12) with a lower G_r

Figure 7-5 Predicted crack amount increase over time using the MEPDG (TDC model)

7.4 Perpetual Pavement Design (PerRoad) Program

7.4.1 Introduction

The PerRoad program was developed for use in the design of perpetual pavement. The goal of the design is to prevent deep structural distresses, including bottom-up cracking and consolidation/structural rutting, so that all distresses can be quickly remedied from surface, which will result in a structure with perpetual life (Timm and Newcomb, 2006). It has been continuously improved over the years through several projects. The 3.5 version (released in Apr. 2010) was adopted for this study, which is available from Dr. Timm's website.

In this study, the PerRoad program was used to predict bottom-up cracking performance for all ten Superpave projects. In other words, the bottom-up cracking model in the program was adopted to undertake the prediction task. The model was locally calibrated based on MnRoad research project (Timm et al., 2006). In an attempt to make the model suitable for use for Florida

sections and to facilitate comparison of predictions to those by MEPDG, the existing model coefficients were replaced with a new set of coefficients derived from the nationally calibrated BUC model in the MEPDG (see Table 7-6), where k_1, C, and E are parameters defined elsewhere (M. El-Basyouny and M. Witczak. 2005a).

Table 7-6 New coefficients for the BUC model in the PerRoad program

		f_3	f_1	f_2
MEPDG – BUC Model		$0.00432 \cdot k_1 \cdot C$	1.281	3.9492
PerRoad – BUC Model	Existing Coeff.	2.83×10^{-6}	0	3.148
	New Coeff.	$0.00432 \cdot k_1 \cdot C \cdot E^{-1.281}$	0	3.9492

A general flowchart of the calibrated model is presented in Figure 7-6. As shown, Monte Carlo simulation and Endurance Limit are two distinctive features of the model. The former was used to randomly generate pavement structures and loads based on the inputs for use by the response model, and the latter is important to filter small responses that do not cause damage in the AC layer. Details for each model component are described elsewhere (Timm and Newcomb, 2006) and were not included in this report. The remaining parts of this section present the input module for the BUC model in the PerRoad, followed by model prediction results.

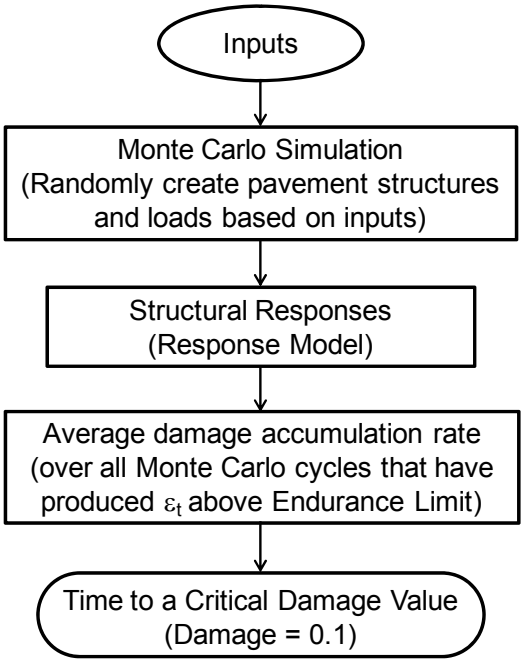

Figure 7-6 Flowchart of the bottom-up cracking model in PerRoad

7.4.2 Input Module

The inputs for the PerRoad program are divided into four categories, including traffic, climate, structure, and analysis type, as shown in Table 7-7. Data characteristics for each input category are described as follows (see also Table 7-7).

- Traffic: The traffic volume (in terms of million ESALs per year) for the year of field evaluation for each project was taken as the base value and applied to the corresponding pavement section for the entire simulation period, without considering annual traffic growth.
- Climate: Seasonal temperature variation of one typical year obtained for each project from MEPDG climatic prediction was applied to each section for the entire simulation period. The annual change in temperature was not considered.

- Structure: A three-layer pavement structure was selected for the simulation. Thickness for AC and Base were obtained from design values. Modulus for Base and Subgrade were determined based on back-analysis of FWD data obtained at the time of field evaluation. The change in Base and Subgrade moduli due to moisture variation in the unbound materials was not considered. Seasonal AC layer modulus was predicted using the stiffness-pavement temperature relationship which requires PG-grade and air temperature. The change in AC modulus due to aging was not considered.
- Analysis type: Deterministic analyses were conducted for all projects.

Table 7-7 Summary of input data characteristics for PerRoad

Inputs	Description
Traffic	Multi-year data: - Based on current ESALs/Year as measured (No growth is counted)
Climate	Multi-year data: - Based on typical one-year data (averaged for each season) from MEPDG climatic prediction
Structure	- Three-layer - AC modulus (one-year data) predicted from initial data: PG-Grade and air temperature (for stiffness-pavement temperature relation) - GB, SG moduli (current data) obtained from FWD data (No moisture effect)
Analysis Type	- Deterministic analysis

7.4.3 Model Prediction Results

The predicted damage rate in terms of damage per million ESALs (D/MESAL) and crack status for bottom-up cracking for each Superpave section are presented in Table 7-8. It shows that at the time of evaluation, two out of ten sections (Projects 4 and 7) have cracked, two (Projects 10 and 11) did not but were about to crack, and rest of the sections were far from crack

initiation. It can also be seen that the predicted BUC performance was affected by a combination of damage rate and traffic volume. In other words, a higher damage rate and/or a higher traffic resulted in worse cracking performance (i.e., shorter crack initiation time) of Projects 4, 7, 10, 11 than for the rest of the Projects. It is noted that the PerRoad program does not predict crack amount.

Table 7-8 Predicted bottom-up cracking using PerRoad

Project (UF) ID	Time of Evaluation (Year)	PerRoad Prediction			
		Bottom-Up Cracking			
		D/MESAL	Traffic (MESAL/Year)	t_i (Year)	Status
1	11	0.0026	0.5	50+	U
2	11	0.0013	1.1	50+	U
3	11	0.0014	1.2	50+	U
4	11	0.0129	1.0	7.6	C
6	11	0.0040	0.5	48.0	U
7	11	0.0174	2.3	2.5	C
9	7	0.0386	0.1	44.4	U
10	7	0.2945	0.04	9.4	U
11	6	0.0095	1.4	7.3	U
12	6	0.0079	0.03	50+	U

7.5 Energy Ratio Based Model (ER Model)

7.5.1 Introduction

During the course of developing an energy-based criterion for top-down cracking performance in HMA, the research team at UF identified a parameter called energy ratio (ER), which was defined as the ratio of dissipated creep strain energy limit ($DCSE_f$) over the minimum dissipated creep strain energy ($DCSE_{min}$) required for good top-down cracking performance (Roque et al., 2004). The ER parameter was then used to develop an ER criterion, together with a minimum $DCSE_f$ criterion to form a system (of two energy-based criteria) that is capable of distinguishing HMA layers that are cracked (bad performance) from those that are not (good

performance). It should be noted that these criteria were developed using properties of aged field cores taken from Florida pavements.

The ER model was developed based on these two energy-based criteria for use in design of new and rehabilitated flexible pavements (Wang et al., 2007). In this study, the ER model was adopted to predict top-down cracking performance for all ten Superpave projects. A general flowchart of the prediction procedure is presented in Figure 7-7. As shown, the material property sub-models were developed and introduced into the ER model to facilitate the prediction of mixture properties required to determine ER, when measured properties from field cores are not available. Details for these material property sub-models and the other major components are described elsewhere (Wang et al., 2007) and were not included in this report. The remaining parts of this section present the input module for the ER model, followed by model prediction results.

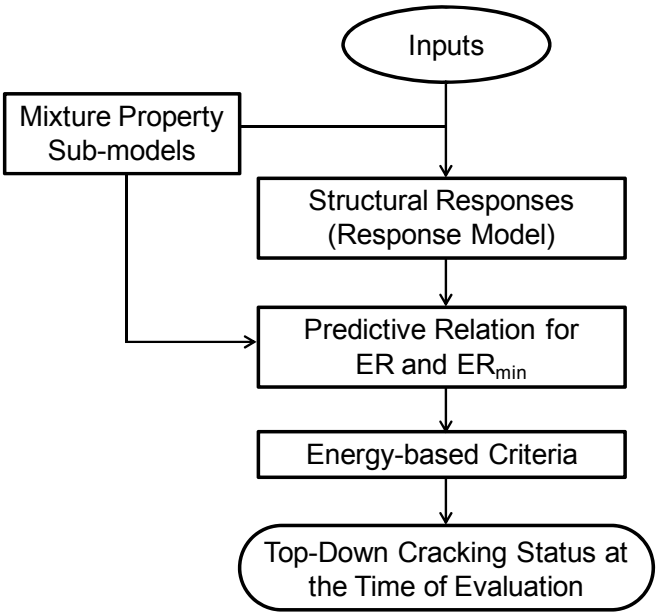

Figure 7-7 General flowchart of ER model

7.5.2 Input Module

The inputs for the ER model are divided into five categories, including traffic, climate, structure, AC damage and fracture property, and analysis type, as shown in Table 7-9. Data characteristics for each input category are described as follows (see also Table 7-9).

Table 7-9 Summary of input data characteristics for ER model

Inputs	Description
Traffic	Multi-year data (ESALs in 20 Years): - Based on current ESALs/Year as measured (No growth is counted)
Climate	Mean annual air temperature (MAAT): - From MEPDG climatic prediction (Not required, if AC damage and facture properties are from field cores)
Structure	- Three-layer - AC modulus (current data) predicted from initial data: Gradation, binder type, volumetric information (for AC stiffness model) - GB, SG moduli (current data) obtained from FWD data (No moisture effect)
AC damage and fracture properties	Current data (m, D_1, S_t, $DCSE_f$): - Measured from field cores (Option One) - Predicted using material property sub-models (Option Two)
Analysis Type	- Deterministic analysis

- Traffic: The traffic volume (in terms of million ESALs per year) for the year of field evaluation for each project was taken as the base value and applied to the corresponding pavement section for the entire simulation period, without considering annual traffic growth.
- Climate: Mean annual air temperature (MAAT) obtained for each project from MEPDG climatic prediction was used for the corresponding pavement section.
- Structure: A three-layer pavement structure was selected for the simulation. Thickness for AC and Base were obtained from design values. Modulus for Base and Subgrade were determined based on back-analysis of FWD data obtained at the

time of field evaluation. The change in Base and Subgrade moduli due to moisture variation in the unbound materials was not considered. AC layer modulus at the time of evaluation was predicted using the AC stiffness aging sub-model which requires gradation, binder type, and volumetric information measured at the unaged condition.

- AC damage and fracture property: AC damage and fracture properties at the time of field evaluation can be measured from field cores (Option One) or predicted using material property sub-models (Option Two). In this study, properties determined from both options were used by the model. The predictions based on measured properties, which are more accurate than those based on predicted properties, were presented in the following part of this section.
- Analysis type: Deterministic analyses were conducted for all projects.

7.5.3 Model Prediction Results

The predicted energy ratio (ER), minimum required energy ratio (ER_{min}), and crack status for top-down cracking for each Superpave section are presented in Table 7-10. It shows that at the time of evaluation, two out of ten sections (Projects 4 and 9) were predicted to be cracked, for which ER is less than ER_{min} and/or $DCSE_f$ is below 0.75 kJ/m^3 (i.e., one or both of the energy-based criteria were not satisfied). The rest of the sections were predicted to be uncracked. However, it is not clear how far away these uncracked sections are from crack initiation as the ER model does not predict crack initiation time.

Table 7-10 Predicted top-down cracking using the ER model

Project (UF) ID	Time of Evaluation (Year)	ER Model Prediction Top-Down Cracking			
		$DCSE_f$ (kJ/m^3)	ER	ER_{min}	Status
1	11	1.68	2.15	1.12	U
2	11	2.77	2.43	1.41	U
3	11	1.40	3.95	1.47	U
4	11	1.22	1.29	1.40	C
6	11	0.99	1.40	1.07	U
7	11	1.49	2.69	1.75	U
9	7	0.45	0.84	0.77	C
10	7	1.07	3.96	0.76	U
11	6	1.30	2.90	1.54	U
12	6	1.08	1.47	0.75	U

7.6 Performance Model Evaluation

7.6.1 Introduction

Four prediction tools were adopted in the prior sections to undertake performance prediction. Two out of the four tools (HMA-FM-E and ER Model) were used for prediction of top-down cracking, one (PerRoad Program) for bottom-up cracking, and one (MEPDG Program) for both top-down and bottom-up cracking. In total, two BUC models and three TDC models were included in this study:

- BUC models: The BUC model in the MEPDG program and the PerRoad program
- TDC models: The TDC model in the MEPDG program, the HMA-FM-E model, and the ER model

The model evaluation process was completed in two stages: first, the models (BUC models followed by TDC models) were compared qualitatively in terms of their main features. In the second stage, prediction results obtained using these models (BUC predictions followed by

TDC predictions) were compared to field observation-based cracking performance presented in Table 7-11, which was determined based on the following two sources (see Sections 2.2 and 2.3).

- The crack rating history from construction through 2009 for each Superpave section was obtained from the flexible pavement condition survey (PCS) database, which is maintained by the Florida Department of Transportation (FDOT).
- Field trips were made to these Superpave sections for performance inspection and preparation of coring locations by the UF research team in 2009. The cracked sections exhibited different amount of cracking, while the uncracked sections were in an acceptable condition. An inspection of core samples from the cracked sections clearly indicated the presence of top-down cracking. No bottom-up cracking was observed.

Table 7-11 Observation-based cracking performance

Project (UF) ID	Time of Evaluation (Year)	Observation-Based TDC Performance	
		t_i (Year)	Cracking Status at Evaluation
1	11	16 (P)	U
2	11	10	C
3	11	9	C
4	11	< 11	C
6	11	11	C
7	11	18 (P)	U
9	7	< 7	C
10	7	< 7	C
11	6	9 (P)	U
12	6	< 6	C

Note: An inspection of core samples indicated that no bottom-up cracking occurred.

7.6.2 Comparison of Model Features

Six main features of the BUC models were compared in this part, including fatigue model, critical condition concept, damage model, endurance limit, crack amount model, and critical value(s). Comparison of each of the features is described as follows (see also Table 7-12):

- Fatigue model: The fatigue sub-models in MEPDG and PerRoad have a similar form. The difference is the number of cycles to failure (N_f) in MEPDG is a function of both tensile strain at bottom of AC layer and AC modulus, while it is a function of tensile strain only in PerRoad.
- Critical condition concept: Neither of the models requires critical condition concept.
- Damage model: The damage sub-models in these two programs are conceptually the same as both sub-models are based on Miner's Law. However, the damage accumulation process in MEPDG is much more involved than PerRoad.
- Endurance limit: The option for setting an endurance limit to filter small responses that do not cause damage is included in both MEPDG and PerRoad.
- Crack amount model: The crack amount in MEPDG is a function of damage. While, no crack amount sub-model is available in PerRoad.
- Critical value(s): Crack amount for crack initiation (CA_i) and 10% damage are critical values used for determination of crack initiation by MEPDG and PerRoad, respectively.

Table 7-12 Qualitative comparison of BUC models

	Models for Bottom-Up Cracking	
	MEPDG	PerRoad
Fatigue model (Number-of-load-cycles to failure)	$N_f = f(\varepsilon_t, E)$	$N_f = f(\varepsilon_t)$
Critical condition concept (Energy-based failure criteria)	Not required	Not required
Damage model	$D = \Sigma (n_i/N_f)$ (Miner's Law)	$D = \Sigma (n_i/N_f)$ (Miner's Law)
Endurance limit	User defined	$\varepsilon_t = 70\ \mu\varepsilon$
Crack amount model	CA = f (D) (in % lane area)	N/A
Critical value(s) for crack initiation	$CA = CA_i$	D = 0.1

Similarly, six main features were compared for the TDC models. Each of the comparisons is described as follows (see also Table 7-13):

- Fatigue model: The number of load cycles to failure (N_f) in MEPDG is a function of tensile strain and AC modulus. No fatigue model is required by HMA-FM-E model and ER model.
- Critical condition concept: The critical condition concept is used by both HMA-FM-E model and ER model, which is based on HMA fracture mechanics. In HMA-FM-E model, a damage recovery and accumulation process was developed based on this concept to accumulate damage in terms of a normalized dissipated creep strain energy until it reaches 1.0 (the threshold), which determines crack initiation (or propagation). In ER model, two energy-based failure criteria were developed based on this concept to distinguish cracked pavement sections from those that were not. No critical condition concept is required by MEPDG.
- Damage model: The damage sub-model in MEPDG is based on Miner's Law. It is not required by either HMA-FM-E model or ER model.

- Healing model/Endurance limit: The healing sub-model in HMA-FM-E model was developed to consider recovery of dissipated creep strain energy based on mixture's healing potential, which was assumed to be a function of the daily lowest stiffness, initial fracture energy, and age of the mixture. No healing sub-model is available in either MEPDG or ER model.
- Crack amount model: The crack amount is a function of damage in MEPDG, and it is a function of relative crack depth in HMA-FM-E model. No crack amount sub-model is available in ER Model.
- Critical value(s): Crack amount for crack initiation (CA_i) and 0.25 in. crack depth are critical values used for determination of crack initiation by MEPDG and HMA-FM-E model, respectively. The critical value is not required by ER model because it does not predict crack initiation.

Table 7-13 Qualitative comparison of TDC models

	Models for Top-Down Cracking		
	MEPDG	HMA-FM-E	ER Model
Fatigue model (Number-of-load-cycles to failure)	$N_f = f(\varepsilon_t, E)$	Not required	Not required
Critical condition concept (Energy-based failure criteria)	Not required	$\Sigma\ DCSE_{norm}(\Delta t_i) = 1$ (HMA-FM)	$ER = ER_{min}$ and $DCSE_f = 0.75$ kJ/m^3 (HMA-FM)
Damage model	$D = \Sigma\ (n_i/N_f)$ (Miner's Law)	Not required	Not required
Healing model (or Endurance limit)	N/A	$h = f(S_{low}, FE_i, t)$	N/A
Crack amount model	$CA = f(D)$ (in ft/500 ft)	$CA = f(CD_r)$ (in ft/100 ft)	N/A
Critical value(s) for crack initiation	$CA = CA_i$	CD = 0.25 in	Not required

7.6.3 Comparison of Prediction Results

In this sub-section, BUC predictions using MEPDG and PerRoad were compared to the field observation-based bottom-up cracking performance, followed by a comparison of TDC predictions using MEPDG, HMA-FM-E model, and ER model to the observation-based top-down cracking performance.

7.6.3.1 Comparison of BUC Predictions

The predicted crack initiation times (t_i) for BUC in all ten Superpave sections using MEPDG and PerRoad are presented in Figure 7-8. As shown, crack initiation times predicted by MEPDG are greater than 30 years for nine out of all ten Superpave sections, except for Project 7 (11.9 years). Overall, no section was predicted to be cracked at the time of field evaluation.

The predictions by PerRoad are generally equivalent to or smaller than those by MEPDG. In particular, four out of ten sections (Projects 4, 7, 10, and 11) have a crack initiation time of less than 10 years. Two of these sections (Projects 4 and 7) were predicted to be cracked, and the other two (Project 10 and 11) were predicted to approach crack initiation at the time of evaluation.

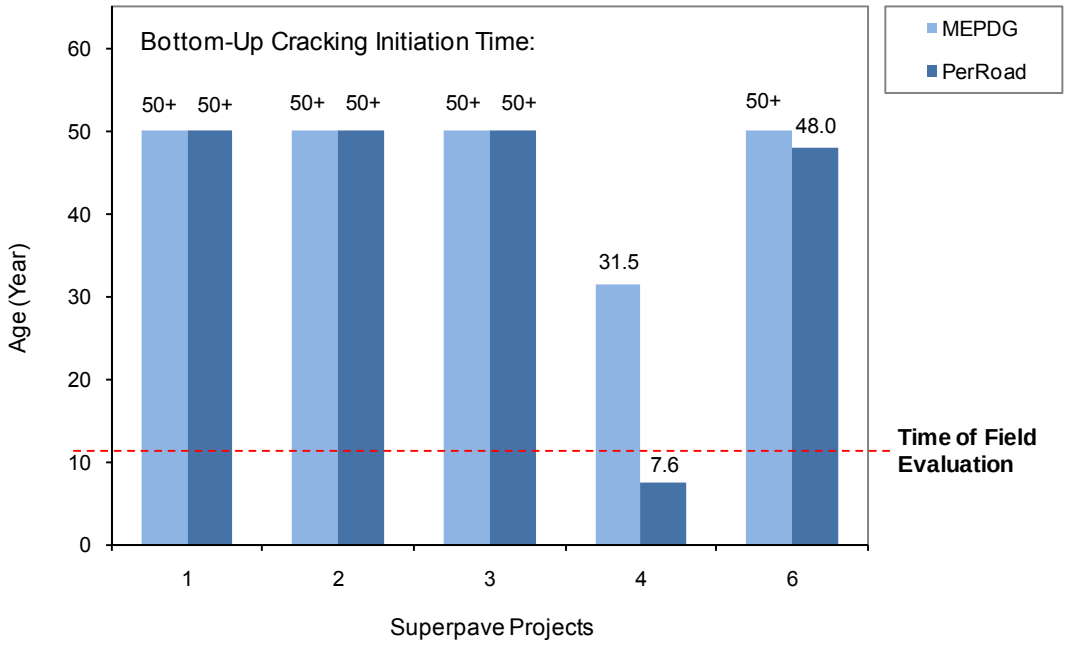

(a) Projects 1 to 4 and 6

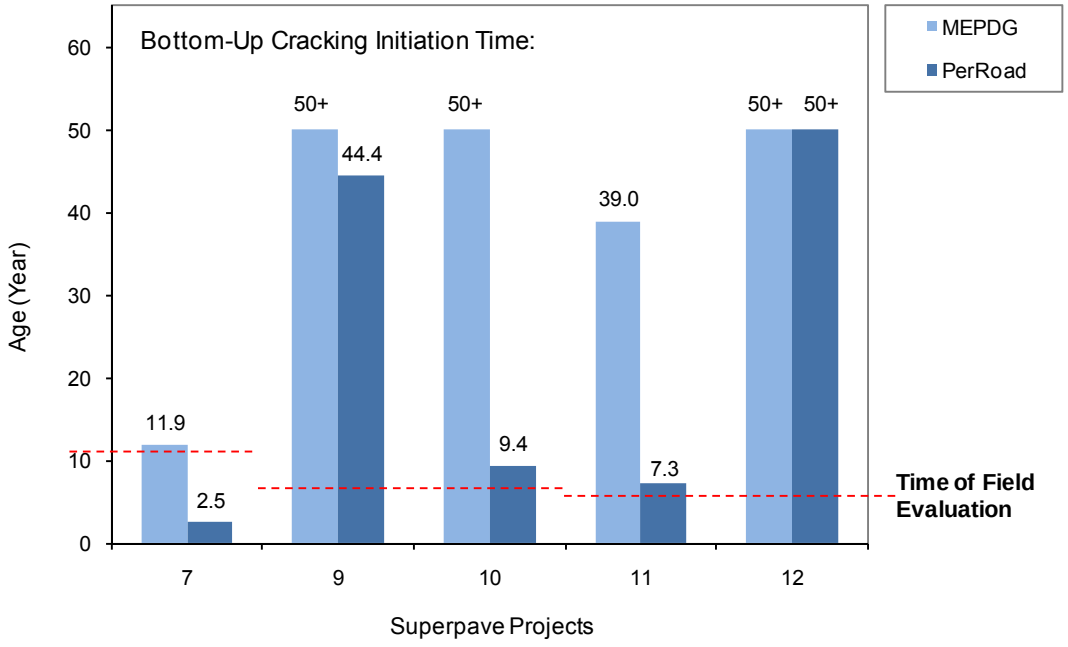

(b) Projects 7 and 9 to 12

Figure 7-8 Comparison of predicted t_i for BUC using MEPDG and PerRoad

As mentioned in Section 7.6.1, no bottom-up cracking occurred at the time of field evaluation, as indicated by an inspection of core samples. So, the BUC predictions by MEPDG which showed no cracking for all sections are consistent with field observations, while the predictions by PerRoad which showed two cracked sections appear to be less accurate than MEPDG. As indicated by the qualitative comparison of model features in Section 7.6.2, PerRoad is quite similar to MEPDG in terms of all main features, but most of them are less sophisticated than MEPDG. Therefore, predictions by MEPDG are potentially more accurate than PerRoad. It should be noted that comparison of crack amount development over time was not possible as PerRoad does not predict crack amount.

7.6.3.2 Comparison of TDC Predictions

Figure 7-8 shows the predicted crack initiation times for TDC in all ten Superpave sections using MEPDG and HMA-FM-E model. As shown, crack initiation times predicted by MEPDG are greater than 25 years for eight out of all ten Superpave sections, except for Project 4 (17.2 years) and Project 7 (7.3 years). Overall, only Project 7 was predicted to be cracked at the time of field evaluation.

The predictions by HMA-FM-E model are generally smaller than those by MEPDG except for Project 7. In particular, six out of ten sections (Projects 3, 4, 6, 7, 9, and 11) have a crack initiation time of no greater than 10 years. Four of these sections (Projects 3, 4, 6, and 7) were predicted to be cracked, and the other two (Project 9 and 11) were predicted to approach crack initiation at the time of evaluation.

The field observation-based crack initiation times for TDC are also presented in Figure 7-8. It can be seen that eight out of ten sections (Projects 2, 3, 4, 6, 9, 10, 11, and 12) have a crack

initiation time of no greater than 11 years. So, the TDC predictions by HMA-FM-E model are clearly closer to the field observation and more accurate than MEPDG.

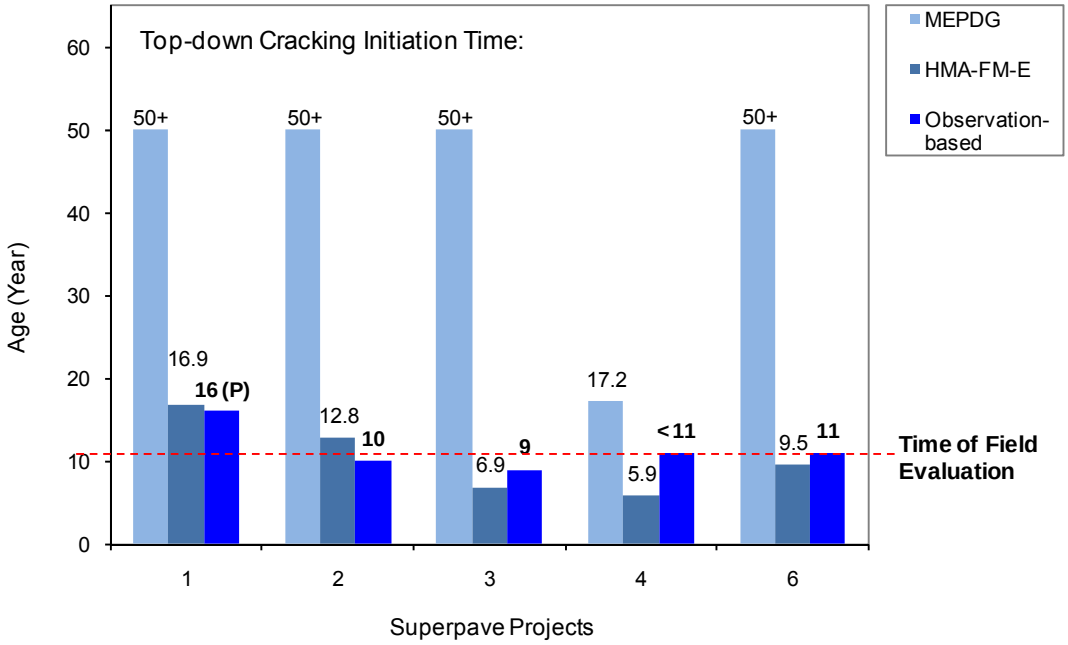

(a) Projects 1 to 4 and 6

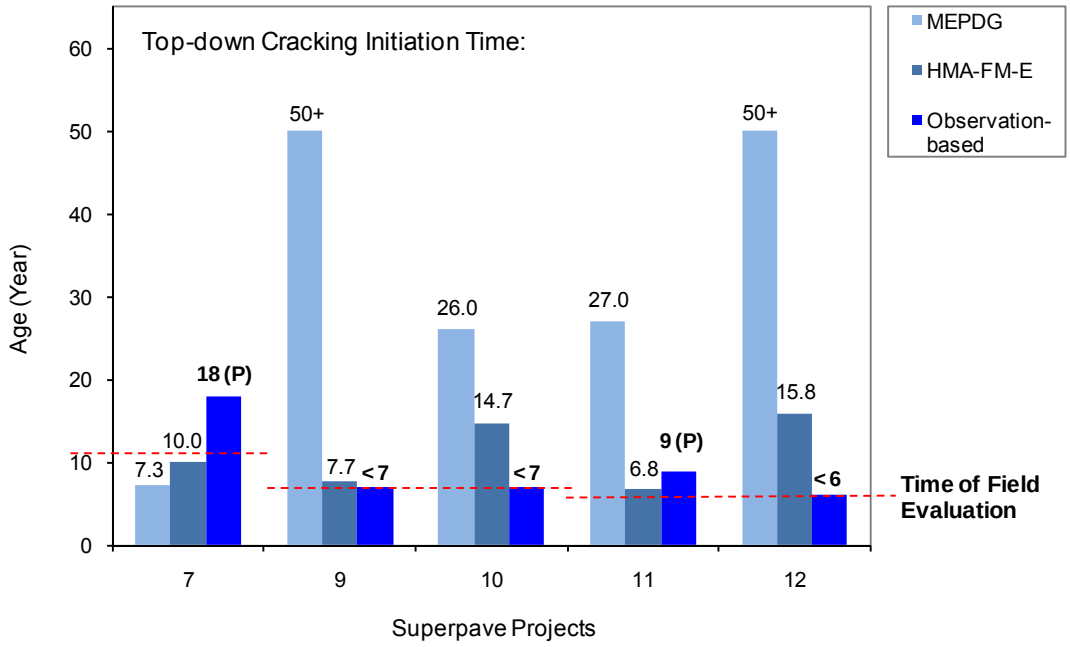

(b) Projects 7 and 9 to 11

Figure 7-9 Comparison of predicted t_i for TDC using MEPDG and HMA-FM-E model

As indicated by the qualitative comparison in Section 7.6.2, HMA-FM-E model is based on the critical condition concept, for which distress is stepwise discontinuous. While MEPDG is based on the traditional fatigue approach, for which distress is continuous. In other words, these two models are based on very different fundamental assumptions: discontinuous vs. continuous distress. Clearly, the discontinuous distress mode is closer to the actual top-down cracking pattern in the field. Therefore, the predictions by HMA-FM-E model are potentially more accurate than MEPDG. Besides, the introduction of sub-models that account for effects of healing and transverse thermal stresses also added prediction accuracy to the HMA-FM-E model.

The increase of crack amount over time was also compared since both HMA-FM-E model and MEPDG predict crack amount. Figure 7-10 presents a series of comparisons of

predictions by these two models and the observation-based performance for individual Superpave project. In an attempt to put the predicted crack amount by different models into the same scale, the crack amount (CA) was normalized by the maximum crack amount (CA_{max}) defined by each model. In other words, the comparison was undertaken in terms of a normalized crack amount: CA/CA_{max}.

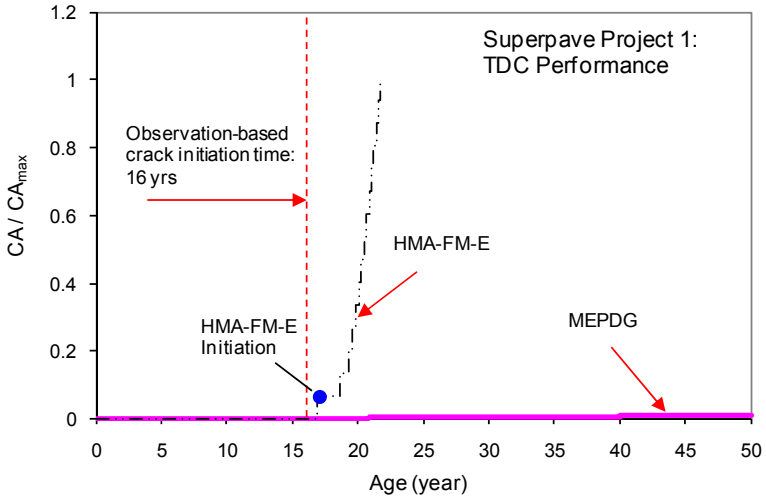

(a)

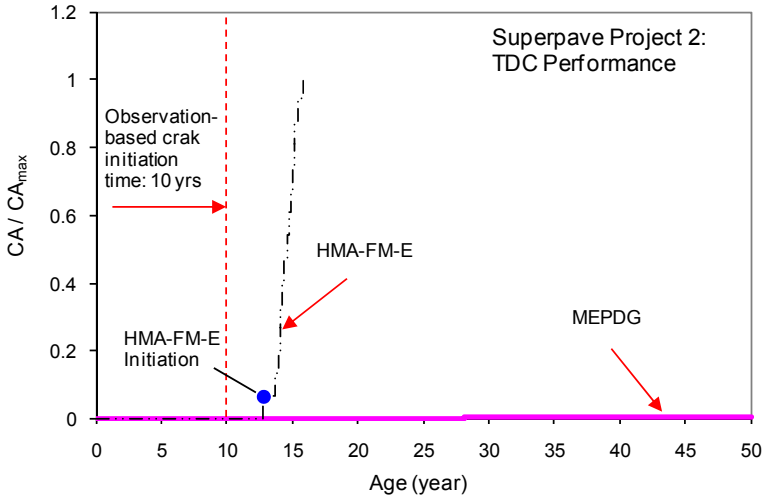

(b)

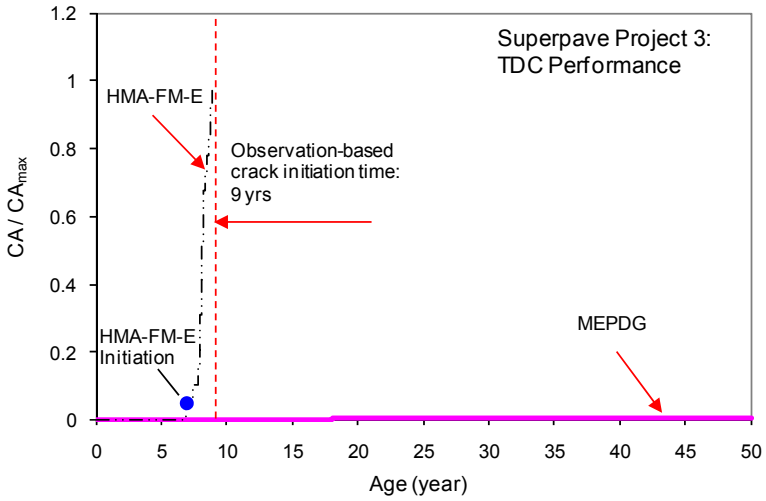
Superpave Project 3:
TDC Performance
HMA-FM-E
Observation-based
crack initiation time:
9 yrs
HMA-FM-E
Initiation
MEPDG
CA / CAmax
Age (year)

(c)

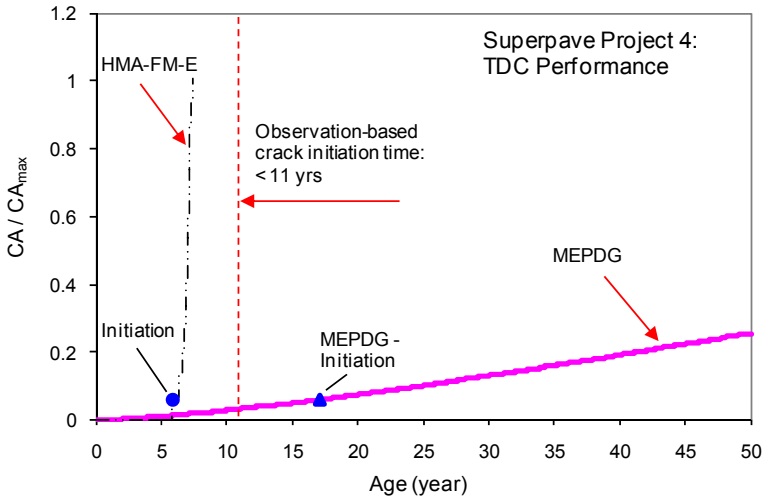
Superpave Project 4:
TDC Performance
HMA-FM-E
Observation-based
crack initiation time:
< 11 yrs
MEPDG
Initiation
MEPDG -
Initiation
CA / CAmax
Age (year)

(d)

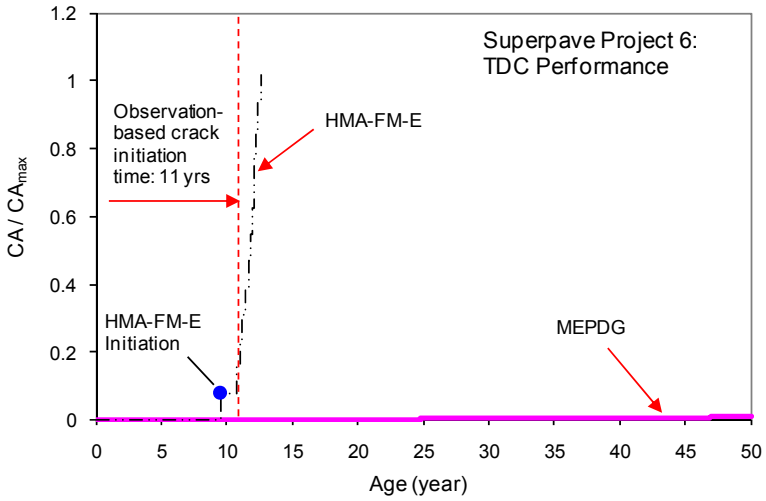
Superpave Project 6:
TDC Performance
Observation-based crack initiation time: 11 yrs
HMA-FM-E
HMA-FM-E Initiation
MEPDG
CA / CAmax
Age (year)

(e)

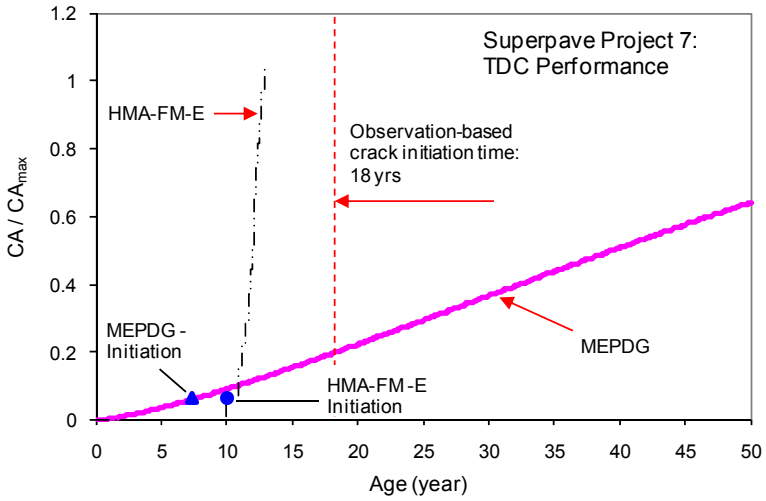
Superpave Project 7:
TDC Performance
HMA-FM-E
Observation-based crack initiation time: 18 yrs
MEPDG - Initiation
HMA-FM-E Initiation
MEPDG
CA / CAmax
Age (year)

(f)

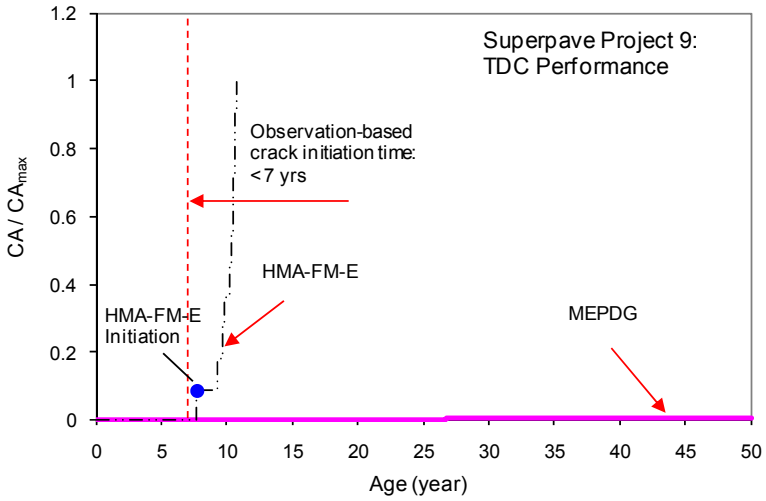
Superpave Project 9:
TDC Performance
Observation-based
crack initiation time:
<7 yrs
HMA-FM-E
HMA-FM-E
Initiation
MEPDG
CA / CAmax
Age (year)

(g)

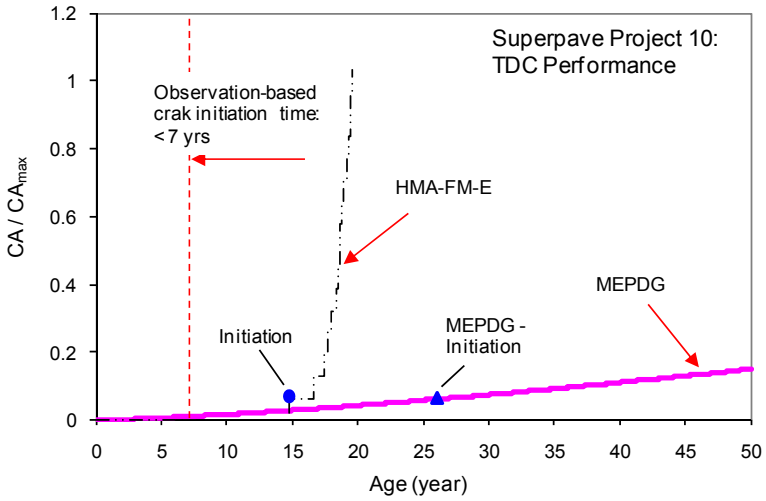
Superpave Project 10:
TDC Performance
Observation-based
crak initiation time:
<7 yrs
HMA-FM-E
MEPDG
Initiation
MEPDG -
Initiation
CA / CAmax
Age (year)

(h)

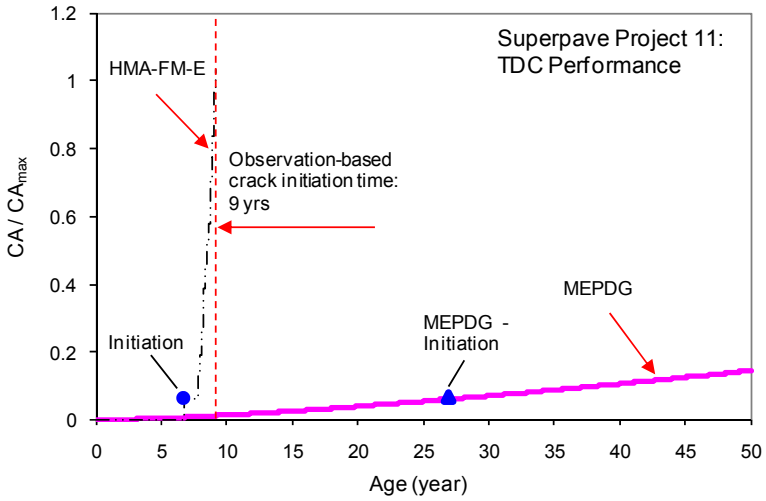

(i)

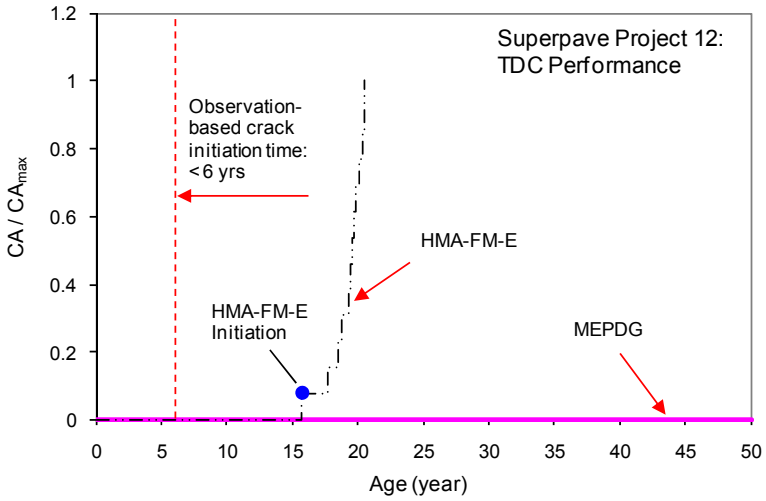

(j)

Figure 7-10 Comparison of predicted crack amount increase over time using different models

Overall, the predictions by HMA-FM-E model showed a much shorter crack initiation time than MEPDG for all the projects, except for Project 7. This trend is consistent with our prior findings from Figure 7-9. Also, the predicted crack propagation times to failure (i.e., when CA/CA_{max} is equal to 1) by HMA-FM-E model are generally within the range of 2 to 5 years.

They are much shorter than those predicted by MEPDG, generally greater than 40 years. From a practical point of view, the HMA-FM-E model predictions make more engineering sense.

The ER model predictions were not included in the prior comparisons because the model predicts neither crack initiation time nor crack amount. Nevertheless, it is a prediction tool to distinguish cracked sections from those that did not crack. In other words, it predicts crack status. Therefore, the ER model predictions were compared to the observation-based crack status, together with the predictions by MEPDG and HMA-FM-E model.

As shown in Table 7-14, Predictions by MEPDG are correct for only two out of all ten projects, while those by HMA-FM-E model are correct for five out of ten projects. Apparently, HMA-FM-E model did a better job than MEPDG, which is consistent with our prior findings. In addition, the ER model was found to correctly predict crack status for five out of ten projects. As indicated by the qualitative comparison, ER model is also based on the critical condition concept, even though in a much simpler form than the HMA-FM-E model. It appeared that the ER model is useful for relative evaluation of TDC performance, as its capability to distinguish cracked from uncracked pavements outperformed MEPDG.

Table 7-14 Comparison of predicted TDC crack status with observation-based performance

Project (UF) ID	Time of Evaluation (Year)	Observation -Based Crack Status	TDC Prediction		
			MEPDG	HMA-FM-E	ER Model
1	11	U	G	G	G
2	11	C	B	B	B
3	11	C	B	G	B
4	11	C	B	G	G
6	11	C	B	G	B
7	11	U	B	B	G
9	7	C	B	B	G
10	7	C	B	B	B
11	6	U	G	G	G
12	6	C	B	B	B

Note: ″G″ denotes a correct prediction, and ″B″ denotes an incorrect prediction.

7.7 Closure

Cracking performance predictions for ten Superpave projects in Florida were completed using four prediction tools selected based on the best knowledge of the research team and availability. Following a qualitative comparison of the prediction tools divided into BUC performance models (Two models) and TDC performance models (Three models), prediction results in terms of bottom-up cracking and top-down cracking were compared separately to field observation-based cracking performance data. The findings may be presented in the following two parts.

7.7.1 Bottom-Up Cracking Models

Crack initiation times predicted by PerRoad for all ten projects are generally no greater than those by MEPDG. In other words, PerRoad predicts earlier bottom-up crack initiation than MEPDG in most cases. Comparison of crack amount development over time was not possible since PerRoad does not predict crack amount.

Comparison of predictions by MEPDG and PerRoad to field performance data was also undertaken, but limited to crack status due to the availability of field data. It was found that bottom-up crack status predicted by MEPDG appeared to be closer to the field observation-based data than PerRoad at the time of field evaluation. MEPDG has similar but more sophisticated features than PerRoad as indicated from the qualitative comparison. So, its predictions are potentially more accurate than PerRoad. However, this needs to be further verified when more field data is available.

7.7.2 Top-Down Cracking Models

Crack initiation times predicted by HMA-FM-E model for all ten projects are generally smaller than those by MEPDG, except for Project 7. In other words, HMA-FM-E model predicts earlier top-down crack initiation than MEPDG in most cases. Comparison of predicted crack amount development over time by these two models also showed a similar trend. It was also found that crack propagation times to failure predicted by HMA-FM-E model were typically within the range of 2 to 5 years, which are much shorter than those by MEPDG. It appeared that the HMA-FM-E model predictions make more engineering sense from a practical perspective.

Comparison of predictions by MEPDG and HMA-FM-E model to field performance data was undertaken in terms of crack initiation time. It was found that the predicted TDC initiation times by HMA-FM-E model are closer to the field data and therefore more accurate than those by MEPDG. As indicated from the qualitative comparison, these two models are based on very different fundamental assumptions (i.e., critical condition vs. traditional fatigue approach). It appeared that the critical condition concept based HMA-FM-E model is more promising than MEPDG for the following reasons:

- The critical condition approach assumes a discontinuous distress mode, which is much closer to the actual cracking pattern in the field as compared to the continuous distress mode centered on by the traditional fatigue approach.
- A healing sub-model was developed and incorporated into the HMA-FM-E model, which is capable of taking into account effect of mixture healing potential on cracking performance.
- Also, effect of transverse thermal stresses on top-down cracking performance was considered in the HMA-FM-E model.

The ER model was one of the top-down cracking models also evaluated in this study. Unlike the other two models, the ER model does not predict crack initiation time nor crack amount. So, the comparison of ER model predictions to the field data was limited to observation-based crack status. It was found that the model made correct predictions for five out of all ten projects. It appeared that this model is suitable for relative evaluation of TDC performance.

In conclusion, the HMA-FM-E model appeared to be the best choice for further development into a top-down cracking model for use in the design of flexible pavements. The key to further improve its accuracy is to more accurately predict changes in mixture damage, fracture, and healing properties with aging.

CHAPTER 8
DEVELOPMENT OF DATABASE FOR SUPERPAVE MIXTURES IN FLORIDA

8.1 Introduction

One of the primary objectives for this research was to continue to obtain material properties, structural characteristics and performance data for the Superpave projects included in the existing Florida Department of Transportation (FDOT) monitoring database. Florida Gulf Coast University (FGCU) was sub-contracted to manage the database and assure the quality of the data in the database. The following work was conducted on the database.

- Upgrade the current database version to latest Microsoft Access version
- Enhance the overall structure of the database
- Design new forms to account for the extension of the Superpave project
- Facilitate ease of use
- Modify existing forms to make the database more user friendly
- Data entry

8.2 Database Management and Quality Assurance of Data in Database

8.2.1 Upgrade Database

The codes on the current UF database version were updated to the latest Microsoft Access software. Since the UF database was designed using Microsoft Access older than the 2007 version, upon opening the database (using Microsoft Access 2007 version) several pop-ups were shown. It gave errors such as the example presented in Figure 8-1 below. These errors messages do not impact the operation of the database. They are warnings that the database

contains some extra references that are no longer needed. Nevertheless, they are a disturbance to the users. In order to fix this problem these references were removed. This was done from the "Visual Basic Editor" built into Access. A troubleshooting manual was written to help with errors likely to be encountered with the database when updating to the current 2007 version of Access. It included a step-by-step process, with screenshots, showing how to remedy the problems the user may encounter due to the update.

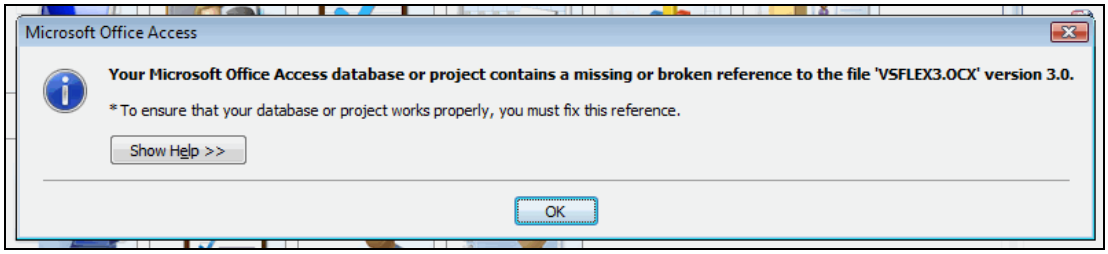

Figure 8-1 Example of possible error messages upon opening the database

8.2.2 Enhance Overall Structure of the Database

The overall interface of the database was redesigned to accommodate the new information and data collected during the Continuation of Superpave Projects Monitoring (CSPM) phase. Throughout this report "Extension" will be used interchangeable to refer CSPM phase. These are data that were collected from 2008 until now. Previously the main interface of the database included icons with little or no information to the users. With the CSPM award, the main interface was redesigned. It was structured into four (4) major modules including General Information, Project Database, Publications/Reports, and User guide. Figures 8-2 and 8-3 are presentations of the main interface of the database before and after the CSPM were awarded. The user guide that provides step by step processes on how to navigate and locate information on the database. In addition, the importance of each module is defined with the intent of providing the

users the necessary information including meaning and content of each module. This step was necessary to make the database user-friendly and provide effective communication by providing definition of each module to the users.

Once the user activates in one of the four major modules on the main interface, the definition and content of each particular module is displayed. Users also have access to the sub-modules contained in the particular module. In addition, users have the option to go back to the main interface or access information from the other 3 major modules of the database (See Figure 8-4). This pattern is consistent throughout the database. The users can access the main interface and the four major modules of the database at anytime.

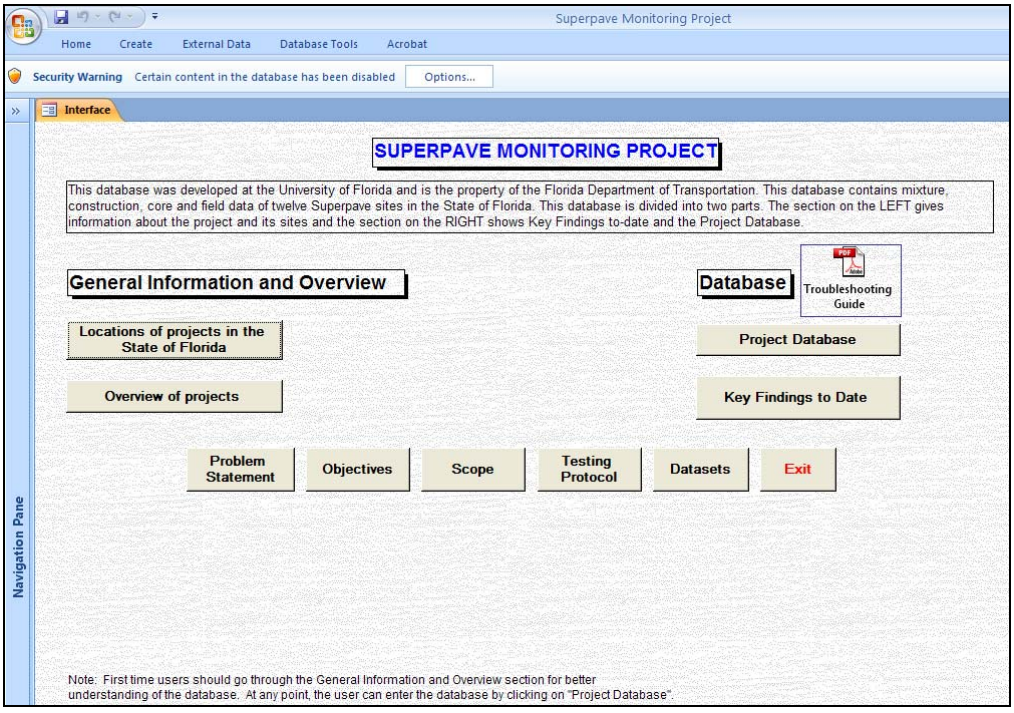

Figure 8-2 Layout of the main interface of the database before the CSPM was awarded

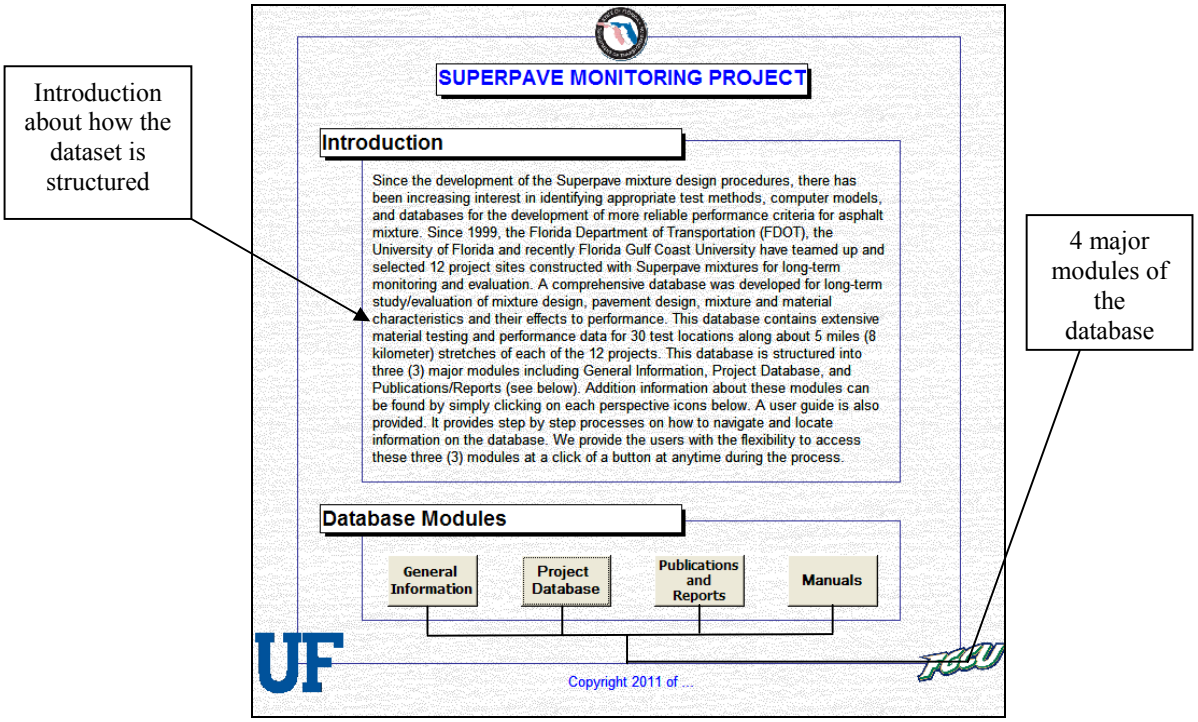

Figure 8-3 Layout of the main interface of the database after the CSPM was awarded

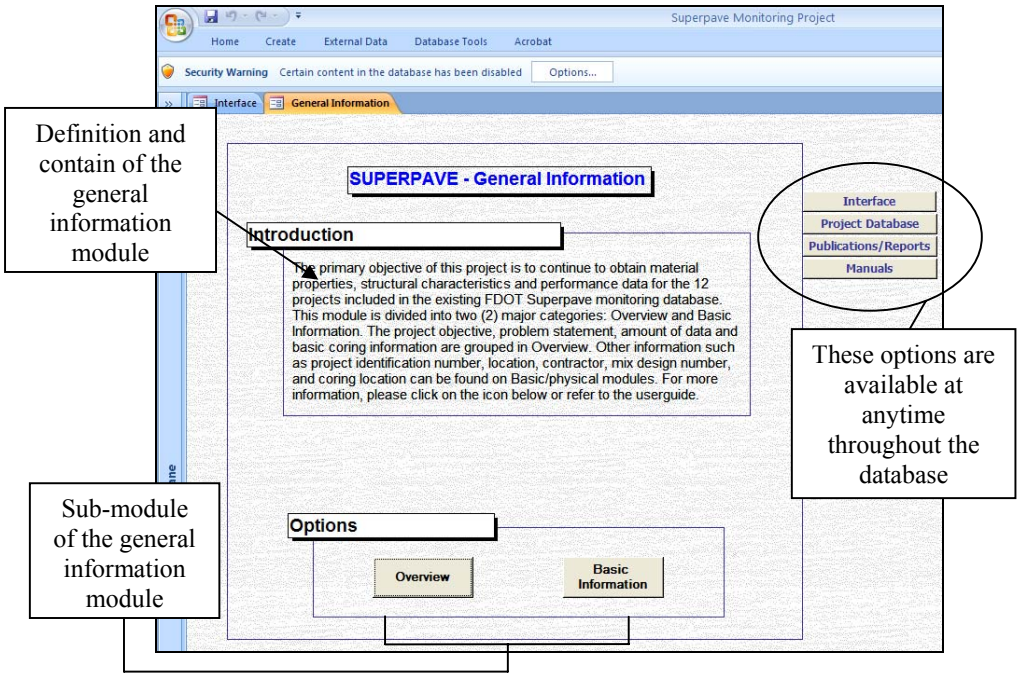

Figure 8-4 Layout of the general information module

8.2.2.1 Grouping

The database is designed to avoid unwanted errors. The original database version contained the controls which allowed Microsoft Access to automatically handle populating fields on the form and update the tables with the database. This would cause problems when moving from the Location data at the top of the form and the core data information at the bottom of the form, as it would prompt to save the data. This could lead to some unwanted changes being saved that the user might likely not notice. This problem was fixed by forgoing Access's automatic handling and manually coding the processes that handle populating fields on the form and updating the tables with in the database.

As mentioned before, the database was structured into for major modules. General information module contains information such as project scope, testing protocol, location of the projects, and key findings to date. Construction data, laboratory test results and field condition survey are located in the project database. All the journal articles and conference proceedings, reports and presentations made at the Florida Department of Transportation (FDOT) can be accessed in the main interface of the database. A flow chart which described how the database was structured is presented in Figure 8-5. It includes the modules and sub-modules of the database.

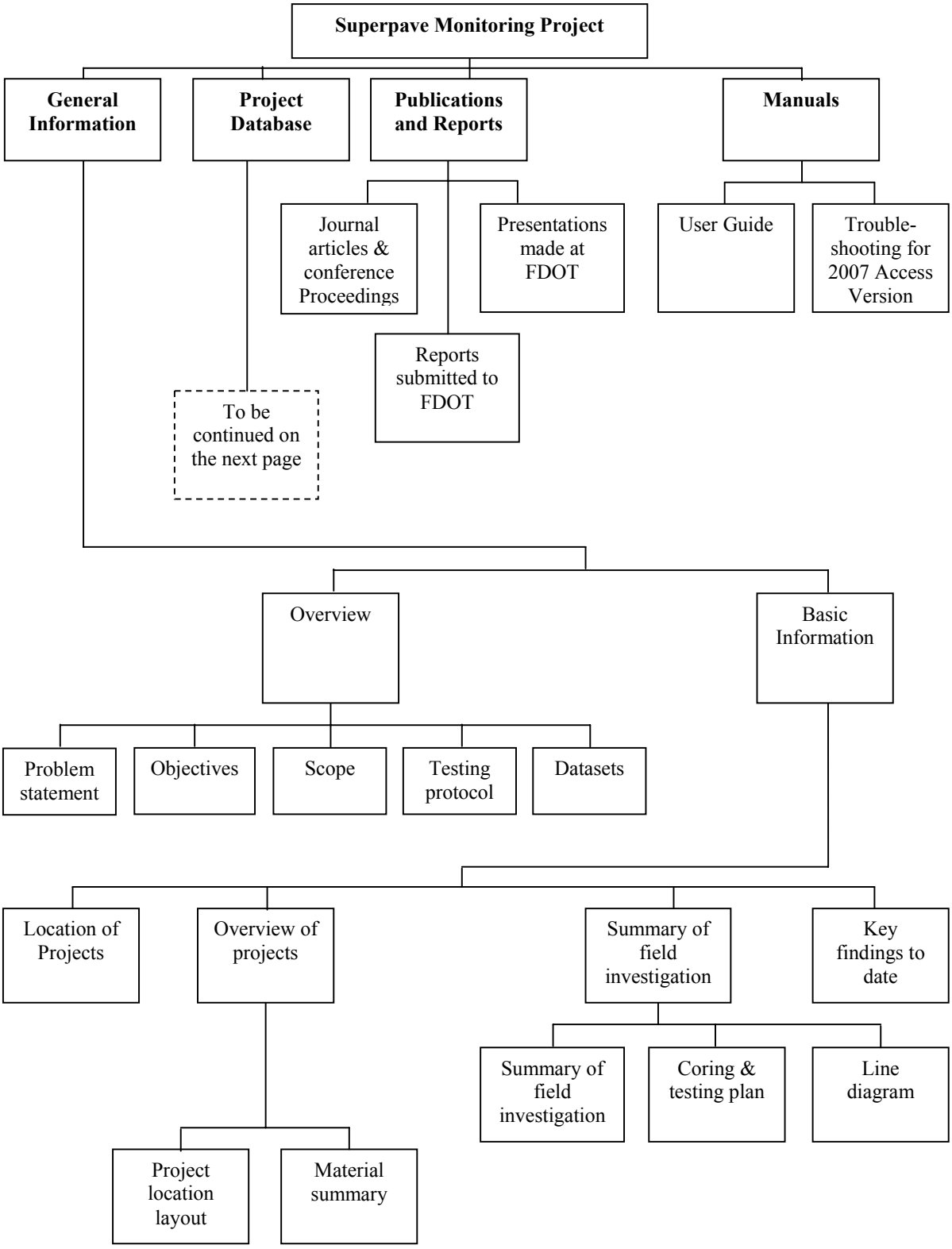

Figure 8-5 Flow chart of the Superpave monitoring project database

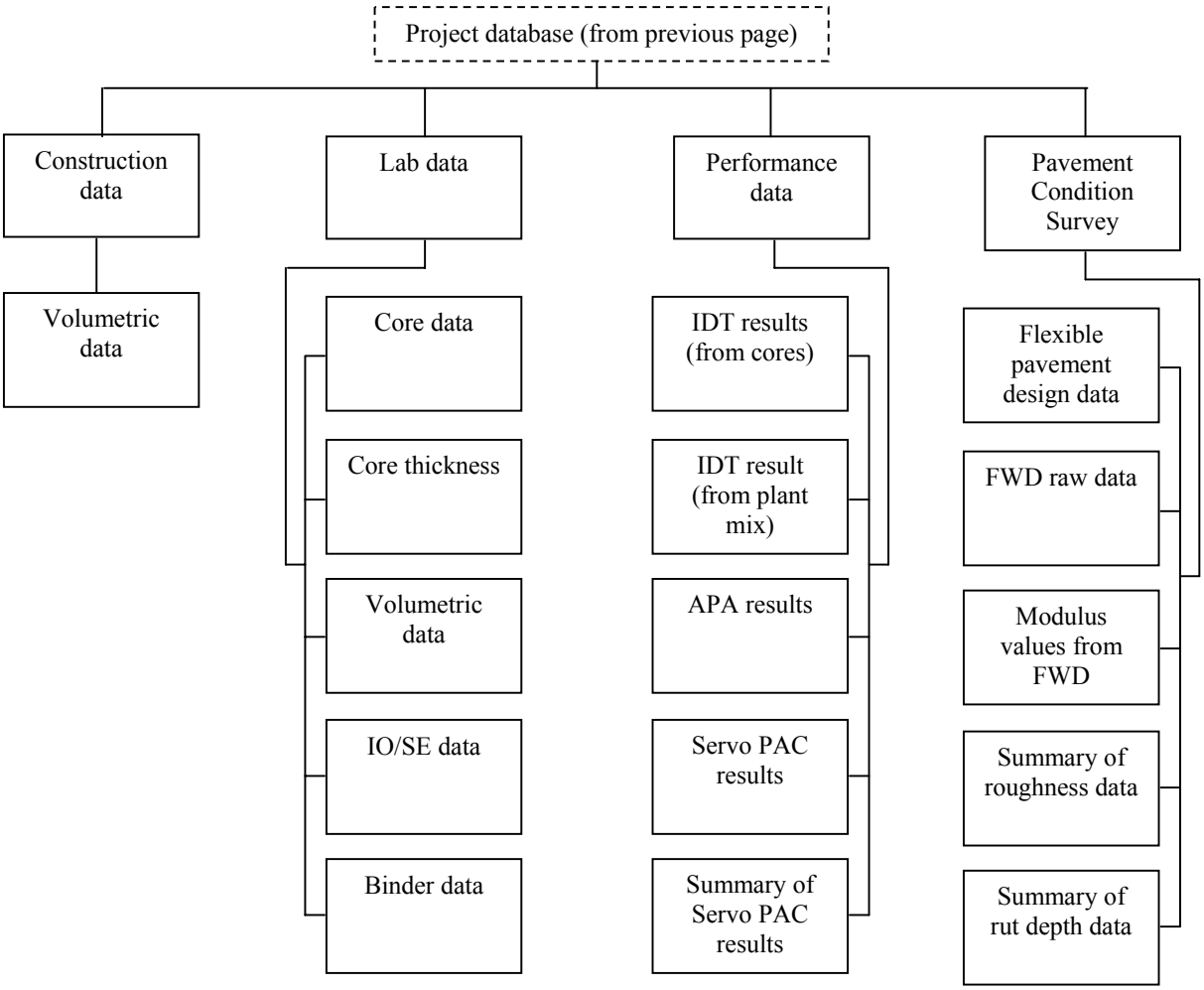

Figure 8-5 Flow chart of the Superpave monitoring project database (continued)

The "Project Database" interface was also redesigned. This option provided better grouping of the data. This version of the database showed a form that gave the users the option of choosing the database form for a specific module or sub-module. For example data that were collected during construction are grouped together (Figure 8-6). Information such as Project ID and type of layers (Layer A or Layer B) is required to retrieve information. Mix Design is another input parameter that can be used to retrieve information.

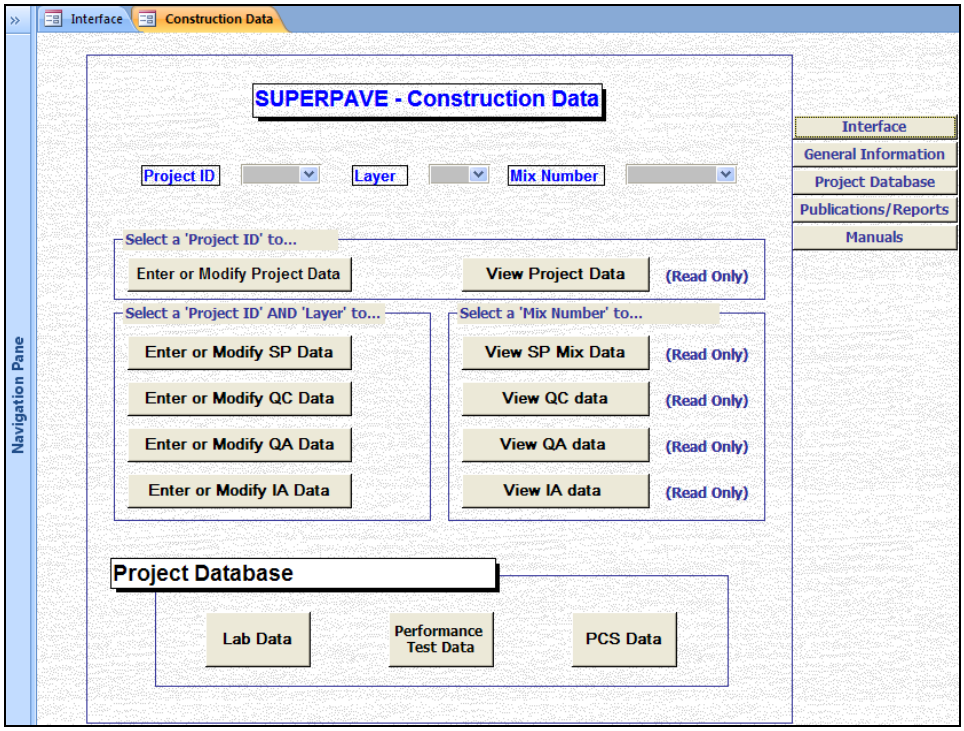

Figure 8-6 Example of how information in the database is grouped

8.2.2.2 Coring Scenario

Each of the projects was about five-miles long. All of them were cored on the travel lane within one year after construction. This will be referred to as “Round-I” throughout the database/report. Projects 1 to 9 were cored about two years after construction (round-II). Cores were taken on projects 1, 2, and 3 at about 4 years after construction (Round-III). The projects were divided into 30 locations. A total of 180 cores were taken on Round-I and 90 cores were taken on Round-II and Round-III. All projects were cored for the CSPM phase. A selected number of locations (2 to 3 locations) were identified for coring in the CSPM phase. A total of 33 cores were taken per locations.

Since all projects were not cored during all rounds and a selected of locations were selected on CSPM phase, careful design procedures were incorporated so that the users were not

misled. To meet this goal, time of coring was selected as the primary variables to retrieve information. This was necessary because when time of coring is activated, the database only prompted the appropriate information requested. For example, if one selects core data parameters from the lab data sub-module, the users are prompted to enter the time of coring. If Round-II is selected, only projects 1 to 9 are shown (see Figure 8-7). Similarly, if Project 1 is selected for CSPM phase, only locations 5 and 15 are shown (see Figure 8-8). Similar procedures were used throughout the database. All these measures were necessary to avoid confusion and effective use of the database.

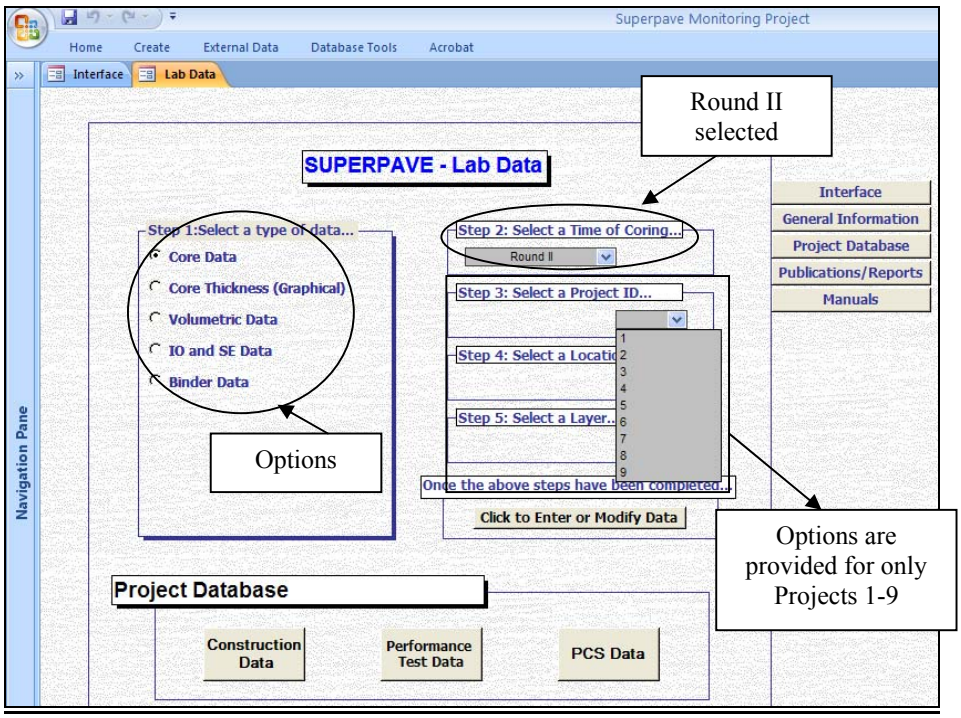

Figure 8-7 Options that isolated data for Round-II (Example of core data for Round II – only the appropriate projects are shown)

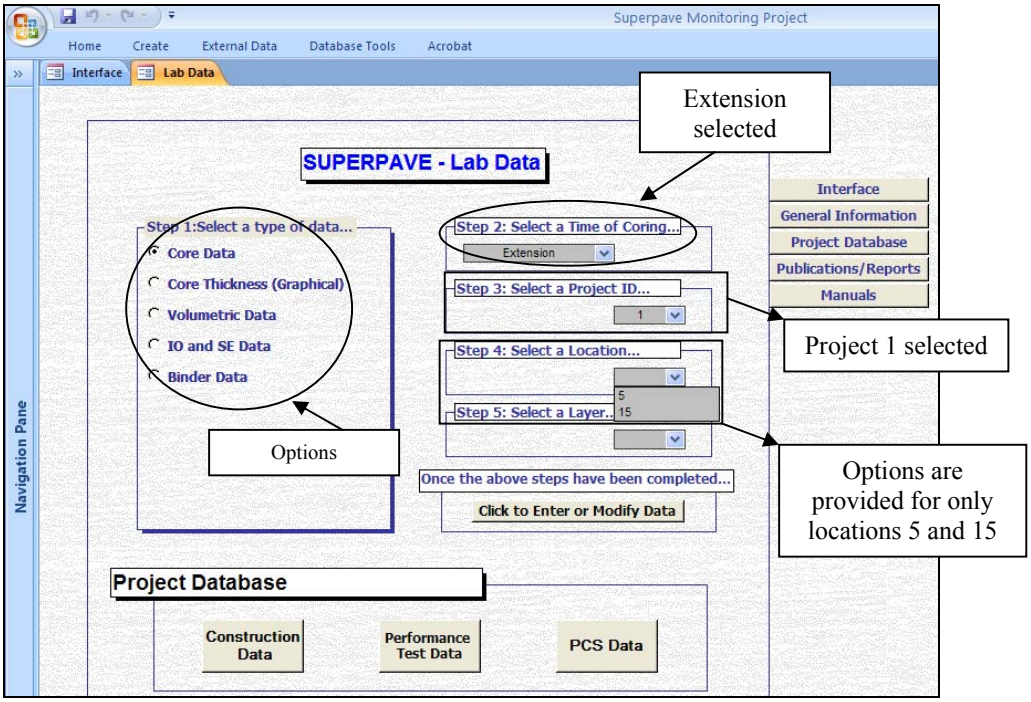

Figure 8-8 Options that isolated data produced during Continuation of Superpave Projects Monitoring (CSPM) phase only (Example of core data extension: Project 1 – only locations 5 and 15 are shown)

8.2.3 Design New Forms

New forms were designed to accommodate the new information and data collected during the Continuation of Superpave Projects Monitoring phase. As mentioned before, in the database the Continuation of Superpave Projects Monitoring (CSPM) Phase is referred as "Extension." In Round I, 6 cores were drilled per locations. For Rounds II and III, 3 cores were taken per locations. A total of 33 cores per location were obtained under the CSPM phase. Figure 8-9 represents a schematic diagram that shows the amount of cores and the coring layout for each particular time of coring.

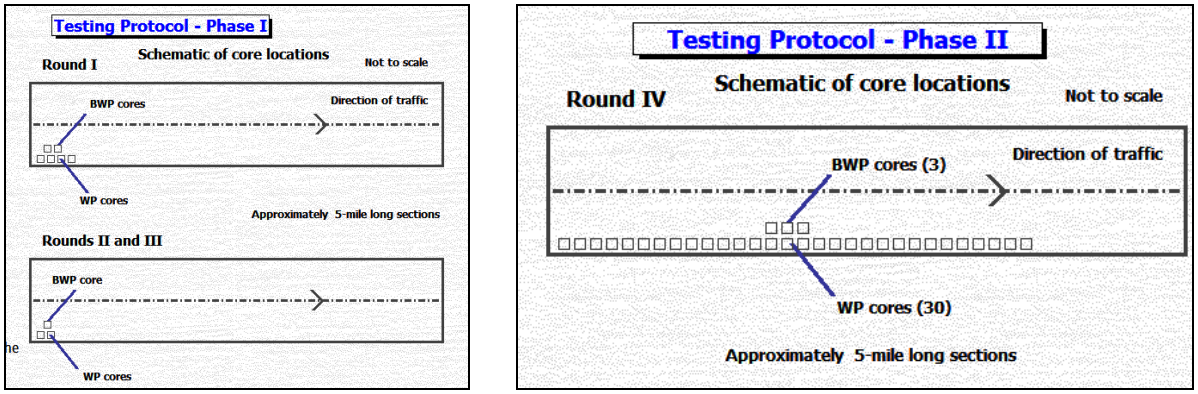

Figure 8-9 Layout of testing protocol for all the different times of coring

8.2.4 Facilitating Ease of Use

The database expanded rapidly with more data and features being added. The database is currently 290 mega bytes. This makes it very essential to make modifications and improvements so that the user can navigate through the database effectively. Every effort was made to ensure that the user is not misled or misguided. For Example, a) if the input parameters were insufficiently entered, then the database prompts the user to input the missing parameters such as "project id", and b) if data were not available, then the appropriate message is displayed instead of blank forms or tables. A thorough diagnosis test was conducted to ensure that response prompts such as "Save Dialogues" are updated and the responses are similar to common programs such as Microsoft Word.

For example under the "Enter or Modify Core Data" icon, since not all the projects were cored say for Round-II, the users are forced to enter the data in sequence starting from: a) time or coring, b) project ID, c) location, and d) layer. This measure was taken to eliminate the option of obtaining inputs data that are not currently available in the database. Also, if new data are added, users are prompted with a dialogue message to save the data accordingly (see Figure 8-10).

Similar measures/features were incorporated throughout the database. Without these measures the database would be filled with empty entries that may affect future tasks.

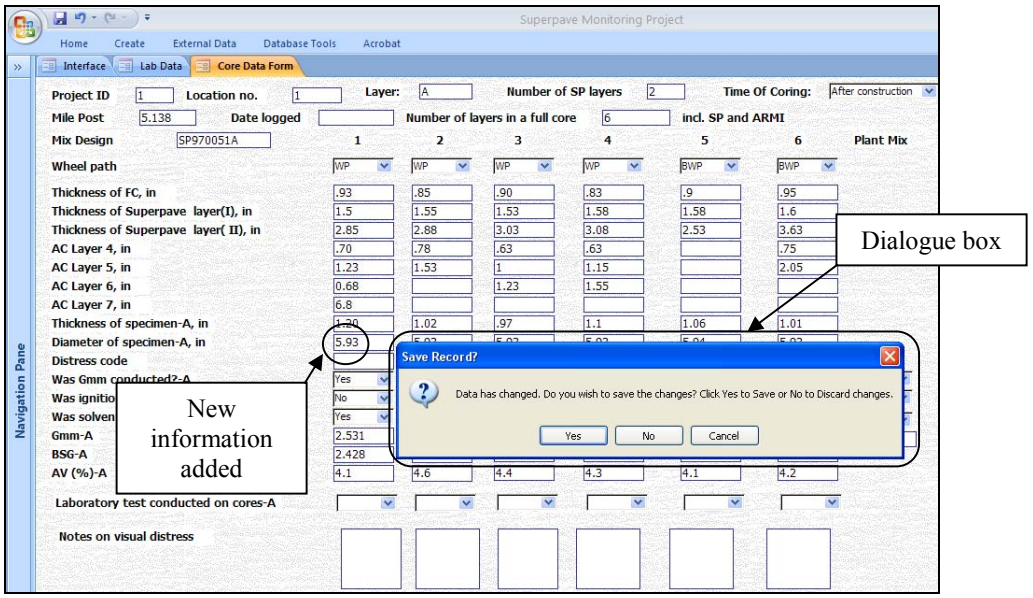

Figure 8-10 Example of modification that made the database more user-friendly

8.2.5 Modify Existing Forms

Additional options were provided to allow the users to isolate only the data generated or collected during the CSPM phase only. These modifications also help make the database more user-friendly and effective. For example, the core data information was able to fit nicely in one page since 6 to 3 cores were taken during Round I and Round II/III, respectively. The "Core Data" forms were modified to accommodate all the 33 cores that were drilled per locations during the CSPM phase (Figure 8-11). By simply clicking a button, users can view all 33 cores taken for a particular location in CSPM phase. In addition, only the locations that were cored for the particular project (for example project 1 - Location 5, 15, and 25), are displayed in the form. A similar approach was incorporated when retrieving information throughout the database. These

measures were taken to ensure that the new forms are consistent in style and format as compared to the existing database.

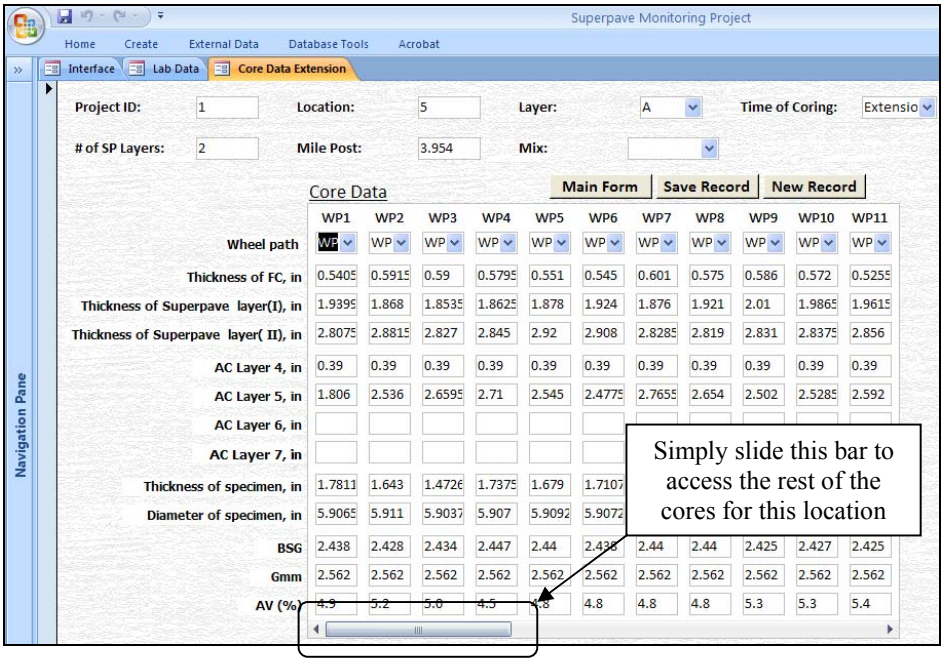

Figure 8-11 Completed core data CSPM phase entry form

8.2.6 Data Entry

The database was consistently updated to include new information and data that are completed up to date. For example; a) all the core data that were provided by the UF Research team on all the projects are currently loaded in the database; b) All the reports, papers, and publications are loaded into the database. More data can be input as they become available; c) The information under CSPM phase for the "Overview of Projects," "Problem Statement," "Objectives," "Scope," "Testing Protocol," and "Datasets" were updated. The data related to the "Summary of Field Investigation" (summary, plans, and line diagrams) has been added and a

new form has been created to access the information (see Figure 8-12). This form is accessible from the "Interface Form" by clicking on the button labeled "Summary of Field Investigation."

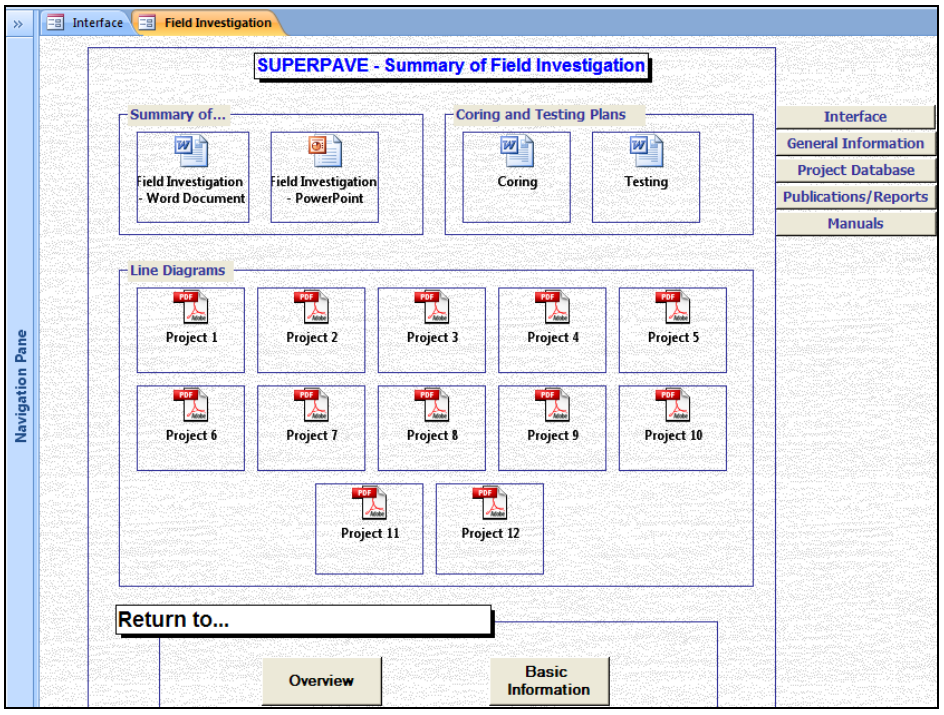

Figure 8-12 Summary of field investigation form

8.3 Closure

A comprehensive and user friendly database was developed for Superpave projects, to compile results of the comprehensive material testing and performance data collected for these project sections. All data generated have been updated to the existing database, including also any interpretation performed on the data and identified as such. This will form one of the most extensive datasets of research quality Superpave data on real world projects.

CHAPTER 9
CLOSURE

9.1 Summary and Findings

This study was conducted to continue to evaluate the performance of Superpave mixtures designed and constructed in Florida using the Superpave mix design system. The work was a follow-up to an earlier monitoring project conducted on the same pavements from 1999 to 2005. Whereas the first project focused on construction variability and establishment of a comprehensive database, the follow-up effort primarily focused on the continuous monitoring of material properties and field performance of Superpave projects for identification and evaluation of: reasonable and effective mixture design guidelines and criteria; performance-related laboratory properties and parameters; relations to predict fundamental mixture properties from component properties and mixture volumetric properties; and the best choice for further development of pavement performance prediction models.

The research framework was composed of six sub-tasks: 1) field data collection; 2) laboratory testing; 3) performance assessment using basic mixture characteristics and Dominant Aggregate Size Range – Interstitial Component (DASR-IC) analysis; 4) material property model development; 5) performance model prediction and evaluation; and 6) database update and further development. Findings associated with these sub-tasks follows:

- Field Performance
  - It was identified that the average field rut depth measured by transverse profilograph (TP) for Superpave projects varied from 0.14 to 0.54 inch for six to eleven year-old pavements. A discrepancy of rut depth measurements between the

TP and the road surface profilograph (RSP) was identified, where the rut depth measured by the RSP was generally lower and less accurate than rut depth measured by the TP. The results showed that the average rut depth measured using the RSP was approximately three times less than the rut depth measured using the TP.

- In most cases, top-down cracking, which initiates at the surface of the pavement and propagates downward, was identified as the dominant crack type in the Superpave projects, which were subjected to around six to eleven years of aging in the field. Actual crack depths measured from cores varied from 0.40 to 3.30 inch, which corresponded to approximately 10 to 50 % of the total thickness of asphalt concrete layer.
- Four of the six projects, constructed with mixtures containing granite aggregates, exhibited moisture damage in the form of stripping within the first six to seven years after construction. Stripping was particularly prominent at the interface between top and bottom Superpave layers. Three of the four projects (Project 9, 10 and 12) had fine-graded mixtures with rubber modified binder (ARB-5) in the top layer and PG64-22 binder in the bottom layer. The fourth project (Project 11) had a coarse-graded mixture with SBS-modified binder in the top layer and PG64-22 binder in the bottom layer.

- Test Results
  - Binder test results from six to eleven year-old cores from the field indicated that most of binders still exhibited parameters that met the Superpave specification

requirement, including parameters from dynamic shear rheometer (DSR) and bending beam rheometer (BBR).

- For most cases, resilient modulus decreased over time, which clearly indicates the presence of permanent damage and the existence of incomplete healing beyond some level of aging. The top layer generally exhibited higher rates of reduction in resilient modulus than the bottom layer. This reflects that the effect of permanent damage induced by traffic load is more severe for top layer than for the bottom layer.
- For mixtures not affected by moisture damage, creep rate of the top and bottom layers generally decreased over time, which indicates that oxidative aging had a predominant effect on change in creep rate. Also, it seemed clear that mixtures with higher initial fracture energy (FE) exhibited higher rate of reduction in FE with aging. For most projects, the top layers exhibited higher rates of reduction in FE than the bottom layers.
- For mixtures affected by moisture damage, creep rate generally increased over time as opposed to the effect of oxidative aging, which indicates the effect of non-healable permanent damage induced by moisture. Also, an increase in air voids over time was observed in these mixtures, which appears to be related to the displacement of material caused by moisture damage. In addition, unusually high rates of reduction in FE were observed regardless of the initial FE magnitude or layer depth.

- DASR-IC Analysis
  - Mixtures having DASR porosity within the acceptable range clearly exhibited better field rutting performance in terms of lower Rut Depth/ESALs than mixtures with high DASR porosity. Mixtures with marginal DASR porosity exhibited either good or bad rutting performance in the field.
  - A parameter called disruption factor (DF) was developed as part of this study to evaluate the effect of IC components on performance. Mixtures with DF considered to be acceptable generally exhibited better cracking performance in terms of longer crack initiation times in the field than mixtures with the either low or high DF.
- Material Property Models
  - Unique relationships were identified between initial fracture energy and three DASR-IC parameters: DASR porosity, DF, and effective film thickness (EFT). It was found that initial fracture energy generally decreases with increasing DASR porosity and DF. Also, a positively proportional relation was identified between initial fracture energy and EFT (i.e., initial fracture energy was found to increase with increasing EFT). It is noted that these trends appear to hold only when DASR porosity, DF, and EFT are within the ranges considered to be acceptable.
  - A new parameter, namely the ratio of the coarse portion divided by the fine portion of finer aggregates (CFA/FFA) representing the fineness of the interstitial component gradation, was introduced to develop a relationship to predict initial creep rate. Results indicated that initial creep rate generally increased with increasing CFA/FFA. As with the initial fracture energy relationship, this trend

appears to work best when DASR porosity, DF, and EFT were within ranges considered to be acceptable.

- Performance Model Prediction
  - For bottom-up cracking models, PerRoad program generally predicts earlier crack initiation than MEPDG. A comparison of predicted bottom-up crack status to the field observation-based data showed that the MEPDG predictions appeared to be closer to the field data than PerRoad at the time of field evaluation. However, it must be noted that bottom-up cracks were not observed on any of the Superpave projects.
  - For top-down cracking models, the enhanced HMA-FM model (HMA-FM-E) generally predicts earlier crack initiation and faster crack growth than MEPDG. A comparison of predicted top-down cracking to the field observation-based data showed that the HMA-FM-E model appeared to accurately predict observed time to initiation and resulted in predictions of crack growth that were reasonable and consistent with field data. The existing TDC model in MEPDG was found to be inadequate in terms of predicting initiation or propagation of TDC. In addition, it was found that the ER model is suitable for relative evaluation of TDC performance, while it predicts neither crack initiation time nor crack amount.
- Database Development
  - The overall structure of the database was redesigned to: provide better grouping of the data; make the database more user-friendly; provide for greater ease of navigation in the database; and to allow data to be located more easily.

- New forms were designed to accommodate new information and data collected during phase II project as well as any future work performed on these pavements. These modifications also help make the database more user-friendly and effective.
- The database was consistently updated to include new information and all data obtained to date.

9.2 Conclusions

The following key conclusions were drawn based on the findings of this study.

- Parameters from binder tests did not appear to be consistently correlated with field performance of asphalt mixtures in terms of either rutting or cracking, but especially for cracking. Binder test results indicated that no single binder-related parameter obtained provided consistent performance-related information.
- The trend of change in mixture property as a function of age in the field appears to be strongly affected by moisture damage. In particular, the fracture resistance of asphalt mixtures was identified to be significantly influenced by moisture damage, which obviously affects mixture performance in the field.
- Fine-graded granite mixtures with rubber modified binder (ARB-5) appeared to be susceptible to moisture damage. In other words, mixtures composed of fine-graded granite and rubber modified binder appear to be a problematic combination for resistance of moisture damage. It is also possible that construction difficulties may have reduced the quality of mixtures related to moisture damage resistance.
- DASR porosity, which reflects the characteristics of coarser aggregate structure, is the most dominant parameter to control rutting performance. The DASR porosity

criteria introduced appears to accurately distinguish the field rutting performance of Superpave mixtures.

- The existence of an acceptable range of disruption factor (DF) was identified to achieve better cracking performance. The DASR porosity alone appears unable to clearly differentiate field cracking performance of Superpave mixtures. DASR porosity criteria combined with DF criteria appeared to distinguish the relative cracking performance of Superpave mixtures in the field.
- It appears that introduction of DASR-IC criteria as performance-related design parameters to current mix design guidelines and specifications will lead to better and more consistent field rutting and cracking performance of Superpave mixtures.
- Mixtures with acceptable range of DASR-IC parameters exhibited more consistent and predictable initial mixture properties and better mixture performance in the field than those with DASR-IC parameters outside ranges identified as acceptable.
- Basic forms of material property models identified to predict changes in mixture properties over time (aging) can serve as the foundation for further development of relationships based on additional field data and laboratory studies using the more advanced laboratory conditioning procedures currently being developed in other ongoing FDOT research.
- The HMA-FM-E model was clearly determined to be the best choice for further development of a top-down cracking prediction model for use in mixture and pavement design in Florida. The key to improvement is to continue to improve the material property models, a process which was initiated as part of this study, to

more accurately predict changes in mixture damage, fracture, and healing properties with time (aging).

9.3 Recommendations and Future Works

Based on extensive evaluations performed in this study, recommendations for further investigations on the continuation of Superpave projects monitoring in Florida are summarized below.

- Further investigations using the healing test currently being developed in other FDOT research are needed to assess the healing characteristics, and to determine the healing properties of in-place mixtures. Healing has been determined to be one of the most critical factors affecting cracking performance of asphalt mixtures.
- Further investigations using composite specimen tension tests are needed to evaluate the influence of Open Graded Friction Course (OGFC) and interface condition on cracking performance of in-place mixtures since this is another critical issue for evaluating the cracking behavior of asphalt mixtures.
- The DASR-IC model, including DASR porosity and DF and associated performance-related criteria is recommended for introduction to existing mixture design and specifications and to establish guidelines for improved field performance of Superpave mixtures. The challenge is to make the system more practical for implementation. Development of software is recommended to make the system for more user-friendly.

- Further development of healing and aging models for asphalt binder and mixture are needed to accurately predict the performance-related properties as a function of time and environment.
- Further development and evaluation of complete mixture property models is needed to account for the effect of non-healable permanent damage related to load and moisture based on additional field data and laboratory data using more advanced laboratory conditioning procedures. The IC parameters identified in this study should be used as the foundation to enhance the mixture property models.
- Pavement performance prediction models should also be further developed and calibrated once the enhanced material property models are developed.
- Further investigations of moisture damaged projects are needed to identify various factors that may have contributed to moisture damage and to fully understand or verify mechanism and effect of moisture damage.
- Future monitoring efforts for existing Superpave project sections need to be continued to refine and to enhance the Superpave mix design guidelines and specifications for evaluating long-term performance of Superpave mixtures.

LIST OF REFERENCES

AASHTO, “Standard Method of Test for Bulk Specific Gravity of Compacted Bituminous Mixtures Using Saturated Surface-Dry Specimens,” AASHTO T 166, Washington, D. C., 2001.

AASHTO, “Standard Method of Test for Percent Air Voids in Compacted Dense and Open Bituminous Paving Mixtures,” AASHTO T 269, Washington, D. C., 2001.

Asphalt Institute, “Superpave Mix Design,” Superpave Series No.2 (SP-2), Third Edition, Asphalt Institute, Lexington, KY, 2001.

ASTM, “Standard Practice for Computing International Roughness Index of Roads from Longitudinal Profile Measurements,” ASTM E 1926, West Conshohocken, PA, 2008.

ASTM, “Standard Practice for Computing Ride Number of Roads from Longitudinal Profile Measurements Made by an Inertial Profile Measuring Device,” ASTM E 1489, West Conshohocken, PA, 2008.

Birgisson, B., Roque, R., and Gale, C. Page, “The Use of a Performance-Based Fracture Criterion for the Evaluation of Moisture Susceptibility in Hot Mix Asphalt,” Transportation Research Board, National Research Council, Washington, D. C., 2004.

Birgisson, B., Roque, R., Mang, T., and Masad, E., “Development and Evaluation of Test Methods to Evaluate Water Damage and Effectiveness of Antistripping Agents,” Final Report of Florida Department of Transportation, University of Florida, Gainesville, FL, June 2005.

Buttlar, W. G., Roque, R., and Reid, B, "Automated Procedure for Generation of Creep Compliance Master Curve for Asphalt Mixtures,″ In Transportation Research Record: Journal of the Transportation Research Board, No. 1630, Transportation Research Board of the National Academies, Washington, D.C., pp. 28-36, 1998.

Buttlar, W. G., and Roque, R., “Development and Evaluation of the Strategic Highway Research Program Measurement and Analysis System for Indirect Tensile Testing at Low Temperatures,” In Transportation Research Record: Journal of the Transportation Research Board, No. 1454, National Research Council, National Academy Press, Washington, D. C., pp. 163-171, 1994.

D’Angelo, J., Dongre, R. N., “Practical Use of Multiple Stress Creep Recovery Test: Characterization of Stylene-Butadiene-Stylene Dispersion and Other Additives in PMA

Binders," In Transportation Research Record: Journal of the Transportation Research Board, Washington, D. C., 2009.

Deme, I. J., and Young, F. D., "Ste. Anne Test Road Revisited Twenty Years Later," Proceedings of the Canadian Technical Asphalt Association, Vol. 32, pp.254-283, 1987.

El-Basyouny, M., and Witczak, M., ″Calibration of the Alligator Fatigue Cracking Model for the 2002 Design Guide,″ In Transportation Research Record: Journal of the Transportation Research Board, No. 1919, Transportation Research Board of the National Academies, Washington, D.C., pp.77-86, 2005a.

El-Basyouny, M., and Witczak, M., ″Calibration of the Longitudinal Fatigue Cracking Model for the 2002 Design Guide,″ Presented at the Transportation Research Board 84th Annual Meeting, Washington, D.C., January 2005b.

ERES Consultants, NCHRP 1-37A Final Report, ″Guide for Mechanistic-Empirical Design for New and Rehabilitated Pavement Structures″, Prepared for: National Cooperative Highway Research Program, Transportation Research Board, National Research Council, March 2004.

FDOT, "Standard Specifications for Road and Bridge Construction," Florida Department of Transportation, Tallahassee, FL, 2007.

FDOT, "Flexible Pavement Condition Survey Handbook," Florida Department of Transportation, Tallahassee, FL, 2009.

Guarin, A., "Interstitial Component Characterization to Evaluate Asphalt Mixture Performance," Ph.D. Dissertation, University of Florida, Gainesville, FL, 2009.

Kandhal, P. S., and Chakraborty, S., "Evaluation of Voids in the Mineral Aggregates," NCAT Report No.96-4, National Center for Asphalt Technology, March 1996.

Kim, B., Roque, R., and Birgisson, B., ″ Effect of Styrene Butadiene Styrene Modifier on Cracking Resistance of Asphalt Mixture,″ In Transportation Research Record: Journal of the Transportation Research Board, No. 1829, Transportation Research Board of the National Academies, Washington, D.C., pp. 8-15, 2003.

Kim, J., Roque, R., and Birgisson, B., "Integration of Thermal Fracture in the HMA Fracture Model," Journal of the Association of Asphalt Paving Technologists, Vol. 77, pp.631-662, 2008.

Lottman, R. P., "Predicting Moisture-Induced Damage to Asphaltic Concrete: Ten Year Field Evaluation," National Cooperative Highway Research Program Synthesis of Highway Practice 175., Transportation Research Board, Washington, D. C., unpublished manuscript, 1986.

Mehta, Y., Roque, R., Lopp, G., and Villiers, C., "Evaluation of the Road Surface Profiler and the Transverse Profilograph for Determination of Rut Depth Measurements," Transportation Research Board, Washington, D. C., 2001.

Mehta, Y., Roque, R., "Evaluation of FWD Data for Determination of Layer Moduli of Pavements," Journal of Materials in Civil Engineering, ASCE, 2003.

Mirza, M. W., and Witczak, M. W., "Development of Global Aging System for Short and Long Term Aging of Asphalt Cements," Journal of the Association of Asphalt Paving Technologists, Vol. 64, pp. 393-430, 1995.

Myers, L. A., Roque, R. and Birgisson B., "Propagation Mechanisms for Surface-Initiated Longitudinal Wheel Path Cracks," In Transportation Research Record: Journal of the Transportation Research Board, No. 1778, National Research Council, National Academy Press, Washington, D. C., pp. 113-122, 2001.

Nukunya, B., Roque, R., Tia, M., and Birgisson, B., "Evaluation of VMA and Other Volumetric Properties as Criteria for the Design and Acceptance of Superpave Mixtures," Journal of the Association of Asphalt Paving Technologists, Vol. 70, pp. 38-69, 2001.

Roque, R., Lopp, G., Li, W., and Niu, T., "Evaluation of Hybrid Binder Use in Surface Mixtures in Florida," Final Report of Florida Department of Transportation, University of Florida, Gainesville, FL, June 2009.

Roque, R., Birgisson, B., Kim, S., and Guarin, A., " Development of Mix Design Guidelines for Improved Performance of Asphalt Mixtures," Final Report of Florida Department of Transportation, University of Florida, Gainesville, FL, January 2006.

Roque, R., Birgisson, B., Drakos, C. A., and Dietrich, B., "Development and Field Evaluation of Energy-Based Criteria for Top-Down Cracking Performance of Hot Mix Asphalt," Journal of the Association of Asphalt Paving Technologists, Vol. 73, pp. 229-260, 2004.

Roque, R., Birgisson, B., Sangpetngam, B., and Zhang, Z., "Hot Mix Asphalt Fracture Mechanics: A Fundamental Crack Growth Law for Asphalt mixtures." Journal of the Association of Asphalt Paving Technologists, Vol. 71, pp.816-827, 2002.

Roque, R., Birgisson, B., Tia, M., and Nukunya, B., "Evaluation of Superpave™ Criteria for VMA and Fine Aggregate Angularity," Final Report of Florida Department of Transportation, University of Florida, Gainesville, FL, March 2002.

Roque, R. and Buttlar, W. G., "The Development of a Measurement and Analysis System to Accurately Determine Asphalt Concrete Properties Using the Indirect Tensile Mode," Journal of the Association of Asphalt Paving Technologists, Vol. 61, pp. 304-332, 1992.

Roque, R., Buttlar, W. G., Ruth, B. E., Tia, M., Dickson, S. W., and Reid, B., "Evaluation of SHRP Indirect Tension Tester to Mitigate Cracking in Asphalt Pavements and Overlays," Final Report of Florida Department of Transportation, University of Florida, Gainesville, FL, August 1997.

Roque, R., Zou, J., Kim, Y. R., Beak, C., Thirunavukkarasu, S., Underwood, B. S., and Guddati, M. N., ″Top-down Cracking of HMA Layers: Models for Initiation and Propagation,″ NCHRP Web-Only Document 162, National Cooperative Highway Research Program, Transportation Research Board of the National Academies, 2010.

Sangpetngam, B., Birgisson, B., and Roque, R., "Development of Efficient Crack Growth Simulator Based on Hot-mix Asphalt Fracture Mechanics," In Transportation Research Record: Journal of the Transportation Research Board, No. 1832, Transportation Research Board of the National Academies, Washington, D.C., pp.105-112, 2003.

Sangpetngam, B., Birgisson, B., and Roque, R., "Multilayer Boundary-element Method for Evaluating Top-down Cracking in Hot-mix Asphalt Pavements," In Transportation Research Record: Journal of the Transportation Research Board, No. 1896, Transportation Research Board of the National Academies, Washington, D.C., pp.129-137, 2004.

Schmidt, J. and Graf, P. E., "The Effect of Water on the Resilient Modulus of Asphalt Treated Mixes," Proceedings of the Association of Asphalt Paving Technologists, Vol. 41, pp.118-162, 1972

T. F. Fwa and C. B. Oh, Effect of Moisture Content on Measured Properties of Asphalt Mixtures," Transportation Research Record No. 1492, National Academy Press Washington, D. C., pp.61-70, 1995.

Timm, D. H., Comparing PerRoad and the MEPDG, Presented at the Ohio Transportation Engineering Conference (OTEC), Oct. 2008.

Timm, D. H., and Newcomb D. E., ″Perpetual Pavement Design for Flexible Pavements in the U.S.,″ International Journal of Pavement Engineering, Vol. 7, No. 2, pp.111-119, June 2006.

Timm D. H., Newcomb, D. E., and Selvaraj, I.., ″A Practical Guide to Low-volume Road Perpetual Pavement Design," International Conference on Perpetual Pavement, Ohio, May 26, 2006.

Villiers, C., Roque, R., and Dietrich, B., "Interpretation of Transverse Profiles to Determine the Source of Rutting within Asphalt pavement," In Transportation Research Record, No. 1905, National Research Council, Washington, D.C., pp. 73-81, 2005.

Wang, J., Birgisson, B., and Roque, R., ″Development of a Windows-Based Top-Down Cracking Design Tool for Florida Based on the Energy Ratio Concept″, In Transportation Research Record, No. 2037, pp.86-96, 2007.

White, T. D., J. E. Haddock, A. J. Hand, and H. Fang, "Contribution of Pavement Structural Layers to Rutting of Hot Mix Asphalt Pavements," NCHRP Report 468, TRB, NRC, Washington, D.C., 2002.

Witczak, M. W., and Fonseca, O. A., "Revised Predictive Model for Dynamic (Complex) Modulus of Asphalt Mixtures," In Transportation Research Record: Journal of the Transportation Research Board, No. 1540, National Research Council, National Academy Press, Washington, D. C., pp. 15-23, 1996.

Zhang, Z., "Identification of Suitable Crack Growth Law for Asphalt Mixtures Using the Superpave Indirect Tensile Test (IDT)," Ph.D. Dissertation, University of Florida, Gainesville, FL, 2000.

Zhang, Z., Roque, R., Birgisson, B., and Sangpetngam, B., "Identification and Verification of a Suitable Crack Growth Law," Journal of the Association of Asphalt Paving Technologists, Vol. 70, pp. 206-241, 2001.

Zou, J., and Roque, R., ″Top-Down Cracking: Enhanced Performance Model and Improved Understanding of Mechanisms,″ Accepted for publication in the Journal of the Association of Asphalt Paving Technologists, Vol. 80, 2011.

APPENDIX A
ANALYSIS PROCEDURE TO DETERMINE THE SOURCE OF RUTTING USING TRANSVERSE PROFILOGRAPH MEASUREMENT

A.1 Introduction

Permanent deformation, commonly referred as rutting, is one of major failure mode for asphalt pavements. Identification of the right source of rutting is an important factor for highway agencies to obtain the necessary information required for proper rehabilitation. As introduced in Chapter 2.4.3, transverse profilograph has been widely used and considered as one of the most accurate devices to measure rut depth, especially for the project level. It will provide cross section profile, wheel path rut depth, imperfections and superelevations.

Conventionally, single measurement of absolute rut depth has been used by many state agencies including FDOT to evaluate rutting performance. However, many researchers recognized in their relative study that absolute rut depth cannot provide enough information to interpret the performance of rutting. (White et al., 2002; Villiers et al., 2005) Rut depth can be a general indicator of pavement structural performance, but it does not provide sufficient information to detect the cause of rutting on asphalt pavement.

New approach was introduced based on the integration of transverse profilograph and falling weight deflectometer (FWD) data to evaluate the contributions of different pavement layers on rutting performance and especially, to identify the presence of instability rutting within the asphalt surface layer. (Villiers et al., 2005) In this study, the sources of rutting were categorized by four different groups as shown below and the analysis method was developed based on the process of elimination represented in Figure A-1. This approach can be used regardless of the magnitude of absolute rut depth.

- Significant Reduction in Air Voids - Asphalt Layer Compaction
- Subgrade (Existing Soil) Compaction
- Base Layer Compaction
- Instability

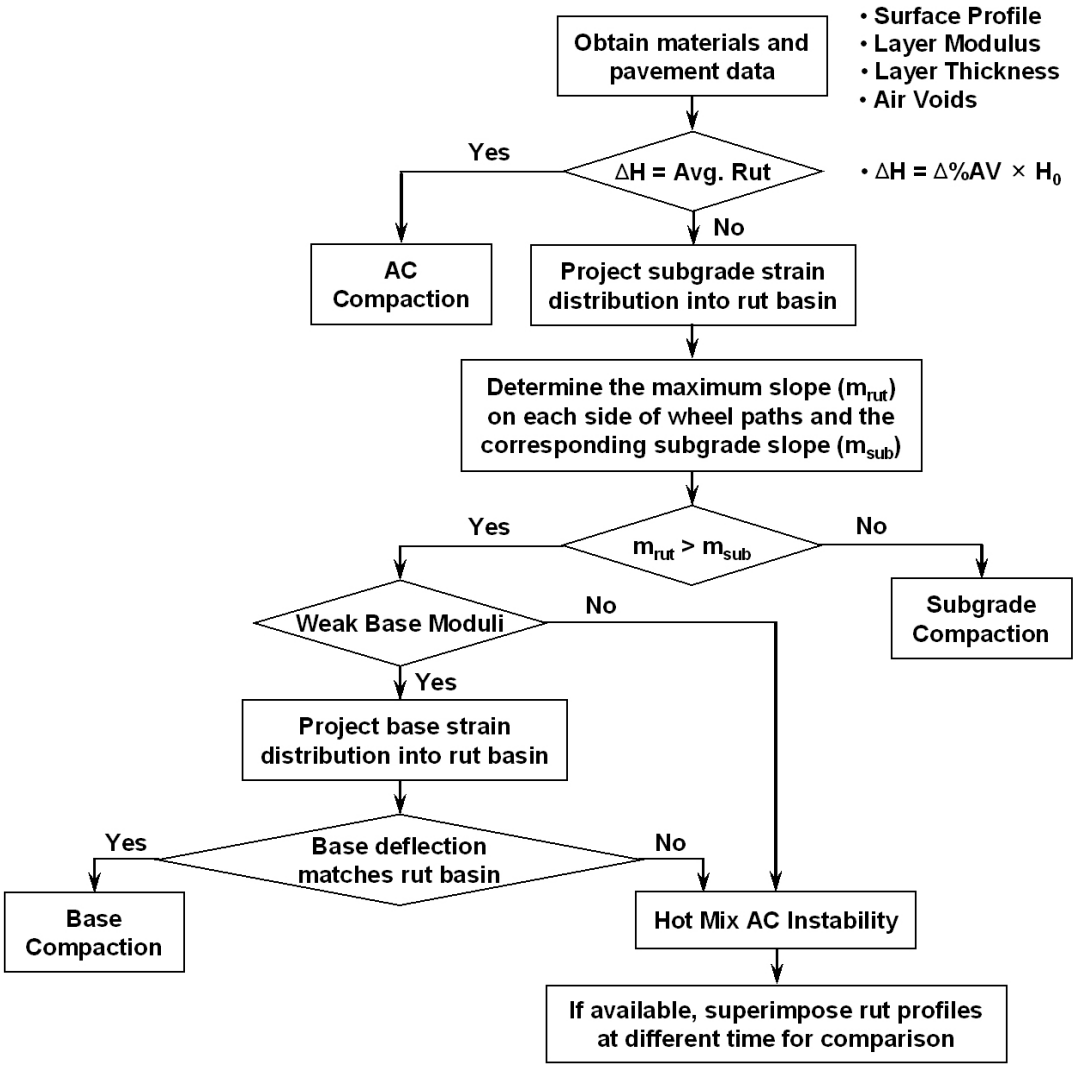

Figure A-1 Schematic approach of elimination process to determine the source of rutting

A.2 Digitalization of Graphs

This task includes conversion of transverse profile graphs obtained from the fields into an electronic format of the Microsoft Excel files. This conversion process will be referred as "digitalization of graphs" throughout the report. This process included identifying each point on the graph and inputting the values into the Excel sheet. Table A-1 shows the summary of available graphs for digitalization. The bold character in the table indicates the graphs that were digitalized in the project duration. The 101 graphs were digitalized in this project duration.

Table A-1 Summary of available graphs for digitalization

	Location 6	Location 12	Location 18	Location 24	Location 30
*Project 1	RI, RII, RIII, **Ext.**	RI, RII, RIII, **Ext.**	RI, RII, RIII, **Ext.**	RI, RII, RIII, **Ext.**	RI, RII, RIII, **Ext.**
*Project 2	RI, RII, RIII, **Ext.**	RI, RII, RIII, **Ext.**	RI, RII, RIII, **Ext.**	RI, RII, RIII, **Ext.**	RI, RII, RIII, **Ext.**
*Project 3	RI, RII, RIII, **Ext.**	RI, RII, RIII, **Ext.**	RI, RII, RIII, **Ext.**	RI, RII, RIII, **Ext.**	RI, RII, RIII, **Ext.**
*Project 4	RI, RII, RIII, **Ext.**	RI, RII, RIII, **Ext.**	RI, RII, RIII, **Ext.**	RI, RII, RIII, **Ext.**	RI, RII, RIII, **Ext.**
*Project 5	No Longer Exist				
*Project 6	RI, RII, RIII, **Ext.**	RI, RII, RIII, **Ext.**	RI, RII, RIII, **Ext.**	RI, RII, RIII, **Ext.**	RI, RII, RIII, **Ext.**
*Project 7	RI, RII, **RIII**, **Ext.**	**RI**, RII, **RIII**, **Ext.**	RI, RII, **RIII**, **Ext.**	RI, RII, **RIII**, **Ext.**	RI, RII, **RIII**, **Ext.**
*Project 8	RI, RII, **RIII**, **Ext.**	RI, RII, **RIII**, **Ext.**	RI, RII, **RIII**, **Ext.**	RI, RII, **RIII**, **Ext.**	RI, RII, **RIII**, **Ext.**
*Project 9	**RI, RII, Ext**	**RI, RII, Ext**	**RI, RII, Ext**	**RI, RII, Ext**	**RI, RII, Ext**
*Project 10	**RI, RII, Ext**	**RI, RII, Ext**	**RI, RII, Ext**	**RI, RII, Ext**	**RI, RII, Ext**
*Project 11	**RI, Ext**	**RI, Ext**	**RI, Ext**	**RI, Ext**	**RI, Ext**
*Project 12	**RI, RII, Ext**	**RI, RII, Ext**	**RI, RII, Ext**	**RI, RII, Ext**	**RI, RII, Ext**

*Note: Here, RI – Round I, RII – Round II, RIII – Round III, Ext. – Extension;
Bold character indicates the data digitalized in this report duration (101 graphs are done in this semester)

A.3 Verification of Layers Moduli and Prediction of Strain Profile

A.3.1 Determination of Layers Moduli

The layer moduli for all the projects were determined and documented based on the analysis procedures introduced in Chapter 2. Since backcalculation is user dependent and the interpretation of transverse profiles analysis (which will be described later) depends on the accuracy of layer moduli, the analysis was verified for selected projects. The moduli of different layers were determined by using Failing Weight Deflectometer (FWD) deflections taken in May 2010 and backcalculation software named the BISDEF computer program.

It was also noticed that the analysis from the Mehta and Roque (2003) was carried out by matching the deflection point right underneath of the initial deflection (D_0) and the outer most deflection (D_6) (see Figure A-2, Approach 1). This time, the first round of analysis was carried out by matching D_0, D_3 or D_4 and D_6 (see Figure A-2, Approach 2). The second round of analysis is carried out as a single trial by keeping asphalt modulus constant and combining base and subbase moduli. This backcalculation method was presented in Mehta and Roque (2003).

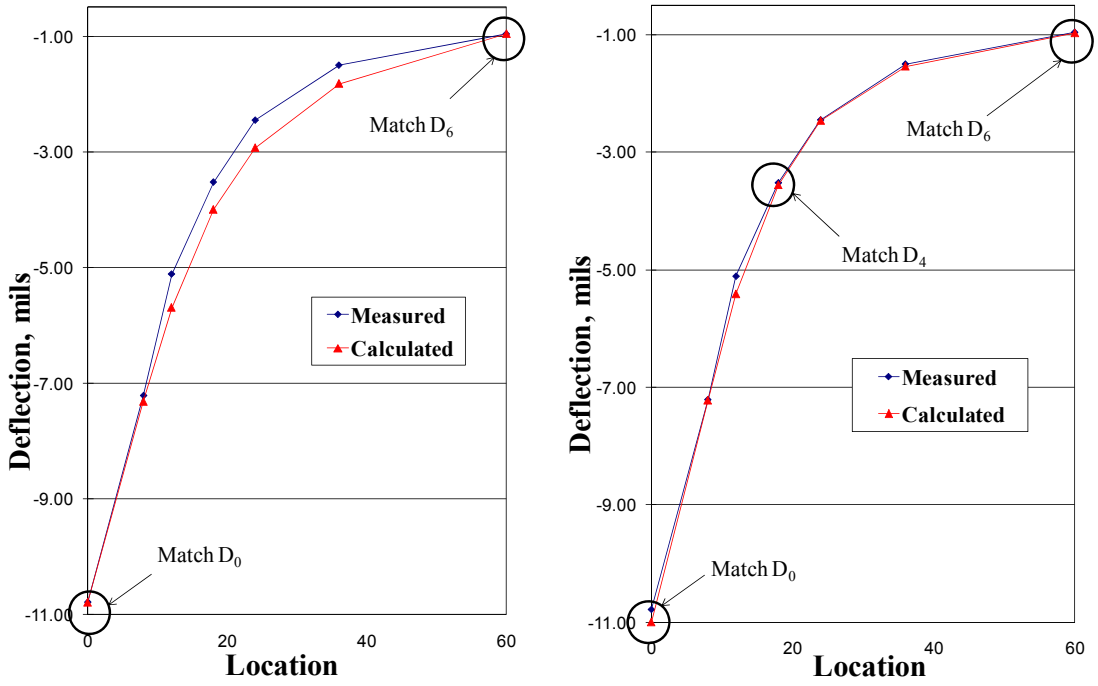

(a) Approach 1 (b) Approach 2

Figure A-2 Graphical representation of comparison of two approaches of first round analysis in determining layer moduli for Project 1

Table A-2 shows the results of the comparison of two approaches for Project 1. Even though percentage difference between approach 1 and 2, in the first round of analysis are as high as 106 %, the percentage difference in the second round of analysis are below 10 %. Similar information was obtained for Project 2.

Table A-2 Results of comparison of two approaches for 1st and 2nd round of analysis for Project 1

First Round of Analysis				
	Approach 1	Approach 2	Average	% Difference
Asphalt	247.8	229.3	238.5	14.1
Base	30.6	25.8	28.2	27.8
Subbase	115.4	740.5	427.9	106.0
Subgrade	45.9	46.9	46.4	2.4
Second Round of Analysis				
	Approach 1	Approach 2	Average	% Difference
Asphalt	250.0	229.3	239.7	8.6
Base	44.1	45.9	45.0	4.1
Subgrade	45.0	45.2	45.1	0.3

With the same objective of validating the modulus obtained from the backcalculation, The Federal Aviation Administration's (FAA) computer program named BACKFAA was used to analyze a selected number of locations of Projects 1 and 2. Results of Project 2 analysis are shown in Table A-3. Results indicate that embedded model used for the analysis within BISDEF and BACKFAA are identical. Based on the information obtained from these two processes, it can be concluded that the modulus values reported in Mehta and Roque (2003) are valid for the further analysis.

Table A-3 Comparison of BISDEF and Backfaa analysis of Project 2

	Deflection (mils)							Layer	Moduli (ksi)
	Location 8							AC	305.0
Measured	-7.00	-4.59	-3.72	-3.05	-2.41	-1.60	-0.69	LR Base	130.0
Predicted (BISDEF)	-7.03	-4.87	-4.03	-3.16	-2.51	-1.60	-0.69	Subbase	16.6
Predicted (Backfaa)	-7.03	-4.86	-4	-3.14	-2.49	-1.58	-0.67	Subgrade	43.6
	Location 10							AC	330.0
Measured	-5.55	-3.78	-3.04	-2.5	-2.11	-1.58	-1.06	LR Base	130.0
Predicted (BISDEF)	-5.67	-3.78	-3.12	-2.55	-2.18	-1.69	-1.06	Subbase	190.0
Predicted (Backfaa)	-5.67	-3.77	-3.1	-2.53	-2.16	-1.68	-1.04	Subgrade	26.0
	Location 12							AC	380.0
Measured	-7.13	-5.09	-4.03	-3.08	-2.43	-1.61	-0.77	LR Base	74.0
Predicted (BISDEF)	-7.19	-5.16	-4.23	-3.23	-2.52	-1.61	-0.77	Subbase	31.3
Predicted (Backfaa)	-7.18	-5.14	-4.21	-3.21	-2.5	-1.59	-0.75	Subgrade	35.8
	Location 13							AC	435.0
Measured	-5.81	-3.9	-3.08	-2.35	-1.8	-1.09	-0.50	LR Base	80.5
Predicted (BISDEF)	-5.83	-4.05	-3.24	-2.39	-1.80	-1.09	-0.50	Subbase	40.6
Predicted (Backfaa)	-5.83	-4.04	-3.23	-2.37	-1.78	-1.07	-0.49	Subgrade	54.5
	Location 17							AC	365.0
Measured	-7.69	-5.45	-4.13	-3.2	-2.52	-1.51	-0.61	LR Base	69.0
Predicted (BISDEF)	-7.69	-5.53	-4.51	-3.39	-2.56	-1.51	-0.61	Subbase	18.1
Predicted (Backfaa)	-7.69	-5.51	-4.49	-3.37	-2.54	-1.49	-0.59	Subgrade	45.4
	Location 25							AC	300.0
Measured	-8.44	-5.92	-4.51	-3.38	-2.57	-1.63	-0.88	LR Base	42.8
Predicted (BISDEF)	-8.57	-5.92	-4.71	-3.45	-2.62	-1.69	-0.88	Subbase	61.0
Predicted (Backfaa)	-8.57	-5.91	-4.69	-3.43	-2.6	-1.67	-0.86	Subgrade	30.8
	Location 28							AC	214.0
Measured	-5.93	-3.41	-2.5	-2.12	-1.71	-1.32	-0.83	LR Base	170.0
Predicted (BISDEF)	-5.98	-3.41	-2.69	-2.16	-1.84	-1.40	-0.83	Subbase	170.0
Predicted (Backfaa)	-6	-3.4	-2.67	-2.15	-1.82	-1.38	-0.81	Subgrade	35.4

A.3.2 BISAR Analysis

The layer moduli were used to determine the vertical strain distribution on the surface of the subgrade layer using BISAR, a multi-layer linear elastic analysis computer program. A 4,082 kg (9,000 lb) load, which is identical to the load used during the FWD testing, was applied on the surface of the asphalt pavement for each section. The resulting strain distribution for Projects 1 to 12 (except Projects 5 and 8) is presented in Figure A-3 to Figure A-7.

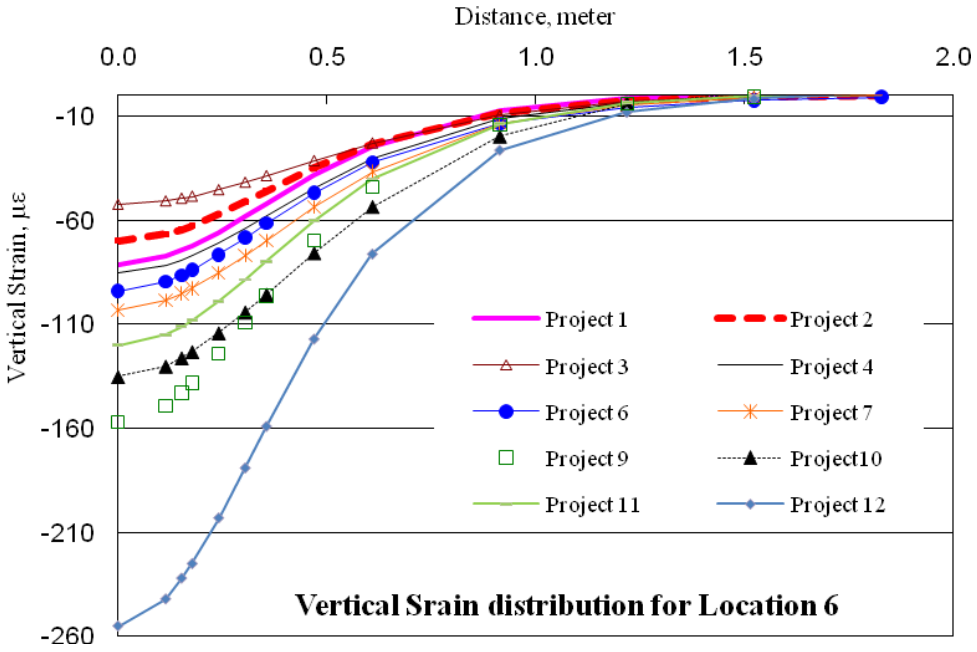

Figure A-3 Vertical strain distribution at the surface of the subgrade for Location 6

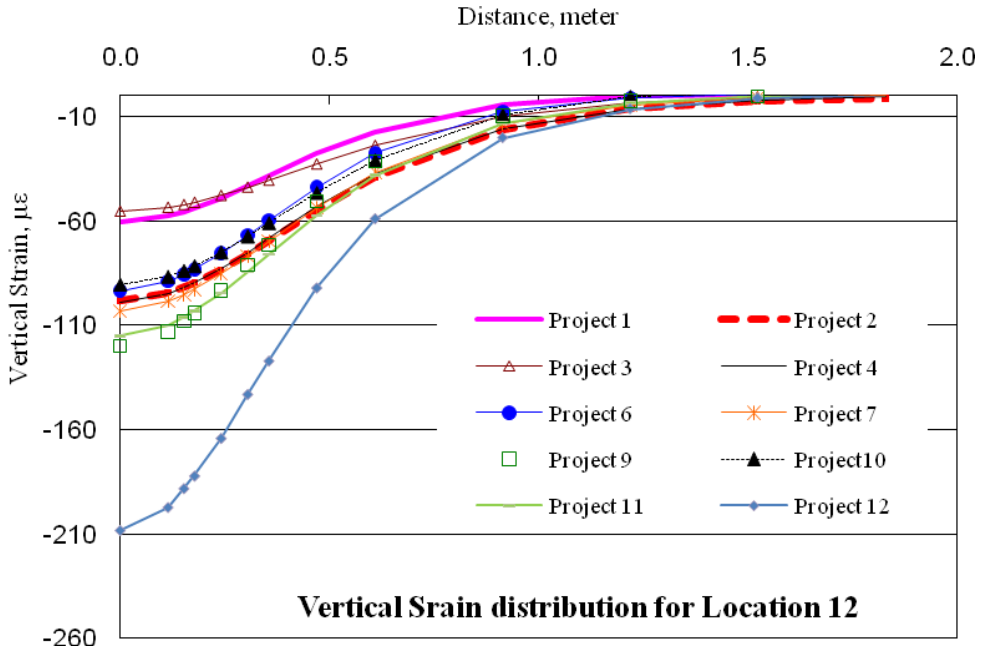

Figure A-4 Vertical strain distribution at the surface of the subgrade for Location 12

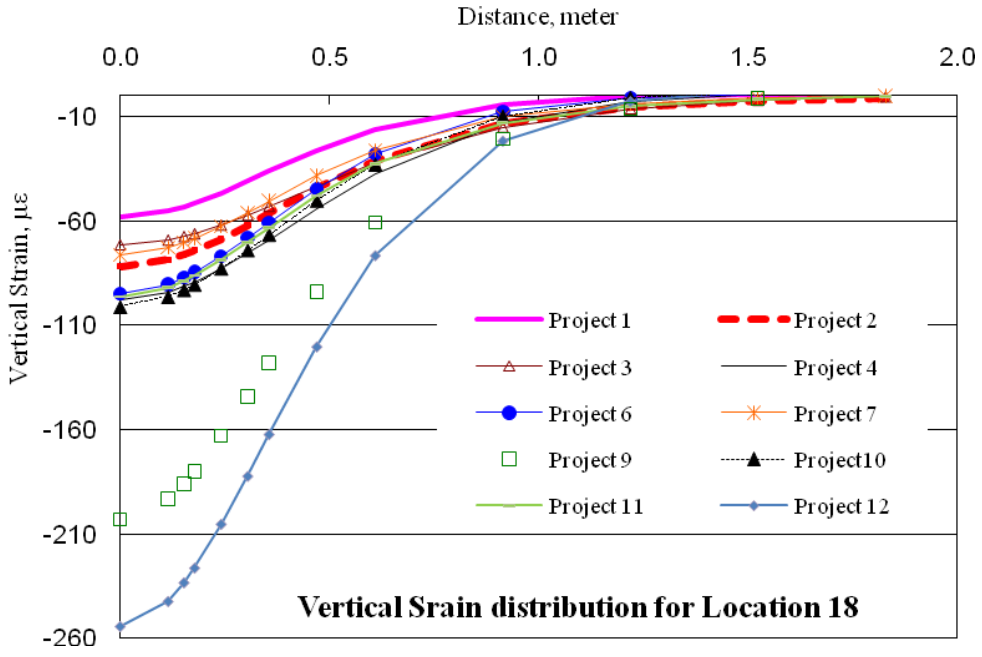

Figure A-5 Vertical strain distribution at the surface of the subgrade for Location 18

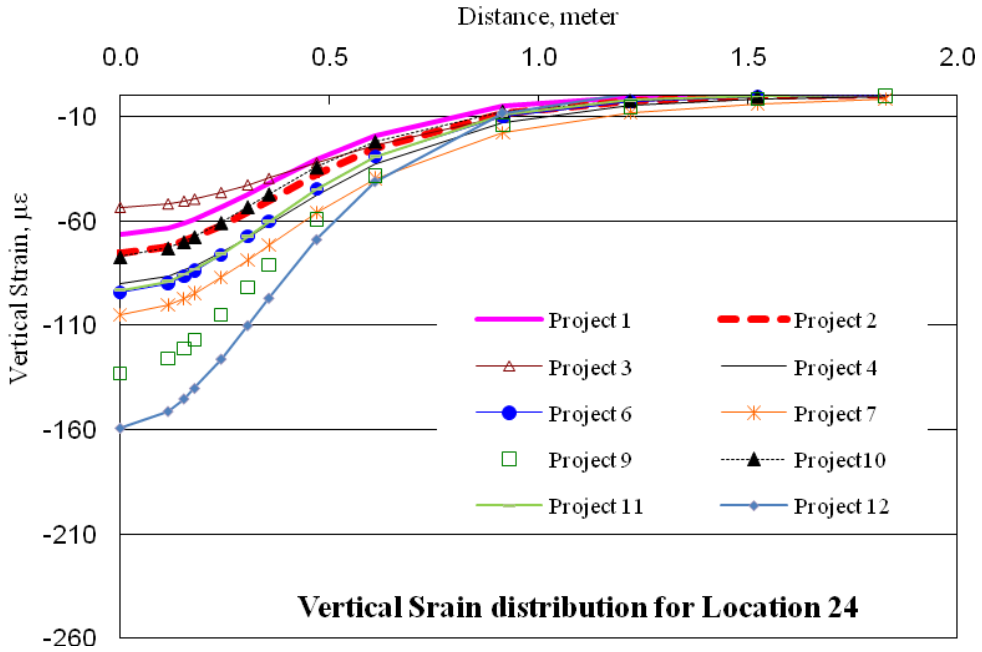

Figure A-6 Vertical strain distribution at the surface of the subgrade for Location 24

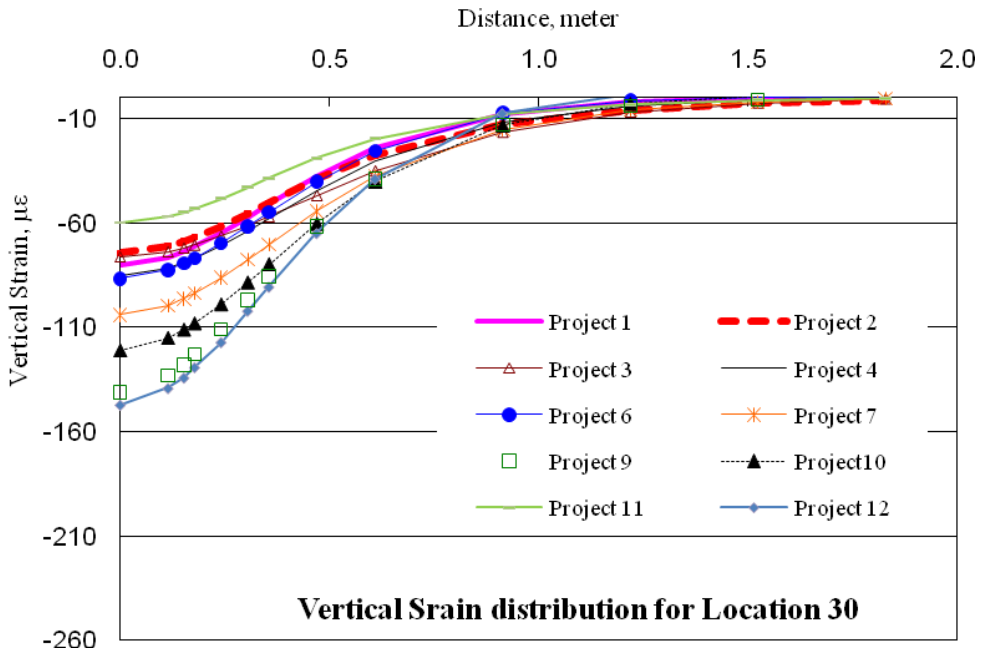

Figure A-7 Vertical strain distribution at the surface of the subgrade for Location 30

A.4 Interpretation of Transverse Profile

The shape of the subgrade strain obtained from the BISAR analysis was projected into the rut profile. Figure A-8 illustrates schematically the process of projecting the distribution of the subgrade strain into the rut basin. A Microsoft Excel spread sheet was used to remove the cross slope from the transverse profile measurements. The slope on each corner of the wheel path was calculated and compared with the corresponding slope in the subgrade deflection. The slope was taken one foot from the intersection of datum line and profile. The percentage difference of the slope of surface and subgrade is shown in Figure A-9 to Figure A-18.

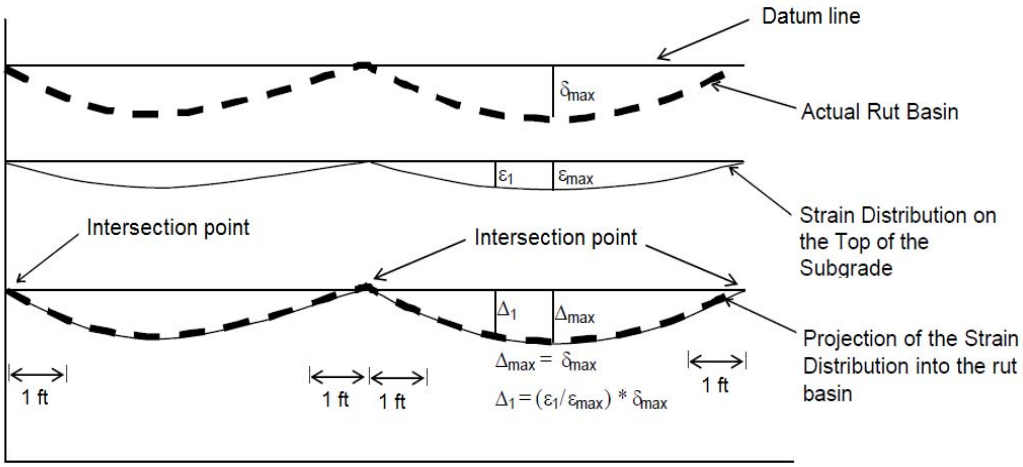

Figure A-8 Schematic representation of projecting the distribution of the subgrade strain into the rut

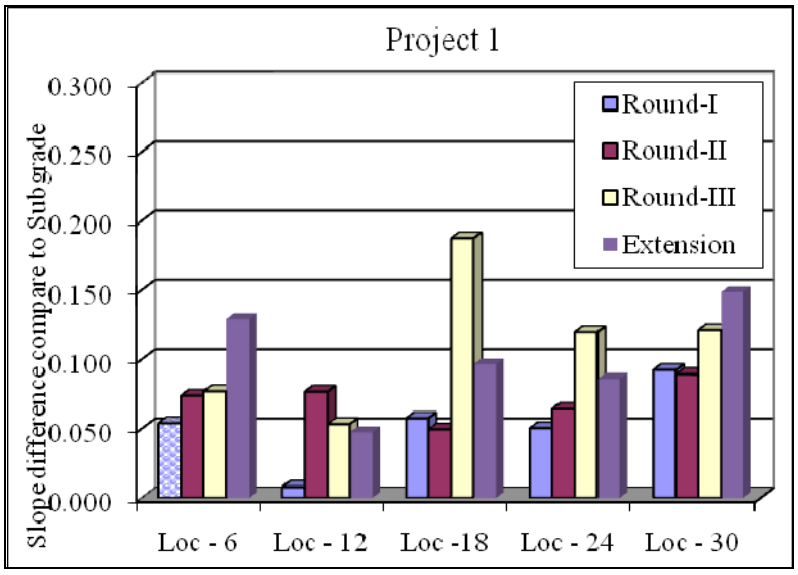

Figure A-9 Overall difference in slope for Project 1

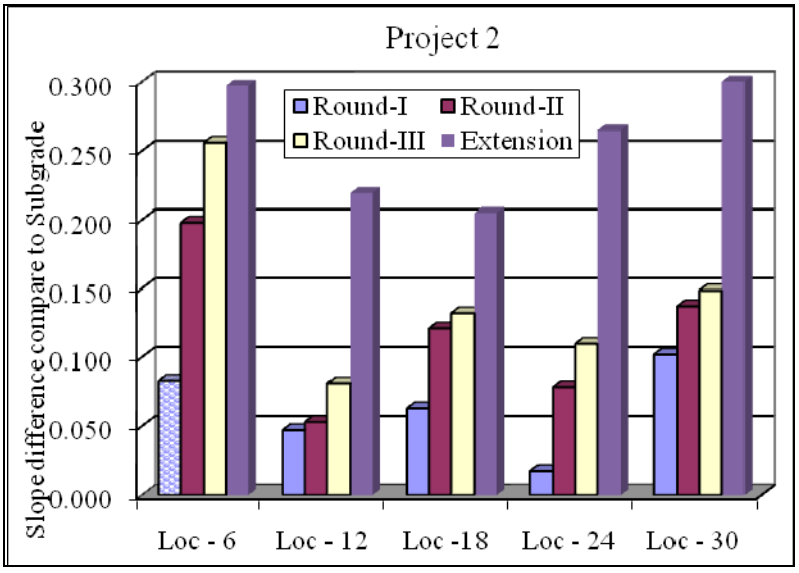

Figure A-10 Overall difference in slope for Project 2

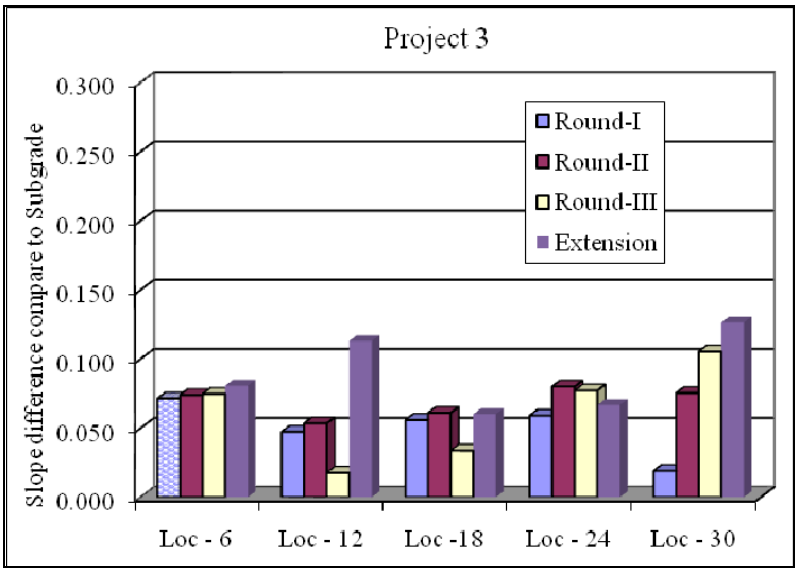

Figure A-11 Overall difference in slope for Project 3

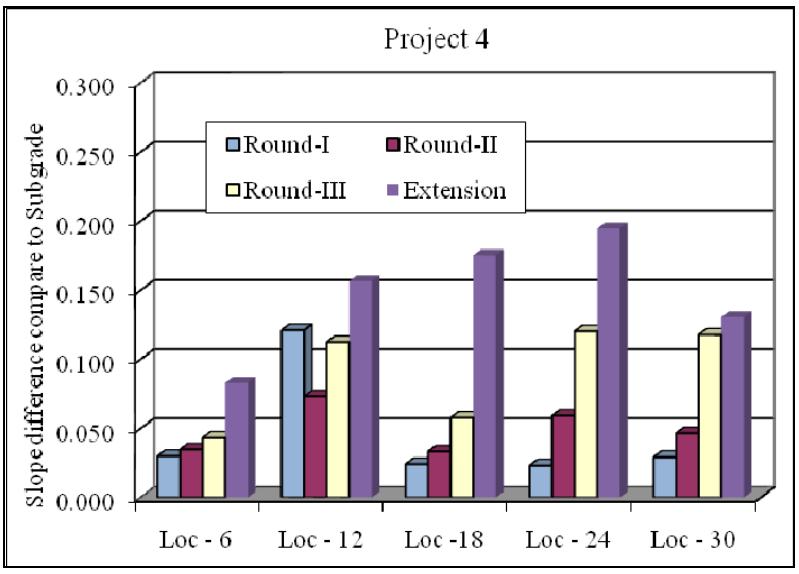

Figure A-12 Overall difference in slope for Project 4

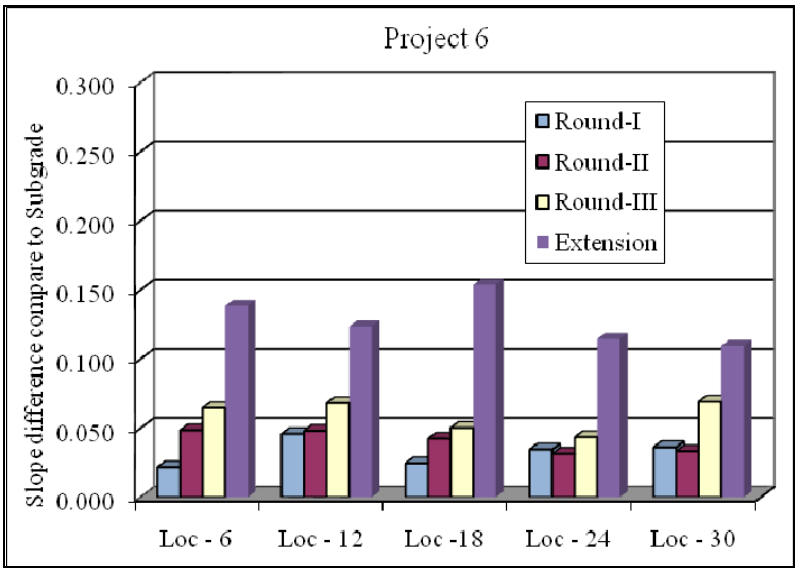

Figure A-13 Overall difference in slope for Project 6

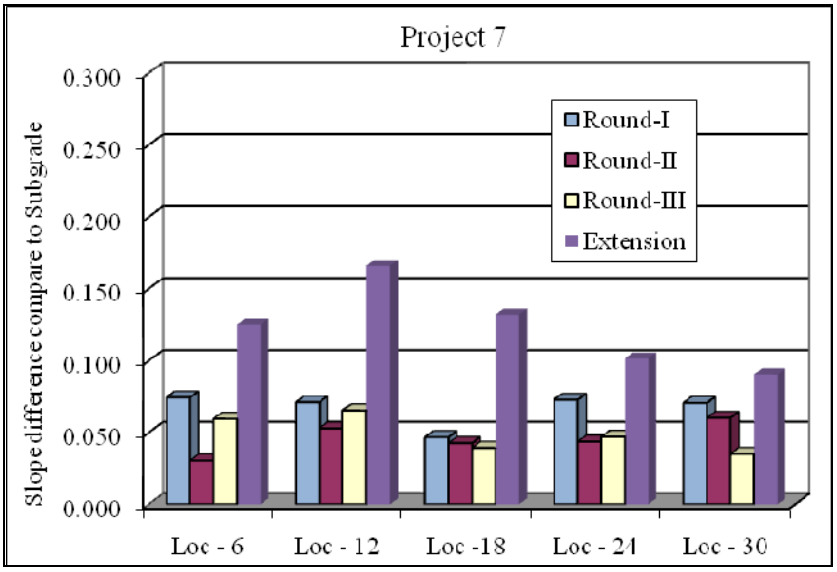

Figure A-14 Overall difference in slope for Project 7

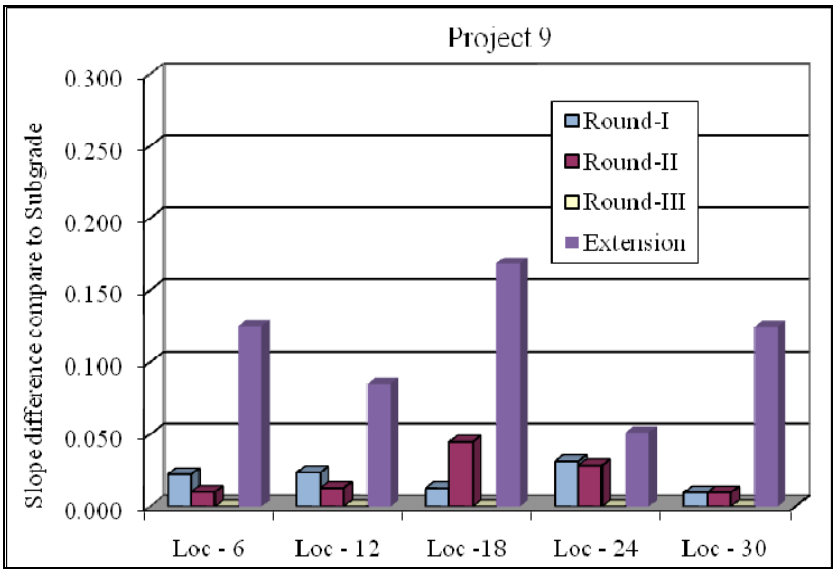

Figure A-15 Overall difference in slope for Project 9

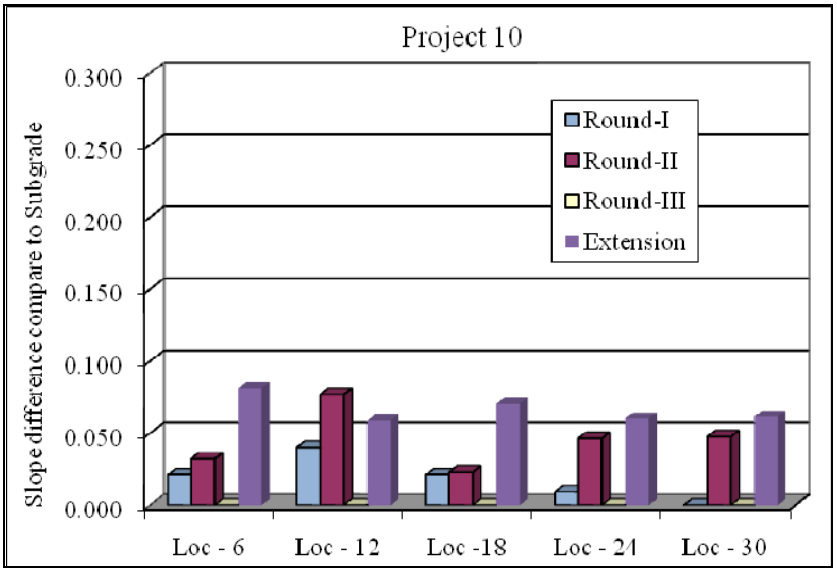

Figure A-16 Overall difference in slope for Project 10

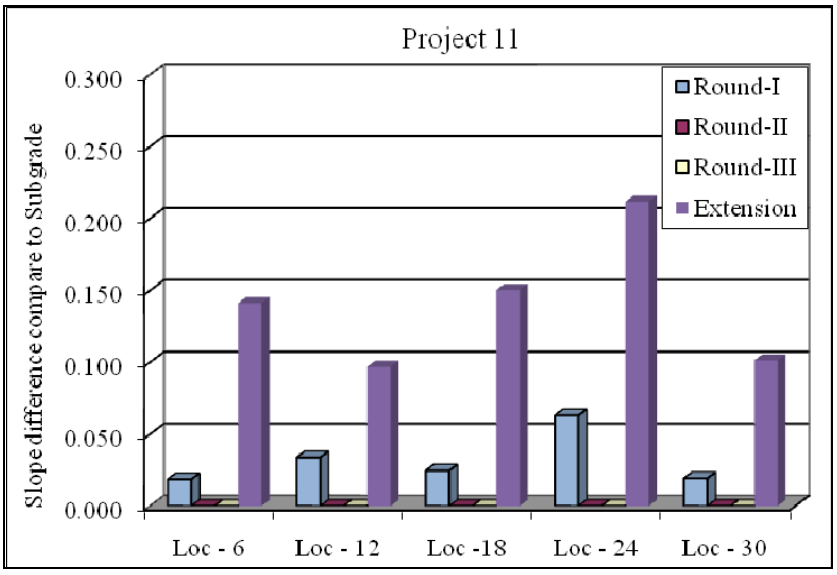

Figure A-17 Overall difference in slope for Project 11

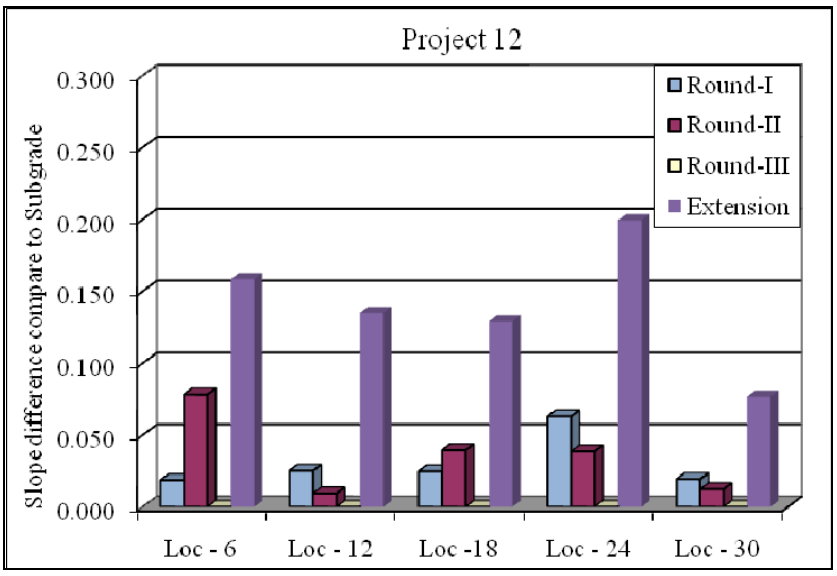

Figure A-18 Overall difference in slope for Project 12

The plot for all the projects except Project 5 and 8 were obtained and presented in Figure A-19. Project 5 is discarded from the analysis. Project 8 FWD data is not available. This Project

was constructed with a HMA overlaid on PCC. Subgrade modulus of such layer configuration could not be obtained from linear elastic backcalculation software currently available. The summary of remaining Projects, based on the approach that was developed by Villiers et al. (2005) is as follows.

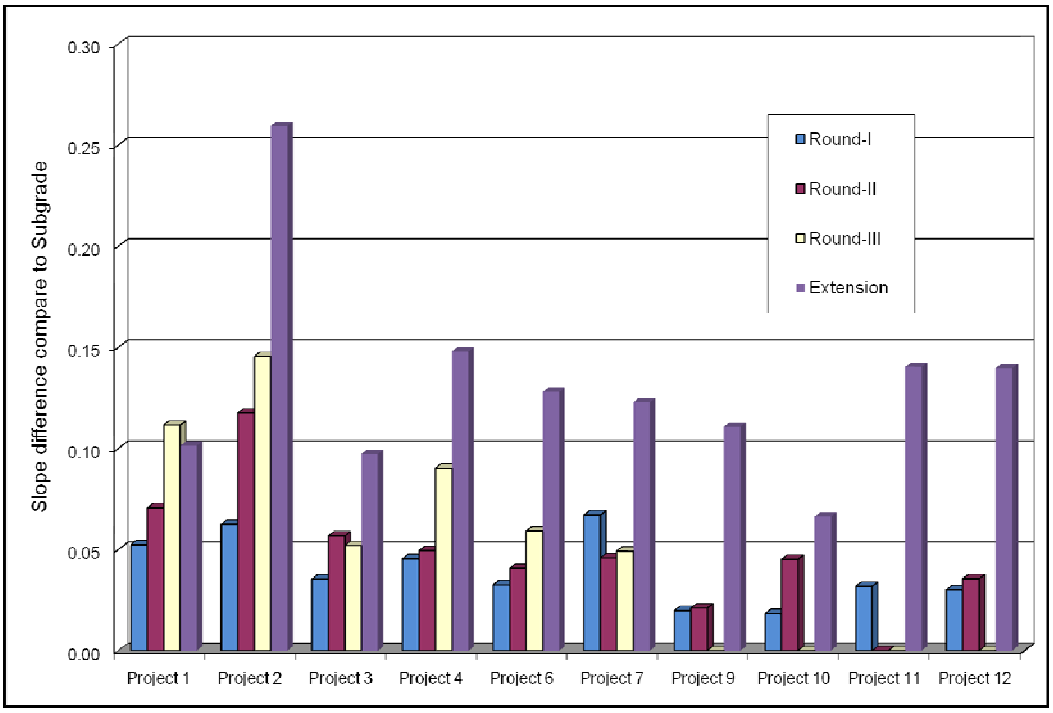

Figure A-19 Average slope difference in Projects 1 to 12 (Except Project 5 and 8)

Table A-4 summarizes the possible major source of rutting determined by the analysis conducted for each Superpave project over time.

Table A-4 Major source of rutting determined for Superpave projects

Project (UF) ID	Time of Construction	Time of Measurement		Major Source of Rutting
		Round	Date	
1	Jan, 1998	Round I	Dec, 1999	Instability
		Round II	Dec, 2000	Instability
		Round III	Feb, 2003	Instability
		Round IV	Aug, 2009	Instability
2	May, 1998	Round I	Dec, 1999	Instability
		Round II	Dec, 2000	Instability
		Round III	Feb, 2003	Instability
		Round IV	Sep, 2009	Instability
3	May, 1998	Round I	Dec, 1999	Subgrade Compaction
		Round II	Dec ,2000	Subgrade Compaction
		Round III	Feb, 2003	Subgrade Compaction
		Round IV	Sep, 2009	Subgrade Compaction
4	Oct, 1998	Round I	Dec, 1999	Subgrade Compaction
		Round II	Mar, 2001	Subgrade Compaction
		Round III	Mar, 2003	Instability
		Round IV	Jul, 2009	Instability
6	Aug, 1998	Round I	Aug, 1999	Reduction in Air voids
		Round II	Feb, 2001	Subgrade Compaction
		Round III	Mar, 2003	Subgrade Compaction / Instability
		Round IV	Jul, 2010	Subgrade Compaction / Instability
7	Sep, 1998	Round I	May, 2000	Reduction in Air voids
		Round II	May, 2001	Subgrade Compaction
		Round III	Mar, 2003	Subgrade Compaction
		Round IV	Jul, 2010	Subgrade Compaction / Instability
8	Oct, 2000	Round I	Oct, 2001	Was not included because the moduli could not be obtained to the pavement structure. PCC overlay with HMA
		Round II	Oct, 2002	
		Round III	Jan, 2005	
		Round IV	Dec, 2009	
9	May, 2002	Round I	Feb, 2003	Subgrade Compaction
		Round II	Nov, 2003	Subgrade Compaction
		Round III	Jun, 2009	Subgrade Compaction / Instability
10	Nov, 2002	Round I	May, 2003	Subgrade Compaction
		Round II	Jun, 2004	Subgrade Compaction
		Round III	Jun, 2009	Subgrade Compaction
11	Mar, 2003	Round I	Jan, 2004	Subgrade Compaction
		Round II	Jun, 2005	Subgrade Compaction
		Round III	Jun, 2009	Instability
12	May, 2003	Round I	Dec, 2003	Subgrade Compaction
		Round II	Feb, 2005	Subgrade Compaction
		Round III	Dec, 2009	Instability

Based on the results analyzed using the new develop approach, the following summary was made on the projects evaluated.

- Instability was present in Project 1 for all the time tested. Except for Project 2, the change in slope (CS) as compared to the subgrade was higher on Project 1 as compared to the other projects for any given time tested. However, it was noticed a 10% reduction in CS from 2003 (Round-III) to 2009 (Extension). When the different profiles were superimposed, it was noted that a possible shift in traffic wander compacted the dilated portion. As a result, the rutted area was widening in the lateral direction.
- Instability was present in Projects 2 for all the time tested. The change in slope (CS) as compared to the subgrade was higher on this project than any other projects for any given time tested.
- There is not enough to conclude that instability was present in Projects 3 and 10. It appears that the source of rutting may primarily due to subgrade compaction for these two projects. For the all the rounds tested, the CS difference as compared to the subgrade was the lowest on these two projects.
- Similarly to Projects 3 and 10, the source of rutting appeared to be primarily due to subgrade compaction for Projects 4, 9, 11, and 12 for the first two rounds tested. However, sign of instability has been observed on these projects, especially during the Continuation of Superpave Projects Monitoring (CSPM) phase.
  - Project 4 CS was almost double on the last two rounds, respectively.
  - Project 9, may be categorized on the border line between subgrade compaction and instability for CSPM phase.

  - Projects 11 and 12 showed sign of instability for CSPM phase. The CS as compared was equal to 0.14 (see Figure A-19). This value was identical to Project 4.

- A similar pattern as compared to Projects 4, 9, 11, and 12 was observed on Projects 6 and 7. Sign of instability has been noticed on these projects, especially during the Continuation of Superpave Projects Monitoring (CSPM) phase. However, the primary cause of rutting on the first two rounds tested was associated to reduction in air voids

Additional analysis and validation is needed to confirm above observations.

A.5 Closure

An approach that integrates Falling Weight Deflectometer (FWD) and core data along with 3.6 meter transverse profile measurements was developed. It can be used to assess the contributions of different pavement layers on rutting, and identifies the presence (or absence) of instability within the asphalt surface layer.

APPENDIX B
SOFTWARE DEVELOPMENT

B.1 Program Description

The objective of this task is to create a user-friendly option to interpret the data collected for a transverse profile. To meet this task objective a computer program was developed using Microsoft C#. The program has the capability to display the results using graphical and tabulation formats. More information related to the input, output and detailed functionality from this program is provided below.

B.2 Inputs

Data input can be generated using the following two processes:

- Transverse profile measurements can be entered manually via a form within the program.
- Transverse profile measurement can be imported from a Microsoft Excel file. This Excel file has to be generated using specific format that is compatible to the Microsoft C# Program.

B.3 Outputs

Following is the brief summary of available output features;

- Plot of the Transverse Profile – The data provided can be used to generate two plots: one that contains the slope of the road (similar to the data obtained from the

field), and one where the data is run through an algorithm to remove the cross slope from the transverse profile measurements

- Value of a Point on the Plot – The co-ordinates of plot after removing the cross slope could be find out by clicking on the graph (This could not be done on the graph before removing the cross slope).
- Slopes of the Depression of the Wheel Paths – Four slopes (one for each corner of a wheel path) are generated and displayed in two formats: a plot of the slopes are superimposed on the plot of the transverse profile, and the numerical values of the slopes are displayed as a table to the user.
- Rut Depths Measurement for Various Time Frame – The rut depth of each wheel path was generated and displayed in two formats: a plot the depths were superimposed on the plot of the transverse profile for multiple time frame (Round I, Round II, …etc.), and the numerical values of the rut depths are displayed in table to the user.
- Plot of the Subgrade Profile – The data provided for subgrade profile could be plotted for the visual comparison with surface profile.
- Additional Display for each "Location" – Comparison of multiple locations could be carried out at one time. Graph of each location could be plotted on separate tab for better viewing.
- Slope of Subgrade Profile – Four slopes (one for each corner of a wheel path) are generated and displayed in two formats: a plot of the slopes is superimposed on the plot of the transverse profile, and the numerical values of the slopes are displayed as a table to the user.

- Detailed results – A window containing slope of surface and subgrade profile, coordinate of the graphs is shown.
- Comparison of Surface and Subgrade profile – A graph can be generated which will show the comparison of the average difference between the slopes generated for surface and subgrade profiles.

B.4 Detailed Functionality

Figure B-1 shows the screenshots of the computer program. This could be divided in two parts; plotting area and data input fields. Detail functionality of the computer program could be divided in following four parts.

- GUI: Data Input
- GUI: Plot Area
- GUI: Detailed Profile Information
- GUI: Project Summary

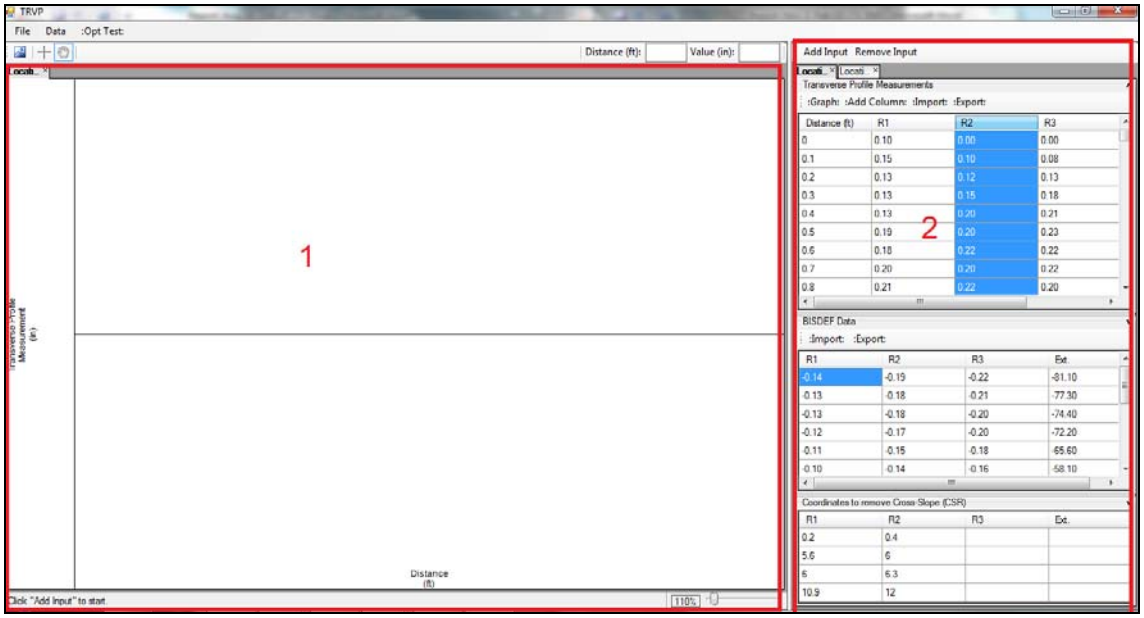

Where,
1 - The plotting area of the program
2 - The data input fields

Figure B-1 GUI display of computer program

B.4.1 GUI: Data Input

Following are the GUI input features added to expedite data evaluation process. See Figure B-2 for more details.

A – Add or Remove of "Location" – The user can add/remove an input form; currently treated as an individual "Location" of a project. When adding a form, a window will prompt the user for the window to define the name; name can be any user define name.

B – Multiple Inputs – The user can have multiple "Locations," represented by tabs, open at the same time. Each of these tabs has their own tables for data input.

C – Transverse Profile Measurement – Transverse profile measurement has "graph", "add column", "import" and "export" tabs which are explained as follows.

- Graph – Once clicked the graph button will take the data from the “Measurement Input Fields,” generate the plots and display them.
- Add column – This will add another column of “Measurement Input Fields” to the form. This is done to allow multiple transverse profiles to be plotted on the same graph.
- Import – Once clicked the user will be prompted to provide a Microsoft Excel file. The program will then take the data in the file and automatically populate the “Measurement Input Fields” (provided it is in the format compatible to C#).
- Export – This will take the data in the “Measurement Input Fields” and create a Microsoft Excel file in the proper format.

D – BISDEF Data – Much like the “Transverse Profile Measurement” buttons; the user is able to import/export directly from/to a Microsoft Excel file. The header of the “Transverse Profile Measurement” should match with the header of “BISDEF Data” table.

E – Coordinate to Remove Cross-Slope – When removing the slope from the original profile to create the horizontal or flat profile; four (4) key points are determined. These four points determine the shape of the horizontal profile, and also where the slopes of the wheel path ruts are located. The program will automatically try to generate the best numbers. In addition to that the user can manually input their own values and have the program use them.

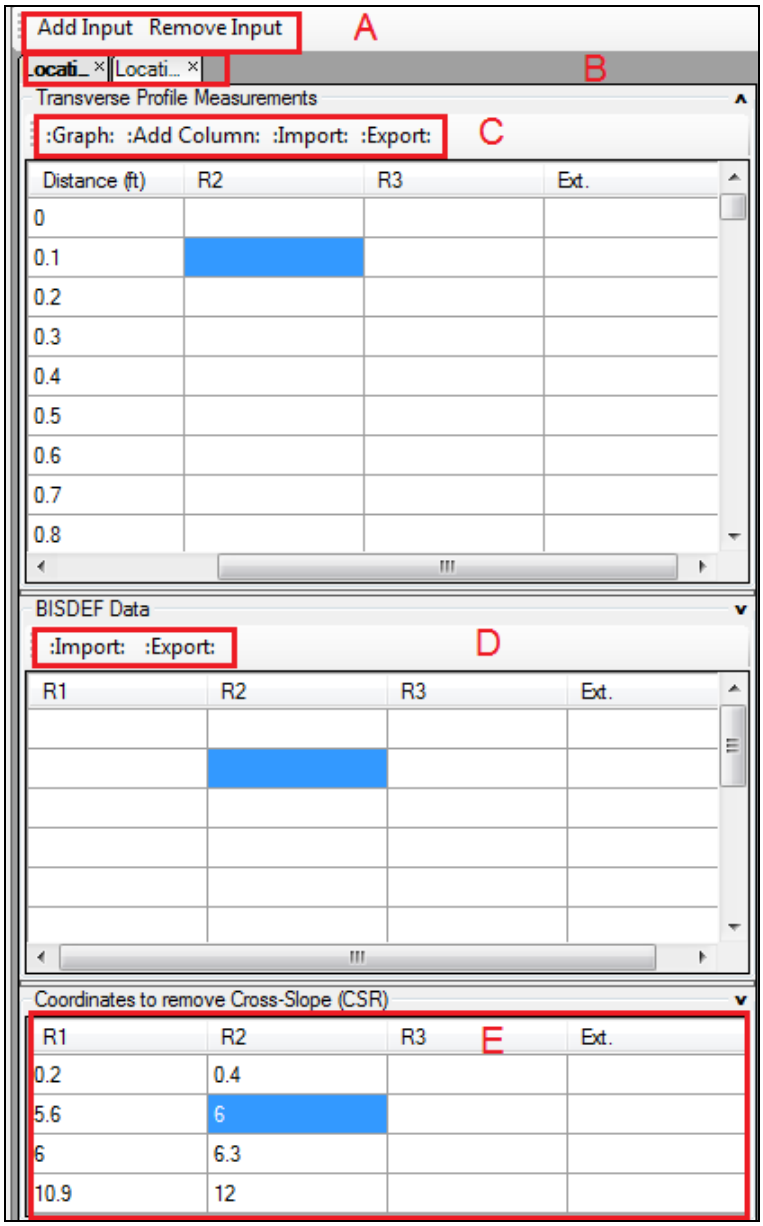

Where,
A – Add or remove of "Location"
B – Multiple input
C – Transverse profile measurement (graph, add column, import, export buttons)
D – BISDEF data
E – Coordinate to remove cross-slope

Figure B-2 The GUI data input field in the program

B.4.2 GUI: Plot Area

Figure A-3 shows the display for plot area. The parts of the display are explained as follows.

1. New graph – This tool is used to create new plot tab which could plot graphs.

2. Precision Pointer Tool – If this tool is selected when a user clicks on a point on a plotted profile then the "Distance and Value Fields" will be updated with data from the point (see Figure A-4).

3. Hand Tool – With this tool selected the user can click on the plot and drag the mouse to move the plot (see Figure B-5).

4. Distance and Value Fields – These fields will display the values of a point on a plot selected by the "Precision Pointer Tool" (see Figure A-4 from the "Precision Pointer Tool" above).

5. Legend of the graphs – Legend of the graph is displayed on top right hand side of the plot area.

6. Zoom Scale Tools Panel – These functions provide a similar but limited version of the "Zoom Tools" describe above and will be removed when the "Zoom Tools" are completed. They are currently still in place for testing purposes.

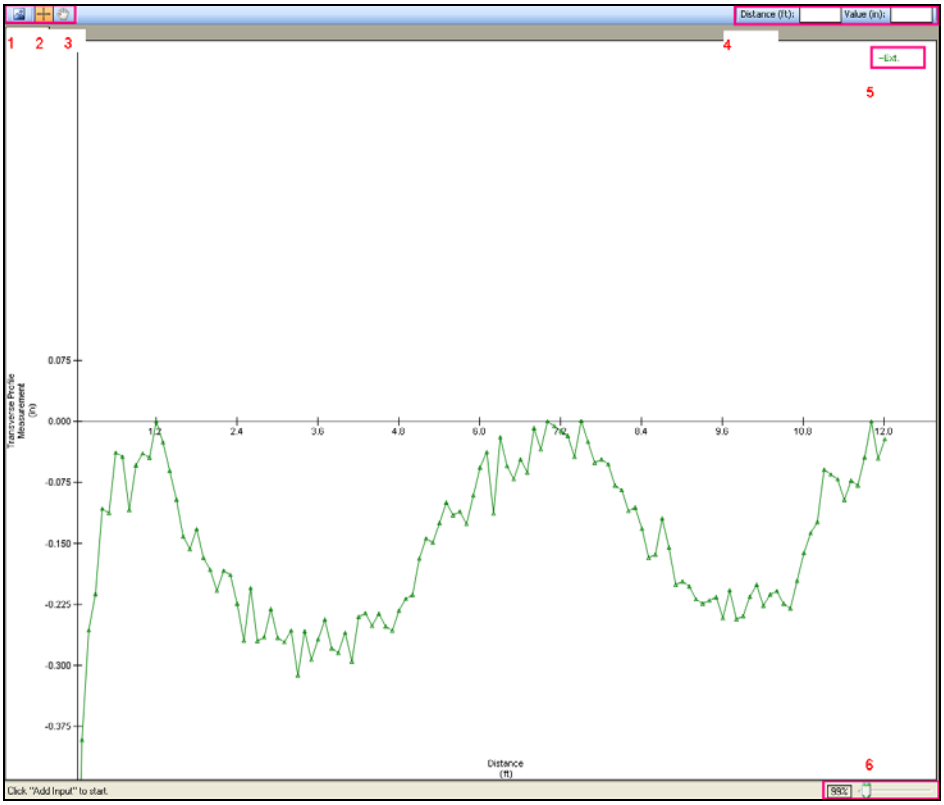

Where,
1 – New graph
2 - Precision pointer tool
3 – Hand tool
4 – Distance and value fields
5 – Legend of the graph
6 – Zoom scale tools panel

Figure B-3 GUI plot area

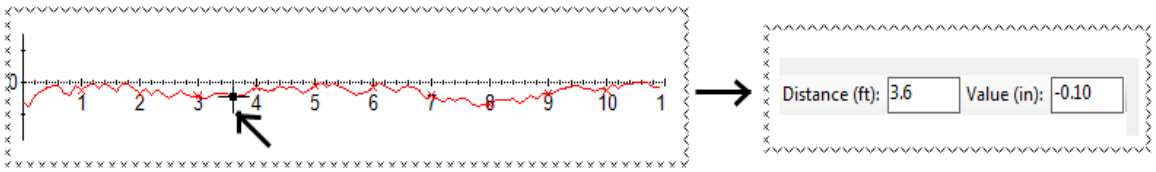

Figure B-4 Precision pointer example

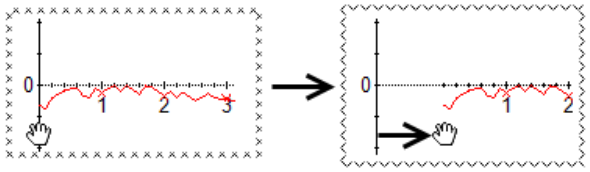

Figure B-5 Hand tool example

B.4.3 GUI: Detailed Profile Information

The graph shows graphical depictions of the profiles and aspects relating to them, such as slope, rut depth, etc. The detail information about the graph input and output could be seen from Figure B-6.

The user may now right-click on a column header of a profile and selects "View Detailed Information" and a window will pop-up containing the numerical values. Following is the description of each subsection in the "detailed Profile Information" window.

1 – Measurement Values with Cross-Slope intact – These are the values the user input to the "Transverse Profile Measurements" table.

2 – Measurement Values without Cross-Slope – These are the values generated by the program after removing the slope from the above (Measurement Values with Cross-Slope intact) values and are the values of the horizontal surface profile.

3 – Rut Depth values – This table contains the lowest depth from the right wheel path, the lowest depth from the left wheel path, and the rut depth generated from the average of these two depths.

4 – Surface Profile Slope values – This table contains the values of the slope for the two corners of each wheel path for the surface profile.

5 – BISDEF (Subgrade) Slope values – This table contains the values of the slope for the two corners of each wheel path for the subgrade profile.

6 – BISDEF Curve Generation Values – This table contains the values used to generate the BISDEF (Subgrade) profiles. The first column contains the value input by the user in the "BISDEF Data" table. The second contains the values generated by the program to create the subgrade profile for the right wheel path. The third column is the same but for the left wheel path.

7 – Surface/Subgrade Slope Comparisons (Right wheel path) – This table contains the values of the comparisons (value difference, the percent difference, average difference, and average percent difference) of the surface and subgrade slopes for the right wheel path.

8 – Surface/Subgrade Slope Comparisons (Left wheel path) – This table contains the values of the comparisons (value difference, the percent difference, average difference, and average percent difference) of the surface and subgrade slopes for the left wheel path.

9 – Surface/Subgrade Slope Comparisons (Average of both wheel paths) – This table contains the values of the average of comparisons (difference and percent difference) of the surface and subgrade slopes of both wheel paths.

10 – Coordinates to remove Cross-Slope (CSR) – This table contains the four values (distances) used to remove the slope to create the horizontal profile generated by the program, or specified by the user. Also, these points determine where the slopes of the surface profile are located.

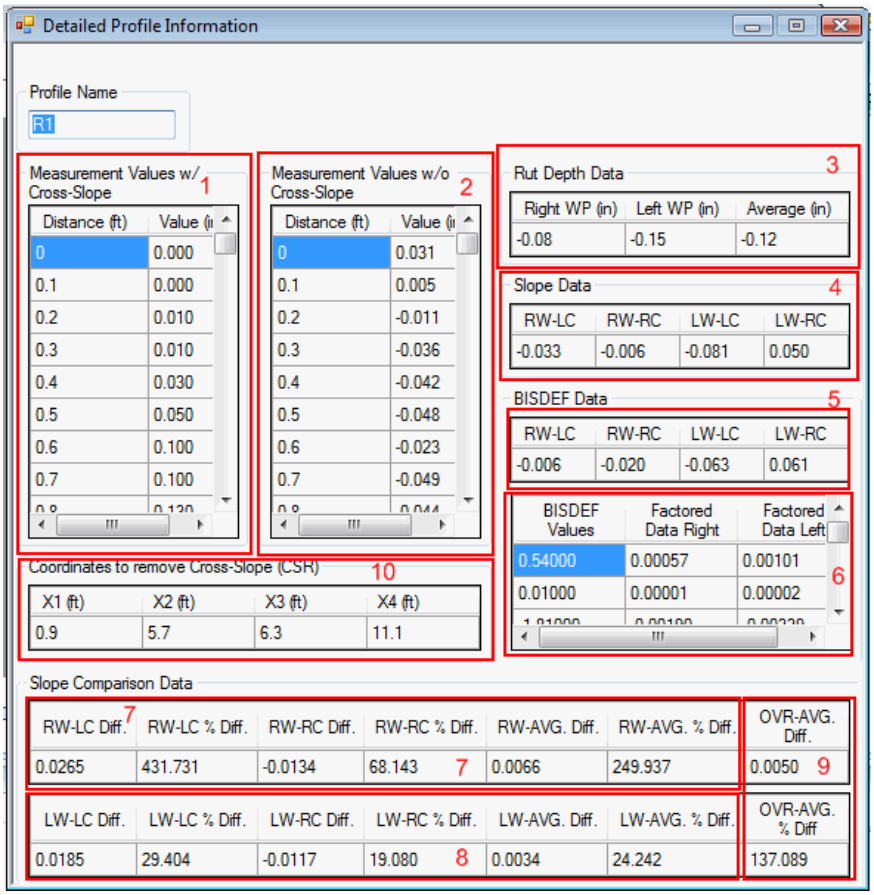

Where,
1 – Measurement values with cross-slope intact
2 – Measurement values without cross-slope
3 – Rut depth values
4 – Surface profile slope values
5 – BISDEF (subgrade) slope values
6 – BISDEF curve generation values
7 – Surface/subgrade slope comparisons (Right wheel path)
8 – Surface/subgrade slope comparisons (Left wheel path)
9 – Surface/subgrade slope comparisons (Average of both wheel paths)
10 – Coordinates to remove cross-slope (CSR)

Figure B-6 Detailed profile information

B.4.4 GUI: Project Summary

An option to display a "Project Summary" is now available. This summary shows the surface/subgrade slope comparison summarized above, as shown in the graph labeled Figure B-7

Project Summary. The bars on the graph represent the difference in the slopes for each profile associated for a location. In this example, the Blue Bar represents “Round I”, the Red Bar; “Round II” and the Green Bar; “Round III”. A key showing this on the graph is planned but not implemented yet.

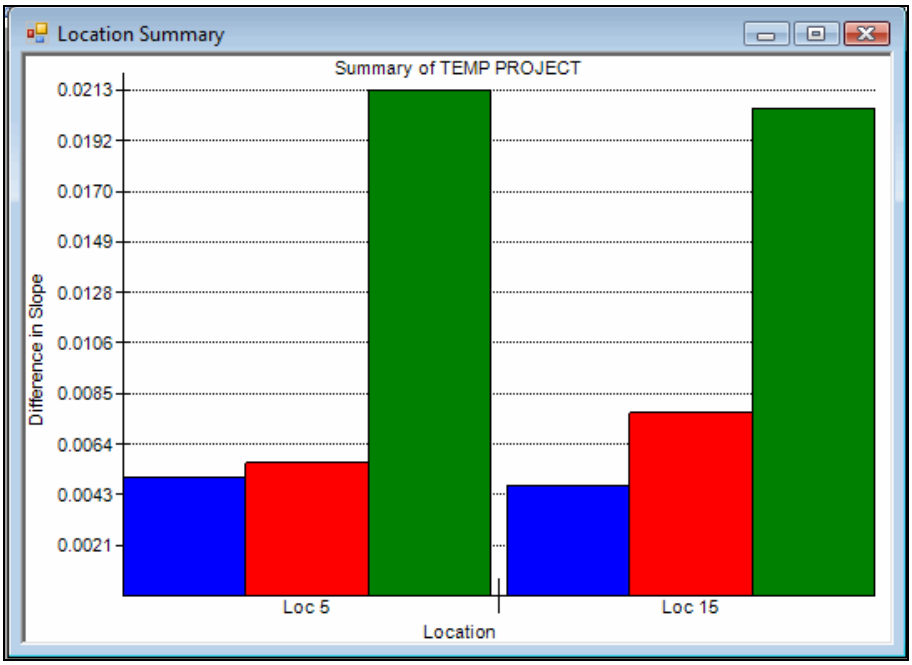

Figure B-7 Project summary

B.5 Data Evaluation with Program

Evaluation of surface and subgrade profile slopes, their plot and comparison is complicated and time consuming process with excel sheet. This obstacle has been removed by developed program. Table B-1 shows the comparison of slope difference determined by excel sheet and new program for Location 6 of Project 1. From the results, it is apparent that new program expedites the process of analysis without compromising in accuracy.

Table B-1 Comparisons of slope difference determined by excel sheet and new program for Location 6 of Project 1

	LW-LC	**LW-RC**	**RW-LC**	**RW-RC**	**Average**
New program					
Round-I	0.083	0.023	0.081	0.003	**0.048**
Round-II	0.055	0.080	0.163	0.006	**0.076**
Round-III	0.038	0.039	0.171	0.059	**0.077**
Extension	0.144	0.114	0.193	0.060	**0.128**
Excel sheet					
Round-I	0.086	0.023	0.081	0.003	**0.048**
Round-II	0.048	0.078	0.163	0.006	**0.074**
Round-III	0.037	0.039	0.173	0.059	**0.077**
Extension	0.148	0.114	0.193	0.065	**0.130**

Where,
1. LW-LC – Left Wheel Left Corner
2. LW-RC – Left Wheel Right Corner
3. RW-LC – Right Wheel Left Corner
4. RW-RC – Right Wheel Right Corner
5. Average – It is average of all four corner values